

Self-Assembling Peptides for Cartilage Regeneration

Andres Barco

Submitted in accordance with the requirements for the
degree of Doctor of Philosophy

The University of Leeds
School of Mechanical Engineering

September 2017

The candidate confirms that the work submitted is his/her own and that appropriate credit has been given where reference has been made to the work of others.

This copy has been supplied on the understanding that it is copyright material and that no quotation from the thesis may be published without proper acknowledgement.

The right of Andres Barco to be identified as author of this work has been asserted by her in accordance with the Copyright, Designs and Patents Act 1988

Acknowledgements

It would only be right to start off by thanking one of the best supervisors a person could ask for, Eileen Ingham. Your constant support, patience and guidance over the years has been admirable, even in time of darkness. Without all your help I wouldn't be who I am today and for that I have everything to thank you for. I wish you well in the future and hope to keep in contact. I would also like to thank my other supervisors and mentors: John Fisher for his witty engineering insights and all the lovely chocolate biscuits. Phil Davies for his constant support and guidance at the beginning of my project, without you I think I would have given up. Hazel Fermor for always being there when I needed help and being an excellent mentor. Your enthusiasm for science is truly inspirational and I feel very privileged to have had the opportunity to work with you all – all the best for the future!

A big thank you to all my lab peers both in engineering, biology and chemistry for making my time here enjoyable to work in. Particular thanks to Imran Asif, James Warren and Fiona Walker for their infinite sources of wisdom, kindness, advice and laughs – you guys were always there to listen to my PhD stories and kept me sane! I would also like to thank the EPSRC for giving me the funding for this excellent opportunity, without it, my growth and learning would have not been possible.

My time at Leeds would have not been the same without each and every one of my friends that I made over the years. You helped me take a step back when I needed it the most and you enabled me to cope with the hard times throughout the last 5 years and for that I will always be grateful – you are too numerous to name but I'm sure you know who you are.

I would like to give a big special thanks to my family and friends back home. Mum, Auntie Lilianna and Uncle Jorge, we have been through a lot together in the past 6 months but your love, support and encouragement is more than I could have ever wished for and I could have not done this without you all! My sister, Carolina, for her constant nagging and entertainment, you've known how to cheer me up when I've been down. To my cousin, Felipe, for his words of wisdom and always a person I could come talk to when times got hard. Lastly to my dad, for all your help and encouragement throughout the years.

Start by doing what's necessary, then do what's possible and suddenly you are doing the impossible.

Abstract

Loss of glycosaminoglycans (GAGs) in osteoarthritic (OA) cartilage contributes to a decrease in mechanical properties and function *in vitro*, and is considered to be a major contributor to disease progression. The aims of this investigation were to test the hypothesis that a combination of self-assembling peptides (SAPs) and chondroitin sulfate (glycosaminoglycan; GAG) would restore the biomechanical properties of GAG depleted porcine condylar cartilage, ideally to a level intrinsic to native porcine condylar cartilage.

The SAPs investigated were members of the P₁₁ series which have been designed to spontaneously self-assemble into three-dimensional fibrillar hydrogels, in response to physiological conditions. Initial studies were carried out to determine which of three peptides (P₁₁-4, P₁₁-8 and P₁₁-12) demonstrated high β -sheet percentage, long-woven fibrillar networks and high stiffness; when mixed with chondroitin sulfate at two different GAG molar ratios (1:16 and 1:64) in physiological conditions, using FTIR analysis, transmission electron microscopy and rheology. The β -sheet percentage, dimensions of fibrils and stiffness were dependent upon the peptide, GAG molar ratio and Na²⁺ salt concentration. P₁₁-4 and P₁₁-8: GAG mixtures had high β -sheet percentage ranging from 50.6-91 % and 81.7-92 %, respectively. Fibril lengths of the P₁₁-4 and P₁₁-8: GAG mixtures were in the range 498- 3518 nm and the elastic shear modulus (G') ranged from 4,479-10,720 Pa and 7,722-26,854 Pa, respectively. P₁₁-4 and P₁₁-8: GAG mixtures were selected for further investigation.

In order to produce a GAG depleted cartilage model, porcine femoral condylar cartilage was subjected to three different methods of GAG depletion (1) coating the surface with chondroitinase ABC (2) injecting chondroitinase ABC into the cartilage (3) washing the condyles in sodium dodecyl sulfate (SDS). GAG depletion was successfully achieved following two 24 hour washes in 0.1 % (w/v) SDS and buffer washes. Histological analysis of safranin O stained sections revealed an absence of GAGs. Quantification of GAGs using the dimethylmethylene blue assay revealed that 75 % of GAGs had been removed.

In order to assess the effects of peptide: GAG mixtures on the biomechanical properties of the GAG depleted porcine condylar cartilage a biomechanical test method was developed. A series of indentation tests using different loads, followed by finite element analysis of the data were performed on native and GAG depleted porcine condylar cartilage; to identify a suitable load for detection of a significant difference in the deformation, equilibrium elastic modulus and permeability between the native and GAG depleted porcine condylar cartilages. A load of 0.31 N was identified as the most appropriate.

GAG depleted porcine condylar cartilage was injected with P₁₁-4 and P₁₁-8 alone, P₁₁-4 and P₁₁-8 : GAG mixtures at a molar ratio of 1:64 and chondroitin sulfate alone. The average percentage deformation of the medial condylar cartilage samples injected with P₁₁-4 alone and P₁₁-4: GAG mixture was 15.5 % and 8.7 % and for P₁₁-8 alone and P₁₁-8: GAG mixture was 11.4 % and 9.1 % respectively; compared to 6.3 % for the native cartilage and 12.6 % for the GAG depleted cartilage. The average equilibrium elastic modulus of the medial cartilage samples injected with P₁₁-4 alone and P₁₁-4: GAG mixture was 0.16 MPa and 0.43 MPa and for P₁₁-8 alone and P₁₁-8: GAG, 0.23 MPa and 0.35 MPa, respectively; compared to 0.49 MPa for the native cartilage and 0.21 MPa for the GAG depleted cartilage. Statistical analysis (ANOVA) showed that a mixture of P₁₁-4: GAG, but not P₁₁-8: GAG restored both the percentage deformation and equilibrium elastic modulus of the GAG depleted cartilage to levels that were not significantly different to the native cartilage.

This study has shown that the use of P₁₁-4 in combination with chondroitin sulfate has future potential for development as a minimally invasive treatment for early stage osteoarthritis.

Table of Contents

Acknowledgements.....	iii
Abstract.....	iv
Table of Contents.....	vi
List of Figures.....	xi
List of Tables.....	xvi
List of Abbreviations	xviii
Chapter 1 Literature Review and Research Goals	1
1.1 Introduction.....	1
1.2 The Anatomy of Hyaline Articular Cartilage	2
1.2.1 Composition and Structure of Cartilage.....	2
1.2.2 Microstructure of Cartilage	2
1.2.3 Macrostructure of Cartilage	7
1.2.4 Function of Cartilage.....	8
1.2.5 Lubrication Mechanisms of Cartilage	11
1.2.6 Wear of articular cartilage.....	14
1.3 Osteoarthritis.....	16
1.3.1 Introduction.....	16
1.3.2 Pathophysiology of Osteoarthritis.....	16
1.3.3 Relevance of OA Models.....	18
1.3.4 Structural and histological signs of OA	21
1.3.5 Biochemical and biomechanical changes of OA cartilage.....	23
1.4 Cartilage Treatments and Research	30
1.4.1 Early Intervention for Cartilage Defects.....	30
1.4.2 Surgical Procedures for Cartilage Repair.....	31
1.4.3 In Vitro Tissue Engineering of Cartilage	39
1.5 Introduction to Peptides	50
1.6 Introduction into self-assembling peptides (SAPs)	51
1.6.1 Self-assembly mechanism	51
1.6.2 Uses of self-assembling peptides in tissue engineering.....	53
1.7 Rationale.....	56
1.8 Aim and Objectives.....	57
1.8.1 Objectives	57
Chapter 2 Materials and Methods	58
2.1 Materials.....	58

2.1.1	Equipment	58
2.1.2	Chemicals.....	59
2.1.3	Peptides.....	60
2.1.4	Glycosaminoglycan (GAG; chondroitin sulfate)	61
2.1.5	Software	61
2.2	Methods.....	61
2.2.1	General Methods.....	61
2.2.2	Cartilage Tissue acquisition	63
2.2.3	Histological techniques.....	67
2.2.4	Histological staining methods.....	69
2.2.5	Biochemical Methods	70
2.2.6	Biomechanical Methods.....	71
2.2.7	Statistical analysis.....	79
Chapter 3 The effect of GAG molar ratio and Na⁺ ion concentration in two different salt solutions on the biochemical, morphological and biomechanical properties of peptides: P₁₁-4, P₁₁-8 and P₁₁-12.....		80
3.1	Introduction.....	80
3.2	Aims and objectives.....	82
3.3	Methods.....	82
3.3.1	Dissolution of peptides, peptide: GAG mixtures and Na ⁺ salt solutions.....	82
3.3.2	Measurement and adjustment of pH	84
3.3.3	Fourier Transform Infra-Red Spectroscopy (FTIR).....	84
3.3.4	Transmission Electron Microscopy (TEM)	88
3.3.5	Rheology.....	90
3.3.6	Statistical analysis.....	95
3.4	Results.....	96
3.4.1	Self-assembly of peptides and peptide-GAG mixtures at varying molar ratios in the presence of two different physiological Na ⁺ salt solutions with varying Na ⁺ ion concentrations.....	96
3.4.2	Morphology of peptides and peptide-GAG mixtures at varying molar ratios in the presence of two different physiological Na ⁺ salt solutions with varying Na ⁺ ion concentrations.....	98
3.4.3	Determination of elastic and viscous shear moduli of peptides and peptide-GAG mixtures at varying molar ratios in the presence of two different physiological Na ⁺ salt solutions with varying Na ⁺ ion concentrations using Rheology.....	107

3.4.4	Summary of the effect of GAG molar ratio and Na ⁺ salt solution on the elastic shear modulus (G') of the peptide and PEP: GAG mixtures.....	117
3.5	Discussion	117
Chapter 4 Development of GAG depleted cartilage models		126
4.1	Introduction.....	126
4.2	Aims and objectives.....	126
4.2.1	Objectives.....	126
4.3	Experimental Methods.....	127
4.3.1	Acquisition of porcine femoral condyles.....	127
4.3.2	Treatment of porcine femoral cartilage with chondroitinase ABC.	127
4.3.3	SDS and PBS washes of porcine condylar cartilage – Model 3.....	130
4.3.4	Histological Characterisation.....	131
4.3.5	GAG Quantification.....	132
4.3.6	SDS Quantification in GAG depleted cartilage (Model 3)	132
4.4	Results.....	133
4.4.1	Evaluation of native and GAG depleted porcine femoral condyles	133
4.4.2	GAG quantification of native and GAG depleted porcine femoral cartilage.....	144
4.5	Discussion	146
4.6	Conclusion	148
Chapter 5 Development of methods for the determination of the biomechanical properties of native and GAG depleted cartilage.....		149
5.1	Introduction.....	149
5.2	Aims and objectives.....	151
5.2.1	Objectives.....	151
5.3	Experimental methods.....	151
5.3.1	Acquisition of porcine femoral condyles.....	151
5.3.2	GAG depletion of porcine femoral condylar cartilage.....	151
5.3.3	Biomechanical characterisation of porcine femoral cartilage.....	151
5.4	Results.....	153
5.4.1	Cartilage thickness measurements.....	153
5.4.2	Percentage deformation	154
5.4.3	Equilibrium elastic modulus and permeability	158
5.5	Discussion	161
5.6	Conclusion	165

Chapter 6 Investigation of the effects of injection of peptide-GAG mixtures to GAG depleted cartilage.....	167
6.1 Introduction.....	167
6.2 Aims and objectives.....	168
6.2.1 Objectives.....	168
6.3 Experimental Design.....	168
6.4 Experimental Methods.....	169
6.4.1 Acquisition of porcine femoral condyles.....	169
6.4.2 GAG depletion of porcine femoral condylar cartilage.....	169
6.4.3 Preparation of peptides, peptide: GAG mixtures and chondroitin sulfate GAG control.	169
6.4.4 Injection of peptides, PEP: GAG mixtures and chondroitin sulfate (GAG) into GAG depleted porcine condylar cartilage.....	171
6.4.5 Biomechanical characterisation of porcine femoral condylar cartilage.....	172
6.4.6 Determination of self-assembly of peptides and PEP: GAG mixtures <i>in situ</i> in GAG depleted porcine condylar cartilage.....	173
6.5 Results.....	175
6.5.1 Preliminary study to determine the effects of injecting water and just a needle (without water) on the deformation properties of native condylar cartilage.....	175
6.5.2 The effects of injecting P ₁₁ -4 and P ₁₁ -8 alone and in combination with GAG, at a molar ratio of 1:64 on the deformation properties of GAG depleted porcine condylar cartilage.	181
6.5.3 Equilibrium elastic modulus and permeability	189
6.5.4 Summary of the effects of injecting GAG-depleted porcine medial condylar cartilage with peptides and PEP: GAG mixtures on the percentage deformation, elastic modulus and permeability values for all groups tested.....	192
6.5.5 Fluorescence recovery after photobleaching (FRAP) analysis to determine self-assembly of injected fluorescein-doped P ₁₁ -4 and P ₁₁ -8 and fluorescein-doped PEP: GAG mixtures in GAG depleted condylar cartilage.....	192
6.6 Discussion.....	201
6.7 Conclusion	207
Chapter 7 Conclusions and Future Studies.....	208
7.1 Major conclusions.....	208
7.2 Future studies	211
7.2.1 Histological and GAG quantification of PEP: GAG treated cartilage.	211

7.2.2	Testing of mild and moderate GAG depleted porcine cartilage models.....	211
7.2.3	Testing of higher GAG molar ratio of PEP: GAG mixtures – 1:16.....	211
7.2.4	Development of friction test to study the bio-tribological properties of the PEP: GAG mixtures.....	212
7.2.5	Use of natural whole joint GAG depleted models in knee simulator to investigate the effects of PEP: GAG mixtures on function.....	212
7.2.6	Leakage study to the asses the stability of the PEP: GAG gel over a prolonged time period.....	213
7.3	Potential for Clinical Translation	213
7.3.1	Arthroscopic delivery system.....	214
7.3.2	Pre-clinical studies in animal models of osteoarthritis.....	214
7.4	Significance of the study	214
	References.....	215

List of Figures

Figure 1: Collagen triple helix with arrangement of amino acids within each procollagen alpha chain	3
Figure 2: The intracellular and extracellular events in the formation of a collagen fibril.....	4
Figure 3: (Left) Schematic of ECM of articular cartilage (Barnes Baili, 2011), (Right) Proteoglycan aggrecan monomer molecule. Adapted from:	5
Figure 4: Stratified structure of cartilage demonstrating zonal arrangement. Adapted from:	8
Figure 5: Stress-strain curve for articular cartilage under uniaxial constant strain rate loading	9
Figure 6: Friction coefficient plotted as a function of fluid viscosity and shear velocity divided by the load (Stribeck Curve) with the corresponding film thickness for boundary, mixed and hydrodynamic lubrication mechanisms	12
Figure 7: Histological images of healthy and osteoarthritic cartilage.....	21
Figure 8: Severe OA, Safranin O/fast green staining. (A) Human, (B) and (C) rabbit.	22
Figure 9: Involvement of synovium in OA pathophysiology.....	23
Figure 10: The role of mechanical loading in osteoarthritis.....	28
Figure 11: Autologous chondrocyte implantation procedure using tibial periosteum for cartilage repair	34
Figure 12: Diagrammatic representation of the collagen I/III membrane showing rough and smooth side.....	36
Figure 13: Chondrocyte-Seeded Type I/III collagen membrane for autologous chondrocyte transplantation.....	37
Figure 14: Complications after ACI (diagnosed by clinical exam, MRI, and arthroscopy). Adapted from:.....	38
Figure 15: Hyalograft-C scaffold displayed as a commercialised product (left), MTT assay showing the encapsulated chondrocytes in an injectable chitosan-based hydrogel for cartilage tissue engineering	43
Figure 16: The three-dimensional poly(lactic-glycolic acid) (3D-PLGA) scaffold.....	47
Figure 17: Hierarchical self-assembly of chiral rod like units.	53
Figure 18: Schematic of self-assembly curve for both nucleated self-assembly & non-nucleated self-assembly of peptides.....	53
Figure 19: One subunit of Chondroitin-6-sulfate.....	62
Figure 20: Dissection equipment.....	64
Figure 21: Dissection of porcine knee joints.	65
Figure 22: Extraction of osteochondral pins.	66
Figure 23: Extraction of Medial and Lateral condyles.....	67
Figure 24: Orientation of cartilage tissue for histology.	68
Figure 25: Indentation apparatus.....	72
Figure 26: Cross-sectional view of the cup holder, showing how the condyle was orientated inside the cup holder and outlining rough distances and heights of relative components.....	72
Figure 27: Medial Porcine condylar cartilage cemented in PMMA.....	74
Figure 28: LVDT calibration.	74
Figure 29: Load cell calibration.	75
Figure 30: Picture of Instron testing equipment.	75
Figure 31: Needle indentation graph interpretation.	76
Figure 32: Finite element model of cartilage.	77
Figure 33: Experimental and modelled cartilage displacement curves.....	78

Figure 34: Equilibrium elastic modulus and permeability of healthy native medial condylar cartilage under a load of 0.31 N (Blue – Healthy condylar cartilage with the ‘no fluid flow’ boundary condition; Red – Healthy condylar cartilage with the ‘fluid flow’ boundary condition).....	78
Figure 35: TEM images of P ₁₁ -8 fibrils, illustrating how the fibril lengths, widths (long and short) and twist pitch was calculated.	89
Figure 36: Schematic of a rotational rheometer.	90
Figure 37: Example of phase angle and its relationship to viscous and elastic materials.	91
Figure 38: Loss, complex and elastic modulus.....	91
Figure 39: Graph demonstrating the Linear Viscoelastic Region.	92
Figure 40: General material behaviour in terms of storage and viscous modulus and phase angle.	92
Figure 41: Example amplitude sweep run at 1Hz and 20Hz showing both the elastic and viscous shear modulus.....	95
Figure 42: Fitted IR amide I' band of P ₁₁ -4, P ₁₁ -8 and P ₁₁ -12 at 10 mg.ml ⁻¹ in the presence of 130 mM (A, C and E) and 230 mM (B, D and F) Na ⁺ salt solution with and without varying chondroitin sulfate molar ratios of 1:16 and 1:64.	97
Figure 43: Morphology of the P ₁₁ -4 peptide in the presence of two Na ⁺ salt solutions at varying chondroitin sulfate molar ratios (1:16 and 1:64) by TEM.	98
Figure 44: Morphology of the P ₁₁ -8 peptide in the presence of two Na ⁺ salt solutions at varying chondroitin sulfate molar ratios (1:16 and 1:64) by TEM.	99
Figure 45: Morphology of the P ₁₁ -12 peptide in the presence of two Na ⁺ salt solutions at varying chondroitin sulfate molar ratios (1:16 and 1:64) by TEM.	99
Figure 46: Images of (a) P ₁₁ -4, P ₁₁ -8 and P ₁₁ -12 in the 130 mM Na ⁺ salt solution at pH 7.4 (b) P ₁₁ -4, P ₁₁ -8 and P ₁₁ -12 in the 230 mM Na ⁺ salt solution at pH 7.4.	100
Figure 47: Widths of fibrils of all peptides in two different Na ⁺ salt solutions at pH 7.4 at varying molar ratios of GAG.	106
Figure 48: Lengths of fibrils of all peptides in two different Na ⁺ salt solutions at pH 7.4 at varying molar ratios of GAG.....	106
Figure 49: P ₁₁ -4, P ₁₁ -8 and P ₁₁ -12 self-supporting gels at 10 mg.ml ⁻¹ in 130 mM and 230 mM Na ⁺ salt solutions.	107
Figure 50: The amplitude sweeps (elastic and viscous modulus vs. shear strain) of P ₁₁ -4, P ₁₁ -8 and P ₁₁ -12 at 10 mg.ml ⁻¹ in 130 mM and 230 mM Na ⁺ salt solutions.	108
Figure 51: The effect of varying the Na ⁺ ion concentration (130 mM or 230 mM) on the mechanical stiffness of the P ₁₁ -4, P ₁₁ -8 and P ₁₁ -12 gels, Strain 0.1 % and temperature 37°C	109
Figure 52: P ₁₁ -4, P ₁₁ -8 and P ₁₁ -12 self-supporting gels at 10 mg.ml ⁻¹ at two different GAG molar ratios (1:64 & 1:16) in 130 mM and 230 mM Na ⁺ salt solutions.....	111
Figure 53: The amplitude sweeps (elastic and viscous modulus vs. shear strain) of P ₁₁ -4, P ₁₁ -8 and P ₁₁ -12: GAG mixtures at 10 mg.ml ⁻¹ in 130 mM and 230 mM Na ⁺ salt solutions.	113
Figure 54: The effect of varying the Na ⁺ ion concentration (130 mM or 230 mM) and GAG molar ratio (1:16 and 1:64) on the mechanical stiffness of the P ₁₁ -4, P ₁₁ -8 and P ₁₁ -12: GAG mixtures.....	114
Figure 55: Varying concentrations of chondroitin sulfate (4.85 mg.ml ⁻¹ and 22.1 mg.ml ⁻¹) in 130 mM & 230 mM Na ⁺ salt solutions.	115
Figure 56: Amplitude sweep: Elastic and viscous modulus vs. shear strain of chondroitin sulfate in both the 130 mM and 230 mM Na ⁺ salt solutions at concentrations of 4.85 and 22.1 mg.ml ⁻¹	116

Figure 57: Frequency sweep: Elastic and viscous modulus vs. frequency of chondroitin sulfate in both the 130 mM and 230 mM Na ⁺ salt solutions at a concentration of 4.85 and 22.1 mg.ml ⁻¹	116
Figure 58: Self-assembly behaviour of P ₁₁ -4, P ₁₁ -8 and P ₁₁ -12 in 130 mM Na ⁺ salt solution with no other salts.....	119
Figure 59: Amino acid residues: a) Glutamine residue b) Serine residue.....	120
Figure 60: Sterile condyles showing the area of interest marked out in permanent marker, Case ABC gel was applied to this area to allow the depletion of GAGs....	129
Figure 61: Porcine femoral condyle showing the area of interest marked out in permanent marker.....	130
Figure 62: Safranin O stained sections of GAG depleted porcine condylar cartilage treated with an agarose gel containing CaseABC and antibiotic/aprotinin solution (model 1) and a porcine condylar cartilage treated with an agarose gel containing only antibiotic/aprotinin solution (control).....	135
Figure 63: GAG content of cartilage from GAG depleted porcine condylar cartilage in model 1 compared to the control sample and untreated native porcine condylar cartilage.	136
Figure 64: Safranin O stained sections of GAG depleted porcine condylar cartilage treated with injections of CaseABC containing antibiotic/aprotinin solution (model 2) and porcine condylar cartilage treated with injections of antibiotic/aprotinin solution alone (control).....	138
Figure 65: GAG content of cartilage from GAG depleted porcine condylar cartilage in models 2 compared to the control sample and untreated native porcine condylar cartilage.	139
Figure 66: Safranin O stained sections of GAG depleted porcine condylar cartilage and untreated native porcine condylar cartilage control from model 3.	141
Figure 67: Safranin O stained sections of GAG depleted porcine condylar cartilage and untreated native porcine condylar cartilage control from model 3.	142
Figure 68: GAG content of cartilage from GAG depleted porcine cartilage in model 3.	143
Figure 69: SDS concentration (ug.ml ⁻¹) after given SDS and PBS washes in model 3, method 4.....	143
Figure 70: GAG content of cartilage from GAG depleted porcine cartilage in Models 1 - 3 vs. native porcine cartilage.	145
Figure 71: Low Load (0.11 N) - Cartilage thickness measurement for native and GAG depleted cartilage (n=5).	153
Figure 72: Medium Load (0.31 N) - Cartilage thickness measurement for native and GAG depleted cartilage (n=6).....	153
Figure 73: High Load (0.51 N) - Cartilage thickness measurement for native and GAG depleted cartilage (n=3).	153
Figure 74: Percentage deformation of native and GAG depleted cartilage over the duration of 1 hour with a load of 0.11 N: (A) Medial condyle (B) Lateral condyle.	154
Figure 75: Final percentage deformation of native and GAG depleted cartilage at 1 hour with a load of 0.11 N.	154
Figure 76: Percentage deformation of native and GAG depleted cartilage over the duration of 1 hour with a load of 0.31 N: (A) Medial condyle (B) Lateral condyle.	155
Figure 77: Final percentage deformation of native and GAG depleted cartilage at 1 hour with a load of 0.31 N.	156

Figure 78: Percentage deformation of native and GAG depleted cartilage over the duration of 1 hour with a load of 0.51 N: (A) Medial condyle (B) Lateral condyle.	157
Figure 79: Final percentage deformation of native and GAG depleted cartilage at 1 hour with a load of 0.51 N.	157
Figure 80: Representative graphs of indentation characteristics obtained experimentally and through FEA model curve fitting of a medial porcine condyle under a load of 0.31 N.	159
Figure 81: Equilibrium elastic modulus and permeability of native and GAG depleted medial condylar cartilage under a load of 0.11 N.	159
Figure 82: Equilibrium elastic modulus and permeability of native and GAG depleted medial condylar cartilage under a load of 0.31 N.	160
Figure 83: Equilibrium elastic modulus and permeability of native and GAG depleted medial condylar cartilage under a load of 0.51 N.	160
Figure 84: Hydrated monomeric peptide being drawn up into a 1 ml syringe, ready for injection into the GAG depleted porcine condylar cartilage.	171
Figure 85: Schematic showing (A) the identification of the flattest region of interest (ROI) of the GAG depleted porcine condylar cartilage.	172
Figure 86: Diffusion profiles for the intensity of fluorescein over a period of time	174
Figure 87: Cartilage thickness measurement of the medial condyles for the: native, native water injected and native injected only groups (n=3 for all groups).	175
Figure 88: Cartilage thickness measurement of the lateral condyles for the: native, native water injected and native injected only groups (n=3 for all groups).	176
Figure 89: Percentage deformation of medial condyles from: native, native water injected and native injected only groups, over the duration of 1 hour with a load of 0.31 N.	177
Figure 90: Percentage deformation of lateral condyles from: native, native water injected and native injected only groups, over the duration of 1 hour with a load of 0.31 N.	178
Figure 91: Final percentage deformation at 1 hour of: native, native water injected and native injected only groups, for the medial and lateral condyles, with a load of 0.31 N.	179
Figure 92: Cartilage thickness measurement of the medial condyles for the: native, GAG depleted chondroitin sulfate (CS) injected only, GAG depleted, P ₁₁ -4: GAG injected, P ₁₁ -4 only injected, P ₁₁ -8: GAG injected and P ₁₁ -8 only injected groups (n=3 for all groups).	181
Figure 93: Cartilage thickness measurement of the lateral condyles for the: native, GAG depleted chondroitin sulfate (CS) injected only, GAG depleted, P ₁₁ -4: GAG injected, P ₁₁ -4 only injected, P ₁₁ -8: GAG injected and P ₁₁ -8 only injected groups (n=3 for all groups).	182
Figure 94: Percentage deformation of medial condyles from: native, GAG depleted chondroitin sulfate (CS) injected only, GAG depleted, P ₁₁ -4: GAG injected, P ₁₁ -4 only injected, P ₁₁ -8: GAG injected, P ₁₁ -8 only injected groups, over the duration of 1 hour with a load of 0.31 N.	183
Figure 95: Percentage deformation of lateral condyles from: native, GAG depleted chondroitin sulfate (CS) injected only, GAG depleted, P ₁₁ -4: GAG injected, P ₁₁ -4 only injected, P ₁₁ -8: GAG injected, P ₁₁ -8 only injected groups, over the duration of 1 hour with a load of 0.31 N.	184
Figure 96: Final percentage deformation at 1 hour of all groups: native, GAG depleted chondroitin sulfate (CS) injected only, GAG depleted, P ₁₁ -4: GAG injected, P ₁₁ -4 only injected, P ₁₁ -8: GAG injected, P ₁₁ -8 only injected, for the medial and lateral condyles, with a load of 0.31 N.	185

Figure 97: Final percentage deformation at 1 hour of medial condyles from: native, GAG depleted, GAG depleted chondroitin sulfate (CS) injected only, P ₁₁ -4: GAG injected, P ₁₁ -4 only injected, P ₁₁ -8: GAG injected, P ₁₁ -8 only injected, with a load of 0.31 N.	186
Figure 98: Final percentage deformation at 1 hour of lateral condyles from: native, GAG depleted, GAG depleted chondroitin sulfate (CS) injected only, P ₁₁ -4: GAG injected, P ₁₁ -4 only injected, P ₁₁ -8: GAG injected, P ₁₁ -8 only injected, with a load of 0.31 N.	187
Figure 99: Representative graphs of indentation characteristics obtained experimentally and through FEA model curve fitting of a medial porcine condyle under a load of 0.31 N.	190
Figure 100: Elastic modulus and permeability of GAG depleted porcine medial condylar cartilage injected with P ₁₁ -4: GAG, P ₁₁ -4 only, P ₁₁ -8: GAG, P ₁₁ -8 only and their corresponding native and GAG depleted condylar cartilage controls, under a load of 0.31 N.	191
Figure 101: Representative FRAP images of GAG depleted porcine condylar cartilage injected with fluorescein-tagged peptide-doped P ₁₁ -4: GAG.	194
Figure 102: Representative FRAP images of porcine GAG depleted condylar cartilage injected with fluorescein-tagged peptide-doped P ₁₁ -4 alone.	195
Figure 103: Representative FRAP images of porcine GAG depleted condylar cartilage injected with fluorescein-tagged peptide-doped P ₁₁ -8: GAG.	197
Figure 104: Representative FRAP images of porcine GAG depleted condylar cartilage injected with fluorescein-tagged peptide-doped P ₁₁ -8 only.	198
Figure 105: Representative FRAP images of porcine GAG depleted condylar cartilage injected with fluorescein-tagged chondroitin sulfate (CS).	199
Figure 106: Representative images of native porcine condylar cartilage viewed under a fluorescein filter and transmitted light.	200
Figure 107: Representative images of porcine GAG depleted condylar cartilage viewed under a fluorescein filter and transmitted light.	201

List of Tables

Table 1: Different descriptions of the Kellgren and Lawrence (K&L) criteria of knee osteoarthritis (OA) adapted from Schiphof <i>et al</i> (Schiphof et al., 2008) and Arden <i>et al</i> (Arden and Nevitt, 2006).	20
Table 2: Clinical, histological and molecular signs of synovitis in OA.	25
Table 3: The different cell sources that have been investigated for use in tissue engineering cartilage, along with the respective reasons for selecting them and their limitations for use.....	40
Table 4: Current clinical products on the market with their associated clinical trials that have been completed or are in the process of completion. Adapted from: (Huang et al., 2016).....	44
Table 5: Equipment used throughout the study.....	58
Table 6: Chemicals and reagents used throughout the study.	59
Table 7: Peptide primary structures, and their net charges at pH 7.4. Positively charged residues are coloured blue, negatively charged residues are red. All peptides were amidated and acetylated.....	60
Table 8: Masses (mg) of peptide and chondroitin sulfate (GAG) weighed out for the different molar ratios. Samples were made up to a total volume of 1 ml in two aqueous Na ⁺ salt solutions, unless otherwise stated.....	63
Table 9: Dissection equipment used throughout the study.	64
Table 10: Concentrations of different salts present in the two physiological salt solutions.....	83
Table 11: Characteristic infrared bands of the peptide (Susi, 1972).	84
Table 12: Secondary structural assignments of amide I' infrared bands.....	86
Table 13: Amino acid side chain absorptions in the amide I' region for the P ₁₁ peptides studied by FTIR spectroscopy.	87
Table 14: Masses of peptide and CS weighed out for the different molar ratios. Samples were made up to a total volume of 4ml in two aqueous Na ⁺ salt solutions.....	93
Table 15: Average widths and twist pitch of the P ₁₁ -4 fibrils in different Na ⁺ salt solutions and GAG molar ratios.	101
Table 16: Average lengths of the P ₁₁ -4 fibrils in different Na ⁺ salt solutions and GAG molar ratios.	101
Table 17: Average widths and twist pitch of the P ₁₁ -8 fibrils in different Na ⁺ salt solutions and GAG molar ratios.	102
Table 18: Average lengths of the P ₁₁ -8 fibrils in different Na ⁺ salt solutions and GAG molar ratios.	102
Table 19: Average widths and twist pitch of the P ₁₁ -12 fibrils in different Na ⁺ salt solutions and GAG molar ratios.	103
Table 20: Average lengths of the P ₁₁ -12 fibrils in different Na ⁺ salt solutions and GAG molar ratios.	103
Table 21: Two-way analysis of variance to determine the effect of GAG molar ratio and Na ⁺ ion concentration had on the length of the P ₁₁ - 4 fibrils.....	104
Table 22: Two-way analysis of variance to determine the effect of GAG molar ratio and Na ⁺ ion concentration had on the length of the P ₁₁ - 8 fibrils.....	104
Table 23: Two-way analysis of variance to determine the effect of GAG molar ratio and Na ⁺ ion concentration had on the length of the P ₁₁ - 12 fibrils.....	104
Table 24: Two-way analysis of variance to determine the effect of GAG molar ratio and Na ⁺ ion concentration had on the width of the P ₁₁ - 4 fibrils.....	105

Table 25: Two-way analysis of variance to determine the effect of GAG molar ratio and Na⁺ ion concentration had on the width of the P₁₁- 8 fibrils.....	105
Table 26: Two-way analysis of variance to determine the effect of GAG molar ratio and Na⁺ ion concentration had on the width of the P₁₁- 12 fibrils.....	105
Table 27: Summary table of the elastic shear modulus (G') of the peptides alone and the PEP: GAG mixtures at 1 Hz.	117
Table 28: Masses of peptide and chondroitin sulfate (GAG) weighed out for the different injection experiments.	170
Table 29: Summary table of the percentage deformation, elastic modulus and permeability and the difference between the GAG depleted medial porcine condylar cartilage sample injected with P₁₁-4: GAG, P₁₁-4 only, P₁₁-8: GAG and P₁₁-8 only and the native and GAG depleted medial porcine condylar cartilage.	192

List of Abbreviations

AC	Articular cartilage
ACI	Autologous chondrocyte implantation
ADAMTS	A disintegrin and metalloprotease with thrombospondin motifs
AFM	Atomic force microscopy
ANOVA	Analysis of variances
BMPs	Bone morphogenetic proteins
BSA	Bovine serum albumin
CACI	Collagen autologous chondrocyte implantation
CaCl₂	Calcium Chloride
CaF₂	Calcium flouride
CaseABC	Chondroitinase ABC
CL	Confidence level
CS	Chondroitin sulfate
D₂O	Deuterium oxide
DCELL	Decellularisation
DCI	Deuterium chloride
DMB	1,9-dimethylemethylen blue
ECM	Extracellular matrix
EDTA	Ethylenediaminetetraacetic acid
ER	Endoplasmic reticulum
FEA	Finite element analysis
FRAP	Fluorescence recovery after photobleaching
FTIR	Fourier transform infrared spectrometer
g	Grams
GAG	Glycosaminoglycan
GF	Growth factors
GLY	Glycine
HA	Hyaluronic Acid
HBSS	Hank's balanced salt solution
HCl	Hydrochloric acid
HYP	Hydroxyproline
ICRS	International cartilage repair system
IGF	Insulin growth factor
IKDC	International knee documentation committee
IL	Interleukin
IR	Infrared
KCl	Potassium chloride
KOOS	Knee injury and osteoarthritis outcome score
KS	Keratan sulfate
LVDT	Linear variable differential transformer
MACI	Matrix associated chondrocyte implantation
Mag	Magnification
ml	Millilitre
mm	Millimetres
mM	Millimolar
MMPs	Matrix metalloproteases
MOCART	Magnetic resonance observation of cartilage repair tissue
MPa	Megapascals
MR	Molar ratio

MRI	Magnetic resonance imaging
MSCs	Mesenchymal stem cells
N	Newtons
NaCl	Sodium Chloride
NaHCO₃	Sodium hydrocarbonate
NaOD	Sodium deuterioxide
NaOH	Sodium Hydroxide
Nm	Nanometres
NS	Not significant difference
NSAIDs	Non-steroidal anti-inflammatory drugs
OA	Osteoarthritis
Pa	Pascals
PACI	Periosteum autologous chondrocyte implantation
PBS	Phosphate Buffered Saline
PBT	Poly butyleneterephthalate
PCL	Poly-caprolactone
PCM	Pericellular matrix
PEG	Polyethylene glycol
PEOT	Poly ethylene oxide-terephthalate
PEP: GAG	Peptide-glycosaminoglycan
PG	Proteoglycan
PGA	Poly-glycolic acid
PGS	Poly glycerol-co-sebacate
PLA	Poly-lactic acid
PLGA	Poly lactic-glycolic acid
PMMA	Polymethylmethacrylate
POC	Poly octanedioil-co-citrate
PRO	Proline
RA	Rheumatoid arthritis
ROI	Region of interest
ROM	Range of motion
SA	Self-assembly
SAL	Surface amorphous layer
SAPL	Surface active phospholipids
SAPs	Self-assembling peptides
SDS	Sodium dodecyl sulfate
SS	Salt solution
ST	Stromelysin
SZP	Superficial zonal proteins
TEM	Transmission electron microscopy
TFA	Trifluoroacetic acid
TGF	Transforming growth factor
TJR	Total joint replacement
TNF	Tumour necrosis factor
UV	Ultra violet
μl	Microlitre
μM	Micromiliter
VAS	Visual analogue scale
VEGF	Vascular endothelial growth factor
WOMAC	Western ontario and McMaster universities osteoarthritis index

Chapter 1 Literature Review and Research Goals

1.1 Introduction

Healthy articular cartilage in the knee has unique properties, allowing it to withstand high compressive, shear and tensile forces that the human body exerts upon it during normal gait or other activities such as running or climbing stairs (Mouw et al., 2005). Articular cartilage is a special type of hyaline cartilage that provides a low friction and wear resistant tissue at the articulating surfaces of bone. This is facilitated by distributing the applied load over a greater surface area which leads to a smooth interaction between the two opposing surfaces (Buckwalter et al., 2005). Unfortunately, articular cartilage is frequently injured in incidences which usually involve sport or trauma from motorized accidents; however it may also degenerate with increasing age (Groh and Herrera, 2009). Due to its avascular nature, the damaged cartilage has a poor propensity to self-repair (Farquhar et al., 1996; Buckwalter et al., 2005).

Cartilage damage and degeneration significantly affects an individual's quality of life. Pain and dysfunction of normal movements are symptoms of cartilage damage, frequently seen in the aging population, which can be attributed to arthritis. Arthritis, defined simply means joint inflammation, however there are two main types of arthritis that affect individuals; osteoarthritis (OA) and rheumatoid arthritis (RA) (Jackson et al., 2001). Osteoarthritis is a degenerative joint disease caused by the degradation of articular cartilage in the joints and rheumatoid arthritis is a chronic inflammatory autoimmune disease with a genetic predisposition. Articular cartilage loss causes proximal bones to rub, leading to pain, discomfort, swelling and limitation in movement. It is estimated that 8.75 million people in the UK suffer from OA (Arthritis Research UK, 2013). Currently there are many ways in which these problems can be overcome and/or managed, however there are limitations to all approaches.

Research is currently focused on development of more advanced methods of cartilage repair, such as autologous chondrocyte implantation (ACI) or the use of biomaterials for tissue engineering of articular cartilage using scaffolds and/or hydrogels. A fundamental knowledge of healthy and degenerated cartilage tissue anatomy, physiology, biomechanical and tribological function is of utmost importance to comprehend cartilage disease and develop novel therapies, for the early intervention in OA.

1.2 The Anatomy of Hyaline Articular Cartilage

Hyaline articular cartilage is the most important structure in synovial joints (e.g. knee and hip joints). It protects the two articulating surfaces from abrasion by allowing smooth movement of the surfaces against each other whilst distributing load evenly (Buckwalter et al., 2005). Articular cartilage is a flexible and tough tissue consisting of chondrocytes (cartilage cells), which are distributed amongst an interlaced network of collagen fibrils and proteoglycans within the extracellular matrix (ECM) (Buckwalter et al., 2005). The work within this thesis is concerned with articular cartilage, therefore the words 'cartilage', 'cartilage tissue' etc. refers to articular cartilage (AC), unless otherwise stated.

1.2.1 Composition and Structure of Cartilage

The main component of cartilage is the ECM which accounts for 95% of the total cartilage dry weight; the remaining 5% is constituted by the cellular component of cartilage. The cellular component consists of chondrocytes, which are the functional element of the ECM (Anderson et al., 1964). The ECM of hyaline cartilage is 70% fluid (water), the remainder is made up of organic collagen molecules (15%), mainly type II collagen, 10% proteoglycans (aggrecan) and 5% glycoproteins (Poole et al., 1982).

The structure of AC can be divided into two hierarchical levels; the micro-scale and the macro-scale. These two scales of viewing the structure of cartilage are of great importance in determining the biomechanical properties of the tissue.

1.2.2 Microstructure of Cartilage

1.2.2.1 Collagen

1.2.2.1.1 Structure of Collagen

Collagen is the major ECM protein. It makes up ~15% of the cartilage ECM. In the body there are 19 types of collagen, however AC is predominantly composed of type II collagen; with smaller amounts of types V, VI, IX, X and XI (Athanasίου et al., 2009; Mow and Ateshian, 1997). All collagens are composed of 3 procollagen alpha chains, coiled around each other to form a triple helix configuration. These polypeptide chains contain approximately ~1000 amino acid residues. The constituent procollagen chains are numbered using Arabic numerals followed by the collagen type with roman numerals in parentheses. For example: Type I procollagen is made up of two pro- α -1 (I) and one pro- α -2 (I), therefore it is a heterotrimer (Cremer et al., 1998). Whereas type II procollagen is assembled of three pro- α -1 (II) chains and is therefore a homotrimer. The individual procollagen alpha chains are each

shaped into a left-handed helix and then all three of the chains coil together to form a right-handed triple helix (Steplewski et al., 2007). The amino acids in the collagen peptide chains are primarily glycine, proline, hydroxyproline, lysine and hydroxylysine. These amino acids are arranged in the following tripeptide sequence: Gly-X-Y, where glycine is repeated every third residue, X is most commonly a proline residue and Y is frequently a hydroxyproline or hydroxylysine residue. This repeat region is encompassed by short unorganised telometric regions (the globular amino terminal and carboxyl terminal), which are prone to proteolytic attack by procollagen peptidase/ procollagen aminoproteinase/ procollagen carboxyproteinase. The cleavage of these terminal peptides allows the spontaneous formation of collagen fibrils (Steplewski et al., 2007).

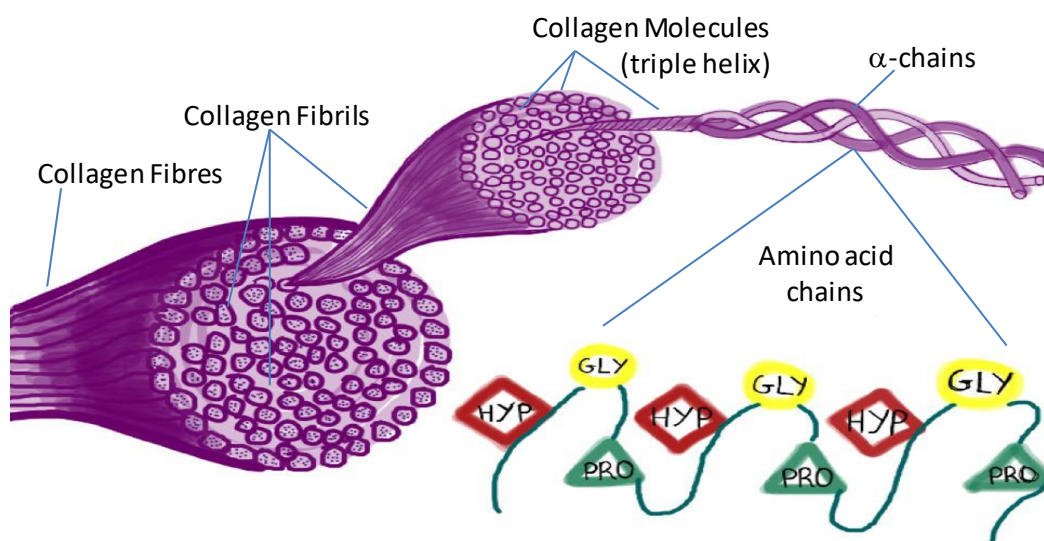


Figure 1: Collagen triple helix with arrangement of amino acids within each procollagen alpha chain. Adapted from: (The collagen molecule: Collagen structure, 2014).

1.2.2.1.2 Synthesis of Collagen

In cartilage, collagen synthesis occurs within chondrocytes. The individual helices gather in the lumen of the endoplasmic reticulum (ER) to form procollagen (Figure 2, (1)). Various proline and lysine amino acids are hydroxylated here and the addition of glucose and galactose to the hydroxylysine residues also occurs (Figure 2, (2,3)). The middle portion of the procollagen chain associates with other molecules to form the triple helix and the propeptide extensions prevent premature assembly of collagen within the ER (Figure 2, (4,5)). Exocytosis of procollagen from the plasma membrane via a secretory vesicle is followed by the cleavage of the globular amino (N-terminal) and carboxyl terminals (C-terminal) via selective proteolysis (Figure 2, (6,7)). The tropocollagen molecule formed then undergoes spontaneous assembly to form collagen fibrils and in turn fibres, which are stabilised by covalent cross-links (Figure 2, (8,9)) (Alberts et al., 2002).

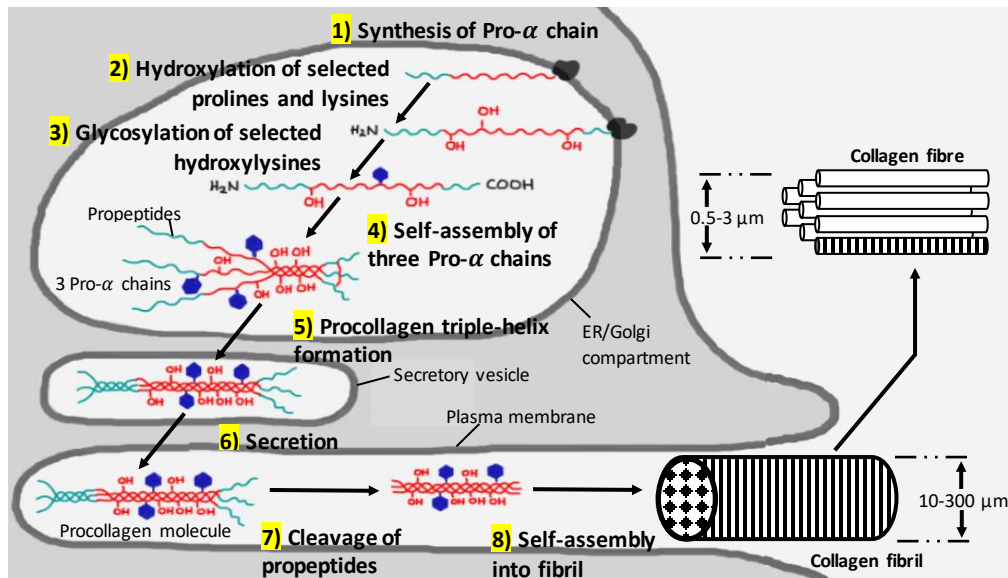


Figure 2: The intracellular and extracellular events in the formation of a collagen fibril. (A) Collagen fibrils assemble in the extracellular space contained within a folding of the plasma membrane. They further assemble to larger collagen fibres which are stabilised by covalent crosslinks. Adapted from: (Alberts et al., 1994).

1.2.2.1.3 Roles of different types of collagen

The most dominant form of collagen in the cartilage ECM is type II collagen (a homotrimer) which constitutes ~80-85% of the total collagen content. Collagen XI and IX (both heterotrimeric) are the second most common forms of collagen, consisting of ~3-10% each. Collagen IX is known to have a slight kink mid-chain where chondroitin sulfate glycosaminoglycans (GAGs) branches off (Steplewski et al., 2007). Collagen type XI is similar to type II, in that it is a straight chain molecule; however, it contains an α -chain at the amino terminal which projects out and forms a covalent cross link to the collagen type II molecule in the fibre backbone at the hydroxylysine residue. Collagen X is also a straight chain specific homotrimer. Although collagen X forms shorter chains than type II and XI, it forms multimeric collagen fibrils.

The specific roles of all the types of collagen are not fully understood, however it is thought that these minor collagens play a role in adjusting the structure of collagen type II (Guilak et al., 2000). Collagen type II makes up the backbone of heteropolymeric cartilaginous fibres of which type IX is thought to play a role in facilitating the interaction of fibrils with proteoglycans. Collagen type VI forms independent microfibrils in the ECM and it plays a role in chondrocyte attachment to the ECM (Cremer et al., 1998; Poole, 1997). Type X is thought to play a role in the organisation and distribution of the matrix components and is present in areas where hypertrophic chondrocytes are found (Cremer et al., 1998; Shen, 2005).

1.2.2.2 Proteoglycans & Glycosaminoglycans

The ECM contains three main types of glycosaminoglycans (GAGs): hyaluronan, chondroitin sulfate and keratan sulfate. A proteoglycan (PG) monomer consists of a core protein (aggrecan), to which numerous GAGs are attached. This proteoglycan monomer has associated chondroitin sulfate and keratan sulfate molecules through simple sugar bonds (Figure 3) (Hardingham and Muir, 1974). In AC, the most important proteoglycan monomer is aggrecan. Aggrecan consists of a protein core onto which GAG chains, made up of chondroitin sulfate and keratan sulfate, are covalently attached (Figure 3) (Mow and Ateshian, 1997). These aggrecan monomers bind, via a linker protein to a hyaluronan molecule, forming a proteoglycan aggregate (Figure 3). This macromolecular complex interacts with the surrounding collagen fibrils to form a fibre-reinforced, porous-permeable composite solid matrix (Poole, 1997), which is known as the solid phase (Figure 3). The most abundant GAG in AC is chondroitin sulfate, however there are other GAGs present in smaller quantities such as; heparin, heparan sulfate, dermatan sulfate and keratan sulfate. The functional properties of PGs are given to them by the individual GAG chains (Mow and Ateshian, 1997).

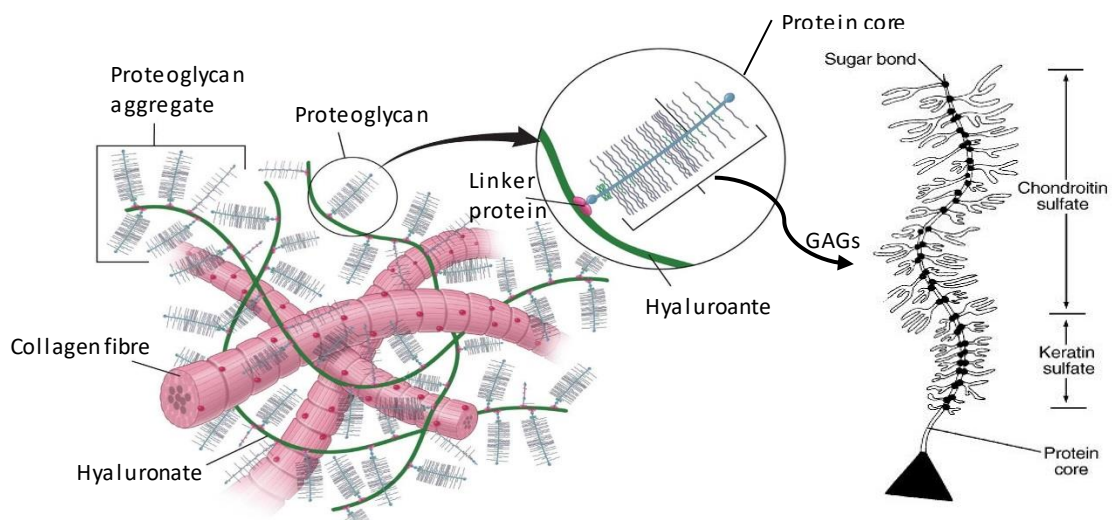


Figure 3: (Left) Schematic of ECM of articular cartilage (Barnes Baili, 2011), (Right) Proteoglycan aggrecan monomer molecule. Adapted from: (Brinker and Miller, 1999).

1.2.2.2.1 Roles of collagen and proteoglycan in articular cartilage

Both the collagen and PGs bind water in different ways, which is essential to the function of healthy cartilage (Mankin et al., 1999). In the solid phase, proteoglycan monomers (Figure 3) with GAGs rich in sulfate and carboxylate groups, are highly negatively charged in contact with water. A swelling pressure, resisted by the surrounding collagen network is created as a result of the repulsion force induced by the negatively charged molecules (Jaffe et al., 1974). The balance of these two forces determines the degree of cartilage hydration and any disruption of this balance will cause an increase in tissue hydration (Mankin, 1982).

The fluid phase of cartilage contributes to the healthy function of cartilage. It is this phase that influences the mechanical behaviour of cartilage when it is loaded. As the cartilage is loaded under compressive force, water is able to flow through the porous structure, which creates a frictional drag force on the matrix. The applied load causes the fluid to be extruded and this reduces the pore size and hence permeability of the ECM. Hence as the permeability of the ECM decreases, the drag force increases further (Maroudas et al., 1968). This mechanical mechanism provides cartilage with a protective feedback feature which enables the cartilage to stiffen by reducing the rate fluid flow through its matrix, when it experiences high and increasing loads (Mow et al., 1980). The combination of fluid and solid matrix properties provides AC with the viscoelastic, biomechanical and low friction properties for efficient load distribution.

However, in degenerative cartilage these properties become compromised. The increased water content (tissue hydration) attributed to degenerative cartilage seems surprising as there is also a loss of glycosaminoglycans, which are themselves highly hydrophilic. Maroudas et al., explained this paradox as a degeneration of the collagen network, which allows the fibrillated tissue to swell even more, in spite of the relatively low osmotic pressure created by the decreased GAG content. Therefore, the swelling seen in degenerate cartilage is not due to any changes in the state of water but to a breakdown in the collagen network.

The main disaccharide unit of GAGs in AC is chondroitin sulfate. It is formed by the linkage of D-glucuronic acid to N-acetylgalactosamine. These galactosamine residues can be sulfated either in positions 4 (C4S) or 6 (C6S); the sulfate groups alongside the carboxyl groups of glucuronic acid, are ionised, therefore giving rise to a global negative charge. In normal healthy cartilage, the concentration of C4S and C6S present in the synovial fluid has been shown to vary between 13.4- 23.4 nmol.ml⁻¹ and 64.3-141.9 nmol.ml⁻¹ respectively and the ratio of C6S:C4S has been shown to fluctuate between 4.3 to 6.9 (Nakayama et al., 2000; Nakayama et al., 2002). However, this ratio has been reported to decrease with increasing age and severity of the disease, most commonly OA, which is why this ratio has been suggested as a clinical marker for damage in articular cartilage in early OA (Sharif et al., 1996; Bayliss et al., 1999). Within the layers of cartilage, the proteoglycan composition changes with depth. The proteoglycans in the upper layers contain a lower amount of keratan sulfate and a higher amount of chondroitin sulfate (Zanetti et al., 1985). Recent studies using various biochemical characterisation techniques have confirmed that there is a topographical variation in the zonal distribution of chondroitin sulfate, and it is more predominantly found in the topmost layers of AC (Crockett et al., 2007; Bayliss et al., 1999).

1.2.3 Macrostructure of Cartilage

Cartilage can be subdivided into four main zones. This zonal structure varies from the surface of AC down to the subchondral bone; through which the cellular (chondrocytes) and structural components (collagen fibre orientation) of the ECM undergo some changes (Figure 4).

1.2.3.1 The Superficial Zone (tangential zone)

This is the articulating surface that provides low friction movement between the two opposing surfaces and resists shear. It consists of two layers; a sheet of very fine fibrils with few polysaccharides and no cells, which forms a clear film often referred to as the lamina splendens, also known as the surface amorphous layer (SAL). Underneath this are flattened ellipsoid-shaped chondrocytes, packed parallel to the articulating surface with collagen fibres also aligned parallel to the surface. They synthesise an ECM with high collagen content and a low proteoglycan concentration, relative to other zones (Buckwalter et al., 2005). Fibronectin and water concentration are also highest in this zone.

1.2.3.2 The Middle Zone (transitional zone)

This zone makes up for around 40-60% of the AC volume. It has a higher Young's modulus than the superficial zone, perpendicular to the AC surface. Chondrocytes in this zone are more rounded than in the superficial layer (Mow and Hung, 1989). They synthesise a matrix that has larger collagen fibrils (arranged loosely and horizontal to the articulating surface), higher proteoglycan content but a lower collagen and water content than seen in the superficial zone matrix (Buckwalter et al., 2005).

1.2.3.3 The Deep Zone (radial Zone)

This zone makes up 30% of the cartilage. Chondrocytes here are spheroidal in shape and arrange themselves parallel to the collagen fibrils and perpendicular to the joint line (Mow and Hung, 1989). This zone contains collagen fibrils with the largest diameter, the highest proteoglycan concentration and the lowest concentration of water (Buckwalter et al., 2005).

1.2.3.4 Calcified Cartilage Layer

The tide mark divides the deep zone from the underlying calcified cartilage, which rests directly on the subchondral bone (Mow and Hung, 1989). This transition reduces the stiffness gradient between the inflexible bone and the more flexible cartilage. The subchondral bone ultimately provides the anchorage for the cartilage tissue as a whole (Radin and Rose, 1986).

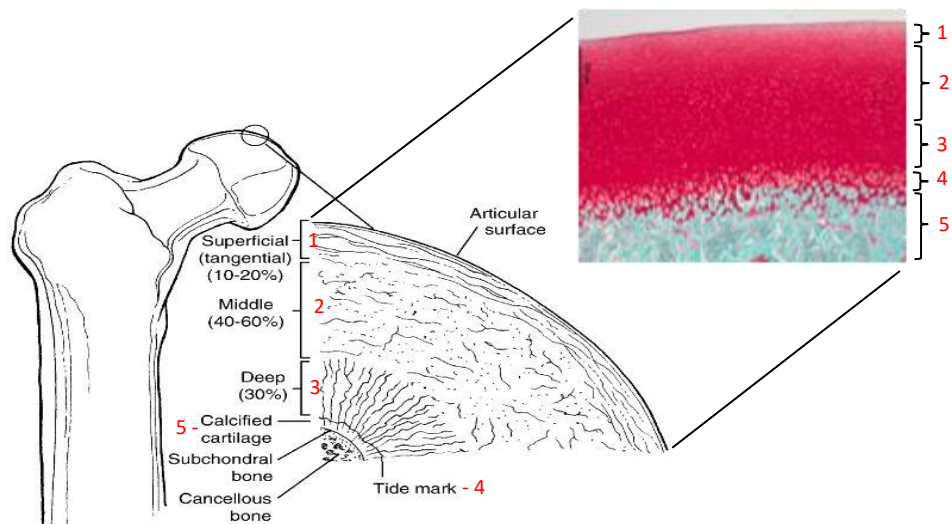


Figure 4: Stratified structure of cartilage demonstrating zonal arrangement. Adapted from: (Brinker and Miller, 1999).

1.2.4 Function of Cartilage

The function of cartilage is best understood when it is viewed as a biphasic structure. This specialist tissue is composed of a solid phase consisting of mostly type II collagen and proteoglycans and the fluid phase, which consists of water and ions. The solid phase has low permeability because of the high resistance to fluid flow, creating high interstitial fluid pressurization in the fluid phase. It is this pressure force that accounts for 90% of the 'load transmission' function of cartilage (Ateshian and Wang, 1997). The low permeability of the solid phase and the high pressurization of the fluid phase both work to establish the stiffness and viscoelastic properties that allow AC to perform its function (Felson et al., 2000).

1.2.4.1 Mechanical properties of articular cartilage

One of the roles of cartilage is to facilitate the load support and load transfer whilst allowing the rotation and translation between bones. The knee experiences a load of approximately 3.5 times body weight and considering the average person weighs about 70 kg, the force experienced in the knee is exceptionally high (Mow et al., 2000). Therefore, the mechanical as well as the biochemical characteristics of AC are proportional to how it performs within the joint. Changes in these characteristics could ultimately affect the loading pattern that the bone experiences and hence, lead to degradation and eventually the total loss of tissue. The ability of cartilage to deform under load plays a crucial role in its mechanical function (Hayes and Mockros, 1971; Mow et al., 1984). The mechanical properties of AC can be described as anisotropic (dependant on orientation), nonlinear (dependant on magnitude of strain) and inhomogeneous (variable within tissue); all of which are due to the changes in macroscopic and microscopic structure throughout its depth (Guilak et al., 2000). AC can best be described

as a viscoelastic material with a solid and fluid phase, in which the interaction of proteoglycans and the collagen network play a crucial role in displaying this behaviour.

When cartilage is put under uniaxial tension, the tissue exhibits non-linear stress-strain characteristics. *In vivo*, this tension is experienced when the cartilage is compressed and the surrounding regions are pulled towards the point of loading. As the cartilage is loaded in tension, the coiled collagen fibrils of the solid matrix begin to uncrimp, which contributes to the initial slope increase in the toe region (Figure 5). Following this initial straightening of the fibres, there is a constant increase in slope as the collagen fibres start to resist the applied tension which eventually leads to the failure of these fibres, as they are stretched to rupture. A study performed by Mow *et al.*, showed that collagen in cartilage exhibits anisotropic behaviour as the tensile modulus was considerably higher in samples that were aligned parallel to the collagen fibres compared to those that were perpendicular to the collagen fibres (Mow and Ateshian, 1997).

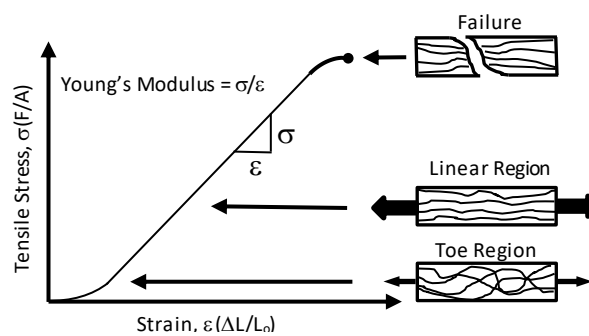


Figure 5: Stress-strain curve for articular cartilage under uniaxial constant strain rate loading.

The tensile Young's modulus of cartilage can be referred to as a measure of the strength of the solid collagenous matrix, which varies depending on the orientation and the depth of the cartilage tissue (Roth and Mow, 1980). Other parameters which also affect this parameter are type of joint, sample location, age, fibre density and diameter, strength of ionic bonds and amount of cross-linking within the cartilage tissue (Schmidt *et al.*, 1990). In healthy human AC, the tensile modulus has been shown to vary between 5 to 25 MPa, depending mostly on the latter conditions (Kempson *et al.*, 1968; Akizuki *et al.*, 1986). The viscoelastic behaviour of AC is also dependant on the interactions of the solid collagenous matrix and its proteoglycans network. Schmidt *et al.* reported that the removal of GAGs from AC affects the collagen fibre orientation, which consequently alters the rate of deformation (creep) of the cartilage samples (Schmidt *et al.*, 1990). Although, this study suggested that the collagen-proteoglycan interactions affect the rate of deformation in AC, it is the inherent stiffness of

the solid collagenous matrix that mainly contributes to the stress-strain behaviour of cartilage in tension (Guilak et al., 2000).

Wong *et al.*, proposed that the loss of tensile integrity in degenerative cartilage and in osteoarthritic cartilage was directly proportional to the amount of collagen degradation as well as the network remodelling (Temple-Wong et al., 2009). Studies by Silver *et al.*, suggested that the elastic modulus (calculated from stress-strain curves) for human AC was influenced by the collagen fibril length and its structure. It was found to be higher in healthy cartilage compared to OA cartilage. They suggested that this increase was due to the presence of PGs within the collagen. However, from the results it was not clear whether the decrease in the elastic modulus in OA cartilage is as a result of the degradation of the collagen network; the loss of PG content; synthesis of catabolic enzymes or a combination of the latter (Silver et al., 2001a; Silver et al., 2004). Nevertheless, the 3D organisation of collagen fibres is known to vary throughout the depth of AC and the orientation of these fibres aids in giving cartilage its unique mechanical properties.

Articular cartilage also exhibits compressive properties that are mainly dependant on the water content and its interaction with the proteoglycan network. The compressive modulus of cartilage ranges from 0.08 to 2 MPa and like the tensile modulus, the compressive modulus can vary depending on location on the joint, age, type of joint and pathology (Schinagl et al., 1997; Athanasiou et al., 1994). Compression of cartilage is governed by the highly charged sulfate and carboxyl groups on the proteoglycans, causing repulsion between them and owing to the expansion in the proteoglycan network. However, this swelling is restricted by the electrostatic forces between the collagen and proteoglycan network. These charged groups have a high affinity for water molecules which restrict the free movement of interstitial fluid through the interconnected pore structure of the solid matrix, setting up a frictional drag coefficient. As a result of these interactions, a Donnan osmotic pressure is created within the cartilage tissue network, which is the major contributor to the compressive stiffness of AC (Ateshian et al., 2003). Interstitial fluid pressures are significantly higher under compression, hence their importance in the load support in the joint. The frictional drag created by the flow of interstitial water through the porous permeable matrix acts as a dissipative mechanism for AC. As this fluid is dispersed through the tissue, the fluid pressure decreases over time and more of the load is supported by the solid matrix, giving rise to the creep and stress-relaxation behaviours in cartilage (Mow et al., 1984; Park et al., 2003; Lai et al., 1981; Mow et al., 1980). In conclusion, the creep and stress-relaxation

behaviour of AC is mainly explained by this biphasic behaviour, as the stresses are dispersed between the solid and fluid phases of cartilage.

1.2.5 Lubrication Mechanisms of Cartilage

Synovial fluid contributes to the low friction articulation within the human joints. Water is the main fluid constituent in AC, as well as the synovial fluid. The synovial fluid contains many inorganic salts, such as calcium, chloride, potassium and sodium as well as other components such as hyaluronic acid and proteins. This interstitial fluid also plays an important role in the transport of nutrients for the chondrocytes and the removal of waste from the tissue. The following section will cover the various lubrication regimes/theories stated for the synovial joints. It is important to note that none of these regimes alone can account for the behaviour of the joints under physiological loading. Therefore, it is suggested that a combination of more than one of the following regimes will be active under any physiological condition that the joint experiences.

1.2.5.1 Fluid Film Lubrication

When two articulating surfaces of AC are separated by a thin fluid layer, there are low levels of friction, and fluid film lubrication exists. The pressure created by this thin layer of fluid between the two bearing surfaces supports the load. The thickness of the film has to be three times greater than the combined roughness of the bearing surfaces, for the fluid film lubrication to subsist and function. Within this type of lubrication theory there are various regimes that can be used to describe the joint lubrication (McNary et al., 2012).

Hydrostatic lubrication, is where the two opposing surfaces are separated and supported by an externally pressured fluid film from the recesses of the cartilage surface. Whereas, *hydrodynamic lubrication* occurs when two surfaces move at relatively high speed and fluid is drawn between them. The film thickness is a function of many different variables such as; geometry, roughness and fluid viscosity (Bassani and Piccigallo, 1992; Neu et al., 2008). In *elastohydrodynamic lubrication*, the asperities of the cartilage surface become of the same order of thickness as the fluid film. Therefore, the pressures generated by the fluid result in the elastic deformation of the bearing surfaces (Dowson, 1995). *Squeeze film lubrication*, is exhibited when the lubricant fluid between the two-bearing surface is viscous in nature and cannot be exuded out of the contact zone, when under load. This resultant pressure keeps the surfaces apart and dissipates the load (Mow and Ateshian, 1997). Lastly, *boosted lubrication* occurs when the joint is under load, this causes the solvent within the synovial fluid to be forced back in to the cartilage ECM, therefore leaving behind highly viscous and

concentrated hyaluronic acid and proteins on the cartilage surface, which have load bearing capabilities (Walker et al., 1968; Longfield et al., 1969).

1.2.5.2 Boundary Lubrication

Boundary lubrication comes into play when the combined asperity height of the two opposing surfaces becomes greater than the fluid film thickness. The articulating surfaces become separated by a mono/multi-layer of boundary lubricant, which prevents direct contact between the two surfaces. In the absence of this continuous and self-replenishing layer, the continuous asperity contact would lead to the degeneration of the cartilage surface by mechanical wear (Mow and Ateshian, 1997; Gleghorn and Bonassar, 2008; Chan et al., 2010). Fluid film lubrication is dependent on the changes in viscosity of the fluid and the fluid forces generated from the joint motion (Figure 6). Nevertheless, the literature states that the lubrication of AC is not completely reliant on the viscosity of the synovial fluid; therefore, this led to further investigation into the lubricating constituents present in the synovial fluid. Research has mainly focused around the study of three proposed boundary lubricant molecules: surface active phospholipids (SAPLs), superficial zonal proteins (SZP) and hyaluronic acid (Chan et al., 2010; Jay and Cha, 1999) and their roles in different lubrication regimes. However, a full discussion of the research into these proposed boundary lubricants is beyond the scope of this thesis.

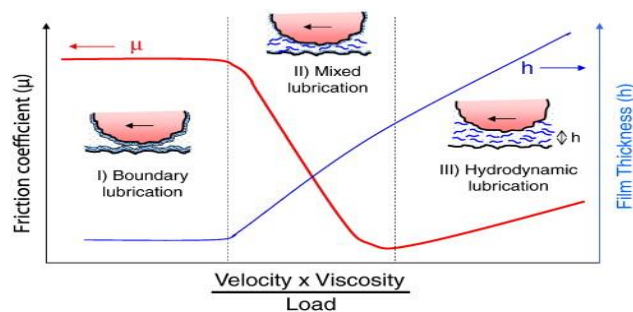


Figure 6: Friction coefficient plotted as a function of fluid viscosity and shear velocity divided by the load (Stribeck Curve) with the corresponding film thickness for boundary, mixed and hydrodynamic lubrication mechanisms (Coles et al., 2010).

1.2.5.3 Mixed Lubrication

This type of lubrication regime comes into play when the interstitial fluid seeps out of the porous cartilage as the load increases. The ability of the cartilage to support the *elastohydrodynamic lubrication* via the secretion of interstitial fluid is reduced and 'mixed lubrication' comes into play. This is a combination of fluid film lubrication and boundary lubrication processes. Throughout the gait cycle, the bearing surfaces of AC undergo a variety of loading conditions (i.e. contact stresses and sliding speeds), diminishing the fluid film layer. As this occurs, the bearing surfaces start to come into contact; this is where boundary

lubrication operates to reduce the friction between the opposing surfaces. Thus, it is likely that under normal physiological conditions, the synovial joint operates under mixed lubrication and may revert to another regime depending on the activity of the individual (Gleghorn and Bonassar, 2008; Neu et al., 2008; Chan et al., 2010).

1.2.5.4 Biphasic Lubrication

Variations of fluid film, boundary and mixed lubrication regimes have been found to operate at the synovial joint. These regimes are attributed to the composition of the articulating surface and the materials present within them. Biphasic lubrication plays an intrinsic role in the tribological function of the cartilage tissue and hence the synovial joints.

McCutchen was the first to propose that the interstitial fluid within the joint cavity was able to carry the load when a force was applied to it. The theory also stated that this fluid exudates from within the cartilage, providing a fluid film to the area that is loaded, keeping the surfaces from coming into contact (McCutchen, 1959). Over the years, many different lubrication mechanisms had been attributed to AC and it had become increasingly clear that the tribological performance of AC was not confined to one single lubrication regime alone. It is considered to have a manifold of lubrication regimes, which can be characteristic of two distinct incompressible and immiscible phases (Greene et al., 2011). These phases are comprised of the solid phase (mainly collagen and proteoglycans) and the fluid phase (interstitial water) (Mow and Lai, 1980). The interaction between these two phases is what controls the deformation of AC, which is the flow of the interstitial fluid through the complex interwoven solid phase. The significance of biphasic deformation in AC on its lubrication was highlighted in the late 1950s by McCutchen *et al.* However, it was not until the 1990s that further studies were carried out; experimentally by Forster *et al.* (1996), and theoretically by Ateshian *et al.* (1997), to confirm the biphasic mechanism (Forster and Fisher, 1996; Ateshian, 1997). The unique structure of AC is crucial to its biphasic and load bearing characteristics. Cartilage is highly porous; this is due to the interwoven nature of the collagen matrix, with pore size varying between 2 - 6.5 nm. The presence of charged groups on the proteoglycan network and these small pores in the matrix contribute to the low permeability value, which varies between 10^{-15} to $10^{-16} \text{ m}^4 \text{Ns}^{-1}$ (Mow and Ateshian, 1997). As the interstitial fluid (fluid phase) is under load, it generates what is known as pressure gradients (drag forces). The pressurization of this fluid phase is able to support the majority of the load applied. However, as time progresses the fluid is exuded into the joint space or into other unloaded areas. Gradually the load is transferred from the fluid phase to the solid phase and as a result the friction is increased.

Forster & Fisher (1996) demonstrated that the friction observed between the two articulating surfaces was mainly due to the solid phases interactions. However, they also suggested that the COF between the articulating surfaces could be kept low as long as the fluid phase load support was very high. This was confirmed by their test measuring the COF in an *in vitro* cartilage specimen against metal and cartilage against cartilage set up for different loading times (Forster and Fisher, 1996).

1.2.5.5 Triphasic Lubrication

Mow *et al.*, established the triphasic material properties of AC as a progression from the original biphasic theory. The proteoglycan aggregates were modelled to be restrained within the collagen matrix, just as in the biphasic theory. These molecules contain a large number of fixed negatively charged groups (SO_3^- and COO^-) along the GAG chains (Mow *et al.*, 1990). Due to these negatively charged molecules, in a water-like environment such as the interstitial fluid, univalent counter ions (e.g. Na^+) are needed to maintain the electro-neutrality. These univalent ions which are present within the interstitial fluid were modelled as an addition to the fluid phase in the biphasic theory (Lai *et al.*, 1991). Although the use of this theory has improved the accuracy in determining the equilibrium response to the deformation of cartilage under load, this ionic phase plays a very small role when compared to the solid and fluid phases of AC (Lai *et al.*, 1991), however it is a factor that should be kept in mind experimentally.

1.2.6 Wear of articular cartilage

The wear of articular cartilage can be classified into two categories, mechanical wear and biochemical degradation, both of which can eventually lead to the destruction and degeneration of AC. In engineering terms, wear is classed as the removal and deformation of a material surface as the result of a mechanical stress applied by an opposing surface or object. Cartilage can last a life time with very minor wear however, this can be hindered by several environmental factors such as, but not limited to; abnormal biomechanical loading, trauma, changes in the structure of the ECM and pathologically induced alterations in the lubrication mechanism. All of the factors can either work in isolation or in concert to increase the cartilage wear past its normal limits. Cartilage tissue is biological in nature and therefore it can suffer from collateral biochemical degradation; this can either be alteration to the collagen network, increased loss of proteoglycans or ionic disturbances in the synovial fluid. It is very hard to determine which of the two types of wear damage, biomechanical or biochemical, follow on from each other. The difficulty of understanding the underlying process of these two types of cartilage wear has focused past and present research, to

determine the frictional and deformation properties of AC, whilst still being aware of any tribological properties.

1.2.6.1 Types of wear

1.2.6.1.1 Mechanical wear

This type of wear can be further subdivided into two groups: fatigue wear and interfacial wear. The latter occurs mostly during boundary and mixed lubrication where there is slight solid-solid contact between the two opposing surfaces. There are two forms of interfacial wear; adhesive wear, which occurs when there is unwanted displacement and attachment of wear debris, from one surface to the other. The other is abrasive wear, in which the material of the softer of the two bearing surfaces is removed from its surface due to rubbing against the harder bearing surface. The harder material can either be the particles between the surfaces, which can be considered as third-body wear or the bearing surface itself (Mow and Ateshian, 1997). However, due to the many lubricating mechanisms within the joint, the contact between the articulating surfaces is hampered, meaning that interfacial wear does not tend to happen frequently. Nevertheless, any disruption to these lubricating mechanisms due to any sort of AC degradation may lead to interfacial wear and accelerate the tissue loss because of the altered biomechanics of the joint and increased contact.

1.2.6.1.2 Fatigue wear

Unlike mechanical wear, fatigue wear is independent of the lubrication phenomenon occurring between the two surfaces of the AC. This type of wear is produced as a result of cyclic loading causing increased stress and strain on the joint by which the material becomes weakened. This produces wear debris that becomes dislodged due to the propagated crack growth at the cartilage surface or in the underlying bulk material. In cartilage, it is manifested in the form of collagen network buckling or loosening (Mow and Ateshian, 1997), by which the collagen fibres become separated from their bundles into individual fibres or even smaller subunits. This results in a dramatic decrease in the mechanical properties and an increase in the tissue permeability, similar to the process seen in OA cartilage.

1.2.6.1.3 Biochemical degeneration

Cartilage loss due to the degeneration of its structural and functional components can be as a result of various pathological causes such as, but not limited to, metabolic disorders, over production of cytokines and matrix metalloproteases (MMPs) and joint haemophilia. This is termed as biochemical degeneration. There is a vast amount of literature that uncovers the underlying mechanisms of these factors and the role they have in cartilage degeneration as well as the onset and progression of OA (Alcaraz et al., 2010; Kapoor et al., 2011; Pitsillides

and Beier, 2011; Ashkavand et al., 2013; Lee et al., 2013). Biochemical degradation can also affect the natural aging of chondrocytes and stimulate chondrocyte hypertrophy as a result of increased metabolic activity. These changes in chondrocyte behaviour alter the composition of the ECM as a result of an increase in the ratio of CS-6 to CS-4, which is similar to the ratio seen in undeveloped foetal cartilage (Sandy et al., 1987; Hickery et al., 2003; Clarkin et al., 2011). Following these events, the biomechanical properties of AC become adversely affected and hence make it susceptible to further mechanical and/or biochemical degeneration, aggravating the OA condition. Therefore, OA is a combination of biological, chemical and mechanical processes.

1.3 Osteoarthritis

1.3.1 Introduction

Osteoarthritis (OA) is one of the most common joint diseases worldwide. This disease is characterised by the progressive loss of articular cartilage and formation of osteophytes which leads to chronic pain and discomfort. The vast literature all points to the same factors that are responsible for the development of OA (Lorenz and Richter, 2006). These mainly include traumatic events either from sporting activities or traffic accidents; however, there are also other factors such as congenital abnormalities, ageing and malnutrition which can all lead to changes in the AC structure (Swoboda, 2001). Unfortunately, cartilage has a poor propensity for self-renewal due to its avascular nature. The repair tissue that it does form as a result of cartilage loss mainly consists of fibrous tissue, which has mechanical properties that are considerably reduced compared to that of healthy AC. Early therapeutic intervention is needed to repair initial cartilage damage and prevent or delay the progression to OA (Arden and Nevitt, 2006). Unfortunately, OA is not normally diagnosed in early stages and predominantly manifest at an advanced stage, when alterations to the joint are pronounced and can be visualised radiographically. The therapeutic options for advanced OA are difficult and limited. There is a real need to understand the underlying molecular mechanisms of cartilage degeneration, in order to develop early intervention therapeutic approaches and diagnostic techniques (Lorenz and Richter, 2006).

1.3.2 Pathophysiology of Osteoarthritis

As noted above, a major problem with understanding of the pathophysiology of OA is that early stage OA cartilage is not easily diagnosed. The morphological and histological features of established OA are well known, however the underlying molecular mechanisms that lead to the development of the disease are still not completely understood. This section aims to

review current literature available on the biochemical and molecular process at different stages of OA that lead to histological and macroscopically visible alterations in AC.

Damage to cartilage, mainly through trauma, involves damage to chondrocytes, which compromises their ability to repair. This leads to loss of proteoglycan content (Lohmander et al., 1989), increased hydration and altered collagen organization (Mankin, 1982). The progressive loss of structure and functionality of AC is driven by an imbalance of anabolic and catabolic processes within the tissue (Sandell and Aigner, 2001). The disturbance of the cartilage organisation results in a decrease in the tensile stiffness and strength that is usually provided by the healthy 3D architecture of the collagen network (Wang et al., 2003). Similarly, the OA process is linked to a loss of proteoglycans, by which proteoglycan monomers are no longer bound to the hyaluronan backbone. This is due to proteolytic enzymes which shorten the chain length of the aggrecan molecule and hence inhibit the formation of the normal macromolecular complex seen in Figure 3 (Mankin et al., 1999; Poole, 1997). It is thought that metalloproteases (MMPs) such as collagenase-1 (MMP-1) and collagenase-3 (MMP-3) are responsible for the degradation of type II collagen (Reboul et al., 1996), whereas stromelysin-1 (ST3) and aggrecanase-1 (ADAMTS-4) are responsible for the degradation of aggrecan (Lark et al., 1997; Tortorella et al., 2000). The breakdown of these complexes leads to a more permeable solid matrix. Even though there is increased water content, the increase in permeability of the matrix results in a decrease in the hydraulic pressure and therefore a reduction in the compressive stiffness (softening) of the cartilage (Akizuki et al., 1987; Lai et al., 1991). Inflammatory cytokines may augment the process of cartilage softening and degradation. Pro-inflammatory cytokines such as tumour necrosis factor- α (TNF- α), interleukin 1- β (IL-1 β) and IL-6 stimulate chondrocytes to secrete catabolic enzymes such as MMPs and aggrecanase, which degrade the cartilage matrix (Martel-Pelletier, 2004). The loss of structure to the ECM and decrease in the mechanical properties leads to the load applied at the surface of the AC to be transferred to the underlying subchondral bone and consequently making it stiffer. Consequently, this causes the impact loads to be transmitted to the weaker damaged cartilage (Mankin, 1982). Small lesions occur which eventually increase in size, revealing naked bone and ultimately the whole layer of the articular cartilage is destroyed (Howell, 1986; Felson, 1993). In summary, the pathophysiological process of OA that causes the morphological and histological change can simply be divided into three stages. Firstly, the ECM breaks down on a molecular level, water content increases and matrix molecules are reduced in size. This compromises the structure of collagen leading to a reduced stiffness. Secondly, chondrocytes try to repair the damage through enhanced proliferation and metabolic activity. Chondrocytes aggregate

around newly formed matrix molecules. Finally, the cells are not able to sustain their reparative activity and as a consequence the regeneration of cartilage is superseded by its degeneration (Lorenz and Richter, 2006).

1.3.3 Relevance of OA Models

One approach to understand the disease progression of OA is via the use of animal models. Animal models have been able to provide radiographical, histological and molecular changes, which can be directly correlated to certain stages of degeneration of human AC (Lorenz and Richter, 2006). Animal models allow direct comparison of diseased and healthy AC in the same animal. Animal models include spontaneous (Huebner et al., 1998), mechanically induced (Pond and Nuki, 1973; Marijnissen et al., 2002), and chemically induced (Dumond et al., 2004) approaches. The relevance of these models to the human situation is, however questionable, not least because animals are quadrupeds and have different loading patterns in joints compared to humans. Nevertheless, most of the current understanding of the pathophysiology of early OA and its progression over time is derived from animal models (Lorenz and Richter, 2006). The type of joint usually studied in animals is the stifle (knee) joint. Nonetheless, other joints include the temporomandibular joint in STR/ort mice (Kumagai et al., 2015), the metacarpophalangeal and middle carpal joints in horses, which have been shown to have great similarities to the human knee joint (McCoy, 2015; McIlwraith et al., 2010). Both small (mouse, rat, rabbit, guinea pig) and large animal (dog, sheep and horse) have been used to develop OA model. However, the choice of animal usually depends on, but is not limited to, the type of experiment, length of study, husbandry costs, ease of handling and outcome measurements. All of which have been associated with the disadvantages of using animal models (Kuyinu et al., 2016). In addition, the length of time needed for each animal to reach skeletal maturity and, as a consequence develop OA is also another limiting factor. Small animal models are usually used to study the pathogenesis and pathophysiology of the OA disease process as well as screening models for therapeutic interventions. Although they are quick, cheap and easy models to implement the efficacy of treatments may not be translatable to humans, which is mainly down to the difference in anatomy, histology and physiology between these animals and humans (McCoy, 2015; Pelletier et al., 2010). Larger animal models are usually used to study the disease process and treatment, as their anatomy is much more like those of humans, which is why studies of cartilage degeneration and osteochondral defects are much more useful in larger animals. They can be used to confirm the efficacy of drugs or treatments before they are taken to clinical trials (McCoy, 2015; Pelletier et al., 2010). The biggest problem however when using animal models is, because there are so many approaches to induce OA, such as but not

limited to: surgical, chemical, non-invasive, mechanical, genetically modified; there is lack of standardisation of these OA models and their outcome measures, making it difficult to compare results between studies. Furthermore, the upscaling of studies from small to large animal model, which are essential for translation of potential therapies to human medicine, still present a great challenge.

1.3.3.1 Kellgren-Lawrence grading system

In humans, the Kellgren-Lawrence grading system (Table 1) is an example of how different stages of OA can be identified. This system of grading based on radiographic features is used by clinicians to classify the extent of joint space narrowing, osteophyte formation, subchondral sclerosis, cyst formation and abnormalities of bone contours. It assigns five grades (0-4) to OA, at different joint sites by comparison with a radiographic atlas (Kellgren and Lawrence, 1957). Over the years many radiologists have added to the atlas databases, and this has helped to provide a more consistent approach to the grading of the individual features mentioned above and allowed better extrapolation between the results of different studies (Altman et al., 1995; Burnett et al., 1994; Schiphof et al., 2008).

Table 1: Different descriptions of the Kellgren and Lawrence (K&L) criteria of knee osteoarthritis (OA) adapted from Schiphof *et al* (Schiphof et al., 2008) and Arden *et al* (Arden and Nevitt, 2006).

Radiological features on which grades are based					
Radiographic Grade	0	I	II	III	IV
Classification	None	Doubtful	Mild/minimal	Moderate	Severe
Description (Kellgren and Lawrence, 1957; Kellgren et al., 1963; Scott et al., 1993)	No features of OA	Doubtful narrowing of joint space and possible osteophytic lipping.	Definite osteophytes and possible narrowing of joint space.	Moderate multiple osteophytes, definite narrowing of joint space and some sclerosis and possible deformity of bone ends.	Large osteophytes, marked narrowing of joint space, severe sclerosis and definite deformity of bone ends.
Alternative A (Jordan et al., 2003; Cooper et al., 1996; Hart et al., 1991)	No features of OA	Minute osteophyte, doubtful significance.	Definite osteophyte, unimpaired joint space.	Moderate diminution of joint space (with osteophytes).	Joint space greatly impaired with sclerosis of subchondral bone
Alternative B (Zhanget al., 2001)	No features of OA	Possible osteophytes only.	Definite osteophytes and possible joint space narrowing.	Moderate osteophytes and/or definite narrowing.	Large osteophytes, severe joint space narrowing and/or bony sclerosis.
Alternative C (Wilder et al., 2002; Williams et al., 2005)	No features of OA	Possible osteophyte lipping.	Definite osteophyte and possible joint space narrowing.	Moderate multiple osteophytes, definite joint space narrowing, some sclerosis, and possible bone contour deformity (bony attrition).	Large osteophytes marked joint space narrowing, severe sclerosis, and definite bone contour deformity (bony attrition).
Alternative D (Williams et al., 2004)	No features of OA	Doubtful pathology.	Minimal osteophytes, possible narrowing, cysts, and sclerosis.	Moderate, as in definite osteophytes with moderate joint space narrowing.	Severe, with large osteophytes and definite joint space narrowing.

1.3.4 Structural and histological signs of OA

1.3.4.1 Early OA

The initial degeneration process of OA is characterised by changes in the cartilage surface, which are no longer smooth (McDevitt et al., 1977). The GAGs remain unchanged compared to normal healthy cartilage, however as the disease progresses, there is a loss of proteoglycans indicated by a reduction in Safranin O staining (Figure 7) and the cells in the superficial layer become round (as opposed to flat), hypertrophic and eventually disappear (Fernandes et al., 2002).

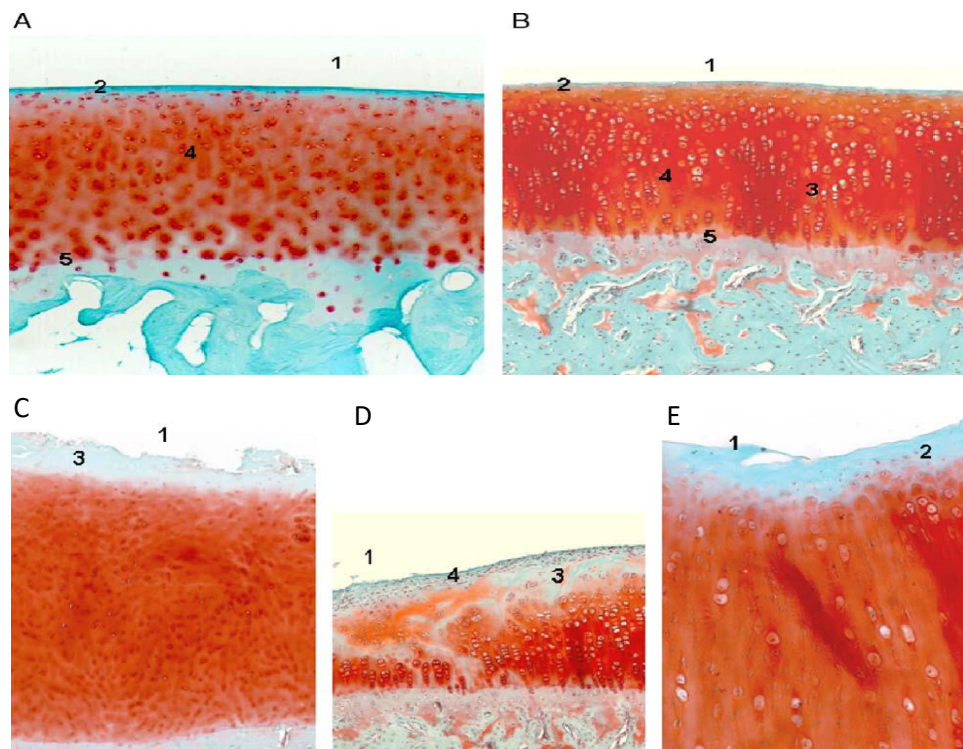


Figure 7: Histological images of healthy and osteoarthritic cartilage. [Top Pictures] Normal knee articular cartilage, Safranin O/fast green stained sections. (A) Human, (B) Rabbit. (1) Smooth surface, (2) cells in the tangential zone are small and flat, (3) cells in the intermediate and radial zone are arranged in columns, (4) the complete cartilage matrix stains with Safranin O, and (5) the tidemark is intact. [Bottom Pictures] Mild OA, (C) Human, (D) and (E) rabbit. (1) Surface irregularities, (2) Hypertrophic cells in tangential zone, (3) staining of Safranin O is reduced and (4) pannus (Lorenz and Richter, 2006).

In the transitional and radial zones the tissue shows mild to moderate hypercellularity. Necrotic chondrocytes have been reported within the tangential zone of experimental OA models (Bluteau et al., 2001). Pelletier *et al.*, as well as many others, have noted that there is a change in the synovial membrane in OA models in dogs and rabbits (Pelletier et al., 1985). Hyperplasia of the synovial lining cells, thickening of the synovial membrane, presence of inflammatory cells and fibrosis have all been reported (Brandt et al., 1991; Sakakibara et al., 1994). The progression of the disease is dependent on the species of animal as well as the

location of the joint as proposed in reviews by; Le Graverand *et al.* (Le Graverand *et al.*, 2002), Lorenz *et al.* (Lorenz *et al.*, 2005), and Young *et al.* (Young *et al.*, 2005).

1.3.4.2 Advanced OA

At a more advanced stage of OA, there are visible signs of complete breakdown of the cartilage (Figure 8). The AC surface demonstrates a rough and uneven surface, with some signs of fissures and cracks, which penetrate down to the calcified bone (Veje *et al.*, 2003). The cells in this very severe OA cartilage, either disappear completely or cluster around the fissures, as the tissue degenerates further. The organisation of cartilage is completely lost and is replaced by fibrous tissue (Miosge *et al.*, 2004). In very extreme cases, the bone is denuded of cartilage creating full-thickness defects (Pfander *et al.*, 1999). A considerable loss of proteoglycan content, visualised by lack of Safranin O in histological sections in all layers of the cartilage is seen, eventually reaching the deep zone (Figure 8). The tidemark between calcified and uncalcified cartilage is obscured (Hayami *et al.*, 2003). Histological studies of human cartilage exhibiting signs of OA, show the presence of fibrocartilage (Goldwasser *et al.*, 1982), as well as the presence of fibrillated tissue with areas of cartilage loss (Squires *et al.*, 2003).

Bock *et al.* were able to distinguish between three types of chondrocytes within OA cartilage via a series of light and electron microscopical analyses. Type I cells exhibited the normal healthy phenotype, in a continuous matrix and small amounts of endoplasmic reticulum. Type II cells, were elongated and more irregular in shape, situated in a fibrillated matrix with an enlarged endoplasmic reticulum. In severe cases of OA, Type III cells were found. These cells contained pyknotic nuclei and partly dissolved cytoplasm within a severely fibrillated matrix (Bock *et al.*, 2001).

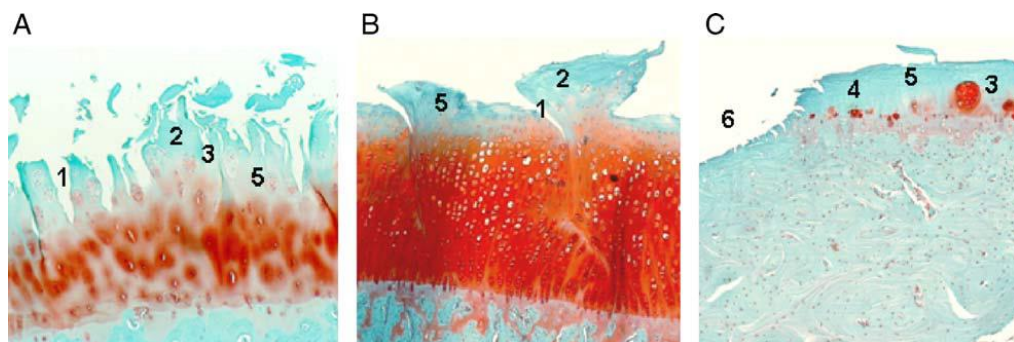


Figure 8: Severe OA, Safranin O/fast green staining. (A) Human, (B) and (C) rabbit. (1-3) The tissue shows deep clefts in the surface from which cells have disappeared from the tangential zone. (4) Lack of cells in the intermediate and radial zone, (5) reduced to no staining of the matrix with Safranin O, and (6) denuded bone (Lorenz and Richter, 2006).

1.3.5 Biochemical and biomechanical changes of OA cartilage

Within the vast literature there is much discussion regarding the biomechanical and biochemical mechanisms involved in the onset and progression of OA. Clinically, OA has been linked to symptoms such as joint swelling, synovitis and inflammatory pain. The synovial membrane contains highly metabolic synoviocytes, which are important in regulating the physiological conditions within the joint capsule and nourishing the chondrocytes via the synovial fluid. They also remove any products of degeneration (Sellam and Berenbaum, 2010). Synovitis has been linked with the structural degradation of the OA disease because of the action of several soluble mediators involved in the pathophysiology. However how this occurs, is open to debate. Sallam & Berenbaum (2010) and later Berenbaum (2013) both proposed the same hypothesis (Sellam and Berenbaum, 2010; Berenbaum, 2013); that as AC degrades due to several factors (some listed in Table 2); cartilage debris becomes dislodged in the joint space. Synovial cells, recognise these fragments as foreign material and mount an inflammatory response leading to the release of inflammatory mediators as depicted in Figure 9.

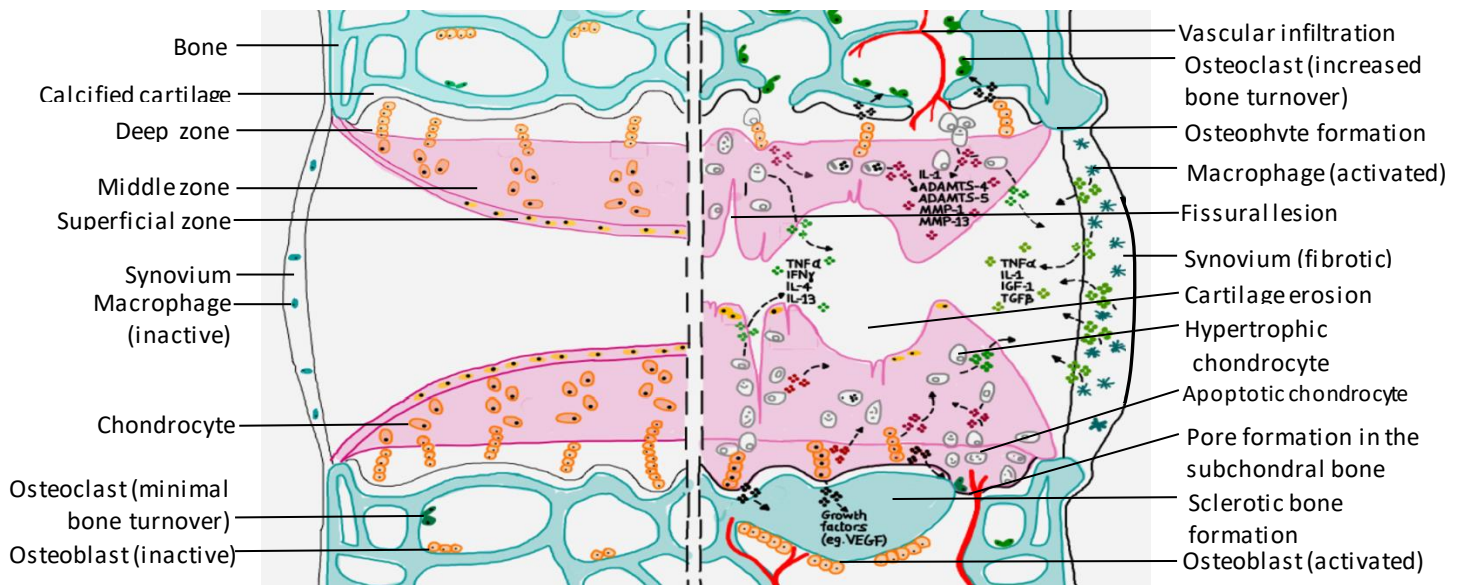


Figure 9: Involvement of synovium in OA pathophysiology. The activated synovial cells produce catabolic and pro-inflammatory mediators, which leads to the excess production of proteolytic enzymes responsible for cartilage and matrix breakdown, creating a positive feedback loop. The inflammatory response is amplified by synovial T & B cells and macrophages. In addition to these inflammatory and degenerative effects, the inflamed synovium also contributes to the formation of osteophytes via the release of bone morphogenetic proteins. Abbreviations - IL: interleukin; TNF: tumor necrosis factor; MMPs: matrix metalloproteinases; ADAMTS: a disintegrin and metalloprotease with thrombospondin motifs and VEGF: vascular endothelial growth factor. Adapted from: (Kuyinu et al., 2016).

Histological changes in OA synovium, reported by Myers *et al.*, show signs of hypertrophy and hyperplasia with an increased number of lymphocytes and macrophages. The permeation of these cells into the synovium and thickness of the synovial lining seem to be closely related (Myers *et al.*, 1990). Inflammatory mediators, detected in the synovial fluid have been suggested to originate from three tissues that have undergone histological modification; cartilage, subchondral bone and synovium. The two most common cytokines involved in the synovial inflammation and hence the pathogenesis of OA are; IL-1 β and TNF- α . Interestingly, a study performed on patients with knee pain both at the early stage and late stage OA suggested that within the synovial fluid, the levels of IL-1 β and TNF- α were higher in patients with early OA than patients with late OA (Benito *et al.*, 2005). The production of these cytokines can have a secondary effect, via the stimulation of chondrocytes and synoviocytes to produce other cytokines (IL-6 & IL-8). These synovial cytokines act on the cartilage matrix and chondrocytes (Sellam and Berenbaum, 2010; Berenbaum, 2013), either independently or in concert with other cytokines to initiate and propagate the inflammation process (Kapoor *et al.*, 2011). In several cell culture studies, IL-1 β and TNF- α have been shown to suppress the synthesis of proteoglycans (Gouze *et al.*, 2001; Saklatvala, 1986), link proteins and type II collagen (Séguin and Bernier, 2003) within AC (Nietfeld *et al.*, 1990; Chadjichristos *et al.*, 2003). Therefore low grade synovitis, generated via pro-inflammatory cytokines as discussed above, as well as other soluble mediators, contributes to the accelerated up-regulation of catabolic factors and down-regulation of anabolic factors, thus leading to the degeneration of AC and progression of OA (Sellam and Berenbaum, 2010; Fernandes *et al.*, 2003; Berenbaum, 2013; Sutton *et al.*, 2009).

As a result of these cytokines, synovial cells as well as OA chondrocytes both produce large quantities of metalloproteinase (MMPs), these include MMP-1, MMP-3, MMP-9 and MMP-13 (Sellam and Berenbaum, 2010). MMP-3 is mainly synthesised at the boundary between hyaline cartilage and synovial fluid, which suggests that this proteinase is produced by the synovium to directly break down cartilage (Blom *et al.*, 2007). Other authors have added to this, indicating that MMPs are able to degrade all components of the ECM (Little *et al.*, 2009). It is clear that these inflammatory mediators play an important role in many physiological processes, their over expression and activation by different cell types contributes to many pathologies, including joint destruction in OA (Sellam and Berenbaum, 2010; Berenbaum, 2013; Little *et al.*, 2009).

Table 2: Clinical, histological and molecular signs of synovitis in OA. (Adapted from Sellam *et al* (Sellam and Berenbaum, 2010)).

Level of Evidence	Evidence of Synovitis in OA	
	Observation	References
Clinical	Effusion, joint swelling, or palpable synovitis	(Krasnokutsky et al., 2008)
	Local signs of inflammation	
	Sudden increase in pain	
	Night pain and morning stiffness	
Histological	Synovial hypertrophy and hyperplasia	(Ayril et al., 2005), (Myers et al., 1990), (Walsh et al., 2007), (Nakamura et al., 1999) and (Alsalameh et al., 1990).
	Infiltration of mononuclear cells (monocytes/macrophages, activated B cells and T cells)	
	Adaptative immune T-cell and B-cell responses to fragments of extracellular matrix	
	Increased angiogenesis	
	Synovitis in the vicinity of degenerative cartilage	
Molecular	Production and/or release of proinflammatory cytokines (TNF, IL-1 β , IL-6, IL-8, IL-15, IL-17, IL-21)	(Benito et al., 2005), (Smith et al., 1997), (Farahat et al., 1993), (Furuzawa-Carballeda and Alcocer-varela, 1999), and (Scanzello et al., 2009).
	Increased production of PGE2 and nitric oxide in the synovium	
	Increased activity of MMPs (MMP-1, MMP-3, MMP-9, MMP-13) and ADAMTS	
	Involvement of macrophages in osteophytes formation via BMPs	
	Insufficient release of anti-inflammatory cytokines (IL-4, IL-10, IL-13, IL-1Ra)	

Alongside these events, the breakdown of aggrecan in the early stages of OA is also a contributing factor to the pathogenesis of OA. The production of aggrecanase ADAMTS (A disintegrin and metalloproteinase with thrombospondin motifs), in particular (ADAMTS)-4 (aggrecanase-1) and ADAMTS-5 (aggrecanase-2) are responsible for the aggrecan degradation (Alcaraz et al., 2010). The production of these proteolytic enzymes is mainly driven by TNF- α but also by IL-1 β and therefore indirectly mediated by synovial macrophages. However, studies using chondrocytes taken from porcine and bovine cartilage explants revealed that the up-regulation ADAMTS-4 but not ADAMTS-5, was dependant on TNF- α and IL-1 β (Tortorella et al., 2001). This finding is in agreement with a similar study performed on human OA synovium (Bondeson et al., 2006).

Several studies have shown that synovial macrophages are responsible for the inflammatory responses in OA (Blom et al., 2007). The depletion of these cells within the synovium

demonstrated a reduction in the formation of osteophytes. Therefore, suggesting the role that TNF- α has on osteophyte formation, perhaps through the stimulation of bone morphogenetic proteins (BMPs) such as BMP-2 and BMP-4 (Blom et al., 2004; Van Lent et al., 2004).

On the whole, the long-established view of OA as a cartilage only disease is no longer valid. This inflammatory disease should be considered as a whole joint pathology that encompasses the synovial tissue, the different layers of cartilage and the subchondral bone, all of which communicate via cell-to-cell interactions, via the release of soluble mediators and mechanical signals. From the literature it is clear that synovial inflammation (synovitis) is not a prerequisite for the development of OA, however it is somewhat involved in the degeneration of cartilage and thus the progression of OA.

During the progressive stages of OA, there is a visible change in the molecular composition and organization of the ECM, which has been linked to the deterioration in the mechanical properties of AC. Some of the current research has focused on the role of chondrocytes in the pathogenesis of these alterations. Chondrocytes are able to respond to sudden structural and mechanical changes in their surrounding matrix, as well as responding to cytokines and various inflammatory mediators (Goldring and Marcu, 2009). The architecture and structural properties of the peri-articular cortical and trabecular bone become compromised, via the cell mediated processes of re-modelling. During the initial stages of remodelling, osteoclasts drive bone resorption, which is then followed by a phase of bone formation, driven by osteoblasts. In normal physiological conditions, the amount of bone lost during the resorption phase is balanced by the bone gained in the formation phases of bone remodelling. Thus, there is no change in the bone mass. However, the architecture and shape of the bone may change (Goldring and Goldring, 2010). The changes to periarticular bone in OA can be subdivided into varying patterns which include; changes in the subchondral plate thickness, changes in the structure of the underlying subchondral bone, formation of osteophytes and the development of subchondral bone cysts. These defined skeletal changes have been linked to changes in the contours of adjacent articulating surfaces, hence altering the homogenous structure of the joint, which further contributes to altered biomechanical properties (Bullough, 2004; Burr, 2004; Radin and Rose, 1986). Radin and co-workers were the first to propose that an increase in the subchondral bone thickness will cause an increase in its stiffness. They speculated that these changes in the bone, adversely affected the biomechanical environment of the cartilage and hence lead to the structural changes. Furthermore, they also made a link between the ability of the adjacent AC to adapt to mechanical load, as a result of the changes in contour and shape to the subchondral plate

(Radin and Rose, 1986), which was later validated by advances in radiography (Buckland-Wright, 2004).

Of the cases of OA reported in the literature, the most common area of OA is the medial compartment of the knee (Andriacchi, 1994; Wise et al., 2012). This is due to the fact that it is subject to greater loads than the lateral compartment. During the development stages of the knee, cartilage thickens in areas that undergo greater loading conditions through the whole joint. This therefore, has an effect on the tibiofemoral mechanics and hence plays a role in the development of OA. Alteration to normal gait mechanics, can change the normal gait patterns under weight-bearing activities; from areas of cartilage which are not adapted to receiving these kinds of loads (Andriacchi et al., 2009; Carter et al., 2004). The aberrant loading of these areas causes the cartilage to become damaged, adversely affecting its mechanical properties.

Injury to AC or other tissue structures within the joint (anterior cruciate ligament) (Chaudhari et al., 2008) as well as the aging process associated with cartilage, all increase the joint laxity. This allows for aberrant motion between the opposing surfaces. At the micro molecular level, this causes fibrillation to the collagen network, loss of proteoglycans, increased surface friction and shear stress, as well as an up-regulation of catabolic factors. This cascade of events, further exacerbates the progression of OA secondary to the damage caused to the AC or the other soft tissues (Vincent et al., 2012; Guilak, 2011).

By and large, chondrocytes are able to modulate their activity in responses to loading and various other factors. However, their ability to modify and repair the surrounding ECM is limited, when compared to the skeletal cells in bone. Therefore, the divergence in adaptation of these two tissue cells disrupts the physiological association between cartilage and bone, which is primordial for the safeguarding of normal joint structure and function and could further contribute to the progression of OA.

Other than pro-inflammatory cytokines and mediators, biomechanical factors also play a crucial role in the events that lead to the commencement and evolution of OA. Under normal physiological conditions; the ECM is able to remain in a constant state of 'slow-turnover', exhibited by a homeostatic balance between anabolic and catabolic events of chondrocytes. This steady state is regulated through the processing of environmental and soluble mediators (cytokines and growth factors), matrix composition and bio-physical factors; including mechanical or interstitial pressure (Guilak, 2011). However, a shift in the direction of degeneration of AC, is indicative that the balance of normal metabolic activity of chondrocytes has been severely compromised. Current research has shown growing

evidence that the interaction between pro-inflammatory cytokines and mediators with mechanical stress, are responsible for the destructive events that occur in OA (Hunter, 2011; Guilak, 2011).

Increasing abnormal stresses applied to any joint, in particular the knee, can lead to alteration in the composition, structure and metabolism of AC. Abnormal loading of the joint may be caused by a variety of factors such as weight gain, trauma, joint instability and malalignment. Obesity has been highlighted as one of the major risk factors for OA incidence, progression and disability (Messier et al., 2000). Although this condition has been associated with increased joint stresses and altered gait, secondary to increase in weight (Messier, 1994); there is also evidence to show the presence of joint inflammation due to obesity (Das, 2001; Visser et al., 1999). This in concert with biomechanical factors promotes the degeneration of AC (Figure 10) (Issa and Griffin, 2012). In addition, a study performed by Felson *et al.* demonstrated that a reduction in weight of only 5 kg could reduce the risk of OA by over 50% (Felson et al., 1992).

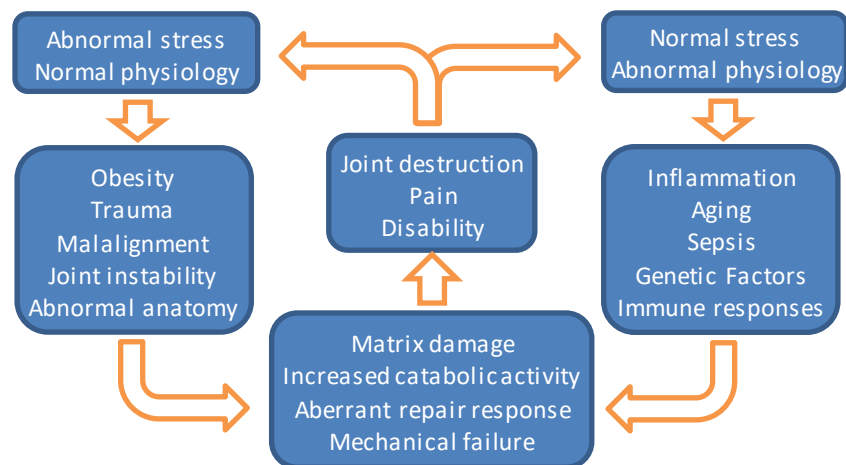


Figure 10: The role of mechanical loading in osteoarthritis. These are some of the biomechanical factors involved in the pathogenesis of OA, which are either due to abnormal loading acting on normal physiology, or normal loading acting in the presence of abnormal physiology. Adapted from: (Moskowitz et al., 2007).

Impact loads have also been associated with the damage incurred to AC. Hyper-physiological stress can increase cellular activity, induce remodelling of the subchondral bone and splitting of the ECM, which are all characteristic signs in early stage OA; indicating that increased loads may be an important factor in the pathogenesis of the disease. The relationship between biomechanical factors and inflammatory cytokines is not fully understood but it is believed that these factors play an important role in these altered loading models of OA. Currently, there is significant evidence from several animal studies, that IL-1 β (Visser et al., 1999), leptin and TNF- α are involved in these processes (Van den Berg, 1997; Bastard et al., 2008). Much of the research carried out today is focused on the understanding of which biophysical signals

are converted into biochemical signals by chondrocytes; in an attempt to better understand cartilage physiology and hence the pathogenesis of OA. Several *in vitro* studies have used a range of different loading configurations of explanted cartilage to show that static compression inhibits matrix biosynthesis; and cyclic and intermittent compression stimulates chondrocyte metabolism (Guilak et al., 1994; Torzilli and Grigiene, 1998; Bonassar et al., 2000). Later studies elaborated that excessive loading, consisting of high loads for an extended period of time had a deleterious effect; resulting in cell death, swelling and tissue disruption (Torzilli et al., 1999; Milentijevic et al., 2003). The reasoning behind these destructive events has been described by many to be due to: the interpretation of these physical signals by chondrocytes through the integrated action of various ion channels; integrin-mediated connections to the ECM and membrane deformations (Kock et al., 2009; Ramage et al., 2009; Mobasheri et al., 2010). The peri-cellular matrix (PCM), which is a shell of collagen fibres encapsulating the chondrocytes, acts like a transducer of the mechanical and physiochemical signals in the cell environment. The PCM together with its enclosed cell form the functional unit known as the chondron. The signals detected by the PCM can influence chondrocyte metabolism, cartilage homeostasis and overall joint health (Halloran et al., 2012). Some studies have commented on the ability of the PCM along with the ECM to regulate the conversion of mechanical loading to physicochemical changes that can be sensed by the chondrocyte (Lai et al., 1991; Mow et al., 1999). These signals can lead to the over production of inflammatory mediators such as cytokines (Chauffier et al., 2012), chemokines and prostaglandins (Gosset et al., 2006). These cytokines are also expressed in the chondrocytes and cells of the subchondral bone when a certain threshold is reached (Sanchez et al., 2012).

Taking into consideration all the points above, it is evident that the inflammatory cytokine network contributes to the pathogenesis of OA. Increased amounts of these pro-inflammatory cytokines in cartilage, subchondral bone and synovium are all believed to be pivotal to the development and progression of the structural and functional changes in the OA joint. Synovitis, has been shown to be one of the major contributors to the symptom severity of OA, the rate of cartilage degeneration, as well as the progression of OA from early to late stage. The aging process and a population increasing in weight, are also factors that can affect joint morphology, cell metabolic activity and mechanical properties of different underlying tissues, associated with the onset and progression of OA. The view of OA is one that has changed vastly over the years. It is now seen as a complex, multi-etiological disease, in which the underlying molecular and biochemical changes are still poorly understood. Focus has to be made in our understanding of the individual roles, mechanism and functions

of the several cytokines (IL-1 β & TNF- α) and MMPs (MMP-3, MMP-9 & MMP-13). This fundamental knowledge will be key to uncovering the underlying disease mechanisms, which will in turn give better solutions for the treatment of OA at both early and late stages.

1.4 Cartilage Treatments and Research

1.4.1 Early Intervention for Cartilage Defects

Early intervention to repair cartilage defects is desirable in order to prevent or delay disease progression to OA. In any patient with cartilage defects, the aim is to provide them with a means by which they will no longer experience pain or discomfort in their joint, and are able to regain normal activities. There are many different therapeutic approaches to achieve this: viscosupplementation, steroid injections, surgical procedures and more recently tissue engineering approaches. The following section will discuss these treatments and their efficacy as well as highlighting current research relevant to this thesis.

1.4.1.1 Pharmacological Treatment

Non-steroidal anti-inflammatory drugs (NSAIDs) are a form of palliative treatment for the early signs of OA. They aim to reduce/manage pain in symptomatic patients by reducing inflammation and restoring mobility. The drugs include painkillers or specific drugs that aim to control/inhibit the production of inflammatory mediators (e.g. MMPs, aggrecanase's, IL-1 β , COX-2 and cathepsins) (Hunter and Matthews, 2011). Examples of oral NSAIDs and topical NSAIDs are discussed by Strand *et al* (Strand *et al.*, 2011) and Roth *et al* (Roth and Fuller, 2011) respectively.

1.4.1.2 Viscosupplementation

As OA progresses further, the analgesic properties of NSAIDs prove insufficient and therapy can be supplemented via intra-articular injections of hyaluronic acid and/or corticosteroids. Glucosamine, CS and hyaluronic acid (HA) have all been tested as successful viscosupplements, with hyaluronic acid being used most frequently (Vangsness *et al.*, 2009; Miller and Clegg, 2011; Sherman *et al.*, 2012; Migliore and Procopio, 2015; Vasiliadis and Tsikopoulos, 2017). HA is a naturally occurring polymer found in the synovial fluid, which becomes sparse in OA synovial fluid.

HA has been vastly researched for its efficacy in controlling pain, reducing inflammation in OA joints and improving joint motion (Chang *et al.*, 2013; 2011; Leighton *et al.*, 2014). Most of the HA therapies available require multiple injections (3 to 5); in order to attain the desired results, due to the rapid degeneration of HA within the joints (Altman *et al.*, 2004). The stabilisation and hence consequent durability of HA within the joint, may reduce the number

of injections required to attain a longer-term result in the treatment of OA (Chevalier et al., 2010). Therefore, a single injection of HA therapy was introduced as an alternative in terms of logistics, cost and tolerability. This not only ensured comfort, but also safety to the patients by removing the risk associated with frequent injections. Altman *et al*/demonstrated the efficacy and safety of a single intra-articular injection of non-animal stabilized hyaluronic acid (NASHA), in patients with knee OA. This 26 week randomized, double blind, multicentre study showed that there was no statistical difference between patients injected with NASHA and those given the placebo (saline solution) (Altman et al., 2004). The nature in which this study was carried out however, via the inclusion of patients with OA at other sites may have skewed the overall results; as there were significant benefits seen over the placebo when the patients selected had OA confined to the knee. Therefore, future studies that scrutinize a local therapy should consider stratifying the population to those that have OA in a single joint. A similar study by Borrás-Verdera *et al.*, also investigated the efficacy and safety, alongside the long-term effects, of a single intra-articular injection of 2% HA + 0.5% mannitol in knee OA patients (Borrás-Verdera et al., 2013). This study was the first to show that a single intra-articular injection of HA was an effective treatment for knee OA as it significantly reduced pain, increased joint functionality and had relatively low incidences of adverse effects.

While clinical studies seem to provide evidence for the therapeutic value of HA injections; *in vitro* studies on the boundary lubrication capabilities of HA are still a matter of debate, as discussed in Section 1.2.5.2. Nevertheless, any form of viscosupplementation is only really considered as an early stage intervention and in most cases to prolong the time before surgical intervention. Currently, there is little evidence supporting the effectiveness of viscosupplementation in severe cases of surface and underlying tissue damage in AC.

1.4.2 Surgical Procedures for Cartilage Repair

There are several therapeutic approaches to treat individuals with cartilage lesions that if left untreated could lead to OA. These include different types of arthroscopy procedures such as lavage, debridement and micro-fracture.

1.4.2.1 Surgical Interventions without cells

1.4.2.1.1 Lavage

Lavage has been reported to be beneficial to patients with cartilage lesions and painful knee joints. This arthroscopic procedure involves a simple thorough rinse of the joint, to remove any tissue debris within the joint space (Livesley et al., 1991). However, this procedure has only proven successful in a handful of patients and in some studies success, has been shown

to be attributed to the 'placebo effect of surgery'. There are currently no convincing scientific or biological explanations which can be related to the beneficial effects of this technique. However, some reports indicate that the effects last up to 1 year or more. It has been speculated that the extensive rinsing, may remove some of the intra-articular active pain signalling molecules. Hunziker *et al.* added that the removal of proteoglycans and aggrecan molecules from the cartilage surface, could promote adhesion of repair cells, which could promote an anti-inflammatory response (Hunziker and Kapfinger, 1998). Nonetheless, evidence is lacking in the literature to support the use of this surgical technique, and most studies comment that there is no substantial relief of pain in patients who have undergone lavage treatment (Gibson *et al.*, 1992; Ontario, 2005).

1.4.2.1.2 Debridement

Debridement involves the removal of free bodies from the joint space as well as excision of osteophytes (Gibson *et al.*, 1992). There is no substantial evidence from *in vivo* studies of beneficial biological effects of this procedure. In addition to this, both experimentally (Messner *et al.*, 2001) and clinically (Neyret *et al.*, 1994), this procedure has been shown to aggravate the OA condition. Several clinical studies (Sprague, 1981; McGinley *et al.*, 1999; Kruger *et al.*, 2000), have reported variable findings, ranging from good pain relief in about 65% of patients, through to moderate pain relief in 50% of patients to very poor pain relief; nevertheless even when results have been reported to be good, it is stressed in the literature that pain relief is only temporary.

1.4.2.1.3 Microfracture

This is a type of reparative treatment is for chondral lesions usually less than 2-3 cm in diameter, for patients who have moderate demands due to their lifestyles (Detterline *et al.*, 2005). This treatment involves the drilling of holes (0.5-1 mm in diameter (Knutsen *et al.*, 2004) and 3 mm in depth (Mithoefer *et al.*, 2005)) through the bone and into the bone marrow cavity. This procedure allows for direct access to the bone marrow, exposing the underlying mesenchymal stem cells (MSCs). These stem cells are believed to initiate the healing process and lead to the formation of fibrocartilage. Microfracture has been widely used; however, it has been reported to only have a short-term improvement in the joint function. The majority of reviews of medium to long term studies, have reported that the tissue formed is not hyaline-like. This is mainly due to the initial hyaline-like tissue formed becoming fibrous in nature and deteriorating as a result of the sub-optimal biomechanical properties of the repair tissue (Matsiko *et al.*, 2013). Unfortunately, this repair tissue eventually fails. Therefore, this type of treatment option only serves to delay the eventual requirement for other reparative methods, or joint replacement in more severe cases. This

said, microfracture can often be combined with other treatment methods to give more promising results in the long term (Nukavarapu, S. P.; Dorcenus, D. L., 2013; Matsiko et al., 2013).

All these operative approaches only result in the short term, temporary removal of pain and do not really have any effect in the long term. In some extreme cases, there have been incidences where these techniques have led to osteonecrosis (Rozbruch et al., 1996); reactive synovitis, chondrolysis and an acceleration of articular degeneration (Tabib et al., 1999). The more common problem is however, that these procedures aim to repair the damaged areas of the cartilage surface, by stimulation of growth of new cartilage tissue. However, these techniques form tissue that is variable in composition, structure and durability. In most cases, they form what is known as fibrocartilage, which is significantly inferior mechanically, to healthy hyaline AC. Inevitably this fibrous repair tissue is prone to failure and therefore the patient's symptoms return. Hence, there is hope for more advanced techniques such as those with viable cells, biomaterials and tissue engineered solutions, that they may have more favourable success rates. These advanced approaches are speculated to reproduce better the composition, structure and durability of the original healthy cartilage. Conversely, as they have not all yet been tested in animals and/or patients, the potential success of more advanced treatments is unknown.

1.4.2.2 Surgical Interventions with cells

Autologous chondrocyte implantation (ACI) is a procedure that is used to treat knee cartilage defects. The aim of this treatment is to regenerate hyaline or hyaline-like cartilage, thereby restoring normal joint function. In the literature, there are three generations of ACI. They have small differences between them, contributing to their success or failure in patients. This section will systematically review each of the generations of ACI from earliest to present literature.

1.4.2.2.1 Autologous Chondrocyte Implantation ACI- 1st Generation

The first generation ACI, originally reported by Brittberg *et al.* in 1994 (Brittberg et al., 1994), was defined as a two-stage procedure. The first stage involved arthroscopic biopsy, where 200 to 300 mg of articular cartilage is removed, from a non-weight bearing area of the joint, usually the femoral condyle or inter-condular notch (The Center for Orthopaedics & Sports Medicine, 2003; Brittberg et al., 1994). Chondrocytes are isolated and cultured for about 4 to 5 weeks to expand the cell population by a factor of about 50 (The Center for Orthopaedics & Sports Medicine, 2003; Brittberg et al., 1994). The second stage involves an open surgical procedure (arthrotomy) where the defected area undergoes removal of the dead/damaged

cartilage and smoothing the surrounding living cartilage (The Center for Orthopaedics & Sports Medicine, 2003; Brittberg et al., 1994). Periosteum taken from the patient's tibia (Figure 11) is then sutured over the defect area and the circumference secured with fibrin glue (2nd Generation ACI). This creates a watertight patch in to which the autologous cultured chondrocytes are injected, where they grow and mature over time (Brittberg et al., 1994).

It is clear from the literature that there has been some controversy between the use of 1st generation periosteum-ACI cover (PACI) and the collagen-ACI cover (CACI). The CACI is made up of a type I/III bilayer collagen membrane derived from porcine peritoneum and skin, which is able to resorb within the body in a matter of months. Bentley *et al.*, reported that the PACI, acts as a watertight seal and that using a CACI, brought about the same if not better results in patients (Bentley et al., 2003). The study showed promising results, with 51/58 (88%) patients (46 underwent CACI and 12 underwent PACI); showing excellent results favouring this hypothesis. Gooding *et al.* carried out a more recent study, consisting of a two-year follow-up of both of the ACI techniques, showing very similar results (Gooding et al., 2006). Furthermore, Gooding *et al.* (Gooding et al., 2006); reported that 26/35 (74%) of patients, treated by CACI had good-excellent results compared to 22/33 (67%) of patients, treated by PACI. They concluded that the PACI technique is not essential for the development and maturation of hyaline cartilage repair and that the CACI technique is better than PACI. This was attributed to its decreased invasive procedure and lower resorption rate compared to the high incidence of graft hypertrophy, delamination and failure rate of the PACI; reported in many recent studies (Minas, 2001; Minas and Bryant, 2005; Zaslav et al., 2009; Harris et al., 2011).

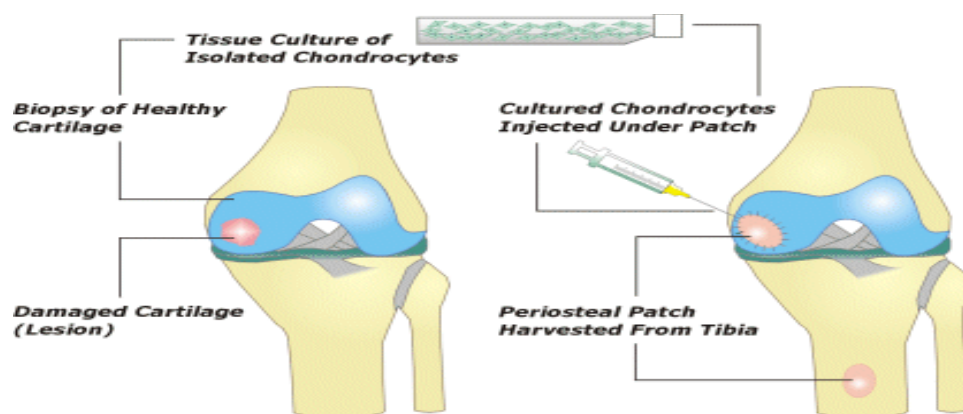


Figure 11: Autologous chondrocyte implantation procedure using tibial periosteum for cartilage repair (Smith, 2005).

1.4.2.2.2 ACI - 2nd Generation

Second generation ACI, also defined as a two-stage procedure, involves an initial arthroscopic biopsy and either an open arthrotomy; or a favoured arthroscopic implantation

of the cultured chondrocytes through cell-seeded, 3-dimensional, bio-absorbable scaffolds (Kon et al., 2008). This technique is somewhat similar to first generation ACI. The difference is that due to advanced methods, prior chondrocyte seeding and the ability for secure graft fixation without sutures means that there is no need for an open arthrotomy, allowing for an all arthroscopic procedure (Marcacci et al., 2002). Several studies using one of the most common 2nd generation ACI (Hyalograft C), show that this technique provides good structural support, allowing for cell to cell contact, cluster formation and ECM production leading to excellent clinical results (Grigolo et al., 2002; Kon et al., 2009; Knutsen et al., 2010). However, despite these favourable clinical results, most of the reported clinical studies are only short to medium term follow ups. Additionally, as reported earlier with the 1st generation techniques, many different approaches may seem favourable in the short term, but the quality of the repair tissue might be influenced in long term results. More recent studies by Gobbi *et al.* (Gobbi et al., 2009) and Nehrer *et al.* (Nehrer et al., 2009), have aimed at reviewing the outcomes of 2nd generation ACI after 5 and 7 year follow-ups, respectively. These studies have reported this specific technique to have good clinical outcomes compared to the 1st generation ACI techniques. However, as a result of the increased complexity of this type of procedure and its method of implantation, there were several drawbacks highlighted by Nehrer *et al.* They reported that the procedure was only successful with young patients sustaining single cartilage defects and implant hypertrophy was high. Although not many cases were reviewed in that particular study, it agrees with the later findings of Gobbi *et al.* (Gobbi et al., 2009) and Marcacci *et al.* (Marcacci et al., 2005). They added that although this method can be very patient specific, it is advantageous in terms of easy handling and application of graft material through minimally invasive techniques. Hence, shortening surgical time and post-operative care of patients (Gobbi et al., 2009; Harris et al., 2011). Nonetheless, further long-term studies (10 years plus) are required to assess the durability of the tissue repair produced using this 2nd generation technique, which will help in further identifying this approach is patient specific or whether it can be used for all types of patients.

1.4.2.2.3 ACI - 3rd Generation

Third generation ACI can be either defined as a one or a two-stage process. It can either consist of an arthroscopic or open surgery, with the implantation of a 3-dimensional matrix containing *in vitro* treated autologous chondrocytes. This particular type of approach uses a matrix associated chondrocyte implantation technique (MACI), which consists of either a protein based polymer, such as collagen or fibrin, or carbohydrate based matrix such as a hyaluronic acid sponge.

Trattnig *et al.*, demonstrated the use of a collagen type I/III MACI and a hyaluronic acid sponge, in 20 human patients to test cartilage regeneration over 52 weeks using high resolution non-invasive magnetic resonance imaging (MRI) (Trattnig *et al.*, 2005). They concluded that both MACI techniques were able to completely fill the defect in terms of thickness, length and homogenous structure, producing regenerated cartilage similar to that of native hyaline cartilage (Trattnig *et al.*, 2005). The reason behind the increasing success of these third-generation ACI techniques is the fact that they do not have to be sutured onto the defect like the PACI & CACI; instead fibrin glue is used, which not only reduces operating times if multiple grafts are needed, but allows for a minimally invasive approach. In addition, the seeding of autologous chondrocytes onto a larger, rougher, less tightly woven collagen type I/III membrane structure (Figure 12), allows for better attachment and even distribution of cells over the implant (Cherubino *et al.*, 2003).

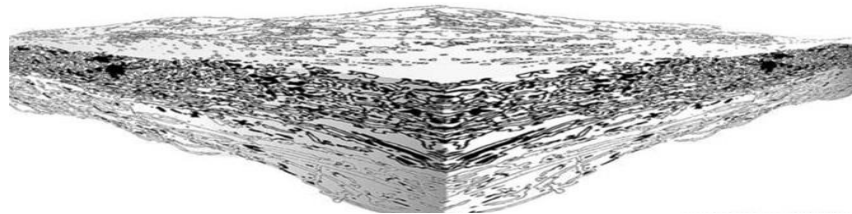


Figure 12: Diagrammatic representation of the collagen I/III membrane showing rough and smooth side (Gibson *et al.*, 2006).

There have been an increasing number of studies comparing the effectiveness of MACI (3rd generation) over the CACI (2nd generation) approaches (Gibson *et al.*, 2006). A 7-year study by Rogers *et al.* reported improved clinical outcome scores for both approaches, with better improvements seen in patients implanted with MACI (Rogers *et al.*, 2010). However, a similar 12-month study showed an increase in knee scores for both approaches, with no significant difference in patient satisfaction between the two approaches (Bartlett *et al.*, 2005). This could be associated with the fact that the MACI operation was performed as an open procedure (arthrotomy) as opposed to an arthroscopic surgery. MACI tends to lend itself for arthroscopic implantation techniques and has shown better long-term results in terms of increased range of motion, decreased pain and decreased post-operative recovery (Laffargue *et al.*, 1999). Although there have been reports of technical difficulties with this arthroscopic procedure, this MACI technique is still in its infancy with the potential to do well (Erggelet *et al.*, 2003; Marcacci *et al.*, 2002).

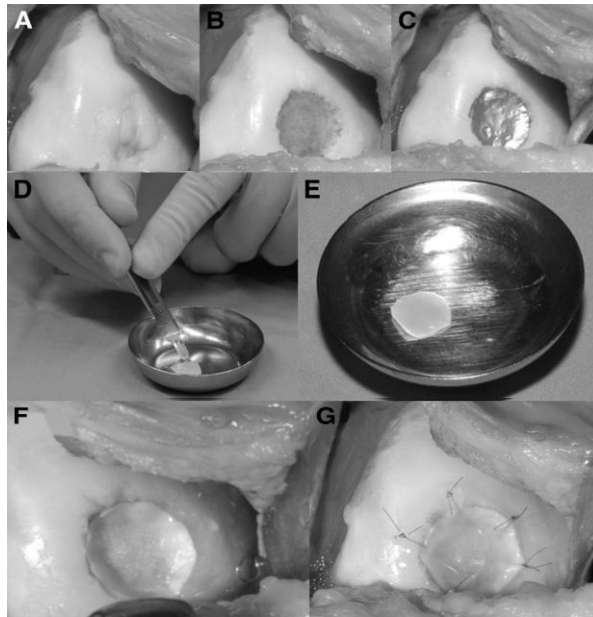


Figure 13: Chondrocyte-Seeded Type I/III collagen membrane for autologous chondrocyte transplantation. Defect Cartilage (A), After debridement of defect (B), Foil template of the size of the cartilage defect (C), Chondrocytes are applied to the rough side of the MACI graft, adherence occurs after a few minutes (D & E), the cell-matrix construct is attached to the defect area (rough side down towards the subchondral bone) (F), bio-resorbable sutures are put in place to fix the cell-matrix graft into place before fibrin glue is applied for additional fixation and sealing (G) (Niemeyer et al., 2010).

It can be concluded that MACI is a reliable 3rd generation ACI technique, with several successful outcomes over the last 5-8 years, for the treatment of defects in the knee. It offers several advantages over the previous generation techniques, in terms of reducing graft hypertrophy, implant morbidity and operating time. The literature shows good mid-term results, suggesting that this technique will be as successful as its predecessor PACI. Nonetheless, longer term follow-ups are needed to fully assess the durability of this ACI technique.

Having reviewed all generations of ACI, it is clear that the failure rate in all generations is relatively low. Failures are higher in 1st generation PACI and considerably lower in 1st generation CACI and 2nd generation techniques. Delamination and hypertrophy is most common in PACI, especially in open arthrotomy procedures. The use of collagen based membranes and second generation techniques has encouraged the use of all arthroscopic implantation, which has greatly improved the complication, failure and re-operation rate of ACI. Third generation techniques are still in their infancy and therefore require long term follow-ups to see their durability in patients. However, up until now they have shown results with minimal complications and revision rates, which is supported by the extensive review performed by Harris *et al* (Figure 14) (Harris et al., 2011).

Complication	% of 1 st generation PACI subjects	% of 1 st generation CACI subjects	% of 2 nd generation ACI subjects	% of 3 rd generation ACI subjects
Hypertrophy of graft	18	3	1	0
Delamination	5	2	2	25
Arthrofibrosis	3	2	2	0
Superficial infection	<1	1	<1	0
Septic knee joint	<1	0	<1	0
Deep vein thrombosis	<1	<1	0	0
Pulmonary embolus	<1	0	0	0
Deaths	0	0	0	0

Figure 14: Complications after ACI (diagnosed by clinical exam, MRI, and arthroscopy). Adapted from: (Harris et al., 2011).

1.4.2.3 Osteochondral grafts

The use of osteochondral grafts is generally reserved for larger articular lesions (>2cm³ diameter) that sometimes cannot be repaired via ACI. These techniques can also be used when lavage and debridement have failed in patients, usually because their lifestyles exert a high demand on their joint, such elite athletes. There are two types of osteochondral graft that can be used. An autograft, taken from a non-load bearing area of the joint from the same donor and an allograft which is taken from a genetically non-identical donor. Autografts are preferred for small to medium defects (<3 cm in diameter) in high demand patients of an older age but larger defects (>3 cm in diameter) tend to use allografts. Both of these osteochondral graft types can be applied to the technique of mosaicplasty, whereby a number of cartilage plugs, extracted from a non-weight bearing region of the joint are implanted back into the defected area (Detterline et al., 2005; Bentley et al., 2012). Both of these techniques have their advantages and disadvantages for their specific uses. Both types of graft take plugs from different location and encompass the same problem. The varying topography of the donor site does not always match that of the recipient's site and hence causes changes in the biomechanics and loading of the joint. Solheim *et al.*, published a long-term follow-up study showing promising results for the autograft, 9 years after surgery (Solheim et al., 2010). However, Haene *et al.* disputed this, arguing that due to the multiple surgeries that are required for autografts, there is damage to surrounding tissue and more risk of chondral tissue damage, they also attributed donor site morbidity to this specific technique (Haene et al., 2012). Furthermore, a randomised control trial carried out by Bentley *et al.* showed that mosaicplasty using autograft tissue was significantly inferior to the preferred ACI (Bentley et al., 2003).

Allografts also have disadvantages, which makes them less favourable than autografts. These include the onset of immune reactions due to the detection of allogenic tissue, which may

carry a risk of disease transmission, reported in a few cases (Haene et al., 2012). Conversely, Gortz *et al.* promoted the use of these grafts, their results showed good to excellent outcomes in up to 80% of cases and most importantly that the larger defects were successfully filled. A very recent study focusing on the outcomes of allograft transplantation in the knee showed favourable outcomes and high satisfaction rates in patients who had an intermediate follow up. They noted that patients with certain etiologies tended to have more favourable results as did younger patients, but there were too few in this study for it to be conclusive (Chahal et al., 2013).

Many of the studies mentioned, particularly the latter, have failed to produce prospective cohort studies in which several comparative cohorts are included. This would further help evaluate the efficacy of osteochondral grafts as a reparative treatment for cartilage defects. Nonetheless it is clear from the literature that autografts are preferred over allografts simply because of no immune rejection and better integration with surrounding tissue (Chahal et al., 2013; Versier and Dubrana, 2011).

1.4.2.4 Joint Replacement

When cartilage degeneration is severe beyond repair, the only option left is to replace the joint with a prosthetic device. These prosthetic devices are known as total joint replacement (TJR). TJR consists of replacing the damaged bone and AC surface with hard smooth bearing components. In the knee, the most common choice of material is metal-on-polyethylene, however ceramics are also being introduced to replace the metal femoral component (Voss et al., 2016; Bergschmidt et al., 2016; Nakamura et al., 2017). This TJR will not only relieve the patient from pain, but it will also improve their quality of life. While the expected lifetime of these conventional TJR is harder to determine, it is not unlimited (Atkinson, 2017). Nevertheless, patients today can look forward to potentially benefitting from new advances that could increase the lifetime of these TJR (Kunčická et al., 2017).

1.4.3 In Vitro Tissue Engineering of Cartilage

The failure of the aforementioned regenerative techniques is mainly due to the insufficient filling of the defect area and the fact that the tissue regenerated is fibrous in nature (Huang et al., 2016). These various surgical/therapeutic approaches have resulted in the formation of fibrocartilage, which is weak in its biomechanical properties compared to the desirable hyaline cartilage found at healthy joints (Cancedda et al., 2003). The ideal treatment would be one in which early cartilage defects are repaired by promoting the formation of hyaline cartilage *in vivo*. Other ways of treating cartilage defects, in the short term, could be to

reduce the further degeneration of cartilage by being able to restore the biochemical and biophysical properties of the damaged cartilage as a result of OA.

Tissue engineering of cartilage is a method by which this might be achieved. In situ tissue engineering approaches, such as ACI have undergone a great deal of change and development in the past few years as discussed above. Moving on from this approach are *in vitro* tissue engineering approaches that focus on developing cartilage constructs for implantation. It involves isolating and expanding cells *in vitro*; seeding them onto biomaterial scaffolds; culturing the cell/scaffold complex to create cartilage equivalents and then finally implanting them back into the body to repair the tissue defect. Choice of cell source is an important factor to be considered as some cells are harder to obtain than others, with many of them not differentiating before they are implanted into the patient (Chung and Burdick, 2008). This following section will systematically review the success of some of the cells sources; as well as some of the material types used in tissue engineering of cartilage, highlighting the reasons for their use and limitations.

1.4.3.1 Cell Source

To this day the optimal choice of cell source has not been identified. However, there is some evidence that the preferred choice of cells is chondrocytes (Chung and Burdick, 2008). Chondrocytes are the naturally occurring cells in cartilage, therefore they do not need to be pre-differentiated *in vitro*. But, the difficulty comes when these cells have to be expanded, as they have a tendency to dedifferentiate. Nevertheless, the use of growth factors and chondro-inducive biomaterials upon which the chondrocytes are seeded, may overcome this problem. A list of the cell sources used to date, where they are taken from, and their limitations is given in Table 3.

Table 3: The different cell sources that have been investigated for use in tissue engineering cartilage, along with the respective reasons for selecting them and their limitations for use.

Chondrocytes	
<p><i>Chondrocyte cells can be obtained from articular (Mesa et al., 2006; Li et al., 2004; Bhattacharjee et al., 2015), auricular (Van Osch et al., 2004; Panossian et al., 2001; Lohan et al., 2014; El Sayed et al., 2010; El Sayed et al., 2013; Ishibashi et al., 2017) costal (Tay et al., 2004; Johnson et al., 2004; El Sayed et al., 2010) or nasoseptal (El Sayed et al., 2010; El Sayed et al., 2013) cartilage.</i></p>	
<p>Reason for Choice (Huang et al., 2016)</p>	<ul style="list-style-type: none"> - Found in native cartilage - Natural choice of cell source. - Have been extensively studied in their role of producing, maintaining and remodelling the ECM (Chung and Burdick, 2008; Li et al., 2004).

<p>Limitations (Vinatier and Guicheux, 2016; Correa and Lietman, 2017)</p>	<ul style="list-style-type: none"> - Limited number of them found within native cartilage, therefore need for expansion (Huang et al., 2016). - Expansion in a monolayer causes dedifferentiation of the chondrocytes (Tay et al., 2004; Li et al., 2004; Albrecht et al., 2011), resulting in decreased production of proteoglycan and collagen type II and hence increased production of collagen type I (Chung and Burdick, 2008; Van Osch et al., 2004). - To minimize this problem, authors have suggested decreasing the passage number or optimise the expansion medium components (e.g. specific growth factors, serums and antibiotics) (Huang et al., 2016; Correa and Lietman, 2017; Bhattacharjee et al., 2015). - Use of other heterotopic chondrocytes such as ‘nasospetal’ or ‘auricular’ chondrocytes are better as alternatives as they are easier to harvest, have lower donor site morbidity and possess higher proliferation rates than articular chondrocytes (El Sayed et al., 2010; El Sayed et al., 2013).
Fibroblasts	
<p>Reason for Choice (French et al., 2004; Lee et al., 2001)</p>	<ul style="list-style-type: none"> - Available in greater abundance compared to chondrocytes - Can be directed to express a chondrogenic phenotype (Chung and Burdick, 2008; French et al., 2004; Zhao et al., 2009; Chee et al., 2016).
<p>Limitations</p>	<ul style="list-style-type: none"> - Require differentiation <i>in vitro</i> prior to implantation into patients (Chung and Burdick, 2008) which has proved to be difficult. - However, the use of certain scaffolds and gene expression factors this can be overcome (Zhao et al., 2009).
Stem Cells	
<p><i>Stem cells can be Bone-marrow derived (Li et al., 2005; Chen et al., 2005; Huang et al., 2016; Beane and Darling, 2012), Adipose derived (Huang et al., 2004; Erickson et al., 2002) or Embryonic (Hwang et al., 2006; Kramer et al., 2000; Beane and Darling, 2012)</i></p>	
<p>Reason for Choice (Vinatier and Guicheux, 2016)</p>	<ul style="list-style-type: none"> - Have “multi lineage potential” (Chung and Burdick, 2008). - Can be extracted from a variety of different tissues, making them an attractive choice for cartilage regeneration (Vinatier and Guicheux, 2016). - Does not express molecules of the Class II major histocompatibility complex, which are responsible for immune rejection, therefore it has been hinted that this cell type could be immunologically privileged (Noel et al., 2007; Du et al., 2016).
<p>Limitations</p>	<ul style="list-style-type: none"> - Bone-marrow derived stem cells produce a mechanically weaker matrix than the one produced by native chondrocytes. - Adipose-derived stem cells produce a low concentration of cartilage specific matrix proteins as well expressing collagen type I. - Embryonic stem cells have the problems of purification as well as the difficulty in differentiating them into chondrocytes as well as well-known ethical issues (Chung and Burdick, 2008; Fontan et al., 2017).

From the literature reviewed in Table 3, the majority of the cells sourced in these studies were all taken from one animal species and implanted into another animal of the same species; to see whether they would express a chondrocytic phenotype and hence produce a

new cartilaginous matrix *in vivo* (Mesa et al., 2006; Van Osch et al., 2004; Panossian et al., 2001; Johnson et al., 2004). One study in particular demonstrated that the use of articular chondrocytes from old animals could produce neocartilage *in vivo*, as well as articular chondrocytes from young donors (Mesa et al., 2006). Therefore, the authors suggested that middle-aged and elderly patients could benefit from using their own “aged” articular cartilage as a source of reparative chondrocytes for cartilage defects owing to the fact that it was also immunologically beneficial.

There has been growing interest in the use of human autologous chondrocytes in synthetic scaffold for cartilage regeneration purposes. Human auricular chondrocytes expanded *in vitro* using several growth factors; demonstrated their potential to produce cartilage grafts of high quality compared to costal chondrocytes. Similarly, bone marrow-derived mesenchymal stem cells (MSCs) on a poly-caprolactone (PCL) scaffold in the presence of certain chondrogenic growth factors, differentiated to a chondrocytic phenotype. The use of these autografts seems a practical and effective way to treat cartilage defects in humans, however the limitations in this technique lies in the multiple operations required before these scaffolds can be implanted. Nevertheless, the use of animal models is an acceptable means to investigate the feasibility of different cell sources, for the use in cartilage tissue engineering.

1.4.3.2 Scaffold Biomaterials

1.4.3.2.1 Natural Biomaterials

Attention has been directed onto natural and synthetic materials for their use as the scaffold material in cartilage repair. Natural scaffold such as hyaluronic acid, collagen, chitosan, gelatin and chondroitin sulfate, have been explored as biocompatible and biodegradable scaffolds for the tissue engineering of cartilage. Despite this, they are prone to variable enzymatic degradation in the body, indicating they are not sufficiently mechanically stable for cells to survive *in vivo* (Chung and Burdick, 2008). Nevertheless, Campoccia *et al.* demonstrated through careful chemical modification, that the esterification of a hyaluronic acid gel, significantly improved its mechanical properties (Campoccia et al., 1998). Moreover, Grigolo *et al.* (Grigolo et al., 2001) showed how the development of HYAFF 11 scaffold, an esterified derivative of hyaluronic acid was able to support *in vitro* growth of viable chondrocytes and maintain their chondrogenic phenotype. Furthermore, a study by Facchini *et al.* (Facchini et al., 2006) showed that the same three-dimensional scaffolds seeded with autologous chondrocytes improved the regeneration of cartilage *in vivo*. This 3D Scaffold is now a commercially available product called Hyalograft-C and has been successfully implanted into human patients with knee cartilage defects, as a tissue engineered

regeneration approach to cartilage repair. A 5-year clinical trial showed promising results post-operatively (Marcacci et al., 2002; Chung et al., 2006; Facchini et al., 2006). Despite supportive evidence of its clinical ability, a review in the European Medicines Agency report (Withdrawal Assessment Report: Hyalograft C Autograft., 2013), raised issues regarding quality control and lack of randomisation in Phase III studies. Commercialisation was ceased in 2013.

Another widely used natural polymer is chitosan, derived from chitin commonly found in the exoskeleton of crustaceans. Its high cationic charges mean it can be ionically cross-linked with a variety of polymers, such as chondroitin sulfate, forming a hydrogel. It forms a semi crystalline biodegradable polymer matrix that can support both chondrogenesis and the expression of cartilage extracellular matrix proteins (Suh and Matthew, 2001; Lahiji et al., 2000). An *in vivo* study by Lu *et al.* showed that a chitosan injection effectively repaired defects of rat knee cartilage (Lu et al., 1999). Like hyaluronic acid, chitosan also has poor mechanical strength and elasticity. However, these can be improved by the addition of a cross linker. Mwale *et al.* showed that the use of chitosan cross-linked with genipin, provided a hydrogel for cartilage tissue engineering (Mwale et al., 2008). Similarly, Yan *et al.* and Hrabchak *et al.* found that this combination was successful in the treatment of osteochondral knee defects in rabbits. The crosslinked material was biocompatible and non-immunogenic, which is a common trait of some natural polymers (Yan et al., 2010; Hrabchak et al., 2010; Jeong and Hollister, 2010).

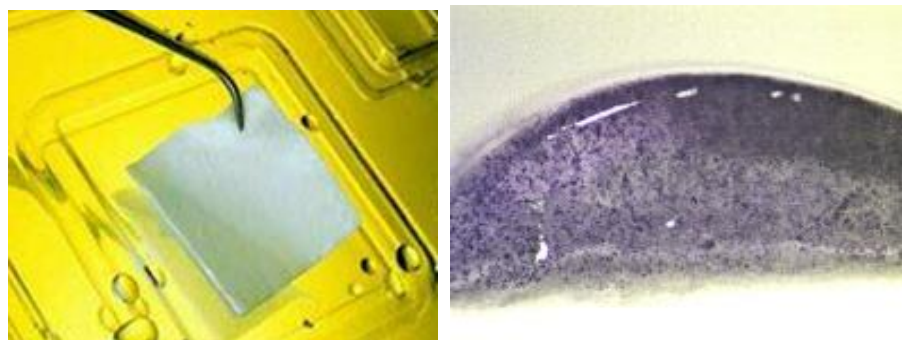


Figure 15: Hyalograft-C scaffold displayed as a commercialised product (left), MTT assay showing the encapsulated chondrocytes in an injectable chitosan-based hydrogel for cartilage tissue engineering (Anika Therapeutics).

The chemical functionalization of hydrogels has been pursued further by Soppimath *et al.*, to develop a 'native-like' environment for cells. These so called "smart" biomaterials have the ability to reversibly gel in response to temperature, ultraviolet light and pH whilst still maintaining the cell viability (Soppimath et al., 2002). This advantageous characteristic means they could be minimally invasively injected into the recipients and form *in situ* at the

defect site, reducing postoperative recovery. Moreover, these biomaterials could play a useful role as carriers, to deliver growth factors that could be released in a controlled manner. Subsequently, stimulating chondrogenic differentiation and *in vivo* proliferation. Wu *et al.*, demonstrated the significance of slow release growth factors, such as transforming growth factor (TGF- β 1) in the promotion of chondrocyte proliferation and matrix synthesis (Wu *et al.*, 2011). Similarly, Kim *et al.* (Kim *et al.*, 2003) and Lee *et al.* (Lee *et al.*, 2004) showed that a combination of TGF- β 1 and the insulin growth factor (IGF-1) in microspheres of chitosan; increased the cartilage ECM synthesis and enhanced the proliferation of chondrocytes in the defected area.

Unfortunately, most of the aforementioned studies utilising hyaluronic acid and chitosan have been short term, very few with FDA approval. The majority of the studies were conducted in animal models, such as nude mice. These promising techniques need to be moved forward into larger animal models, or even clinical trials to test their long term regenerative capacity.

Nevertheless, advances have been made in the production of natural scaffolds for cartilage repair that have undergone extensive animal studies or/and some that have gone through phases I-III clinical trials. These clinical products are summarised in Table 4. The efficacy and success of these clinical products was measured through several common outcome measures. To list a few: International knee documentation committee (IKDC) score; knee injury and osteoarthritis outcome score (KOOS); western ontario and McMaster universities osteoarthritis index (WOMAC); visual analogue scale (VAS) for pain; international cartilage repair system (ICRS) score and the magnetic resonance observation of cartilage repair tissue (MOCART) score. The majority of these are forms/questionnaires; in which treated patients fill in questions about how they feel with their new implant. Other methods include medical evaluations of MRI images and evaluating range of motion (ROM) that patients are able to achieve. Although these questionnaires can be subjective; they have been used for many years and are said to be a reliable way of assessing post-operative success.

Table 4: Current clinical products on the market with their associated clinical trials that have been completed or are in the process of completion. Adapted from: (Huang *et al.*, 2016).

Product	Clinical studies (completed)	Clinical studies (ongoing)	Clinical scores and outcomes.
Biocart™II fibrinogen/hyaluronic acid scaffold seeded with expanded autologous	- Preliminary study (n=8) [2008] - Phase II study (n=40) [2012]	N/A	Showed feasibility to treat cartilage lesion of 1-8 cm ² . IKDC scores

chondrocytes (26,27,29).			improved at 6 & 12 months.
Cartipatch® - Agarose-alginate hydrogel seeded with expanded autologous chondrocytes.	- Multi-centre study (n= 17) [2008] - Phase III study comparing Cartipatch® to mosaicplasty (n=58) [2013]	- Phase III study comparing Cartipatch® to microfracture was terminated.	Largely used to treat osteochondritis dissecans (OCD). Defects ranged from 1.0 to 5.1 cm ² . IKDC scores improved at 2 years over baseline.
Chondrospheres® - Small spheroids of neo-cartilage composed of expanded autologous chondrocytes and their associated matrix.	- Over 7200 patients treated since 2004. - Multi-centre study (n=42) [2009] - Investigator-initiated trial (n=37) [2012]	- Phase II study to finish Nov. 2017 (2-year outcome). - Phase III study to finish Dec. 2020 (5-year outcome).	Improved range of motion (ROM), pain levels were reported at 2 year follow up, however IKDC and WOMAC scores remained unchanged.
NeoCart® - Honeycomb bovine type I collagen scaffold seeded with expanded autologous chondrocytes.	- Phase I study (n=8) [2009] - Phase II study comparing to microfracture (n=30) [2012]	- Phase III study (n=245) to finish Jul. 2017 (1-year outcome measures)	- Ph I - Pain scores and ROM were improved over baseline values at 2 years. - Ph 2 – IKDC, KOOS and VAS scores were all significantly improved vs microfracture.
NOVOCART® 3D - Biphasic type I collagen scaffold seeded with autologous chondrocytes.	- Over 6000 patients treated since 2003. - Prospective study (n=23) [2014] - Other prospective studies (n=30-41) [2009,2014,2012] - Study on treatment of OCD [2011]	- Phase III study (n=233) comparing NOVOCART® 3D to microfracture finish Jul. 2018 (2-year outcome) - Non-interventional study (n=80) to finish Sept. 2019 (3-year outcome) - Phase III study (n=261) comparing NOVOCART® 3D plus to microfracture finish Jun. 2019 (5-year outcome).	- Showed feasibility to treat cartilage lesion of 2-6 cm ² . - Prospective clinical studies have all shown improvements in the IKDC, VAS and MOCART scores at 1 and 2 year follow ups.
RevaFlex™ - Scaffold-free neocartilage disc composed of allogeneic juvenile chondrocytes and their associated matrix.	- Phase I/II study (n=12) [2013]	- Phase III study (n=225) comparing RevaFlex™ to microfracture finish Jul. 2019 (5-year outcome).	- Showed feasibility to treat cartilage lesion <5 cm ² . - Immunological and histological analysis showed no adverse immune response, indicating that allogeneic chondrocytes may be immune-privileged.
CaRes® - Type I collagen hydrogel embedded	- Multi-center study (n=116) [2011]	N/A	IKDC scores were improved from baseline in multi-centre study and in the retrospective

with primary autologous chondrocytes.	- Retrospective study comparing to microfracture (n=20) [2013]		comparative study showed no significant difference in 2 methods.
---------------------------------------	--	--	--

From the literature reviewed in Table 4, it was highlighted that although many of these natural scaffolds are able to promote hyaline cartilage formation, future/current clinical trials have been halted or stopped. The authors did not comment on the reasons for this. Nevertheless, if these longterm clinical studies were to be successful, eventually gaining FDA approval; the clinical application would still need to be thoroughly considered and thought-out for future use in humans. Having said this, there were some clinical products (Chondrospheres[®], NeoCart[®], NOVOCART[®] 3D and RevaFlex[™]), which successfully made it through to Phase III clinical trials and are yet to reveal their long-term success in patients.

1.4.3.2.2 Synthetic Biomaterials

Aside from natural polymers, there are also synthetic polymer scaffolds. Their chemical and physical properties can be modified to alter their degradation rate and mechanical characteristics, which is harder to do in natural polymers. Common synthetic polymers used in cartilage tissue engineering are the family of poly α -hydroxy esters, such as poly-glycolic acid (PGA), poly-lactic acid (PLA) and PCL. The growing research interest of these synthetic polymers is due to their biocompatibility, and FDA approval for clinical use for more than 20 years (Mouw et al., 2005). The physical properties of these scaffolds, such as pore size, polymer crystallinity and fibre size are key features that regulate their degradation rates. Highly porous PGA has been extensively used in cartilage regeneration as it is able to degrade in about 6-8 weeks. These PGA scaffolds have exhibited high rates of initial cell growth, maintenance of chondrocyte function and secretion of ECM similar to that of healthy hyaline cartilage (Mouw et al., 2005; Hooper et al., 1998). Highly crystalline PLA has also been studied for cartilage repair and can take about 6-18 weeks to degrade. This synthetic material has shown good chondrocyte proliferation and GAG production *in vitro*. However, cell growth and matrix production is much lower than that of PGA (Hooper et al., 1998; Lee and Shin, 2007). The pioneers behind the *in vitro* study of the family of poly (α -hydroxy esters) were Vacanti *et al.*; whose team reported the ability to regenerate cartilage in animal models (Vacanti et al., 1991). This led to further fabrication of various structured synthetic polymers scaffolds to culture chondrocytes or mesenchymal stem cells (MSCs) for regeneration of cartilage *in vitro*. Unlike natural biopolymers that are often prepared in a hydrogel form, synthetic polymers can be fabricated into various pre-formed structures, such as fibres, foams and sponges.

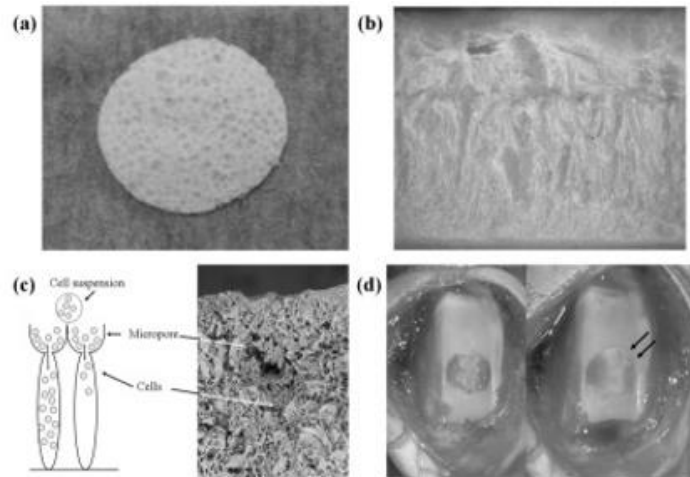


Figure 16: The three-dimensional poly(lactic-glycolic acid) (3D-PLGA) scaffold. The micropore side (cell seeding side) (a) and a cross section (b) of the scaffold. Schematic illustration of cell seeding (left) and scanning electron photomicrograph of cross section of cells seeded in the 3D-PLGA scaffold (right) (c). The cells lie in a uniform array at the palisades, similar to hyaline cartilage. Gross appearance of a cartilage defect in the patella groove of a rabbit implanted with a complex between adherent bone marrow cells and 3D-PLGA scaffold (d). The arrows indicate cell/PLGA scaffold (Jin et al., 2009).

Holland *et al.* highlighted that the manufacturing process of certain synthetic biodegradable polymers has a significant effect on cell migration of chondrocytes and differentiation of MSCs (Holland and Mikos, 2006); which is why the development of nanostructural materials has been an emerging trend in cartilage tissue engineering. Nanostructured scaffolds can be fabricated via a technique called electrospinning. Two detailed studies performed by Li *et al.* showed that chondrocytes cultured in PCL nanofibrous scaffolds maintained their chondrocytic phenotype (Li et al., 2003), similarly MSCs were successfully induced into chondrocytes (Li et al., 2005). Li *et al.* pursued a further *in vivo* study showing that chondrocyte-MSC laden nanofibrous scaffolds, grown in a bioreactor, were able to repair full thickness defects in pig femoral condyles (Li et al., 2009). Despite this, current studies have shown interest in new synthetic biomaterials such as poly glycerol-co-sebacate (PGS) and poly octanedioil-co-citrate (POC) as they have been found to have similar mechanical stiffness to articular cartilage, potentially making them feasible for cartilage tissue engineering, however their regenerative potential is still unknown (Wang et al., 2003; Kang et al., 2006; Jeong and Hollister, 2010). Claire *et al.* proposed a method in which PCL, PGS and POC were fabricated into the same fixed 3D architecture. This enabled the study of solely the material to determine its effects on cartilage regeneration *in vitro* (Jeong and Hollister, 2010). The study reported that POC provided optimal support for cartilage regeneration in terms of maintaining cell phenotype, ECM production and differentiation of chondrocytes. Conversely, PGS and PCL were found to be less favourable as they caused de-differentiation of some chondrocytes and high matrix degradation.

Other synthetic scaffolds used in cartilage regeneration which have both undergone clinical trials are; a commercial product named Bioseed[®]-C (biodegradable polymer scaffold) and INSTRUCT (poly (ethylene oxide-terephthalate)/poly(butylene terephthalate) (PEOT/PBT) scaffold seeded with primary autologous chondrocytes and bone marrow cells). Studies using Bioseed[®]-C in human clinical trials, have reported great clinical success. At 2 years, significant improvements in the KOOS score were reported when compared to baseline values and histological images showed good integration and formation of cartilaginous repair tissue (Ossendorf et al., 2007). At 4 years significant improvements in the ICRS, IKDC and KOOS scores were reported when compared to baseline and MRI examinations showed complete filling in 72.7 %, moderate filling in 25 % and less than 50 % filling in 0.3 % of patients (Kreuz et al., 2009; Kreuz et al., 2011). Over 300 patients have been treated with the Bioseed[®]-C scaffold since 2003 (BioTissue - BIOSEED[®]-C). A recently a long-term follow up study (12 years), highlighted that morphological evaluation by MRI showed moderate to complete filling in 10 of 14 patients. From which qualitative evaluation of the cartilage ultrastructure showed hyaline-like repair tissue in repair site, 12 years after implantation (BioTissue - BIOSEED[®]-C). This scaffold is currently being widely used in Europe with hopes to move into the American market (Huang et al., 2016).

The INSTRUCT scaffold utilises a modern approach of a bio-plotter device to create the desired porous lattice structure (approx. 170 µm diameter fibres, 200 µm pore size, and 56% porosity) (Hendriks et al., 2013). An initial study in nude mice, reported that the softer PEOT polymer of the scaffold functions to support the chondrogenic phenotype, whilst the PBT part, increases the material stiffness (Moroni et al., 2007). Several authors commented on the ability to easily fine tune the mechanical properties of this scaffold by altering the ratio of PEOT to PBT, which also gave rise to varying pore sizes for better cell aggregation, alongside differing rates of degradation (Jansen et al., 2008; Deschamps et al., 2001; Emans et al., 2012). This bio-resorbable scaffold (12 months) has a unique way of being input into patients via a single surgical intervention, whereby the patient's cells and bone marrow aspirate are inserted into a semi-automated machine (INSTRUCT cell processor). The machine isolated the chondrocytes, mixes them with marrow cells, adds fibronectin and seeds them onto a scaffold, all of which can be done in under 1 hour (Moroni et al., 2007; Mechanically Functional Scaffold Technology, 2015; The INSTRUCT Products, 2015). A Phase II trial completed in 2014, with a 2-year outcome, showed improvements in the IKDC and KOOS scores, with 72 % of patient exhibiting hyaline cartilage and 97 % with either fibrocartilage or hyaline cartilage (Hendriks et al., 2013; Slynarski et al., 2015).

From the literature, it is clear that scaffold material, cell source and signalling factors make up the basis of a good tissue engineered construct. Examples of some novel biomaterials used have been reviewed, showing their continuous development as biocompatible scaffold/hydrogels. Not only have these scaffolds been able to meet the mechanical requirements to maintain cell phenotype but they have been able to provide a stable environment in which cells are able to synthesise an ECM, something that was not as well characterised in earlier therapeutic techniques. Furthermore, the incorporation of certain bioactive molecules has shown enhancement in the cartilage regeneration properties as well as cell proliferation. Both natural and synthetic biomaterials have their drawbacks, some of which have viable solutions to them. Aside from this, the prime concern of some of these scaffold materials is that the majority of them are yet to be tested in humans to assess their feasibility.

The current approaches to cartilage repair reviewed in the previous sections have all been shown to have different effects on the regeneration of cartilage. The therapeutic techniques without any active cells have been shown to have only temporary effects on patients, in some cases worsening the condition. Severities of the disease or lesion, age and bone quality have all been reported to have an effect on the surgical outcomes of these therapeutic approaches.

Despite the large number of preclinical and clinical studies reviewed here for cartilage tissue engineering, none of the scaffolds or clinical products discussed were injectable percutaneously. Recent interest has been directed toward the development of self-hardening and injectable materials, that can be used in the percutaneous injection of biomaterials, capable of cartilaginous tissue repair without causing any extra damage to the surrounding tissue. The properties and structures of hydrogels make them ideal candidates for implantation by minimally invasive surgery (Liu et al., 2017; Lum and Elisseeff, 2003; Radhakrishnan et al., 2017). Hydrogels are composed of chains of synthetic or natural macromolecules capable of forming hydrogels after physical, ionic stimuli or covalent crosslinking (Dury and Mooney, 2003; Liu et al., 2017). They are known to exhibit a high level of hydration close to that of the articular cartilage, allowing them to mimic the 3D environment of chondrocytes (Teixeira et al., 2014).

In conclusion, surgeons have a variety of tools that can be used to treat OA cartilage. Age, aetiology, extent of cartilage damage and the lifestyle of the patient, should all be factors that should define the choice of treatment of the patient. The use of minimal invasive surgery should be put into practise where possible in order to avoid open intrusive surgery and put

off joint replacement for as long as possible. One of the most important factors in avoiding the extensive end stage deterioration of cartilage, is to improve the current methods and approaches to diagnose the changes in biochemical and biomechanical properties of cartilage at a much earlier stage of the disease. Equal effort should also be made to develop new methods and biomaterials that can oppose the changes that occur in the ECM of cartilage in early OA, in order to prevent the further progression of the disease. The following section will introduce a novel type of material – self-assembling peptides (SAPs) – that have shown potential as injectable biomaterials for intervention in early cartilage defect and early stage OA. They offer flexibility in function and design, as well as lending themselves to be developed into viable alternatives to joint lubricants that may also have the ability to repair ECM damage.

1.5 Introduction to Peptides

Peptides are short chains of amino acid monomers that through condensation reactions (H_2O produced), form peptide bonds. This covalent bond is as a result of the carboxyl group of one amino acid reacting with the amino group of another (Voet and Voet, 1995; University of Arizona, 2001).

There are 20 main natural amino acids involved in the synthesis of peptides and proteins present in biology. These amino acids are organised according to the polarity of their side chains. All these amino acids have the same basic structure, varying only in their 'R groups' (Ulijn and Smith, 2008). The peptides made from these amino acids are completely ionised at all pH ranges, and therefore can act either as an acid or a base. Cation and anion concentrations in solution can have an effect on the behaviour of these peptides; as these ions can act electrostatically to shield the side chain charges from one another, disturbing any intra and intra molecular interactions (Voet and Voet, 1995).

Proteins that naturally occur in nature are considered to have four levels of hierarchical structure, making them more complex than peptides, which only generally have two levels (Berg et al., 2002). For peptides, the primary structure is the formation of polypeptides. They are made up by a sequence of amino acid residues, determining the specific conformation that is adopted by the peptide. The secondary structure refers to the orientation of the peptide backbone, due to the formation of hydrogen bonding. The main secondary structures are known as α -helix and β -sheet (Berg et al., 2002).

1.6 Introduction into self-assembling peptides (SAPs)

Self-assembling peptides can be thermodynamically driven to self-assemble into well-defined aggregates through weak non-covalent forces. In order of strength, these forces consist of: hydrogen bonding, electrostatic interaction, hydrophobic interactions and Van de Waals (Semino, 2008). The idea behind molecular self-assembly (SA) has become one of the main driving force for the development of these biomaterials. The bottom up approach to the design and synthesis of these functional biomaterials starts with the careful design of the small building blocks that can self-assemble without any external forces and hence lend themselves for the use in nanoscience (Tu and Tirrell, 2004). The structural ordering of the SA process is similar to the one seen in biological proteins, in that there are primary SA, secondary and tertiary SA and finally quaternary folding (Aggeli et al., 2001).

In peptides, one dimensional SA is the formation of singular polypeptide chains. Secondary SA consists in the formation of α -helices and/or β -sheets. Tertiary SA is when either the α -helices and/or β -sheets assemble into 3D structures via side chain interactions of the individual amino acids. The different level of SA are based on protein folding; whilst the last level (quaternary assembly), is when several peptide chains assemble into tape like or globular structures. The SA process can further continue, depending on the physical conditions (pH or ionic strength of solution) into ribbons, fibril or fibres (Aggeli et al., 2001; Aggeli et al., 2003).

1.6.1 Self-assembly mechanism

Self-assembling peptides are able to assemble in one of two ways; nucleated or non-nucleated (classical).

Non-nucleated self-assembly is the free energy change associated with the formation of one dimer unit or higher order aggregates. This stepwise addition of individual units will occur with identical rate constants for each of the associating reactions. Equation 1 gives the free energy change per molecule where; α is the association energy, K_B = Boltzmann constant and T = temperature.

$$\Delta\mu^* = -\alpha K_B T \quad \text{[Equation 1]}$$

Nucleated self-assembly is a more complex self-assembly mechanism. This mechanism involves a critical concentration for the formation of aggregates (nucleation). Below this nucleation point, the majority of molecules in the system will exist as isolated monomers where their φ & ψ angles have any value (Branden and Tooze, 1999). Essentially, the growth or aggregation is inhibited until a particular concentration is reached at which point it will

spontaneously take off. This concentration is known as the critical concentration more commonly known as C^* (Israelachvil, 1992). This mechanism involves two parameters, nucleation energy ($\alpha_n K_B T$) and growth energy ($\alpha_g K_B T$). The latter is associated with the corresponding energy of $\alpha K_B T$, as seen in the non-nucleated SA (Eq 1), however in classical non-nucleated SA the nucleation energy is absent (Israelachvil, 1992).

For peptides to self-assemble in 1D, they must undergo a conformational transition, associated with an entropy loss. This entropy loss is characteristic of the straightening out of a peptide chain from its random coil to its β -strand conformation. This process is described by the energetic parameter, $\varepsilon_{trans} K_B T$. Once this β -strand conformation is reached, further SA can occur once the tape scission energy is increased; $\varepsilon_{tape} K_B T$ (energy required to break tape in 2 pieces) (Aggelli, 2000). This energy is enthalpic in nature, which stems from the intermolecular peptide backbone complementary hydrogen bonds and the side chain interactions. Indeed, SA can only occur when the loss in entropy ($\varepsilon_{trans} K_B T$) is counterbalanced by the gain in enthalpy ($\varepsilon_{tape} K_B T$). The SA mechanism can further continue, where two tapes can associate to form a ribbon structure, stabilised by $\varepsilon_{ribbon} K_B T$. The magnitude of ε_{ribbon} is due to the intermolecular interaction between the side chains. Opposing the stacking of these tapes is what is called the elastic energy $\varepsilon_{elastribbon}$, which originates from the helical nature of tapes. In order for two tapes to stack together, they must both decrease their helical twist to facilitate the presence of each other. Therefore, the ribbon formed has more of a saddle curvature rather than a helical twist. Therefore, if ε_{ribbon} can overcome $\varepsilon_{elastribbon}$, the formation of a ribbon will occur (Aggelli et al., 2001; Fishwick et al., 2003).

Similarly, the stacking of several ribbons one top of one another will form fibrils. This is stabilised by $\varepsilon_{fibril} K_B T$, which is the free energy per stacked peptides in the fibril. This system has an opposing force restricting the formation of fibrils, known as $\varepsilon_{elastfibril}$, which is the energy associated with the untwisting of the ribbons upon stacking. The number of tapes within a fibril is determined by a balance between the gain in attraction (ε_{fibril}), associated with ribbon stacking, and the elastic cost associated with packing of the ribbons in the fibril. Therefore if ε_{fibril} overcomes $\varepsilon_{elastfibril}$, the SA of the fibril will occur. Finally, once a stable fibril is formed, pairs of fibrils are able to entwine edge on edge resulting in the formation of a fibre.

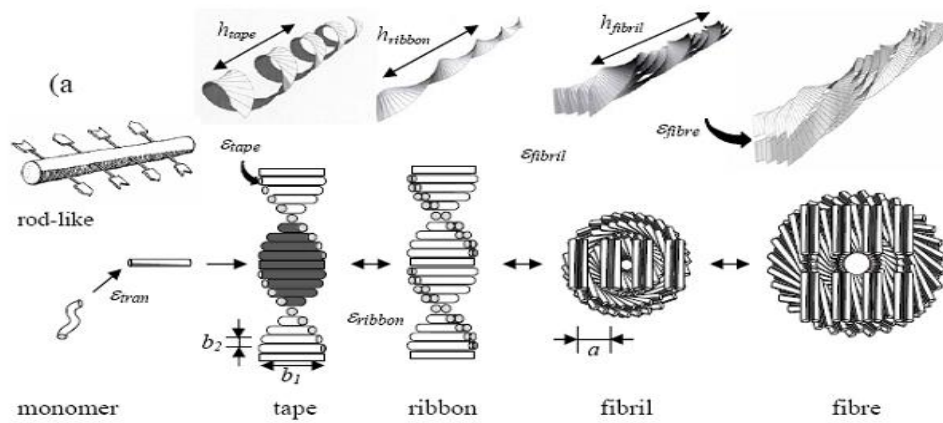


Figure 17: Hierarchical self-assembly of chiral rod like units.

The arrangement of the amino acids within the peptide, along with the changes in energetics, is therefore important to attain the desired SA and functional properties of the SAPs.

In summary, the SA of peptides can be broken down into three distinct phases. The 1st phase is *nucleation*, during which there are stable monomers and some unstable tapes. The monomers and tapes are assembling and disassembling due to there not being enough enthalpic energy to counteract the entropic energy loss. The 2nd phase is the formation of a stable nucleus. Here the enthalpic gain balances the entropic loss and so the first aggregates form (Aggelli, 2000). The concentration at which this occurs is known as C^* . The final stage is the growth stage, where aggregates grow in size until they precipitate out of solution. These three-phases can be seen in what is called a self-assembly curve, which is the fraction of aggregate against the total peptide concentration, a schematic is given in Figure 18.

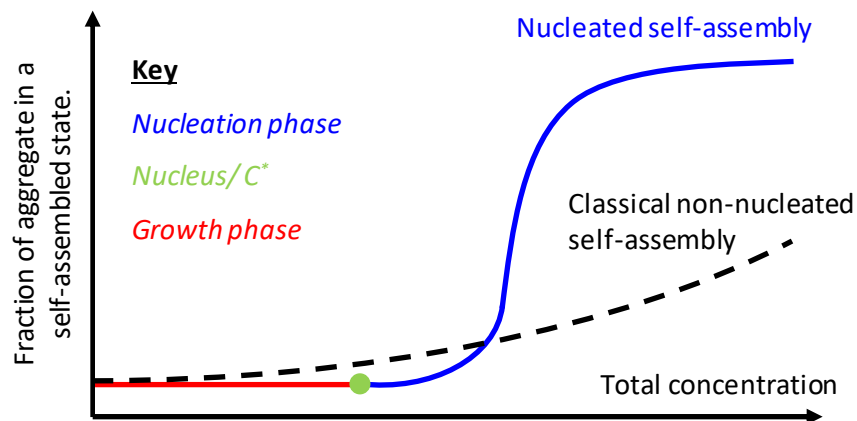


Figure 18: Schematic of self-assembly curve for both nucleated self-assembly & non-nucleated self-assembly of peptides.

1.6.2 Uses of self-assembling peptides in tissue engineering.

Depending on their chemical composition, some β -sheet self-assembling peptides have been shown to be biocompatible with no cytotoxic effects. An example of such peptides is given in a study carried out by Kirkham *et al.*, in which these peptides led to the commercialisation

of a product for dental repair (Kirkham et al., 2007). The use of these peptides was to treat/prevent caries lesion via the insertion of these peptides as a monomeric solution. It was hypothesised that they would polymerise *in situ* via changes in pH or ionic strength; in order to provide a biomimetic scaffold upon which hydroxyapatite nucleation could occur and promote repair. The matrix like structures formed by these peptides not only mimic the biological macromolecules found in the natural ECM of the mammalian skeleton, but are also able to induce the deposition of hydroxyapatite. The reasoning behind this increased mineral deposition of the peptide used (P₁₁-4), was due to the structure of the fibrils formed, which is reminiscent of collagen fibres. The presence of these collagen-like fibres promotes nucleation of hydroxyapatite more readily than normal (Kirkham et al., 2007). The successes of this study led to the commercialisation of a product named, CURODONT™, which is now used to treat caries lesion.

Further uses of SAPs, as biomaterials for the application in tissue engineering, are their use as joint lubricants. Bell *et al.*, was among the first to study the frictional properties of these peptides, which had been designed based on the functional motif of hyaluronic acid, which is commonly used as a viscosupplement and is a very important GAG within the ECM of cartilage (Bell et al., 2006). In static and dynamic friction tests carried out in healthy cartilage pin on plate experiments, it was found that one of the peptides, P₁₁-9, had favourable frictional characteristics, similar if not better than hyaluronic acid. However, this was not the case in damaged cartilage samples (Bell et al., 2006). Nevertheless, the study was able to provide preliminary evidence that these self-assembling peptides are promising candidates in developing effective joint lubricant and could also be used to regulate the AC degeneration in its early stage.

SAPs have also been used for other tissue engineering application such as the formation of hydrogel scaffolds. Kisiday *et al* showed that chondrocytes are able to grow and multiply on a hydrogel scaffold-like material produced by a SAP called KLD-12. The bovine chondrocytes used were not only able to maintain their chondrocytic phenotype and produce cartilage-like ECM, rich in collagen type-II but also showed increased mechanical properties, after 4-weeks of culture *in vitro* (Kisiday et al., 2002).

The examples outlined here are only some of the uses that make these SAPs so promising as scaffolds for tissue engineering and show tremendous promise in the field of regenerative medicine. In depth studies and reviews by several authors cover a vast number of applications for all the different types of SAPs in tissue engineering (Maude et al., 2013; Hosseinkhani et al., 2013; Johnstone et al., 2013; Stephanopoulos et al., 2013; Varaprasad et

al., 2017; Calo and Khutoryanskiy, 2016). A few significant application that SAPs have been used for reduction of blood loss in haemorrhagic sites, which could be used to treat non-compressible torso haemorrhage in battlefield patients (Morgan et al., 2016), wound healing (Schneider et al., 2008; Meng et al., 2009; Loo et al., 2014; Xie et al., 2015), bone repair (Fellah et al., 2006; Ozeki et al., 2011; Short et al., 2015; Xavier et al., 2015; Radhakrishnan et al., 2017), scaffold for regenerating dental pulp (Galler et al., 2012), nucleus pulposus (Collin et al., 2011; Tao et al., 2015; Xu et al., 2015; Miles et al., 2016; Thorpe et al., 2016; Wan et al., 2016; Gullbrand et al., 2017; Wachs et al., 2017) and cartilage (Balakrishnan et al., 2014; He et al., 2014; Kim et al., 2015; Ren et al., 2015; Tatman et al., 2015). Most of the above studies using SAP hydrogels for cartilage regeneration purposes are mixed with cells in complicated multi-step procedures. Some of which use more than one biomaterial to improve the mechanical stiffness's of the gels formed, which can increase the cost of the potential minimally invasive procedure. Nevertheless, these SAP hydrogels have demonstrated good biocompatibility with the host environment and have shown good feasibility to be used as minimally invasive injectable materials for the use in early stages of OA. However, in this study cells will not be used. A much simpler and cheaper approach of mixing the SAPs with a naturally occurring biopolymer in cartilage (chondroitin sulfate), in a one-step procedure, will be investigated to see whether it is able to restore the biomechanical properties of OA cartilage.

In general terms SAP molecules have been labelled as 'Lego bricks', with the ability to spontaneously self-assemble when exposed to an external stimulus to form nanofibrous structures. Their success is thanks to their highly defined structure and the molecular interaction which enable them form fibrillar intricate nanostructures that are very similar in size, shape and porosity to that of natural fibrillar proteins in the ECM. Additionally, their self-assembling properties allow them to form porous network structures. These provide a tissue-like microenvironment and can display cell-binding sites that can be made to specially interact with cells and influence their biological function. From the literature reviewed, their most important characteristic, which makes them favourable for tissue engineering and regenerative medicine is their self-assembling properties and how this can be triggered. The self-assembly of the SAPs used in regenerative medicine was reported to be triggered by shifts in pH or temperature or by the presence of monovalent or divalent electrolyte ions. The combination of all these characteristics makes SAPs very favourable biomaterials for percutaneous injections, specifically in minimally invasive surgery techniques for cartilage regeneration. Therefore, the ideal design requirements for a SAP gel, that could be used in the regeneration of osteoarthritic cartilage should be able to form self-supporting gels in a

physiological environment, show characteristic morphology similar to that of proteoglycan structures found in native cartilage and be strong enough to remain in the area to which it is applied.

1.7 Rationale

Osteoarthritis is considered the most common joint disorder worldwide (Arden and Nevitt, 2006; Lorenz and Richter, 2006). The number of people that will be affected by OA is on the rise because of the aging population in most Western countries and the recent obesity epidemic (Arden and Nevitt, 2006; Zhang and Jordan, 2010). This degenerative joint disease is characterised by the progressive loss of articular cartilage and formation of osteophytes, which leads to pain, loss of function and mobility problems (Berenbaum, 2013; Pitsillides and Beier, 2011; Bach and Hunter, 2014). Cartilage is a unique tissue, demonstrating both viscoelastic and compressive properties provided by its extracellular matrix (ECM). Unfortunately, chondrocytes have a very limited ability to fully repair damaged cartilage (Berenbaum, 2013). Therapeutic interventions are needed. Current treatments are limited in respect to their ability to regenerate/restore hyaline cartilage and alleviate pain. OA is characterised by a loss of GAGs from the cartilage ECM which are essential for its biomechanical function. Restoration of GAGs in articular cartilage during early stages of OA may delay or prevent disease progression. Treatment with chondroitin sulfate (Katta et al., 2008) has been shown to be ineffective in restoration of mechanical properties to GAG depleted cartilage. It is hypothesised that a combination of chondroitin sulfate and SAPs, with the SAPs retaining the GAG *in situ* will be effective. The use of SAPs (Shaha et al., 2010; Kyle et al., 2010), which can transform from injectable liquids into hydrogel bioactive structures *in vivo*; is an attractive approach that could be transferred to the clinic.

The SAPs chosen were a family of peptides from the P₁₁ series that have been de novo designed at the University of Leeds. These SAPs are able to form β -sheet tapes, which self-assemble in one dimension into a hierarchy of well-defined structures. They are advantageous because they are entirely based on natural amino acids and their self-assembly can be triggered by external factors such as pH, ionic strength and temperature (Aggeli et al., 2003; Carrick et al., 2007; Maude et al., 2011). The peptides P₁₁-4, P₁₁-8 and P₁₁-12 were chosen as they systematically vary in charge (net charge of +2 or -2) and hydrogen bonding capacity (glutamine (Q) or Serine (S) based peptides). They were then combined with chondroitin sulfate, which has a -2 charge and a large number of hydrogen bond donors (4) and acceptors (15) groups per repeat monomer unit that will potentially facilitate interactions between the peptides and these GAGs through a combination of electrostatic

and/or hydrogen bonding interactions. Miles *et al.*, carried out a similar study in which these peptides were combined with GAGs at varying molar ratios to investigate if they could restore the *in vitro* biomechanical properties of degenerative intervertebral discs. To date this is the only other study which has combined the use of the P₁₁ peptides and GAG. However, the authors carried out their experiments at room temperature and in only one physiological conditions (130 mM NaCl in Deuterated water (D₂O)), which was relevant to their area of study. Hence this study aims to investigate a range of physiological conditions found within the cartilage tissue.

Therefore, this project will investigate the feasibility of using novel self-assembling peptides combined with chondroitin sulfate (a key component of the ECM), for the restoration of biomechanical properties of GAG depleted cartilage *in vitro*.

1.8 Aim and Objectives

The aim of this project is to use multidisciplinary approaches, to determine whether a combination SAPs and chondroitin sulfate is able to restore the biomechanical properties of GAG depleted porcine condylar cartilage, ideally to a level intrinsic to natural porcine condylar cartilage.

1.8.1 Objectives

- 1) To determine the effects of combining the SAPs (P₁₁-4, P₁₁-8 and P₁₁-12) and chondroitin sulfate (GAG) at two molar ratios (1:64 and 1:16) in two physiological conditions (130 mM and 230 mM Na⁺ salt solutions), on the β -sheet percentage, fibril morphology and biomechanical properties of the SAPs and SAP: GAG mixtures.
- 2) To create a GAG depleted porcine condylar cartilage model and characterise the model biochemically and histologically.
- 3) To develop an indentation testing procedure that gives a significant difference in the deformation, equilibrium elastic modulus and permeability between native and GAG depleted porcine condylar cartilages.
- 4) To determine the GAG content and biomechanical properties of native and GAG depleted porcine condylar cartilage
- 5) To investigate whether the SAPs or SAPs/GAG mixtures are able to restore the biomechanical properties of GAG depleted porcine condylar cartilage.

Chapter 2 Materials and Methods

2.1 Materials

2.1.1 Equipment

A list of the laboratory equipment used throughout the study is shown in Table 5.

Table 5: Equipment used throughout the study.

Equipment	Model/Size	Supplier
Automatic pipettes	Gilson P20-P5000	Anachem Ltd.
Balance	Mettler AE240 Balance	Inte Equipment Trading Ltd.
Bijous	5 ml	Scientific Laboratory Supplies Ltd
Disposable plastic syringes	1 ml, 2 ml, 10 ml, 20 ml	Scientific Laboratory Supplies Ltd
Fourier transform infrared spectrometer (FTIR)	Nicolet 6700	Thermo Scientific.
Freeze drier	Modulyod-230	Thermo Savant
Freezer (-20 °C)	Electrolux 3000	Jencons PLC
Fridge	Electrolux ER8817C	Jencons PLC
Hexagonal mesh copper grids	400 mesh grids	Agar Scientific Ltd.
Histology cassettes	CMB-160-030R	Thermo Fisher Scientific Ltd
Histology moulds	-	Thermo Fisher Scientific Ltd
Histology water bath	MH8515	Barnstead
Hot plate	E18.1 hotplate	Raymond A Lamb
Hot wax dispenser	E66 was dispenser	Raymond A Lamb
Incubator	Heraeus	Jencons PLC
Instron material testing machine	3365	Instron
Linear variable differential transformer (LVDT)	RDP DS-200H	Electrosence
Magnetic stirrer	Stuart SB161	Scientific Laboratory Systems Ltd
Mica carbon sheets	-	Agar Scientific Ltd.
Micro-plate spectrophotometer	Multiscan Spectrum 1500	Thermo Scientific
Microscope (upright)	Zeiss AX10	Zeiss
Microscope	Zeiss with FRAP module	
Microtome	RM2125 RTR	Leica Microsystems
Microtome Blades	SD3050835	Fisher Scientific
Orbital Shaker	IKA KS130 basic	Jencons PLC
Parafilm M	-	Sigma Aldrich Ltd.
pH Meter	Sartorius Docu-pH-meter	Fisher Scientific
Pipette tips	10 µl, 200 µl, 1000 µl	Star Labs
Plate Shaker	IKA KS130 basic	Jencons PLC
Rheometer	Malvern Kinexus Pro	Malvern
Sample vials (7ml)	4013610	Scientific Industries Inc.
Slide holder	E102	Raymond A Lamb
Sonicator	Sonorex RK52H	Bandelin Sonorex Ltd.
Superfrost Plus microscope slide	MIC3022	Scientific Laboratory Supplies Ltd
Syringe needles	32G	Thermo Fisher Schientific Ltd

Tissue Processor	TP11020	Leica Microsystems
Transmission electron microscope	Jeol 1400	Jeol Ltd.
Universals	25 ml	Scientific Laboratory Supplies Ltd
Vortexer	Vortex Genie-2	Scientific Industries Inc.
Water Bath	Grant	Jencons PLC
Well plates, Nunc® (flat bottomed)	96-well plates	Nunc International Corporation
Wax oven	Windsor E18/31	Scientific Laboratory Supplies

2.1.2 Chemicals

Sources of chemicals used throughout the study are shown in Table 6.

Table 6: Chemicals and reagents used throughout the study.

Chemical/reagent	Supplier
1,9 dimethylene blue	Sigma-Aldrich Ltd.
Acetic Acid (glacial)	Thermo Fisher Scientific Ltd
Amphotericin B	VWR International
Aprotinin (10,000 KUI)	Mayfair house
Bovine Serum Albumin	Sigma Aldrich Ltd.
Calcium acetate	Thermo Fisher Scientific Ltd
Calcium chloride (CaCl ₂)	Thermo Fisher Scientific Ltd
Chondroitin sulfate B	Sigma Aldrich Ltd.
Deuterium chloride (DCI)	Sigma Aldrich Ltd.
Deuterium oxide (D ₂ O)	Sigma Aldrich Ltd.
DPX mountant	Thermo Fisher Scientific Ltd
di-sodium hydrogen orthophosphate	VWR International
Ethanol	Thermo Fisher Scientific Ltd
Ethylenediaminetetraacetic acid (EDTA)	VWR International
Fast green	Sigma Aldrich Ltd.
Formic acid	Sigma Aldrich Ltd.
Formamide	Sigma Aldrich Ltd.
Gentamycin	Biochrom A
Hank's balanced salt solution (HBSS)	Sigma Aldrich Ltd.
Haematoxylin (Weigert's)	Atom Scientific
Hydrochloric acid	VWR International
Isopropanol	Thermo Fisher Scientific Ltd
L-cystine hydrochloride	Sigma Aldrich Ltd.
Methyl methacrylate (liquid)	WhW Plastics
Nystatin	Sigma Aldrich Ltd.
OCT embedding media	Leica Biosystems
Papain	Sigma Aldrich Ltd.
Paraffin wax	Thermo Fisher Scientific Ltd
Phosphate Buffered Saline (PBS) without Ca ²⁺ /Mg ²⁺	Lonza
Penicillin	Lonza
Potassium chloride (KCl)	Sigma Aldrich Ltd.
Polymixin B	Calbiochem
Polymethylmethacrylate (PMMA) powder	WhW Plastics
Primixin I.V. (Imipenem Cilastatin)	Medreg

Safranin O	Acros
Sodium acetate	Thermo Fisher Scientific Ltd
Sodium chloride (NaCl)	Thermo Fisher Scientific Ltd
Sodium deuteroxide (NaOD)	Sigma Aldrich Ltd.
Sodium di-hydrogen orthophosphate	VWR International
Sodium dodecyl sulfate (SDS)	Sigma Aldrich Ltd.
Sodium formate	VWR International
Sodium hydrocarbonate (NaHCO ₃)	Thermo Fisher Scientific Ltd
Sodium Hydroxide	VWR International
Stains-all solution	VWR International
Standard pH buffers (pH 4, 7 and 10)	Sigma Aldrich Ltd.
Trizma base	Sigma Aldrich Ltd.
Uranyl acetate	Sigma Aldrich Ltd.
Vancomycin	Sigma Aldrich Ltd.
Xylene	Genta Medical
Zinc acetate	Thermo Fisher Scientific Ltd
Zinc chloride	Thermo Fisher Scientific Ltd

2.1.3 Peptides

P₁₁-4, P₁₁-8 and P₁₁-12 were purchased from CS Bio Co. These peptides were analysed in house to check their composition and purity using elemental analysis and UV spectroscopy.

Table 7: Peptide primary structures, and their net charges at pH 7.4. Positively charged residues are coloured blue, negatively charged residues are red. All peptides were amidated and acetylated.

Peptide	Amino Acid Sequence	Net charge at pH 7.4
P ₁₁ -4	QQR FEW FEQQ	-2
P ₁₁ -8	QQR FOW FEQQ	+2
P ₁₁ -12	SSR FOW FESS	+2

Manufacturer values of peptide percentage purity were checked using UV spectroscopy. The three peptides studied here (Table 7) all contain tryptophan. Therefore, the UV absorption spectra can be used to calculate the molar concentration. The wavelength of 279 nm corresponds to the excitation peak of the indol side chain of the tryptophan residue. Therefore, when the spectra are collected in a 1 mm path length cell, the molar ratio can be calculated using equation 2:

$$\text{Equation 2} \quad - \quad [\text{peptide}]M = \frac{Abs_{279}}{5600 (M^{-1}cm^{-1})}$$

Where 5600 M⁻¹cm⁻¹ is the molar extinction coefficient of the tryptophan residue at 279 nm. Solutions were prepared at 1 mg.ml⁻¹ in water. The pH of these solutions was adjusted (pH > 8 for P₁₁-4 and a pH < 6 for P₁₁-8 and P₁₁-12), to obtain a fully monomerised solution. Peptide solutions were added to the Hellma UV quartz cuvettes with a 1 mm path length. Prior to commencing, spectrometer was auto-zeroed using Hellman UV quartz cuvettes filled with blank solvent (water). Solution absorbance was recorded using a PerkinElmer UV/VIS/NIR

Lambda 900 Spectrometer, controlled by UV WinLab software. Ten measurements of absorbance were recorded, with a ten second pause in-between the successive readings. An average of the absorbance measurements was taken. The in-house peptide content value from UV spectroscopy was calculated using Equation 3:

$$\text{Equation 3} \quad - \quad \text{Peptide content} = \frac{\text{Molarity measured by UV}}{\text{Molarity measured by mass/volume ratio}}$$

Peptides were stored in a freezer and prior to use left to thaw at room temperature.

2.1.4 Glycosaminoglycan (GAG; chondroitin sulfate)

Chondroitin sulfate sodium salt from shark cartilage was purchased from Sigma-Aldrich Ltd, Dorset, UK. This particular GAG is the most abundant in healthy articular cartilage, therefore is the most likely candidate to provide mechanical and biological behaviour similar to that found in the natural tissue (Mow and Ateshian, 1997).

2.1.5 Software

OMNIC software by Thermo Fisher Scientific (Version 7.3, SP1) was used to interpret the peptide spectra data produced by the Fourier transform infrared spectroscopy (FTIR) machine. This program allowed the production of peak fitted graphs, to determine the secondary structure of the peptides, which were saved as CSV files to be further manipulated in Origin Pro 8.6 (OriginLab, SR1). rSpace Kinexus by Malvern Instruments (Version 6.7) was used to control the rheometer and export raw data. Origin Pro 8.6 was used to process, manipulate and present the graphs throughout this thesis.

2.2 Methods

2.2.1 General Methods

2.2.1.1 Weighing of peptides

A Mettler AE240 balance was used to measure masses greater than ≈ 1 mg, while masses less than ≈ 1 mg, were weighed on a Sartorius SC2 balance. The accuracy of the balances were 0.01 mg and 0.1 μ g, respectively. The percentage purities of the three peptides, P₁₁₋₄, P₁₁₋₈ and P₁₁₋₁₂ were 95 %, 79.05 % and 79.7 % respectively. Throughout this study, it was decided to use 10 mg of peptide per 1 ml of Na⁺ salt solution. However, as the peptide purities were not 100%, the amount of peptide to weigh out in order to obtain 10 mg. ml⁻¹ was calculated.

The percentage purities (above) were divided by 100 and then subtracted from 1 to give the number of milligrams (mg) of counter ions in each sample, the remaining weight was the weight of peptide as detailed below:

- For each mg of P₁₁-4, 0.05 mg was counter ions. The remaining weight 0.95 mg, was of actual P₁₁-4.
- For each mg of P₁₁-8, 0.21 mg was counter ions. The remaining weight 0.79 mg, was of actual P₁₁-8.
- For each mg of P₁₁-12, 0.20 mg was counter ions. The remaining weight 0.80 mg, was of actual P₁₁-12.

Therefore for 10 mg.ml⁻¹ to be achieved, 10 mg was divided by the weight of peptide (above) which accounted for the counter ions to give the weight of peptide that was weighed out.

For P₁₁-4= 10.53 mg.ml⁻¹ of Na⁺ salt solution – (1)

For P₁₁-8= 12.65 mg.ml⁻¹ of Na⁺ salt solution – (2)

For P₁₁-12 = 12.50 mg.ml⁻¹ of Na⁺ salt solution –(3)

The concentration of the peptides used in this study was always 10 mg. ml⁻¹.

2.2.1.2 Weighing of chondroitin sulfate (CS) powder – (GAG)

Chondroitin sulfate sodium salt was used as the GAG for all the experiments (unless otherwise stated). Different molar ratios of GAG: peptide were used throughout this study, these were 1:64 and 1:16. Throughout this work the terminology 1:64 & 1:16, refers to one part GAG to one part peptide.

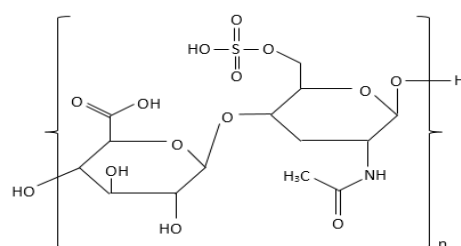


Figure 19: One subunit of Chondroitin-6-sulfate.

To determine the amount of GAG powder to be weighed to make up these molar ratios the following calculations were carried out.

The peptide weight, 10 mg, was divided by the molecular weights of the corresponding peptide to determine the number of moles of peptide.

The number of moles of peptide was then divided by the ratio required, so either 64 for the 1:64 ratio or 16 for the 1:16 ratio. This gave the moles of GAG required, from this using

equation 4 below and rearranging it to calculate the mass, the masses of the GAG for the two molar ratios were calculated. All the masses of the powders for all peptides and molar ratios of GAG are shown in Table 8.

$$\text{Equation 4} \quad - \text{No. of moles} = \frac{\text{mass (g)}}{\text{molecular weight (g.mol}^{-1}\text{)}}$$

Molecular weights of peptides and chondroitin sulfate:

- For P₁₁-4 = 1596 gmol⁻¹ • For P₁₁-12 = 1401 gmol⁻¹ • For P₁₁-8 = 1567 gmol⁻¹ • For CS powder = 54,000 gmol⁻¹

Table 8: Masses (mg) of peptide and chondroitin sulfate (GAG) weighed out for the different molar ratios. Samples were made up to a total volume of 1 ml in two aqueous Na⁺ salt solutions, unless otherwise stated.

	1 part GAG : 64 part peptide		1 part GAG : 16 part peptide	
P₁₁-4	5.3 mg	10.5 mg	21.1 mg	10.5 mg
P₁₁-8	5.4 mg	12.7 mg	21.5 mg	12.7 mg
P₁₁-12	6.0 mg	12.5 mg	24.0 mg	12.5 mg

2.2.1.3 Sterilisation

Solutions, materials and equipment were sterilised using one of three procedures:

- Dry heat sterilisation – items were placed in a hot air oven for 4 h at 180 °C.
- Moist heat sterilisation – items which were not suitable for dry heat sterilisation were sterilised in an autoclave for 20 mins at 121 °C at a pressure of 103 kPa.
- Filter Sterilisation – items were drawn up through a sterile syringe and passed through a Millex®GP filter unit (0.22µm – pore size).

2.2.2 Cartilage Tissue acquisition

Cartilage tissue underwent several modifications to create different models of OA, explained in Chapter 4. Cartilage models and cartilage treated with the SAP: GAG mixtures were subject to several histological, biochemical and biomechanical tests to determine the effects of the SAP-GAG mixtures, which are outlined in Chapter 4, Chapter 5 and Chapter 6.

2.2.2.1 Dissection equipment

The dissection equipment and supplier information used for dissection and extraction of porcine cartilage are listed in Table 9 and shown in Figure 20.

Table 9: Dissection equipment used throughout the study.

Equipment	Size/Model	Supplier
Bench top clamp	-	-
Bunsen Burner	-	Fisher Scientific Ltd
Corer (serrated drill attachment)	9 mm diameter	Mechanical Engineering Workshop
Corer (serrated)	9 mm diameter	Mechanical Engineering Workshop
Corer (smooth)	9 mm diameter	Mechanical Engineering Workshop
E-cut precision blade	-	Fien Industry power tools UK Ltd
Hand drill	-	Bosch
Oscillating saw	-	Fien Industry power tools UK Ltd
Rat toothed forceps	125 mm length	Fisher Scientific Ltd
Scalpel handle	Size 4 & 3	Swann Morton Ltd
Sterile stainless and carbon steel surgical blades	Size 22 & 10	Swann Morton Ltd
Straight pincer forceps	Long and short	Fisher Scientific Ltd



Figure 20: Dissection equipment. A- Hand held oscillating saw. B- Piezo electronic gas igniter. C- E-cut precision blade for multi master drill. D- Sterile stainless steel surgical blade. E- Scalpel handle (size 3). F- Sterile carbon steel surgical blade. G- Scalpel handle (size 4). H- Smooth corer. I- Serrated corer. J- Serrated corer drill attachment. K- Pincer forceps (long). L- Pincer forceps (short). M- Bunsen burner. N- Hand held power drill. O- Bench top vice for holding porcine knee condyles in place.

2.2.2.2 Dissection

Right hand-side porcine legs were supplied by local abattoirs 24 h after slaughter. Pigs were aged ~ 6 months. The knee condyles, both medial and lateral were extracted in a sterile environment using a Bunsen burner and sterile equipment. Condyles were used either directly following extraction or if necessary for use the next day, the condyles were stored in a moist environment at 4 °C overnight.

Porcine knees were dissected as shown in Figure 21. Excess tissue was removed from the femur and surrounding skeletal structures to allow easier access. The knee joint was exposed by severing all surrounding ligaments and excising the joint capsule. First the patella ligament

was cut allowing extraction of the patella to expose the knee joint. Medial and lateral collateral ligaments were cut allowing full flexion of the knee and exposure of the posterior and anterior cruciate ligaments, which were then cut. The knee condyles were fully exposed; cartilage was kept hydrated whilst extracting individual condyles or pins, by covering in phosphate buffered saline (PBS) soaked tissue paper.



Figure 21: Dissection of porcine knee joints. (A) - Whole porcine leg. (B) – Incision made laterally to the knee. (C) – Enlargement of the incision site, parallel to the femur. (D) – Removal of the lateral muscles/tissue. (E) – Removal of the medial lateral muscles/tissue. (F) – Excision of the patella tendon. (G) – Removal of the patella and exposure to the joint cavity. (H) – Collateral ligaments severed. (I) – Cruciate ligaments severed. (J) – Excision of the meniscus ligaments to separate the femur from the tibia. (K) – Removal of excess tissue. (L) – All knee surface exposed.

2.2.2.3 Extraction of condyles and osteochondral pins

Osteochondral pins 9 mm in diameter were extracted from the cartilage surface of the medial and lateral condyles. Usually two pins were taken from each condyle (medial and lateral) for analysis, unless otherwise stated. Pins were initially marked out then a hand held

power drill with a specialist corer drill bit was used to cut into the subchondral bone. A hand held corer was used to loosen the pin and extract it from the joint. The cartilage was carefully removed from the bone, using a scalpel blade, leaving behind just the cartilage. Images of this procedure are shown in Figure 22.

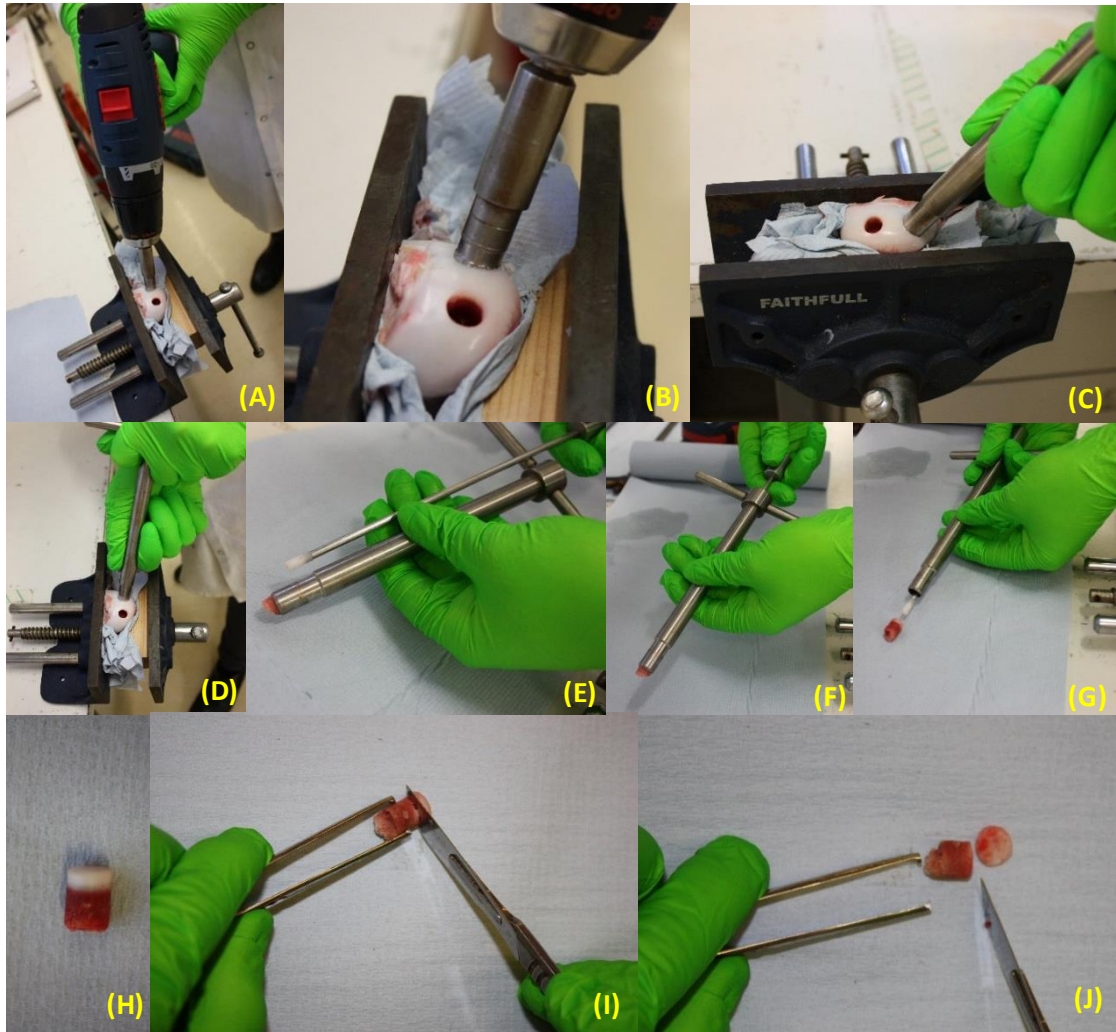


Figure 22: Extraction of osteochondral pins. (A) - Power drill with a specialist corer drill to cut subchondral bone. (B) - The power drill was drilled into the cartilage until the third line last line of the specialist corer drill. (C and D) - A hand held corer was pushed into the cartilage to loosen the pin, force was used to snap the pin and extract it from the joint. (E) – A specialised metal rod with a polyethylene tip was used to remove the pin from the hand held corer. (F) – A piece of PBS soaked blue roll was pushed down the central canal of the hand held corer with the help of the specialised metal rod. (G) Force was applied to the specialised metal rod and the pin was removed from the hand held corer orifice. (H) - Representative image of porcine cartilage pin. (I) – Rat toothed forceps were used to secure the porcine cartilage pin and scalpel with a surgical blade was used to carefully remove the cartilage from the bone. (J) – Cartilage removed from the bone.

Condyles were obtained using a hand held oscillating saw. An incision point to remove both condyles was chosen at the distal end of the patella groove where it meets the anterior area of the condyles. This narrowing ensured that the cut area exposed was small. The saw was

held in the transverse plane towards the posterior area of the condyle. A second incision site was made in-between the two condyles in the sagittal plane. Individual condyles were then placed in sterile 250 ml pots with sterile filter paper soaked in sterile PBS. Images of this procedure are shown in Figure 23.

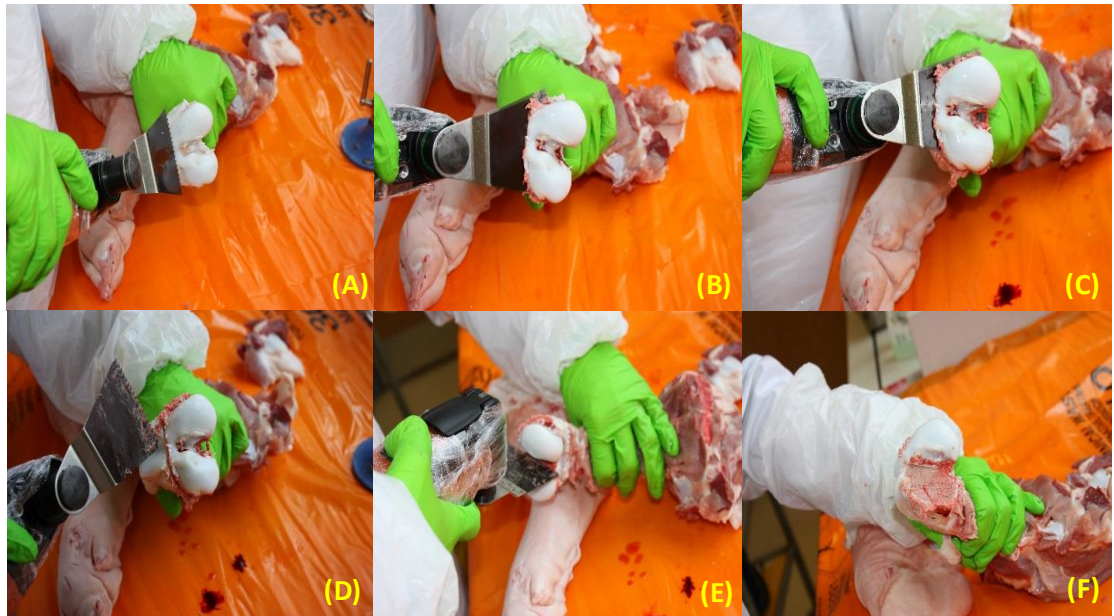


Figure 23: Extraction of Medial and Lateral condyles. A – Cut made at the distal end of the femoral patella groove to reduce cut area of cartilage. B-D – Anterior-posterior cut made to remove the condyles from the femur. E – Lateral cut made to separate the medial and lateral condyles. F – Removal of individual condyles.

2.2.2.4 Storage of tissues

Cartilage tissue removed from osteochondral pins was labelled and placed in histology cassettes (Histicette®). Condyles and the histology cassettes containing the cartilage tissue were placed in sterile 250 ml pots with sterile filter paper soaked in sterile PBS and stored at 4 °C overnight.

2.2.3 Histological techniques

2.2.3.1 Zinc Fixation

Reagents:

Zinc fixative

Tris solution (0.1 M) was made by dissolving 12.1 g of Trizma base in 1000 ml of distilled water using a magnetic stirrer. Calcium acetate (0.5 g) was added and dissolved and the pH adjusted to 7.0-7.4 via the addition of 6 M hydrochloric acid (HCL) or 6 M sodium hydroxide (NaOH) dropwise whilst being stirred using a magnetic stirrer. Zinc acetate (5 g) was dissolved into the solution followed by 5 g of zinc chloride using a magnetic stirrer.

Method:

Cartilage tissue that had been placed in histological cassettes, was fixed using the zinc fixative solution. Fixation took place in a sealed 250 ml pot immersed with 200 ml of the zinc fixative solution for 16 hours to achieve complete fixation of samples.

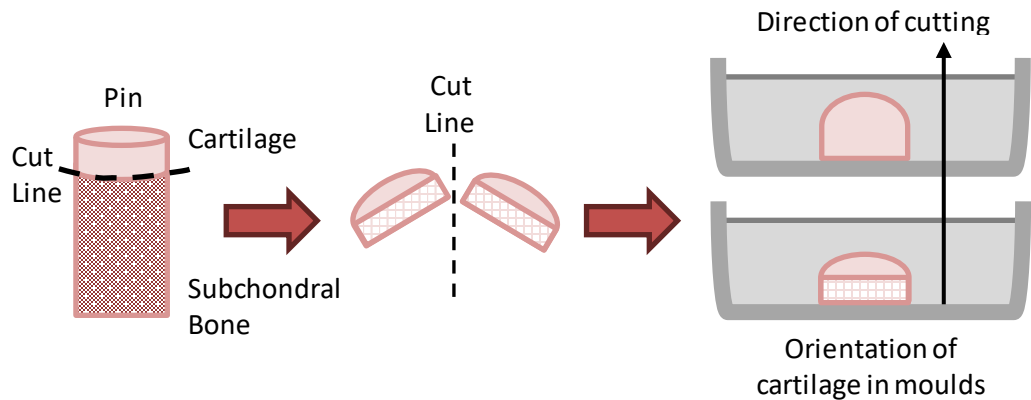


Figure 24: Orientation of cartilage tissue for histology. Pins were bisected to remove the cartilage from the bone and then cut in half before being placed in histology cassettes. Either the cut or cartilage surface was placed face down such that when moulded in wax, sections could be cut to observe the cartilage architecture from different angles.

2.2.3.2 Paraffin wax embedding

Once fixed, samples were placed in a Leica TP 1020 automated tissue processor and processed using program 9 excluding the first step (formalin fixation). The samples were immersed in 70 % (w/v) ethanol for 1 h followed by 1 h in 90 % (w/v) ethanol. Samples were then immersed in absolute ethanol for 2 h 20 min, 3 h 20 min, and then 4 h and 20 min. Immersion of xylene followed in cycles of 1 h, 1 h 30 min, and 2 h. Overall the process took 22 h. Samples were removed from the processor and oriented accordingly into the moulds, as illustrated in Figure 24. Samples were covered in molten wax and left to set overnight at room temperature, after which, excess wax was scraped away using a blunt blade.

2.2.3.3 Sectioning and slide preparation

A microtome (Leica RM2125 RTR) was used to section the wax embedded cartilage to a thickness of 6 μm . Using forceps and a brush, thin sections were transferred to a water bath at 50 $^{\circ}\text{C}$. The sections were transferred onto Superfrost Plus slides and placed directly onto a hotplate at 45 $^{\circ}\text{C}$ to bake on for 1 h and then transferred to slide rack and allowed to air dry at room temperature.

2.2.3.4 Dewaxing and rehydration

Xylene solutions were used to dewax the sections. They were immersed twice in xylene for 10 min sections were then rehydrated in 3 successive immersions in 100% (w/v) ethanol for

3 min, 2 min and then 2 min, followed by immersion in 70% (w/v) ethanol for 2 min. To finish slides were placed in running tap water for 3 min to rehydrate the sections before staining.

2.2.3.5 Dehydration and mounting

Stained sections were dehydrated by immersion in 70% (w/v) ethanol for 5 sec, followed by successive washes in 100% ethanol for 1 min 2 min and 3 min. Sections were then immersed twice in xylene for 10 min. Cover slips were carefully mounted to the slides using 3 drops of DPX mountant, avoiding any bubbles. If any bubbles were present, plastic tongs were used to press and disperse them out of field of view of the section. Slides were left to dry in a fume hood overnight before visualising by microscopy.

2.2.3.6 Microscopy

Bright-field microscopy was carried out using a Zeiss AX10 microscope. Where needed, the tiling function was used to stitch images together to enable visualisation of the full architecture of the sample. Images were captured using the attached Zeiss digital camera controlled through the Zen Zeiss software (image capture and digitalisation).

2.2.4 Histological staining methods

2.2.4.1 Safranin O/ fast green staining

Reagents:

- 0.1% (w/v) Safranin O, 500 mg of safranin O dye was dissolved in 500 ml of distilled water.
- 0.02 % (w/v) Fast green, 100 mg of fast green dye was dissolved in 500 ml of distilled water.
- 1 % (v/v) acetic acid, 5 ml of glacial acetic acid was mixed with 495 ml of distilled water.
- 1 % acid alcohol, 5ml of concentrated hydrochloric acid was added to 495 ml of 70% (w/v) ethanol.
- Weigert's haematoxylin, equal volumes of solution A and solution B (as supplied by the manufacturer).

Safranin O stains proteoglycans whilst fast green stains collagen. Cell nuclei are stained with Weigert's haematoxylin. Following the dewaxing and rehydration (Section 2.2.3.4), slides were placed in Weigert's haematoxylin for 3 min and then run under cold tap water for 3 min. Sections were then immersed in fast green dye for 5 min before being rinsed in acetic acid for 10 to 15 seconds and dabbed dry to remove excess liquid and placed straight into

safranin O for 4 min. Following this, sections were dehydrated and mounted, as described in Section 2.2.3.5.

2.2.5 Biochemical Methods

2.2.5.1 Sample preparation

2.2.5.1.1 Lyophilisation

Cartilage tissue removed from the bone was macerated and placed in a bijoux. Samples were weighed three times and a mean wet weight was calculated. Samples were placed in a freeze dryer (Thermo, Savant ModulyoD) at -50 °C, 0.15-0.2 mbar, and the weight measured every 24 h until constant (~72 hours).

2.2.5.1.2 Papain digestion

For quantification of sulfated proteoglycans, macerated, freeze-dried cartilage samples were digested in papain.

Reagents:

- Digestion buffer, 0.788 g of L-cystine hydrochloride and 1.8612 g of disodium ethylenediaminetetraacetic acid (EDTA) were dissolved in 1 litre of PBS. 6 M HCL or 6 M NaOH were added dropwise whilst using a magnetic stirrer, to achieve pH 6.0.
- Papain digestion solution, 96,012 kU of papain (Sigma A3824, Lot no#2B005436, 31.5 kU/mg) was dissolved in 60 ml of digestion buffer.

Method:

Papain digestion solution (5 ml) was added to each bijoux containing the lyophilised cartilage (~10-20 mg, dry weight) and incubated in a water bath at 60 °C for 36-48 h until fully digested.

2.2.5.2 Water content

The percentage water content was measured by weighing the cartilage before and after lyophilisation (Section 2.2.5.1.1.). The water weight was then calculated by subtracting the dry weight from the wet weight and is presented as a percentage of the tissue wet weight.

2.2.5.3 Quantification of sulfated sugars (GAG)

Quantification of GAGs in tissues was achieved via colorimetric analysis. The method used was pioneered by Farndale *et al.*, such that under acidic conditions the metachromatic change in the 1,9-dimethylmethylene blue (DMB) cationic dye, as it binds to carboxyl or sulfated groups of GAG chains, is detected. This change can be measured spectrophotometrically (Farndale *et al.*, 1982).

Reagents:

- 0.1 M sodium di-hydrogen orthophosphate; 3.45 g of sodium di-hydrogen orthophosphate was dissolved in 250 ml of dH₂O.
- 0.1 M di-sodium hydrogen orthophosphate; 3.55 g of di-sodium hydrogen orthophosphate was dissolved in 250 ml of dH₂O.
- Assay buffer; 137 ml of 0.1 M sodium di-hydrogen orthophosphate was mixed with 63 ml of 0.1 M di-sodium hydrogen orthophosphate. The pH was adjusted to 6.8, using droplets of 6M HCL or 6M NaOH.
- DMB dye; 16 mg of DMB was dissolved into 5 ml of ethanol and 2 ml of formic acid. 2 g of sodium formate was added and the solution was made up to 1 L with dH₂O. pH was adjusted to 3, using formic acid.

2.2.5.3.1 Method of quantification

Standard calibration solutions of chondroitin sulfate B were made up in assay buffer at 0, 3.1, 6.3, 12.5, 25, 50, 100, 150 and 200 µg.ml⁻¹. Test samples that has been lyophilised and papain digested (Section 2.2.5.1.1 & 2.2.5.1.2) were diluted 1:100 in assay buffer. Each of the standards and diluted test samples (40 µl) were added to the wells of a clear 96 well flat-bottomed plate in triplicates. 250 µl of DMB dye were then added to each of the wells and the plates were gently agitated for 2 mins on a plate shaker. Plates were then placed in a micro plate spectrophotometer and their optical densities were read at 525 nm. A standard curve was plotted in Microsoft excel of the mean absorbance of chondroitin sulfate B vs concentration and a linear regression analysis (Section 2.2.7.3) was performed to interpolate the unknown GAG concentrations of the test samples based on their absorbance. Dilution factors were taken into consideration and the GAG concentration was determined per tissue dry weight.

2.2.6 Biomechanical Methods

2.2.6.1 Sample preparation

To assess the time dependant biomechanical behaviour of articular cartilage, porcine condyles were subject to creep indentation. All the equipment used is shown in Figure 25. The porcine condyles were mounted in polymethylmethacrylate cement (PMMA). Once porcine condyles had been dissected and extracted as described in Section 2.2.2.2 & 2.2.2.3, the condyles` height (~18-26 mm) was measured and recorded to determine the height of PMMA needed to allow the condyles to sit below the top end of the cup and a few millimetres (~1 mm) below the indenter tip (illustrated in Figure 26). The distance the indenter tip went

into the cup holder was measured (~6 mm); this was marked out on the inside of the cup in several spots around the circumference of the cylindrical cup with a ruler and permanent pen. From this distance, the height of the condyle was measured down into the cup and another marking was made along the circumference of the cup holder.

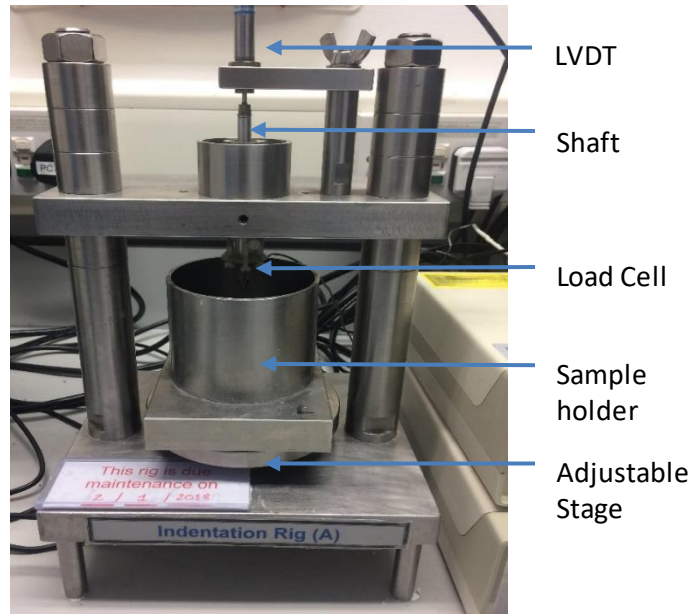


Figure 25: Indentation apparatus. The equipment used to perform creep indentation testing to determine deformation of porcine condylar cartilage. (A) - Indentation rig and components. (B) – Sample holder, stage adjuster and indenter.

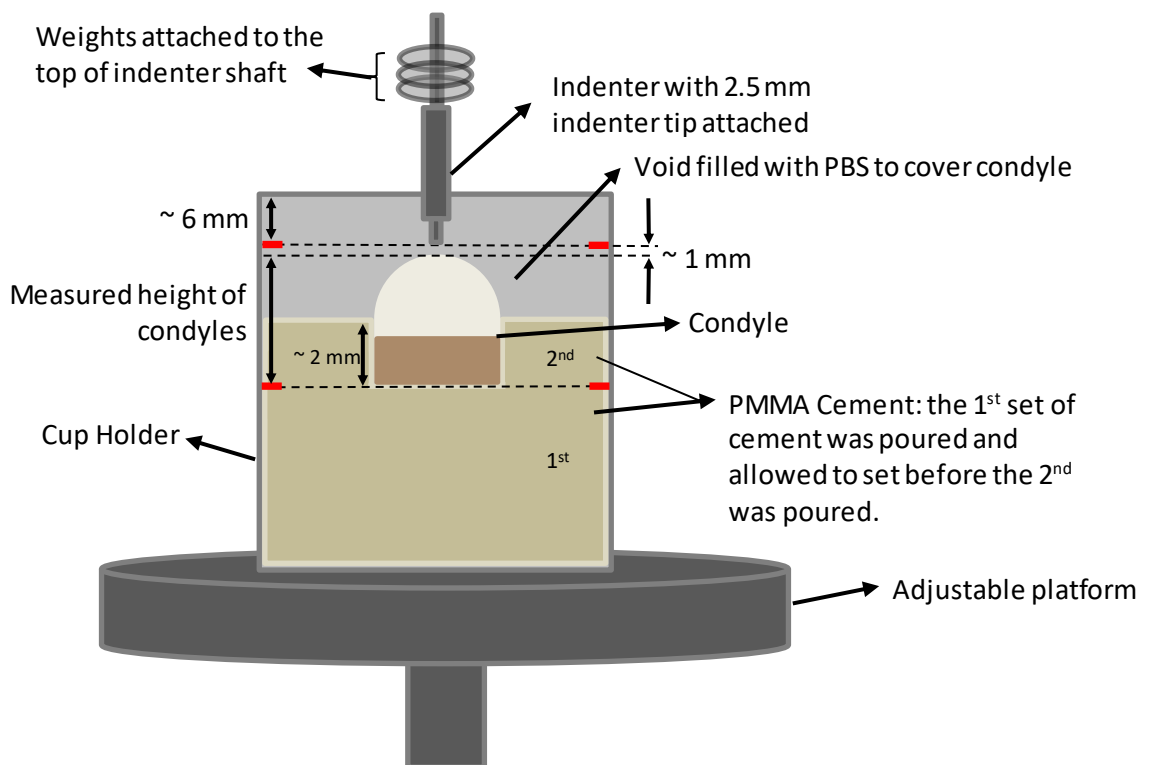


Figure 26: Cross-sectional view of the cup holder, showing how the condyle was orientated inside the cup holder and outlining rough distances and heights of relative components.

PMMA powder was weighed and whilst stirring simultaneously, the methyl-methacrylate liquid was added to the powder until a thick silky paste was achieved. The thick paste was poured into the cup holder up to the lower line previously marked out and left to set. Another batch of PMMA paste was made up of a much thinner consistency (added more methyl methacrylate liquid) and left to one side. Once the PMMA had set hard, the condyle was placed in the centre of the cup holder, with a piece of moistened PBS paper covering the condyle surface. The second batch of PMMA paste was poured into the cup holder carefully, making sure not to pour it directly over the condyle. The PMMA paste surrounded and covered the bottom half (~2 mm) of the condyle. This was left to set and fresh moistened PBS paper towels were placed over the condyle to stop it from drying out. Once the PMMA had set hard and cooled down the sample was ready to test.

2.2.6.2 Method

Generally, PBS was added to the cup holder to completely submerge the condyle whilst testing. Variation from this method is detailed in the relevant Sections. An impermeable, stainless steel flat indenter (2.5 mm diameter) was used to indent the cartilage with a set load over 1 h. The extra load added to the top part of the shaft (Figure 26), is detailed in the relevant Sections. The cup holder was placed on the adjustable platform and the cup holder was raised so that the indenter was positioned about ~1 mm above the cartilage surface. The adjustable platform was then secured with a locking nut at the bottom to avoid shaking and vibration once the cup holder was set to the required height. The lowering of the indenter shaft was controlled via a silicone filled dashpot to reduce the speed of impact, the full load was applied within 0.2 sec. The displacement of the indenter was measured using a linear variable differential transducer (LVDT, RDP D5-200H, 2 mv/V/0.001 sensitivity, ElectroSense, PA, USA) and the resistance force measured using a piezo-electric force transformer (Part No. 060-1896-02, ElectroSense, PA, USA). The data from the LVDT and force sensors were passed through analogue-to-digital converters and acquired at a 10 Hz sampling frequency and stored on a computer using Labview 8 software (National Instruments). Once the condyle had been immersed in PBS for 10 minutes and located in the correct place, the lock holding the indenter tip was released to start the experiment. After one hour of testing, the condyle was removed and the area that had been indented was marked out using a non-permanent pen (Figure 27) and the condyles were stored in plastic Tupperware on moist PBS soaked tissue at 4 °C, to allow the tissue to recover before measuring cartilage thickness.

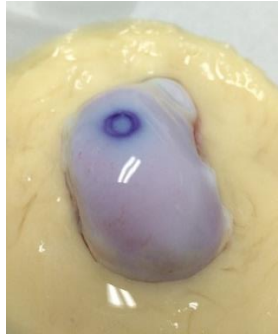


Figure 27: Medial Porcine condylar cartilage cemented in PMMA. The area of interest was marked out using a permanent marker.

2.2.6.3 Calibration¹

Calibration was undertaken to convert the voltage outputs of the LVDT and force transducer into millimetres and Newtons, respectively. The LVDT displacement transducer was calibrated using standard steel slip gauges. The voltage was recorded for each height increase following the addition of the slip gauges (0, 0.005, 0.01, 0.02, 0.05, 0.1, 0.2, 0.5, 1.0, 1.5, 2.0 mm – sizes of slip gauges used). The linear regression fit for the voltage against the displacement of the indenter tip was plotted and the linear trend line calculated. The equation of the line was subsequently used as a calibration factor (Figure 28).

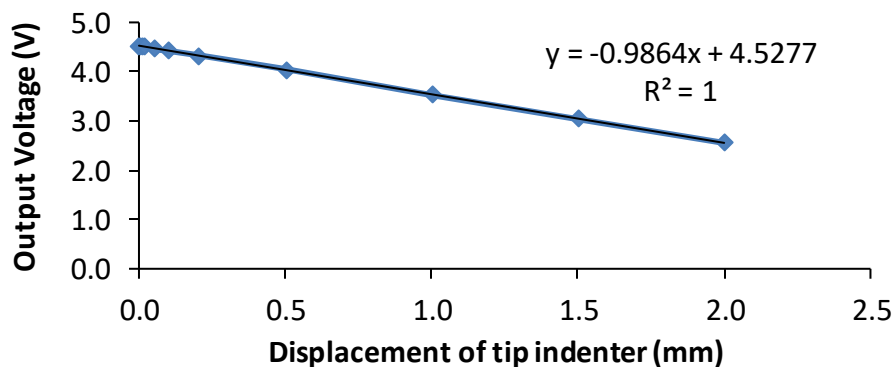


Figure 28: LVDT calibration. Calibration of LVDT from the indentation apparatus using standard height slip gauges to determine factor to convert output voltage to displacement.

The force transducer was calibrated by adding known masses to the top of the shaft incrementally (typically in step of 10.1 grams), while observing the changes in the voltage readings from the force sensor. The shaft to which the weights were being added was fixed, by allowing it to rest on a flat stainless-steel rod. This again, was plotted a linear regression

¹ Methodology developed by Abdellatif Abdelgaied

graph (voltage against load) and the equation of the trend line was used to convert voltage to Newtons (Figure 29).

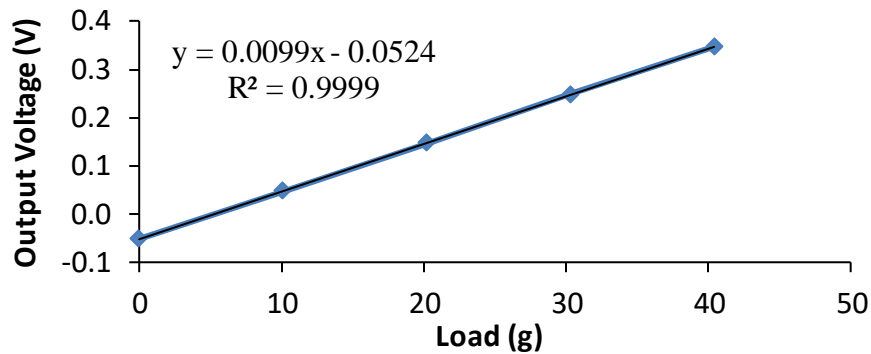


Figure 29: Load cell calibration. Calibration of load cell from the indentation apparatus using standard known masses to determine the factor to convert output voltage into Newton's.

2.2.6.4 Cartilage thickness measurements

Cartilage thickness was measured to normalise the deformation data for each cartilage condyle, so that the percentage deformation could be presented and material properties could be derived. The thickness was measured using an Instron material testing machine (Instron 3365B, INSTRON, University of Leeds - Figure 30A) with a needle attached to a force transducer. Condyles that had previously been cemented in PMMA cement (Section 2.2.6.1) and allowed to recover in a sealed Tupperware box moistened with PBS tissue at 4°C overnight, were fixed to the base of the material testing machine using 4 screws (Figure 30B). This allowed the area of indentation to be located directly underneath the needle indenter. The needle attached to the Instron arm was manually positioned ~1 mm above the cartilage surface (Figure 30C). During testing the arm was controlled via a PC graphic user interface (Bluehill Software V) and lowered at a rate of 4.5 mm.min⁻¹. The resistance to motion was measured using a 500 N load cell.

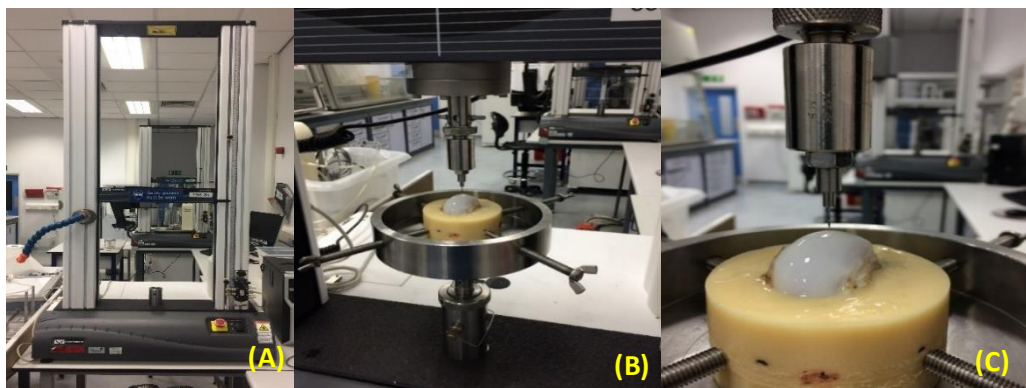


Figure 30: Picture of Instron testing equipment. (A) - Picture of Instron 3365B used for cartilage thickness measurements. (B) - Instron base for attachment of cemented porcine condyle (C) – Starting position of needle (circa 1 mm from cartilage surface) before cartilage thickness indentation method commenced.

The cartilage thickness was defined as the distance between the increase in resistance (measured in Newtons) from the initial needle contact with the cartilage surface and the steep increase in resistance from the needle coming into contact with the stiffer bone (Figure 31). Each condyle was indented 6 times on the periphery of the area that had been previously indented, taking care not to indent inside that area. An average of the thickness was calculated.

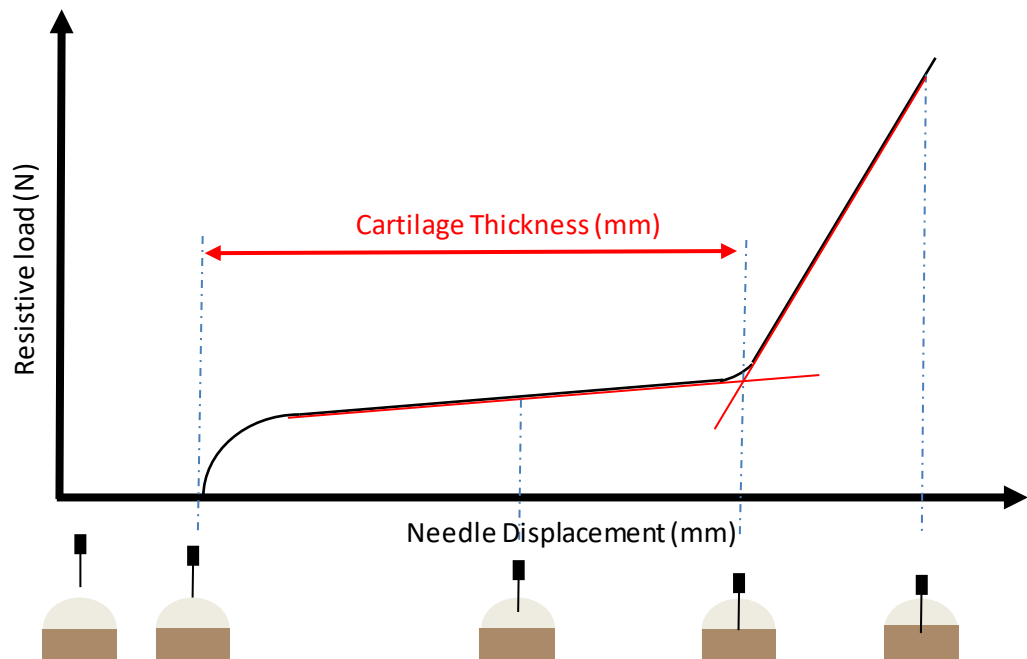


Figure 31: Needle indentation graph interpretation. This diagram shows how the cartilage thickness was determined from the needle indentation.

2.2.6.5 Finite element method for derivation of material properties

Cartilage deformation curves generated in Section 2.2.6.2 along with cartilage thicknesses measured in Section 2.2.6.4 were used to derive the permeability and equilibrium elastic modulus of the cartilage. An axisymmetric poroelastic biphasic finite element model (ABAQUS, version 6.9-1 Dassault Systemes, Suresnes Cedex, France) developed by Pawaskar *et al.* was used to simulate the indentation tests and derive the biphasic material parameters - permeability (k) and elastic modulus (E) of the cartilage samples (Figure 32) (Pawaskar *et al.*, 2010; Pawaskar *et al.*, 2011).

The cartilage was modelled as a poroelastic material and meshed with 900 four-node bilinear displacement and pore pressure elements CAX4P, whereas the subchondral bone was modelled with 225 four-node bilinear elastic elements CAX4. The choice of elements for these regions in the cartilage meant that there was no fluid flow between cartilage and subchondral bone, making it an impermeable boundary, shown in Figure 32. The cartilage model was assigned a water content of 80% and a Poisson's ratio of zero, in order to

maximise the biphasic effect or compressibility (Pawaskar et al., 2010; Jin et al., 2000). The metal indenter was modelled as rigid, since its elastic modulus was at least 5 orders of magnitude greater than that of cartilage.

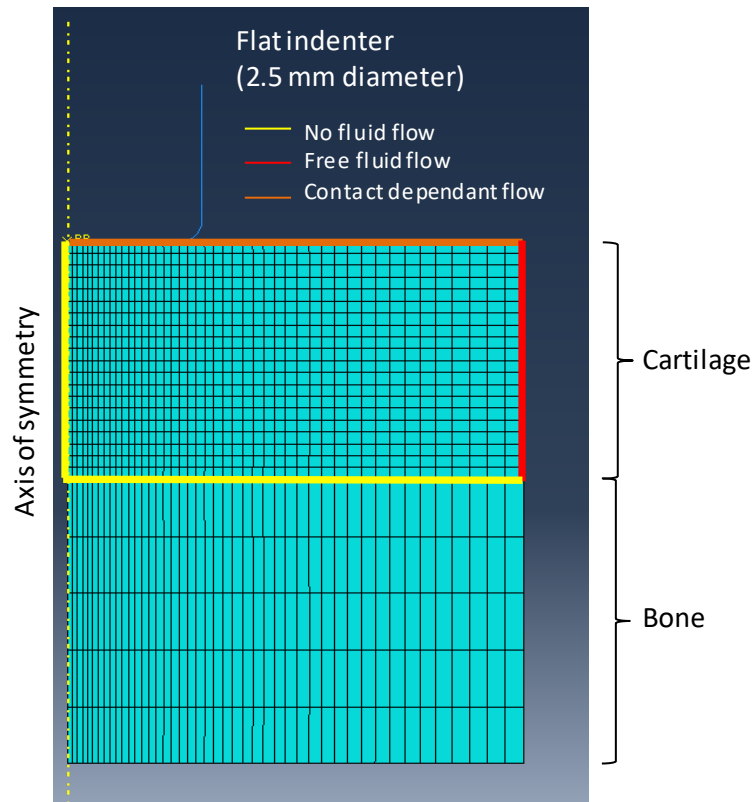


Figure 32: Finite element model of cartilage. This schematic shows the axis of symmetry and the imposed fluid flow restrictions in the model.

The FE model aims to mimic the method that was outlined in Section 2.2.6.2. The load was increased from 0 to a max load (specified in each Section), over 2 seconds through the indenter and applied for 1 hour in total. A graph showing the deformation/time was produced by the FE model based on the material properties (permeability and equilibrium elastic modulus) set, these starting material properties varied depending on the study being done. The closeness of fit between the final 30% of the FE model data and the experimental data was assessed using MATLAB (version 7.4, MathWorks Inc, Boston, MA, USA; Figure 33). The input initial material properties were adjusted to minimise the squared error. An R^2 value greater than 0.75 (75%) was accepted as significant for biological tissue. Equilibrium elastic modulus's and permeability values of each cartilage sample were chosen from the initial material properties that gave the highest R^2 value.

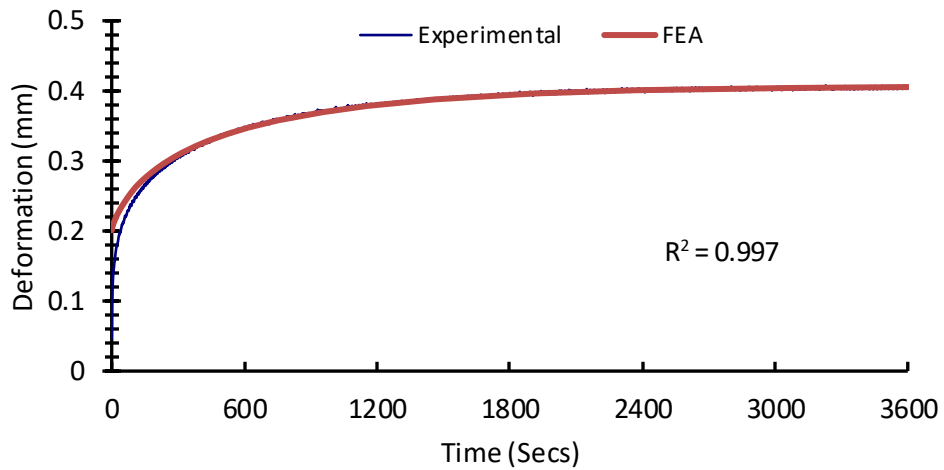


Figure 33: Experimental and modelled cartilage displacement curves. The FE model curve was fitted to the deformation curve produced by the experimental data to reach the highest possible agreement by altering the input material properties.

2.2.6.5.1 Sensitivity Analysis

A sensitivity analysis was carried out to determine if changing the end boundary condition (BC) on the left-hand side of the cartilage pin (red line - Figure 32), from ‘free-flowing fluid’ to ‘no fluid flow’ made a significant difference to the elastic modulus and permeability of the samples being tested. The experimental deformation data from 6 healthy pig condyles was input into the FE model. The same set of data was run twice. (BC-1) the first time the data was run with the left-hand side boundary condition with a ‘free fluid flow’ and (BC-2) the second time it was run with ‘no fluid flow’. The data is shown in Figure 34.

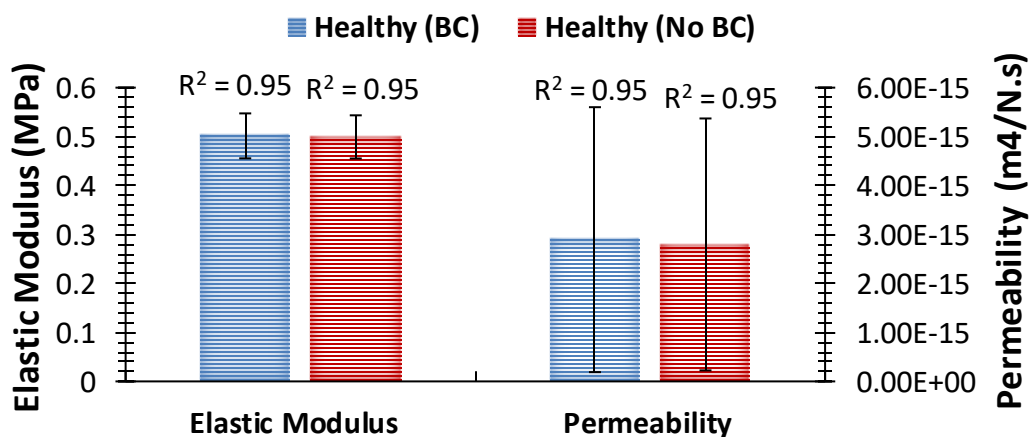


Figure 34: Equilibrium elastic modulus and permeability of healthy native medial condylar cartilage under a load of 0.31 N (Blue – Healthy condylar cartilage with the ‘no fluid flow’ boundary condition; Red – Healthy condylar cartilage with the ‘fluid flow’ boundary condition). Data is expressed as the mean (n=6) ± 95 % confidence limits. The R² values define how close the FE model curve fitting was to the last 70% of the experimental deformation curve, the closer the R² value is to 1, the better the fit. The data was analysed by Student’s t-test; *p<0.05. This revealed that changing the left-hand side boundary condition from ‘no fluid flow’ to ‘fluid flow’ did not significantly affect the elastic modulus nor the permeability of the healthy native cartilage.

The elastic modulus and permeability values of the healthy native cartilage samples with BC-1 were compared to the healthy native cartilage samples with BC-2, to determine if there were any difference. The data was analysed by Student's t-test to determine differences between group means. This showed that the elastic modulus and permeability values of the healthy native cartilage samples run with BC-1 were not significantly different to those of healthy native cartilage samples run with BC-2. Therefore, it was decided to run future FE models with the 'free fluid flow' boundary condition (BC-1) given the results of this sensitivity analysis.

2.2.7 Statistical analysis

2.2.7.1 Confidence limits

Microsoft Excel (version 2013, Microsoft) was used to analyse numerical data produced in this thesis. 95% confidence limits (CL) were chosen over standard error and standard deviation because 95 % CL are the most accurate and honest way of presenting the data of small samples sizes (n=3). 95 % CL take into account the sample size, whereas for the standard error, one has to provide the readership with the sample size so that the region in which the true mean lies, can be calculated. In this study the numerical data has been presented as the mean (n≥3) ± 95 % CL. The ± 95 % confidence intervals (α = 0.05) were calculated using the descriptive statistics option of the data analysis package in Microsoft Excel.

2.2.7.2 ANOVA

An analysis of variance was used when comparing the means of more than two groups. Individual differences between the data sets were identified by performing a Tukey Kramer post-hoc analysis to identify significant differences between group means.

2.2.7.3 Linear regression analysis

When interpolation of results was required, a linear regression analysis was performed on standard curves.

$$\text{Unknown } x = \frac{\text{Mean measured } y \text{ variables}}{y \text{ value of linear regression line equation}}$$

2.2.7.4 Arcsin transformation

When data is presented as a percentage or proportion, data values were transformed to arcsin to allow accurate calculation of the 95 % CL and statistical analysis. After analysis, values were transformed back for presentation.

Chapter 3 The effect of GAG molar ratio and Na⁺ ion concentration in two different salt solutions on the biochemical, morphological and biomechanical properties of peptides: P₁₁-4, P₁₁-8 and P₁₁-12

3.1 Introduction

The overall aim of this research is to investigate the utility of a multi-component system whereby GAGs are delivered into GAG depleted cartilage using a carrier self-assembling peptide (SAP) which is initially delivered as a non-viscous fluid. Subsequently, once in place, the SAPs are triggered by the physiological environment to self-assemble into a gel incorporating the GAGs.

Osteoarthritic cartilage has reduced biomechanical properties and this is primarily due to the gradual loss of GAGs. There is a great deal of interest in the research and development of early intervention treatments to repair or replace damaged cartilage in an attempt to delay the progression of OA and the need for joint replacement. One approach to repair early cartilage degradation is to restore GAG levels with the aim of maintaining functional cartilage material properties (Katta et al., 2008).

Peptides have been shown to readily self-assemble into higher order structures that create very stable hydrogels under physiological conditions and have been used to develop novel materials for regenerative medicine applications (Zhang et al., 2005; Bell et al., 2006; Firth et al., 2006; Kirkham et al., 2007; Galler et al., 2008; Schneider et al., 2008; Kyle et al., 2009; Kyle et al., 2010). The P₁₁-X family of self-assembling peptides (SAPs), are rationally designed 11 residue long peptides, with strategically placed hydrophobic and hydrophilic amino acids, which have been studied extensively (Kyle et al., 2010; Aggeli et al., 2001; Maude et al., 2011). The SAPs in this study, have the ability to form hydrogels from an initial non-Newtonian fluid state upon application of a trigger, they have been shown to be biocompatible and studies have indicated that they have potential as a visco-supplementation treatment for early stage OA (Bell et al., 2006). The combination of these self-recovering peptides with GAGs, which may provide increased bio-functionality, along with their ability to be delivered in a minimally invasive manner, makes them ideal candidates as injectable materials for use as a potential intervention therapy for early stage OA.

A key challenge is the control over the mechanical properties of these hydrogels which can be affected by the concentration of the peptide, the net charge of the peptide and also the environmental conditions such as pH and ionic strength (Aggeli et al., 2001; Miles, 2012). For

potential application in the treatment of early stage OA; SAP-GAG mixtures with three favourable properties would be desirable: high β -sheet percentage, long-woven fibrillar networks which are densely packed and have a high stiffness, all of which must occur in specific physiological conditions. Cartilage contains varying counter ions and the amounts and species depend on the region of the cartilage. These counter ions are important for the biomechanical function of cartilage (Urban, 1994). Urban (1994) summarised the range of ion concentrations in two discreet areas of articular cartilage, at the surface ($[\text{Na}^+]$ 210-230 mM, $[\text{K}^+]$ 7mM $[\text{Ca}^{2+}]$ 4-6 mM, $[\text{Cl}^-]$ 100-110mM) and in deep cartilage ($[\text{Na}^+]$ 260-320 mM, $[\text{K}^+]$ 9-11 mM, $[\text{Ca}^{2+}]$ 8-15 mM, $[\text{Cl}^-]$ 70-90 mM). The primary interest is in replacing depleted GAGs near the surface of cartilage and therefore it was important to investigate the behaviour of P_{11} -X peptides and P_{11} -X-GAG mixtures in the physiological conditions representative of this region.

Fourier transform infra-red spectroscopy (FTIR), has been used to analyse the secondary structure of peptides, in particular the amide I region. The peptides used in this study have been designed to self-assemble into β -sheet character. Therefore, interest lies in analysing the β -sheet percentage of these peptides and peptide: GAG mixtures. Transmission electron microscopy (TEM), allows for high resolution images of the macro and micro-structures of the peptides in a self-assembled state. At the micro-level, the fibril/fibre formation can be analysed morphologically. Thicknesses and of the peptide fibril/fibres can also be calculated. Rheology has previously been used to explore the biomechanical properties of various peptide hydrogels, and also to study their gelation mechanisms during and after flow (Aggeli et al., 1997). Rheology may be used to mimic the mechanical process that these hydrogels would undergo if used *in vivo* in cartilage, such as shear under load. Walking frequency (stride length) is *ca.* 1Hz (60 strides per minute) (Danion et al., 2003; Mason et al., 2005). Therefore, the rheological behaviour of the assembled peptides and assembled peptide/GAG mixtures were compared at 1Hz. The GAG chosen in this study, was chondroitin sulfate. Chondroitin sulfate, is the most abundant GAG in the proteoglycans present in native cartilage. Molar ratios of 1:16 and 1:64 were chosen based on findings presented by Aggeli *et al.* (2001) and Ng *et al.* (2003). Aggeli *et al.* described a model in which the length and width of peptide fibrils could be calculated through theoretical principles and assumptions paramount to concentration dependent self-assembly, which are based upon the monomeric peptide concentration. Furthermore, Ng *et al.* calculated the average individual core-protein end to end length, GAG chain length (average number of disaccharides per chain) and GAG to GAG spacing of two types of aggrecan from foetal and mature cartilage from atomic force microscopy (AFM) images and measurements (Ng et al., 2003). In this study, the peptide

mimicked the role of the core protein in the aggrecan. Therefore, combining information from both these studies, it was possible to determine the amount of GAGs that would be needed to give the correct ratio of GAGs to peptide.

3.2 Aims and objectives

The aims of this part of the study were to determine the effects of combining the SAPs with chondroitin sulfate (GAG) at two molar ratios of 1:16 and 1:64 in 130 mM and 230 mM Na⁺ salt solutions, representative of normal physiological conditions and the physiological environment within the surface of articular cartilage. The specific objectives were:

- 1) To determine the **β-sheet percentage** of the peptides and peptide/GAG mixtures in physiological conditions.
- 2) To assess the **fibril morphology** of the peptides and peptide/GAG mixtures in physiological conditions.
- 3) To determine the **biomechanical properties (stiffness)** of the peptides and peptide/GAG mixtures in physiological conditions.

3.3 Methods

This section summarises the procedures generally used to prepare peptide solutions for FTIR and transmission electron microscopy (TEM). Any exceptions to these procedures are detailed in the appropriate sections.

Peptides and GAG were weighed as detailed in Chapter 2; Sections 2.2.1.1 and 2.2.1.2, respectively. With the exception that in this study for the TEM and FTIR, the concentration (w/v) of peptide used was 5 mg.ml⁻¹.

3.3.1 Dissolution of peptides, peptide: GAG mixtures and Na⁺ salt solutions.

3.3.1.1 Dissolution of peptides for studies of peptide alone.

The appropriate Na⁺ salt solution (300 μl; described below) was added to the weighed peptides. Peptides were then taken to a monomeric state (unless otherwise stated), which was determined by achieving the required pH or [pD] and observing the fluidity of the gels; monomeric peptides were clear and exhibited water like properties (above pH 12 [pD 11.6] for P₁₁-4 and below pH 3 [pD 2.6] for P₁₁-8 and P₁₁-12). Between 50-100 μl of 0.1–3 M HCl or NaOH [DCl or NaOD] aliquots were added during this process before the monomeric solutions were carefully taken to pH 7.4 [pD 7] using 50-100 μl of 0.1–3 M HCl and NaOH [DCl

and NaOD]. The containers were sealed with Parafilm, vortexed for ≈ 40 seconds and sonicated in a water bath at 35 kHz at 37°C for two hours before storage at 4°C overnight to allow the peptides to equilibrate and prevent any contamination. The pH [pD] was re-measured and re-adjusted to pH 7.4 [pD 7] the following day and the final volumes were adjusted to 0.5 ml.

3.3.1.2 Dissolution of peptides and chondroitin sulfate for studies of peptide: GAG mixtures.

The peptides were treated as described in Section 3.3.1.1, except that chondroitin sulfate was added before bringing the pH back to 7.4. Chondroitin sulfate powder was weighed (Chapter 2; Section 2.2.1.2) and 50-100 μl of the appropriate Na^+ salt solution was added. The chondroitin sulfate solution was vortexed for ≈ 40 seconds and sonicated in a water bath at 35 kHz for a further ≈ 5 minutes at 37°C. The chondroitin sulfate solution was added to the monomerised peptide and vortexed for a further 40 seconds. After bringing the PEP-GAG mixture to pH 7.4 [pD 7] and adding the Na^+ salt solution to make the final volume to 0.5 ml, the mixture was vortexed for ≈ 40 seconds and sonicated in a water bath at 35 kHz at 37°C for two hours. Samples were refrigerated overnight (4°C) to allow them to equilibrate and the pH was re-measured and re-adjusted to pH 7.4 [pD 7] the following day. The final volumes of the mixtures were adjusted to 0.5 ml.

3.3.1.3 Dissolution of physiological salts to make up two concentrations of Na^+ salt solutions.

The peptides and PEP-GAG mixtures were studied in two aqueous salt solutions containing varying Na^+ ion concentrations (130mM & 230 mM), unless otherwise stated. These two salt solutions contained all the ions present in cartilage (Urban, 1994). The salts present within these two salt solutions and their concentrations are listed in Table 10. The only species that varied between the two salt solutions was the concentration of Na^+ ions. Throughout this thesis an increase in the salt concentration is described as an increase in the Na^+ ion concentration. The solvent used to dissolve the ions, peptides and chondroitin sulfate in this study was distilled water (H_2O), unless otherwise stated (Section 3.3.1).

Table 10: Concentrations of different salts present in the two physiological salt solutions.

Salt	Salt solution 1 (130mM of NaCl) (mg.ml ⁻¹)	Salt solution 2 (230mM of NaCl) (mg.ml ⁻¹)
KCl	0.522	0.522
CaCl ₂	0.555	0.555
NaCl	5.143	5.143
NaHCO ₃	3.528	11.929

3.3.2 Measurement and adjustment of pH

All samples were adjusted to pH or pD (pH in deuterated solutions) of 7.4 ± 0.3 , unless otherwise specified. Measured pD values quoted here were those following the a 0.4 correction value subtracted from the pH meter reading (Glasoe and Long, 1960). Sample pH was determined using a Sartorius Docu-pH meter and a pH electrode probe. The probe was filled with and stored in a 3 M KCl solution.

Prior to use, the Sartorius Docu-pH meter was calibrated using three different pH standard buffers at pH 4, 7 and 10 (each within ± 0.01 pH units at 25°C). Following this procedure, the value of the pH 7 buffer was rechecked to ensure correct calibration.

The pH of the solutions was adjusted using micro-litre aliquots of 0.05, 0.1, 0.25, 0.5 and 1 M HCl and NaOH [DCl and NaOD for the FTIR study]. After each addition of acid or base, the solution was vortexed (≈ 10 seconds), and its pH or pD rechecked.

3.3.3 Fourier Transform Infra-Red Spectroscopy (FTIR)

3.3.3.1 Background to FTIR analysis of peptides

The application of FTIR spectroscopy to peptides allows their secondary structure to be analysed. When a molecule absorbs IR light, the oscillating dipole moment interacts with the oscillating electric vector of the IR beam (Williams and Fleming, 1995). A bond within a molecule can experience different types of oscillation depending on the energy between its ground state and excited state. The amount of energy absorbed is dependent on changes in the dipole moment. Bonds that are non-polar show weak absorption and those that are polar, such as C=O, show strong absorption. Complex molecules will have a variety of vibrational modes, these will consist of vibrations from individual bonds but there will also be vibrations from functional groups. The main amide vibrational modes are termed A and B and I-VII, which enable the study of peptide secondary structure. Of these modes, amides I to III are of most interest for proteins (Table 11) (Seshadri et al., 1999).

Table 11: Characteristic infrared bands of the peptide (Susi, 1972).

Amide Band	Wavenumber (cm ⁻¹)	Origin
A	~3300	NH Stretching
B	~3100	NH stretching
I	1600-1690	C=O Stretching
II	1480-1575	CN Stretching, NH Bending
III	12229-1301	CN Stretching, NH Bending
IV	625-767	OCN bending mixed with other nodes
V	640-800	Out of plane NH Bending
VI	537-606	Out of plane C=O Bending
VII	~200	Skeletal Torsion

Amide I is the most useful for the secondary structure determination (Susi and Byler, 1986). Arrondo et al. reported that more than 90% of protein studies used solely amide I band for analysis (Arrondo et al., 1993). The reasons why amide I is preferred over amide II and III were initially explained by Jackson and Mantsch (1995) and Cai and Singh (2004):

- Amide I, arises from just one functional group –C=O stretching, which simplifies the assignment (Jackson and Mantsch, 1995).
- Amide II has a strong vibration but is insensitive to secondary structure and may also be obscured by side chain vibrations (Cai and Singh, 2004).
- Amide III, despite it being sensitive to the secondary structure, has a weak vibration (5-10 times less than amide I) and it can be affected by other vibrations (Cai and Singh, 2004).

Amide I stretch is affected by many different intermolecular hydrogen bonding patterns in the peptide backbone, therefore it manifests itself as a featureless peak that occurs at 1600-1690 cm^{-1} . In the same way that the functional groups are located by looking at the absorption ranges, it is also possible to compare the amide band peaks and determine the secondary structure of the sample (Table 12). Different peptide and protein secondary structures have unique hydrogen bonding patterns (C=O or NH groups), which gives rise to exact vibrational frequencies in the amide I band. The assignment of these amide regions to the presence of various secondary structure motifs has been taken from previous studies on proteins with dominant secondary structures, homo-polypeptides and calculated values (Barth, 2007; Pelton and McLean, 2000).

Peptides and proteins are usually studied in aqueous conditions as these are the conditions in which they adopt native structure. However, water (H_2O) has several IR absorption peaks with one present at 1650 cm^{-1} , which is in the middle of the amide I region (Siebert and Hildebrandt, 2007). For this reason, deuterium oxide (D_2O) was used in all FTIR studies rather than H_2O . The D_2O bending absorption has a lower wavenumber, as deuterium has a greater mass than hydrogen. If the samples in the spectra have been made up using D_2O , the amide bands have a prime symbol attached to them e.g. amide I'.

3.3.3.2 Analysis of FTIR data

3.3.3.2.1 Peak fitting and assignment

When peptide samples are subject to FTIR, a spectrum is produced which is then peak fitted. The peak fitting procedure is an iterative process in which chosen peak functions are adjusted and matched to the experimental spectrum as closely as possible. Using more component

peaks may improve the difference between the experimental and fitted spectra; however adding too many peaks may cause the spectra to lose meaning. The recommendation from Thermo-Fisher was to use a minimal number of peak functions to fit the amide I' region, with additional peaks being added if necessary after convergence.

Once the FTIR spectra has had the amide I' region fitted to the component bands, the assignment of the bands to the different secondary structure motifs is the final stage of analysis. Secondary structures can exhibit peak positions over a range of values, depending on the peptide and the conditions under which it is studied. Differences can arise from variation in hydrogen bonding, which introduces ambiguity in assignment. Therefore values which different authors assign to different secondary structure components may overlap, and hence distinguishing each is not easy (Jackson and Mantsch, 1995).

The P₁₁ peptides used in this study were designed to self-assemble into β -sheet character; which can be identified in the amide I region using FTIR (Arrondo et al., 1993; Barth, 2007; Kong and Yu, 2007). Therefore, interest lay in analysing the β -sheet peaks. The peak positions corresponding to the various secondary structures are presented in Table 12 and the peaks for some of the amino acid side chains are listed in Table 13.

Table 12: Secondary structural assignments of amide I' infrared bands.

Amide I' Band	Secondary structure assignment
1613-1630	β -sheet
1642-1649	Unordered
1649-1655	α -helix
1658-1672	β -turn
1673	TFA
1672-1690	β -sheet
1694-1697	β -turn

Adapted from: (Susi and Byler, 1986; Jackson and Mantsch, 1995; Pelton and McLean, 2000; Harris and Chapman, 1995; Kong and Yu, 2007).

3.3.3.2.2 Side chains and trifluoroacetic acid (TFA) in the amide I region

Amino acid side chains exhibit characteristic absorption frequencies in the amide I region and therefore must be considered during the assignment of secondary structures. Chirgadze *et al.* (1975) reported the side chain absorptions in the presence of D₂O. Fortunately, shown in Table 13, the small number of amino acids present in the P₁₁ peptides simplifies this consideration. Furthermore, the IR molar absorption coefficient for most side chains is a lot weaker compared to that of the peptide bond itself. Therefore, only arginine, glutamine and glutamic acid may be detectable in the amide I region of the P₁₁ peptides.

Table 13: Amino acid side chain absorptions in the amide I' region for the P₁₁ peptides studied by FTIR spectroscopy.

Amino Acid	Wavenumber (cm ⁻¹)	Molar absorption coefficient/notes
Arginine	1586	$\epsilon = 500 \text{ M}^{-1} \text{ cm}^{-1}$
	1608	$\epsilon = 460 \text{ M}^{-1} \text{ cm}^{-1}$
Glutamine	1635-1654	$\epsilon = 550 \text{ M}^{-1} \text{ cm}^{-1}$
Glutamic Acid	1567	$\epsilon = 830 \text{ M}^{-1} \text{ cm}^{-1}$
	1706-1775	$\epsilon = 280 \text{ M}^{-1} \text{ cm}^{-1}$
Ornithine	-	No data found, note lysine does not absorb in the amide I' region.
Phenylalanine	-	No absorption
Tryptophan	1618	Little to no absorption.

Adapted from: (Chirgadze et al., 1975; Barth, 2000).

Trifluoroacetic acid (TFA) is frequently used during the purification of peptides, which means it could be present in the peptides as a counter ion bound to the positively charged residues (Cornish et al., 1999). The amount of TFA present in the peptide is dependent on the amount of positively charged residues in the peptide i.e. peptides containing greater numbers of arginine and ornithine will contain more TFA. The TFA band is located at 1673 cm^{-1} . Care had to be taken when assigning the secondary structures of the peptides, as the TFA falls in a β -sheet region and could be incorrectly assigned to it.

3.3.3.3 Method

3.3.3.3.1 Sample preparation

Two sets of solutions of P₁₁-4, P₁₁-8 and P₁₁-12 were prepared in D₂O. One set of peptides was prepared in 130 mM Na⁺ salt solution and the other set was prepared in a 230 mM Na⁺ salt solution as detailed in Section 3.3.1.

3.3.3.3.2 Equipment and data acquisition

Samples were placed in a Thermo HT-32 demountable cell with CaF₂ windows and a copper spacer in-between the windows with a thickness of 0.25 mm. A Thermo Nicolet 6700 FTIR spectrometer, controlled with OMNIC 7.3 SP1 software, was used to record the FTIR spectra. Each spectrum was an average of 32 scans taken at a resolution of 4 cm^{-1} at room temperature, one replicate per sample was analysed. Experiments involved pipetting about $\sim 40 \mu\text{l}$ of the gel/liquid sample into the cell. A background air spectrum, consisting of an empty sample compartment (no cell), was always taken before commencing any sample measurement.

3.3.3.3.3 Processing of spectra

As well as collecting spectra for the background and the sample, spectra of the two Na⁺ salt solutions in D₂O were also recorded using the same path length spacer and then they were

subtracted from the sample spectrum, using the subtract function in OMNIC. Whilst in this function, the region of 1800 to 2100 cm^{-1} was observed while varying the subtraction factor; the appropriate subtraction factor was chosen when a flat baseline was achieved in this region. Subtracted spectra were then baseline corrected with a manually selected baseline, whose points were fixed to the spectral values and interpolated using a spline function.

In order to fit the amide I' band, baseline corrected spectra were processed with the OMNIC peak analysis tool (Bradley, 2007). This tool fitted a series of defined functions which summed to ideally match the experimental spectra as well as possible. In order to achieve this, the second derivative of the amide I' region had to be observed (spectra were analysed in the 1720-1580 cm^{-1} range) to locate large negative peaks. Negative peaks in the second derivative corresponded to actual absorption peaks (Stuart, 2004). Once located, Gaussian-Lorentzian peak functions with constant baseline and a noise of 10 were centrally aligned at wavenumbers corresponding to these negative peaks. Initially, a minimum number of peaks were selected. Peak parameters were optimised by a Fletcher-Powell-McCormick algorithm which minimised the root mean square noise ratio of the residual of the fitted peak sum to the actual spectrum. Once converged, if necessary, new peak functions were manually added in the same manner, where the residual was large and the optimisation was repeated. This process was repeated until it was no longer possible to further improve the residual.

Once the fitted peaks in the amide I' region had been assigned to a secondary structure the proportion of peptide adopting a particular secondary structure was determined from the relative areas using equation 5 (Stuart and George, 1996). The relative areas were calculated for each peak parameter, during the peak fitting, using the peak analysis tool in OMNIC. In this study the percentage of β -sheet was of particular interest.

$$\text{Equation 5} \quad \% \text{ Secondary structure} = 100 \times \frac{\text{Motif total peak area}}{\text{Total secondary structure peak area}}$$

3.3.4 Transmission Electron Microscopy (TEM)

3.3.4.1 Method

3.3.4.1.1 Sample preparation

Two sets of solutions of P₁₁-4, P₁₁-8 and P₁₁-12 were prepared in H₂O. One set of peptides was prepared in 130 mM Na⁺ salt solution and the other set was prepared in a 230 mM Na⁺ salt solution as detailed in Section 3.3.1.

Carbon-coated copper grids (400 mesh grids, Agar scientific) were placed coated side down on the surface of a 10 μl droplet of the sample to be analysed for 1 min and then blotted on

filter paper to remove excess. Grids were then placed on a 10 μl droplet of 2% (20 $\text{mg}\cdot\text{ml}^{-1}$) uranyl acetate for 30 secs for negative staining and then blotted against double folded Whatman 50 filter paper and left to dry. Prepared grids were stored in plastic grid storage boxes. Grids were examined with a JEM-1400 JEOL microscope.

3.3.4.1.2 Image capturing and processing

Digital images were captured using an AMT ERB bottom mounted digital CCD camera on the TEM microscope. AMT image capture engine (Version 602) was used as an interface between the camera and the computer in order to save the pictures as tiff images for further processing. Only one replicate per sample was analysed. Fibril lengths and widths and twist pitch were measured with ImageJ software (Version 1.47), as described in Figure 35. Before any measurement was made the appropriate distance per pixel was set using the software's set scale function. The measurements were then made by tracing over the image with a straight or segmented line tool and then using the software inbuilt measure function to measure the cumulative distances.

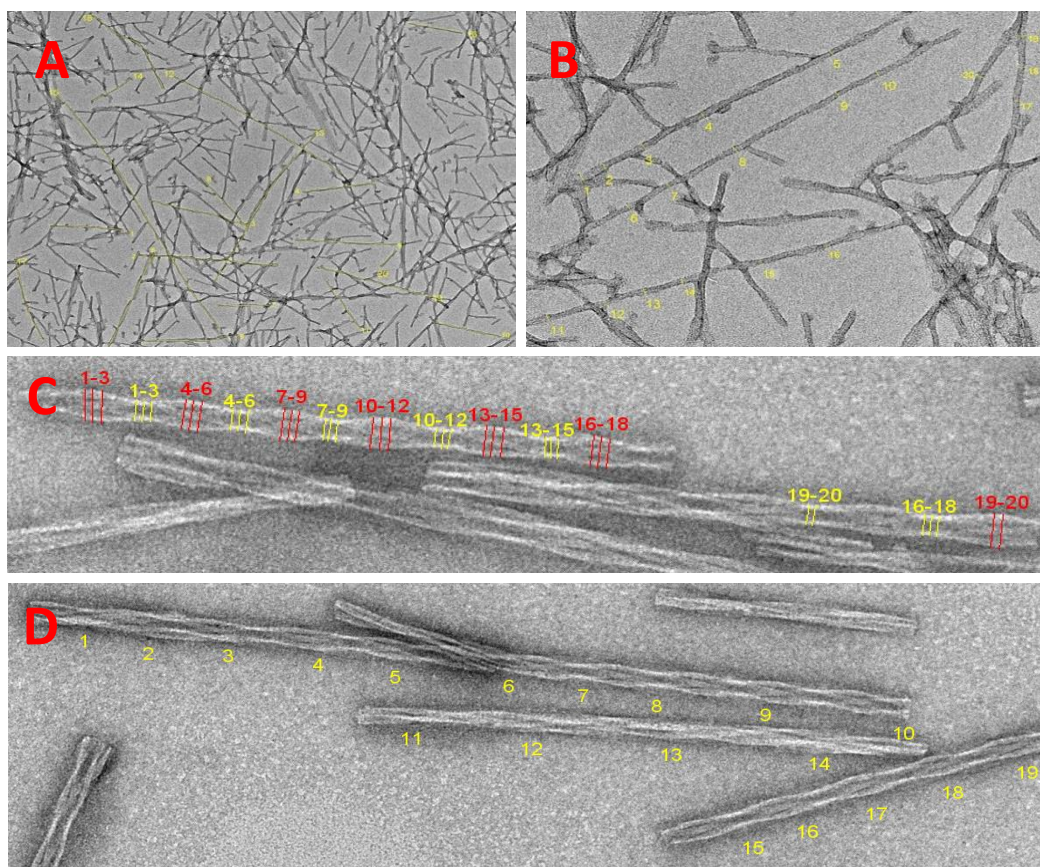


Figure 35: TEM images of P11-8 fibrils, illustrating how the fibril lengths, widths (long and short) and twist pitch was calculated. (A) 20 random fibrils were chosen and the length measured, (B) 20 random fibrils were chosen and the width measured, (C) if the fibrils were twisted the long width (red line) and short width (yellow line) were measured 20 times, (D) the twist pitch was calculated by measuring the first narrowest point to the third, indicative of a full twist. This was repeated all the way down the fibril length and then an average of these values was recorded.

3.3.5 Rheology

3.3.5.1 Background to Rheology

Solids deform when stressed, whereas liquids flow. The rheological properties of a material can be studied by stressing the sample and measuring how much it deforms. To measure the resistance to deformation of a material (elasticity) the shear modulus is measured. The shear modulus is the resistance to movement, the stiffer a sample is the more resistance to movement it has. The modulus is a measure of shear stress divided by the shear strain. A rotational rheometer (Figure 36) measures the shear modulus of a sample by oscillating backwards and forwards, non-destructively, so that it can show the properties under deformation, before it flows. This can be carried out in one of two ways:

- Controlled stress – oscillates top plate with a set force and measures its displacement.
- Controlled strain – oscillates top plate using a set displacement and measures the force.

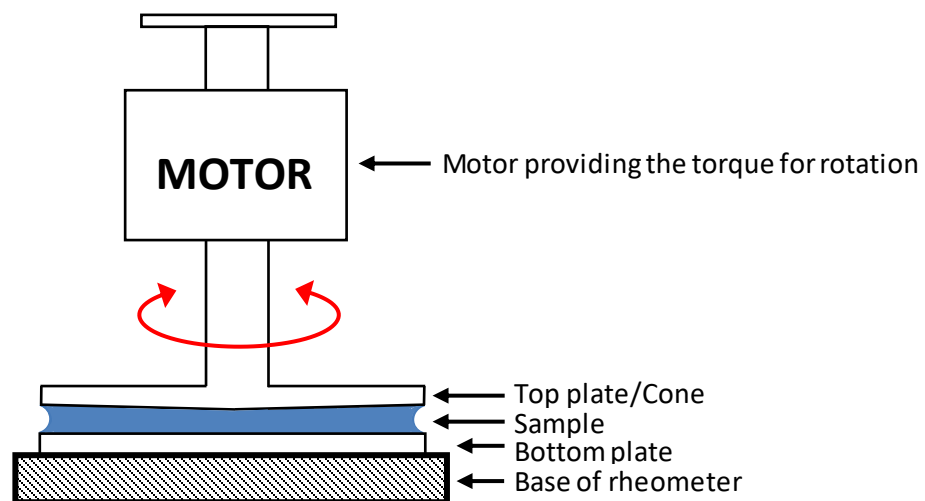


Figure 36: Schematic of a rotational rheometer.

The microstructure of liquids in their natural rest condition represents a minimum energy state. However, when they are deformed, thermodynamic forces immediately act to restore the rest state, just like a spring. Like a spring movement from the rest state represents a storage energy, which expresses itself as an elastic force trying to restore the static *status quo*. At first these restoring forces increase linearly with the distance that any deformation takes the material away from the state of rest, but eventually non-linearity's will occur. The rate at which the force increases with deformation diminishes, until at very large deformations a steady state condition arises and the elastic force becomes constant (Barnes, 2000). Alongside these elastic forces are also viscous forces due to the dissipation and rate of deformation. In conjunction, these two forces produce viscoelastic effects. One way to

measure the viscoelastic profile of a material is to use oscillatory testing. This involves applying an oscillating stress or strain as an input to the sample and resolving the resulting oscillatory strain or stress output to study the microstructure and therefore predict the materials` behaviour.

There are two types of responses; a solid-like response and a liquid-like response. A solid-like response is where the input stress or strain is in phase with the output stress or strain and therefore the phase angle would be zero. Whereas for a liquid-like response, the output stress or strain would be $\pi/2$ out of phase (Phase angle = 90°) with the input (Figure 37).

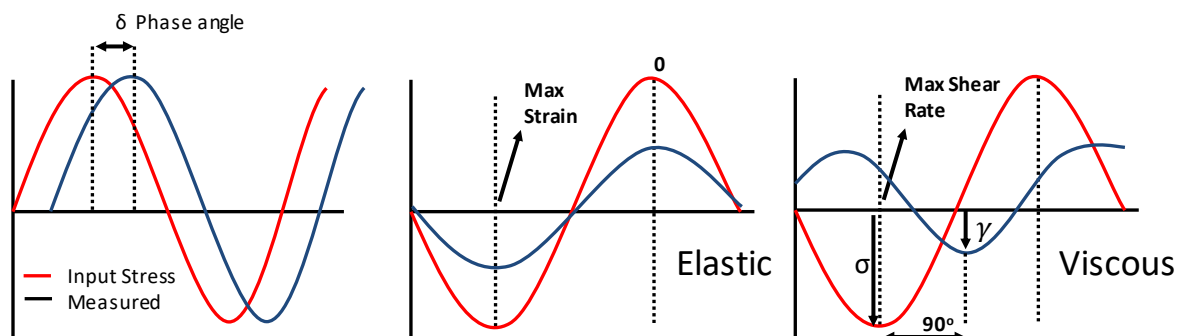


Figure 37: Example of phase angle and its relationship to viscous and elastic materials.
Adapted from (Duffy, 2016).

The solid component at any particular frequency is characterised by the storage modulus ($G' = G \times \cos\delta$) and the liquid like component is described as the loss modulus ($G'' = G \times \sin\delta$), where G is the elastic modulus ($\frac{\sigma}{\gamma}$) and δ is the phase angle. The combination of both these parameter yields the complex modulus (G^*), which is the measure of the overall stiffness of a material and is calculated by how much a sample moves (shear strain (γ)) for a given force (shear stress (σ)). If $G' > G''$, then the phase angle will be less than 45° and exhibit solid-like behaviour. If $G'' > G'$, then the phase angle will be greater than 45° and exhibit liquid-like behaviour (Duffy, 2016).

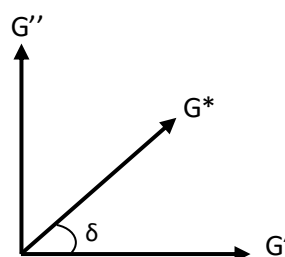


Figure 38: Loss, complex and elastic modulus.

Oscillatory rheometers have two components of the oscillation setup that can be controlled:

1. The oscillation amplitude (strain or stress) – An amplitude sweep can be run to determine the linear viscoelastic region (LVER). This gives an idea of the stability of

the sample and this can also be quantified to indicate how much energy is required to break up the suspension. The larger the force is, the more stable the sample. In the LVER, the storage modulus does not change, therefore this means that it is non-destructive to the material and any subsequent tests (frequency sweeps) can be kept within the LVER (e.g. Figure 39).

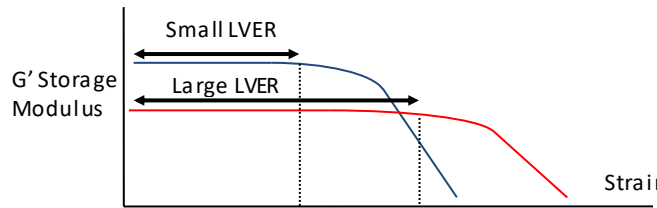


Figure 39: Graph demonstrating the Linear Viscoelastic Region. Adapted from (Duffy, 2015).

2. The frequency (oscillation time-scale) – A frequency sweep is run to determine the response at different timescales and this is carried out within the LVER region.

Generally, there are three types of material behaviour that can be determined from rheological data:

- 1) Viscoelastic liquid; where the phase angle at rest tends towards 90° .
- 2) Viscoelastic solid; where the phase angle at rest tends towards 0° .
- 3) Gel; where the phase angle is independent of frequency.

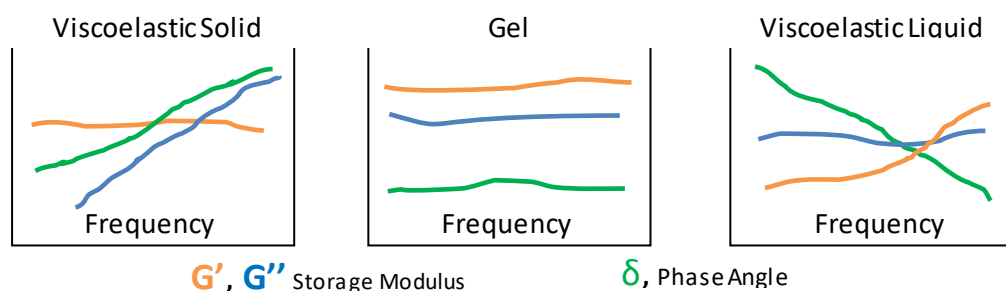


Figure 40: General material behaviour in terms of storage and viscous modulus and phase angle. Adapted from (Duffy, 2016).

Rheology has previously been used to not only look at bulk mechanical properties of various peptide hydrogels, but also to study their gelation mechanisms during and after flow (Aggeli et al., 1997). Self-recovering peptide hydrogels could be ideal candidates for injectable materials and rheometry can be used to mimic the mechanical process of such procedures; such as the shearing effect of an injection or the shear of cartilage under load. The rheology that will be undertaken in this chapter will not only give an insight into the gelation kinetics and gel stiffness, both of which directly affect the final use of these materials, but it will also

be used to determine whether the SAP:GAG systems are reproducible and whether individual samples are repeatable. Hence this will determine whether the preparation method is suitable for future use.

3.3.5.2 Sample preparation

Three replicate samples were measured in triplicate for each peptide alone, chondroitin sulfate alone and PEP: GAG mixture in the two Na⁺ salt solutions. Each sample had a total volume of 4 ml. For each replicate 1 ml was applied to the rheometer.

3.3.5.2.1 Peptide control: P₁₁-4, P₁₁-8, P₁₁-12.

Approximately 40 mg of peptide was weighed into a sample vial, to which 3.5 ml of the appropriate Na⁺ salt solution was added (i.e. 130 mM or 230 mM Na⁺ salt solution). Samples were then sonicated for 10 minutes. The peptide controls were then prepared as described in Section 3.3.1.1.

Once a pH as close to 7.4 had been achieved, peptide samples were placed in a water bath at 37°C for two hours. Samples were stored at 4°C overnight to allow them to equilibrate and the pH was re-measured and re-adjusted to pH 7.4 the following day. This was carried out using minimal microliter volumes of HCL and NaOH aliquots, vortexing for ≈40 seconds after each addition. The final volumes of each solution were adjusted to 4 ml.

3.3.5.2.2 Peptide: GAG samples: P₁₁-4, P₁₁-8, P₁₁-12: GAG (1:16 and 1:64).

It was hypothesised that the introduction of varying molar ratios of chondroitin-6-sulfate (CS), would not only interact electrostatically with the charged peptide but also with the charged Na⁺ salt solutions. Therefore, in order to establish whether these interactions were possible, a mixing study was carried out, whereby a gel would be made by combining the peptide and GAG to produce a peptide-GAG gel. The concentration of peptide was kept the same for each sample (10 mg.ml⁻¹) and the molar ratios of GAG used was 1:16 and 1:64. In order to carry out several repeats (n=3), the volume of the peptide: GAG mixtures were increased from 1 ml to 4 ml, with the concentration remaining at 10 mg.ml⁻¹, as shown in Table 14. The GAG was also found to have some impurities in terms of Na⁺, which was determined using atomic absorption spectrophotometry. There was 0.08312 mg of Na⁺ per mg of CS, therefore this was accounted for in the ratio weights of the GAG.

Table 14: Masses of peptide and CS weighed out for the different molar ratios. Samples were made up to a total volume of 4ml in two aqueous Na⁺ salt solutions.

	1 part GAG : 64 part peptide		1 part GAG : 16 part peptide	
P ₁₁ -4	19.4mg	42.1 mg	77.6 mg	42.1 mg
P ₁₁ -8	19.7 mg	51.5 mg	79.0 mg	51.5 mg
P ₁₁ -12	22.1 mg	50.2 mg	88.4 mg	50.2 mg

Approximately 40 mg of peptide was weighed into a sample vial, to which 3 ml of the corresponding Na⁺ salt solution was added (i.e. 130 mM or 230 mM Na⁺ salt solution). Samples were sonicated for 10 minutes at 37°C. The peptides were monomerised as described in Section 3.3.1.1. For each peptide, the appropriate pre measured amount of GAG (Table 14) was hydrated in 950 µl of the corresponding Na⁺ salt solution. This GAG suspension was vortexed for ≈40 seconds and then sonicated for 5 minutes at 37°C. The GAG suspension was added to the monomerised peptide and vortexed for a further ≈ 40 seconds on a low setting. The pH was adjusted to pH 7.4 or as close to it as possible and then placed in a water bath at 37°C for two hours. Samples were stored at 4°C overnight to allow them to equilibrate and the pH was re-measured and re-adjusted to pH 7.4 the following day. This was carried out using the remaining 50 µl volume of HCl and NaOH aliquots to make the total volume up to 4 ml.

3.3.5.2.3 GAG control: chondroitin sulfate alone.

The highest and the lowest weights of chondroitin sulfate mixed with the peptides (19.4 mg and 88.4 mg; Table 14), were selected as controls. The pre-weighed chondroitin sulfate was hydrated in 3.95 ml of the corresponding Na⁺ salt solution. Samples were vortexed for ≈ 40 seconds and then sonicated for a further 10 minutes at 37°C. The pH was adjusted to 7.4 using the remaining 50 µl volume of HCl and NaOH aliquots to make the total volume up to 4 ml.

3.3.5.3 Method

All rheological measurements were carried out on the Malvern Kinexus Rheometer. rSpace Kinexus by Malvern Instruments was used to control the rheometer and export raw data. A coned-plate geometry (50 mm diameter, gap of 0.0330 mm) was used with a cone angle of 1°. All tests were run at 37°C, using a solvent trap (SU0005 PLC) so that the atmosphere was kept saturated to ensure minimal evaporation of the peptide: GAG samples.

Samples were firstly subjected to an amplitude sweep, which determined the linear viscoelastic region (LVER) of the sample. Therefore, two amplitude sweeps were performed in a shear strain controlled mode from 0.01-100%. One at 1 Hz and another at 20 Hz with a 10-minute pause in-between the two amplitude sweeps to allow the peptides to equilibrate. Both components of the shear modulus (elastic and viscous) at both 1Hz and 20 Hz were overlaid in Origin Pro. A strain value that lay within the LVER (preferably in the middle), in which the elastic shear modulus (G') and the viscous shear modulus (G'') were independent of the strain amplitude was chosen (i.e. Figure 41).

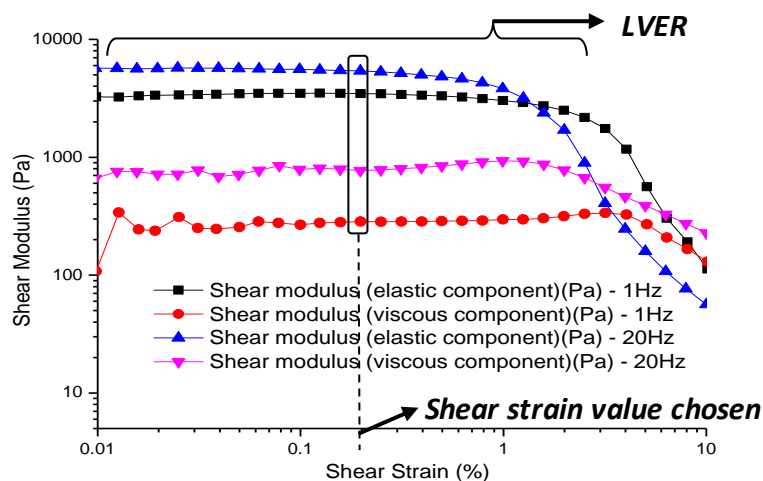


Figure 41: Example amplitude sweep run at 1Hz and 20Hz showing both the elastic and viscous shear modulus. Strain value that lay in the middle of the LVER was chosen.

Frequency sweeps were then run to determine the dynamic modulus of the hydrogel samples. The sweeps were run between 1 and 20 Hz at the pre-determined strain that was established from the amplitude sweep. Peptide hydrogels were allowed to equilibrate for 15 minutes once loaded, prior to the start of testing. Visual observations were recorded in the form of images of the gels after 48 hours, prior to testing.

3.3.6 Statistical analysis

3.3.6.1 Analysis of variance (ANOVA)

Throughout this part of the study various ANOVA's were used to determine the source of variation within the data. For determination of the length and width of peptide fibres/fibrils using TEM, the null hypothesis was that neither the GAG molar ratio nor concentration of Na^+ ions would have any effect on the lengths and widths of a given peptide (P_{11-4} , P_{11-8} or P_{11-12}). Therefore, the data for each peptide lengths and peptide widths was analysed by two-way ANOVA using SPSS. The analysis enabled understanding of whether the independent factors (GAG molar ratio, Na^+ salt concentration or their combined effects) had a significant effect on the lengths and/or widths of each peptide fibres/fibrils.

3.4 Results

3.4.1 Self-assembly of peptides and peptide-GAG mixtures at varying molar ratios in the presence of two different physiological Na⁺ salt solutions with varying Na⁺ ion concentrations.

FTIR analysis was used to study the secondary structure of peptides P₁₁-4, P₁₁-8 and P₁₁-12 in the presence and absence of chondroitin sulfate at molar ratios of 1:16 and 1:64 (peptide: GAG) in two concentrations of Na⁺ salt solution.

The FTIR data showed that the self-assembled peptide conformation was rich in β -sheet for P₁₁-4, P₁₁-8 and P₁₁-12 alone in 130 mM and 230 mM Na⁺ salt solutions and in the majority of the peptide-chondroitin sulfate mixtures in both Na⁺ salt solutions, as shown in Figure 42. Of particular interest, was the relative β -sheet percentage formed by the SAPs alone, which was indicative of a self-assembled hydrogel state. Increasing the Na⁺ ion concentration had different effects which were dependent upon the peptide

The addition of chondroitin sulfate at molar ratios of 1:16 and 1:64 in conjunction with the two Na⁺ salt solutions had a very different effect on the percentage of β -sheet formed. The addition of the GAG to P₁₁-4 at the lower molar ratio (1:64), resulted in a decrease in the peaks observed in the region of 1672-1690 cm⁻¹ (anti-parallel β -sheet conformation), which was indicative of a decreased percentage of β -sheet formed when compared to the peptide alone (Figure 42A & B). The addition of the GAG to P₁₁-4 at the higher molar ratio (1:16), however resulted in an increase in the overall percentage β -sheet, regardless of the concentration of Na⁺ ions in the salt solution.

On the other hand, the addition of the lower molar ratio of GAG to P₁₁-8 and P₁₁-12 in the 130 mM Na⁺ salt solution caused the percentage of β -sheet formed to initially increase but when the molar ratio of the GAG was increased, the percentage of β -sheet formed decreased. The effect was greater for P₁₁-12 than P₁₁-8 (Figure 42). It was notable that the addition of the GAG to P₁₁-12 had a detrimental effect on the percentage of β -sheet formed, especially at the higher GAG molar ratio (Figure 42E & F).

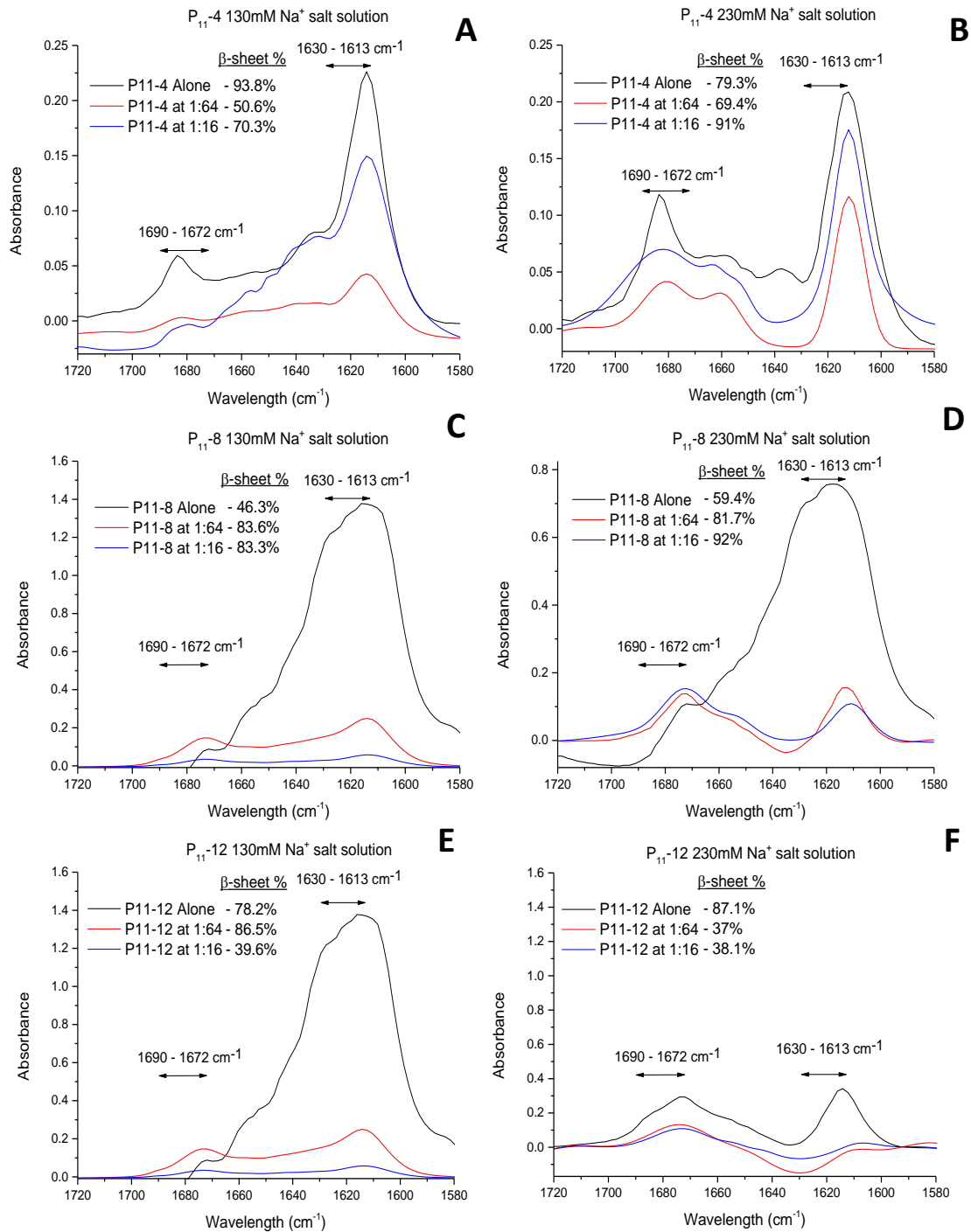


Figure 42: Fitted IR amide I' band of P₁₁-4, P₁₁-8 and P₁₁-12 at 10 mg.ml⁻¹ in the presence of 130 mM (A, C and E) and 230 mM (B, D and F) Na⁺ salt solution with and without varying chondroitin sulfate molar ratios of 1:16 and 1:64. The β-sheet percentage was calculated by adding the total area of the peaks showing β-sheet and then dividing them by the areas of all the individual peaks combined for each graph and multiplying by 100. The β-sheet regions are defined by the peaks in the wavelength region of 1630-1613 cm⁻¹ and 1690-1672 cm⁻¹.

3.4.2 Morphology of peptides and peptide-GAG mixtures at varying molar ratios in the presence of two different physiological Na⁺ salt solutions with varying Na⁺ ion concentrations.

Physical differences between the fibre morphology of the peptides P₁₁-4, P₁₁-8 and P₁₁-12 in the presence and absence of chondroitin sulfate at molar ratios of 1:16 and 1:64 in two concentrations of Na⁺ salt solution were observed by TEM. Representative images are shown in Figure 43 - Figure 45. Varying networks of entangled fibres or bundles were observed, which are essential for gel formation.

The TEM images for peptides alone at both Na⁺ ion concentrations (Figure 43– Figure 45: A & D) showed that the gels were composed of fibrils and fibres, as was the case with the peptide: GAG mixtures (Figure 43– Figure 45; B & E; C & F).

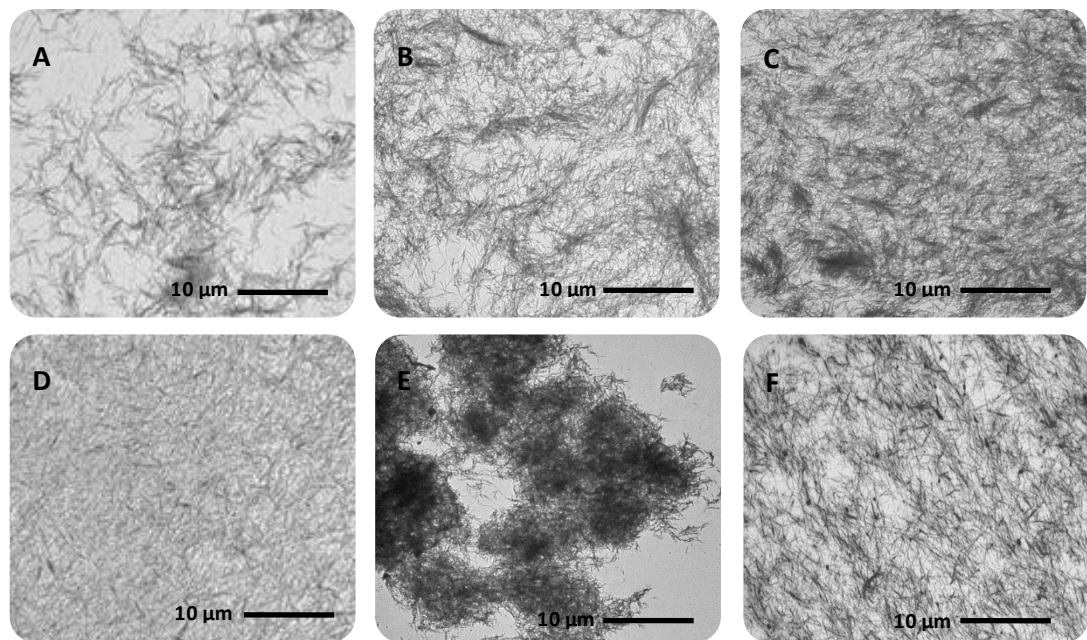


Figure 43: Morphology of the P₁₁-4 peptide in the presence of two Na⁺ salt solutions at varying chondroitin sulfate molar ratios (1:16 and 1:64) by TEM. (A) P₁₁-4 in a 230 mM Na⁺ salt solution, (B) P₁₁-4 at 1:64 GAG molar ratio in a 230 mM Na⁺ salt solution, (C) P₁₁-4 at 1:16 GAG molar ratio in a 230mM Na⁺ salt solution, (D) P₁₁-4 in a 130mM Na⁺ salt solution, (E) P₁₁-4 at 1:64 GAG molar ratio in a 130mM Na⁺ salt solution, (F) P₁₁-4 at 1:16 GAG molar ratio in a 130mM Na⁺ salt solution. Magnification of 500. Individual scale bars (10 μm) are shown for each image.

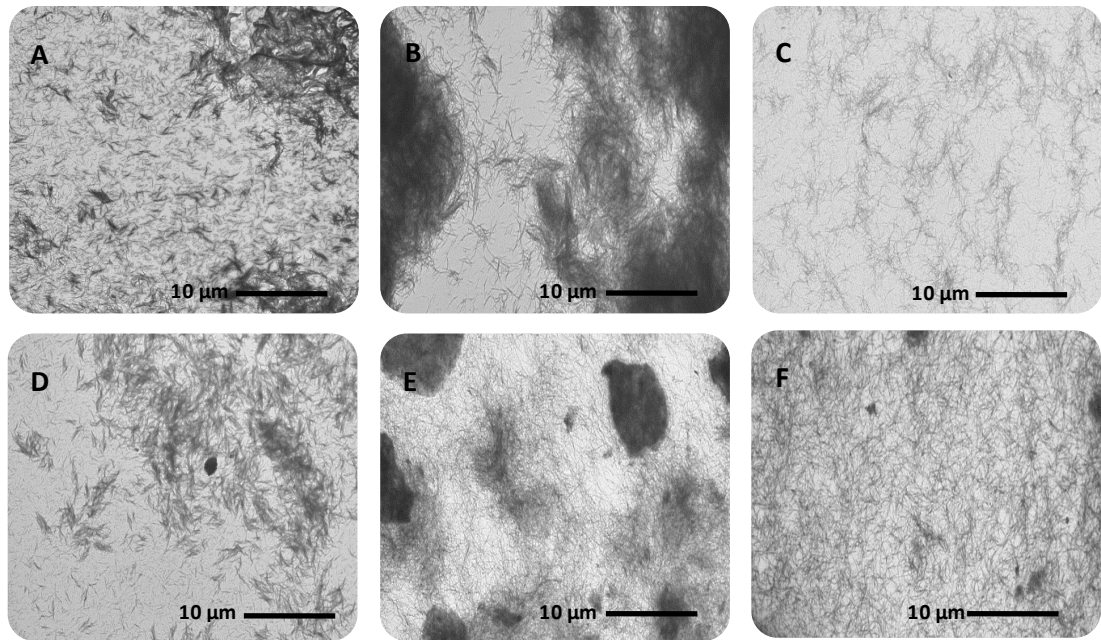


Figure 44: Morphology of the P₁₁-8 peptide in the presence of two Na⁺ salt solutions at varying chondroitin sulfate molar ratios (1:16 and 1:64) by TEM. (A) P₁₁-8 in a 230mM Na⁺ salt solution, (B) P₁₁-8 at 1:64 GAG molar ratio in a 230mM Na⁺ salt solution, (C) P₁₁-8 at 1:16 GAG molar ratio in a 230mM Na⁺ salt solution, (D) P₁₁-8 in a 130mM Na⁺ salt solution, (E) P₁₁-8 at 1:64 GAG molar ratio in a 130mM Na⁺ salt solution, (F) P₁₁-8 at 1:16 GAG molar ratio in a 130mM Na⁺ salt solution. Magnification of 500. Individual scale bars (10 μm) are shown for each image.

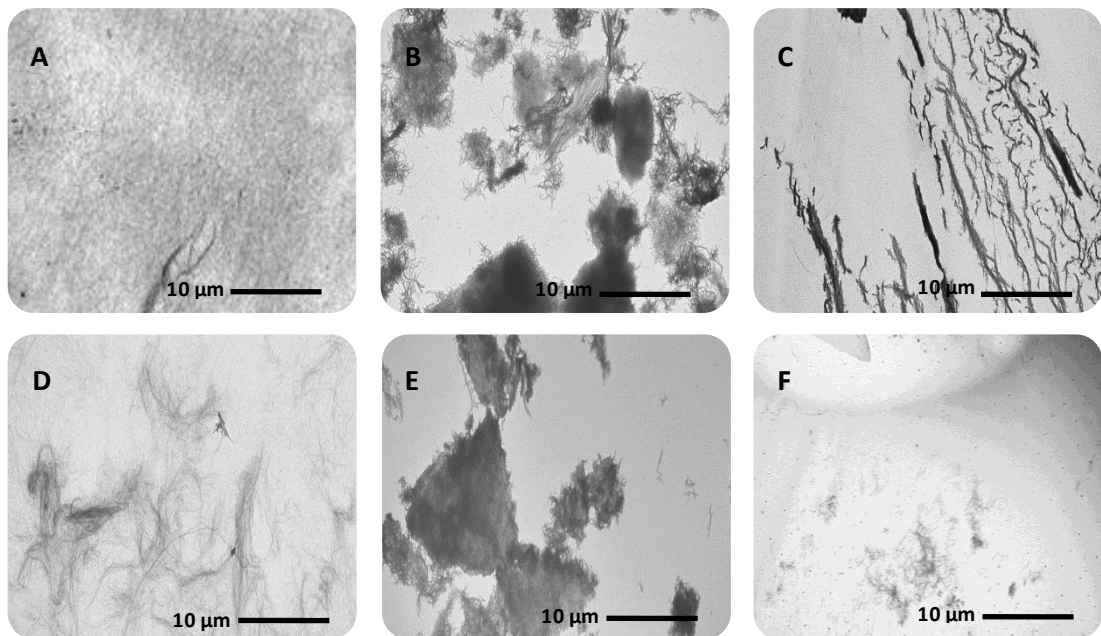


Figure 45: Morphology of the P₁₁-12 peptide in the presence of two Na⁺ salt solutions at varying chondroitin sulfate molar ratios (1:16 and 1:64) by TEM. (A) P₁₁-12 in a 230mM Na⁺ salt solution, (B) P₁₁-12 at 1:64 GAG molar ratio in a 230mM Na⁺ salt solution, (C) P₁₁-12 at 1:16 GAG molar ratio in a 230mM Na⁺ salt solution, (D) P₁₁-12 in a 130mM Na⁺ salt solution, (E) P₁₁-12 at 1:64 GAG molar ratio in a 130mM Na⁺ salt solution, (F) P₁₁-12 at 1:16 GAG molar ratio in a 130mM Na⁺ salt solution. Magnification of 500. Individual scale bars (10 μm) are shown for each image.

The physical properties of P₁₁-4, P₁₁-8 and P₁₁-12 alone in 130 mM and 230 mM Na⁺ salt solution are shown in Figure 46. The P₁₁-4 and P₁₁-8 peptide samples had a cloudy gel appearance when compared to the clear gel produced by the P₁₁-12 peptide sample. All three peptides exhibited shear softening (i.e. if sheared they would flow but after some time, they would return to their original gel state). This characteristic was exaggerated in the lower Na⁺ salt concentration. The peptide underwent a range of different physical states, ranging from isotropic fluid to nematic liquid crystalline/gel, however once equilibrium was reached at pH 7.4, the sample exhibited nematic gel characteristics. The liquid crystalline properties were established using a high resolution digital camera, with the sample placed in-between crossed polarized film/lenses (Figure 46C – E).

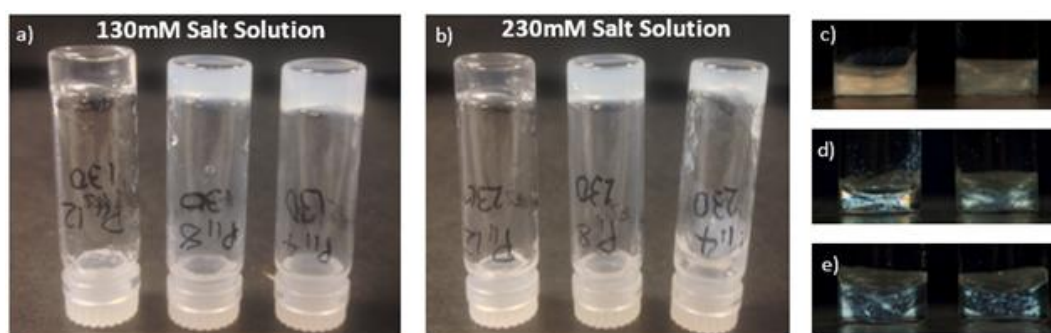


Figure 46: Images of (a) P₁₁-4, P₁₁-8 and P₁₁-12 in the 130 mM Na⁺ salt solution at pH 7.4 (b) P₁₁-4, P₁₁-8 and P₁₁-12 in the 230 mM Na⁺ salt solution at pH 7.4. Images show their physical properties 3 days after the gels were made (from left to right: P₁₁-12, P₁₁-8 and P₁₁-4) (c-e) Photographs of bulk samples exhibiting the birefringent gels of P₁₁-4, P₁₁-8 and P₁₁-12, respectively.

Overlapping of the fibrils and fibres made it difficult to definitively assess the morphology, hence regions in which individual fibrils could clearly be observed were chosen to measure fibre lengths and widths. The peptides in different salt solutions exhibited a twist pitch, meaning two widths were recorded; a wide width and a narrow width (where the twist occurred), values of twist pitch are presented in Figure 47, along with their corresponding widths. Average lengths ranging from *ca.* 410 to 990 nm for the peptides alone and *ca.* 498 to 3518 nm for the peptide-GAG mixtures were recorded (Figure 48).

The average widths and lengths of the P₁₁-4: GAG mixtures are summarised in Table 15 and Table 16 and represented in Figure 47 and Figure 48, respectively. From the TEM images for P₁₁-4, it was observed that in the 230 mM Na⁺ salt solution the fibrils were thicker and longer than those formed in the 130 mM Na⁺ salt solution. The average fibril width for P₁₁-4 in the 130 mM and 230 mM Na⁺ salt solutions was 9.96 ± 0.48 nm (\pm SEM) and 12.42 ± 0.22 nm, respectively at their widest point (Table 15). The average fibril length in the 130 mM and 230 mM Na⁺ salt solution were 468.68 ± 66.34 nm and 532.13 ± 54.24 nm, respectively (Table 16). However, in the 230 mM Na⁺ salt solution, P₁₁-4 exhibited a twist pitch of 236.26 nm

(Figure 47 – Image *1), and at its narrowest point (where the twist occurred) it had an average width of 8.58 ± 0.12 nm.

As the Na^+ ion concentration and GAG molar ratio were increased the average lengths of the P_{11} -4: GAG fibrils were also increased, compared to P_{11} -4 alone. However, this was not the case for the average widths of the P_{11} -4: GAG mixtures, as these were affected independently by the two variables (Na^+ ion concentration and GAG molar ratio). As the Na^+ ion concentration was increased, the average width of the P_{11} -4: GAG fibril at the GAG molar ratio of 1:64 decreased, however at the 1:16 GAG molar ratio the average widths of the fibrils were increased. On the other hand, as the GAG molar ratio for the P_{11} -4: GAG mixtures in the 230 mM Na^+ salt solution was increased, the average width of the fibrils was also increased, however for the P_{11} -4-GAG mixtures in the 130 mM Na^+ salt solution, the average width of the fibrils was decreased.

Table 15: Average widths and twist pitch of the P_{11} -4 fibrils in different Na^+ salt solutions and GAG molar ratios.

Widths (nm)		
<u>P_{11}-4 130mM</u> 9.96 ± 0.48	<u>P_{11}-4 130mM 1:64</u> 18.17 ± 1.60	<u>P_{11}-4 130mM 1:16</u> 12.63 ± 0.41
<u>P_{11}-4 230mM</u> [12.42 ± 0.22] ^{*w} [8.58 ± 0.12] ^{*s} <i>Twist pitch = 236.26 nm</i>	<u>P_{11}-4 230mM 1:64</u> 14.15 ± 0.92	<u>P_{11}-4 230mM 1:16</u> [21.44 ± 0.27] ^{*w} [13.02 ± 0.41] ^{*s} <i>Twist pitch = 330.78 nm</i>

The widths were determined from TEM images at a magnification of 30,000 using the software imageJ. 20 fibrils were measured for each sample. The data is presented as the mean ($n=20$) \pm SEM. The twist pitch was calculated using the measure tool in imageJ. It was measured for an individual fibre from its first narrowest point to the third, indicative of a full twist (*W = Wide width and *S = Short width).

Table 16: Average lengths of the P_{11} -4 fibrils in different Na^+ salt solutions and GAG molar ratios.

Lengths (nm)		
<u>P_{11}-4 130mM</u> 468.68 ± 66.34	<u>P_{11}-4 130mM 1:64</u> 498.08 ± 41.24	<u>P_{11}-4 130mM 1:16</u> 674.17 ± 76.38
<u>P_{11}-4 230mM</u> 532.13 ± 54.24	<u>P_{11}-4 230mM 1:64</u> 973.66 ± 79.75	<u>P_{11}-4 230mM 1:16</u> 1075.85 ± 125.09

The lengths were determined from TEM images at a magnification of 12,000 using the software imageJ. 20 fibrils were measured for each sample. The data is presented as the mean ($n=20$) \pm SEM.

The average widths and lengths of the P_{11} -8 fibrils at different GAG molar ratios and Na^+ ion concentrations are summarised in Table 17 and Table 18 and represented in Figure 47 and Figure 48, respectively. For the measured P_{11} -8 fibrils, they were thicker and longer in the 130 mM Na^+ salt solution, when compared to the P_{11} -8 fibrils in the 230 mM Na^+ salt solution. The average fibril width for P_{11} -8 in the 130 mM and 230 mM Na^+ salt solutions were $20.42 \pm$

0.25 nm and 19.16 ± 0.31 , at their widest point and 10.66 ± 0.15 nm and 14.45 ± 0.25 nm, at their narrowest point, respectively (Table 17). In both of these conditions the fibrils exhibited a twist pitch of 379.24 nm and 345.23 nm, respectively (Figure 47 – Image*3 & 4). The average fibril length in the 130 mM and 230 mM Na⁺ salt solutions was 445.27 ± 40.74 nm and 410.68 ± 32.81 , respectively (Table 18).

As the Na⁺ ion concentration increased, the length of the P₁₁-8 fibrils/fibres decreased regardless of the GAG molar ratio. However, as the GAG molar ratio increased the length of the fibrils/fibres increased regardless of the Na⁺ ion concentration. Interestingly in the P₁₁-8: GAG mixtures there were multiple types of structure observed, fibrils were by far the most common type but there were instances of nanotube formation. The P₁₁-8: GAG fibrils were longer in the 130 mM Na⁺ salt solution, when compared to the P₁₁-8: GAG fibrils in the 230 mM Na⁺ salt solution. The widths of the fibres of the P₁₁-8: GAG mixtures were increased with an increased Na⁺ ion concentration and GAG molar ratio. Similarly, the P₁₁-8: GAG fibrils were thicker in the 130 mM Na⁺ salt solution, when compared to the P₁₁-8: GAG fibrils in the 230 mM Na⁺ salt solution.

Table 17: Average widths and twist pitch of the P₁₁-8 fibrils in different Na⁺ salt solutions and GAG molar ratios.

Widths (nm)		
<p>P₁₁-8 130mM $[20.42 \pm 0.25]^*w$ $[10.66 \pm 0.15]^*s$ <i>Twist pitch = 379.24 nm</i></p>	<p>P₁₁-8 130mM 1:64 $[16.40 \pm 0.32]^*w$ $[8.96 \pm 0.37]^*s$ <i>Twist pitch = 196.41 nm</i></p>	<p>P₁₁-8 130mM 1:16 16.81 ± 1.21</p>
<p>P₁₁-8 230mM $[19.16 \pm 0.31]^*w$ $[12.03 \pm 0.31]^*s$ <i>Twist pitch = 345.23 nm</i></p>	<p>P₁₁-8 230mM 1:64 17.22 ± 1.13</p>	<p>P₁₁-8 230mM 1:16 $[19.90 \pm 0.49]^*w$ $[10.98 \pm 0.33]^*s$ <i>Twist pitch = 229.97 nm</i></p>

The widths were determined from TEM images at a magnification of 30,000 using the software imageJ. 20 fibrils were measured for each sample. The data is presented as the mean (n=20) ±SEM. The twist pitch was calculated using the measure tool in imageJ it was measured for an individual fibre from its first narrowest point to the third, indicative of a full twist (*W = Wide width & *S = Short width).

Table 18: Average lengths of the P₁₁-8 fibrils in different Na⁺ salt solutions and GAG molar ratios.

Lengths (nm)		
<p>P₁₁-8 130mM 445.27 ± 40.74</p>	<p>P₁₁-8 130mM 1:64 2682.16 ± 545.21</p>	<p>P₁₁-8 130mM 1:16 3518.32 ± 432.47</p>
<p>P₁₁-8 230mM 410.68 ± 32.81</p>	<p>P₁₁-8 230mM 1:64 799.13 ± 57.47</p>	<p>P₁₁-8 230mM 1:16 827.87 ± 50.37</p>

These were determined from TEM images at a magnification of 12,000 using the software imageJ. 20 fibrils were measured for each sample. The data is presented as the mean (n=20) ±SEM.

From the TEM images for P₁₁-12, it was observed that increasing the Na⁺ ion concentration in the salt solution increased the widths of the fibrils, however the fibril length was

decreased, as shown in Table 19 and Table 20 and represented in Figure 47 and Figure 48. The average width of P₁₁-12 in the 130 mM and 230 mM Na⁺ salt solutions was 4.95 ± 0.15 nm and 22.72 ± 0.32 nm respectively at the widest point. The fibrils in the 230 mM Na⁺ salt solution exhibited a twist pitch of 397.81 nm, at the narrowest point the average width of the P₁₁-12 fibrils was 15.11 ± 0.36 nm. In the 130 mM Na⁺ salt solution at a magnification of x500, P₁₁-12 showed a less dense network of fibrils and fibres compared to the image seen in the 230 mM Na⁺ salt solution at the same magnification.

The average widths and lengths of the fibrils in the P₁₁-12: GAG mixtures varied depending on the amount of Na⁺ ions in the salt solution or GAG molar ratio (Table 19 and Table 20; Figure 47 and Figure 48). An increase in the Na⁺ ion concentration resulted in increased widths and lengths of the fibrils, regardless of the GAG molar ratio. However, as the GAG molar ratio increased the length of the fibrils was increased regardless of the Na⁺ ion concentration; as well as the width of only the P₁₁-12: GAG fibrils in the 230 mM Na⁺ salt solution. Overall the lengths and widths of the P₁₁-12: GAG fibrils were greatest in the higher Na⁺ ion concentration and GAG molar ratio (Figure 47 and Figure 48). The longest fibrils formed by the P₁₁-12 peptide were seen in the GAG molar ratio of 1:16 in both 130 mM and 230 mM Na⁺ salt solutions.

Table 19: Average widths and twist pitch of the P₁₁-12 fibrils in different Na⁺ salt solutions and GAG molar ratios.

Widths (nm)		
<u>P₁₁-12 130mM</u> 4.95 ± 0.15	<u>P₁₁-12 130mM 1:64</u> 31.84 ± 1.96	<u>P₁₁-12 130mM 1:16</u> 14.24 ± 0.96
<u>P₁₁-12 230mM</u> [22.72 ± 0.32] ^{*w} [15.11 ± 0.36] ^{*s} <i>Twist pitch = 397.81 nm</i>	<u>P₁₁-12 230mM 1:64</u> 34.24 ± 2.12	<u>P₁₁-12 230mM 1:16</u> 83.89 ± 4.94

The widths were determined from TEM images at a magnification of 30,000 using the software imageJ. 20 fibrils were measured for each sample. The data is presented as the mean (n=20) ± SEM.

Table 20: Average lengths of the P₁₁-12 fibrils in different Na⁺ salt solutions and GAG molar ratios.

Lengths (nm)		
<u>P₁₁-12 130mM</u> 990.96 ± 75.79	<u>P₁₁-12 130mM 1:64</u> 588.55 ± 59.02	<u>P₁₁-12 130mM 1:16</u> 1802.74 ± 334.82
<u>P₁₁-12 230mM</u> 893.60 ± 100.13	<u>P₁₁-12 230mM 1:64</u> 1374.98 ± 114.16	<u>P₁₁-12 230mM 1:16</u> 1880.11 ± 137.65

These were determined from TEM images at a magnification of 12,000 using the software imageJ. 20 fibrils were measured for each sample. The data is presented as the mean (n=20) ± SEM.

3.4.2.1 Analysis of the effects of Na⁺ ion concentration and GAG molar ratio on the lengths and widths of fibrils of P₁₁₋₄, P₁₁₋₈ and P₁₁₋₁₂.

The effect that the Na⁺ ion concentration in the salt solution and the GAG molar ratios had on (a) the lengths (Table 21 to Table 23) and (b) the widths (Table 24 to Table 26) of the fibrils formed; was determined by 2-way ANOVA for each peptide and was found to vary from peptide to peptide. The null hypothesis was that neither of the independent variables (GAG molar ratio and concentration of Na⁺ ions) would have any effect on the lengths and widths of the peptide fibrils.

The results of the analyses revealed that both Na⁺ ion concentration in the salt solution, GAG molar ratio and their combinations, all had a significant effect ($p < 0.05$) on the length and widths of the fibrils; in all the peptide hydrogels except in P₁₁₋₁₂, where the Na⁺ ion concentration in the salt solution did not have a significant effect on the length of the fibrils formed ($p = 0.084$) (Table 23).

Table 21: Two-way analysis of variance to determine the effect of GAG molar ratio and Na⁺ ion concentration had on the length of the P₁₁₋₄ fibrils.

Source	df	Mean Square	F	Sig.
Salt Solution (SS)	1	2.95E+06	23.991	.000
GAG Molar Ratio (MR)	2	1.43E+06	11.665	.000
MR * SS	2	4.83E+05	3.927	.022
Error	114	1.23E+05		

Statistical significance was determined at $p < 0.05$. Independent variables: GAG molar ratio (MR) and Salt Solution (SS). Dependant variable: Length.

Table 22: Two-way analysis of variance to determine the effect of GAG molar ratio and Na⁺ ion concentration had on the length of the P₁₁₋₈ fibrils.

Source	df	Mean Square	F	Sig.
Salt Solution (SS)	1	7.08E+07	43.084	.000
GAG Molar Ratio (MR)	2	3.30E+07	20.109	.000
MR * SS	2	1.85E+07	11.283	.000
Error	114	1.64E+06		

Statistical significance was determined at $p < 0.05$. Independent variables: GAG molar ratio (MR) and Salt Solution (SS). Dependant variable: Length.

Table 23: Two-way analysis of variance to determine the effect of GAG molar ratio and Na⁺ ion concentration had on the length of the P₁₁₋₁₂ fibrils.

Source	df	Mean Square	F	Sig.
Salt Solution (SS)	1	1.76E+06	3.037	.084
GAG Molar Ratio (MR)	2	9.92E+06	17.093	.000
MR * SS	2	1.81E+06	3.113	.049
Error	114	5.80E+05		

Statistical significance was determined at $p < 0.05$. Independent variables: GAG molar ratio (MR) and Salt Solution (SS). Dependant variable: Length.

Table 24: Two-way analysis of variance to determine the effect of GAG molar ratio and Na⁺ ion concentration had on the width of the P₁₁- 4 fibrils.

Source	df	Mean Square	F	Sig.
Salt Solution (SS)	1	174.947	13.379	.000
GAG Molar Ratio (MR)	2	397.873	30.428	.000
MR * SS	2	411.463	31.467	.000
Error	114	13.076		

Statistical significance was determined at $p < 0.05$. Independent variables: GAG molar ratio (MR) and Salt Solution (SS). Dependant variable: Width.

Table 25: Two-way analysis of variance to determine the effect of GAG molar ratio and Na⁺ ion concentration had on the width of the P₁₁- 8 fibrils.

Source	df	Mean Square	F	Sig.
Salt Solution (SS)	1	360.995	31.244	.000
GAG Molar Ratio (MR)	2	518.656	44.890	.000
MR * SS	2	81.586	7.061	.001
Error	114	11.554		

Statistical significance was determined at $p < 0.05$. Independent variables: GAG molar ratio (MR) and Salt Solution (SS). Dependant variable: Width.

Table 26: Two-way analysis of variance to determine the effect of GAG molar ratio and Na⁺ ion concentration had on the width of the P₁₁- 12 fibrils.

Source	df	Mean Square	F	Sig.
Salt Solution (SS)	1	2.69E+04	238.950	.000
GAG Molar Ratio (MR)	2	1.24E+04	110.568	.000
MR * SS	2	1.24E+04	110.333	.000
Error	114	1.13E+02		

Statistical significance was determined at $p < 0.05$. Independent variables: GAG molar ratio (MR) and Salt Solution (SS). Dependant variable: Width.

Perusal of the data indicated that in the 230 mM Na⁺ salt solution, the P₁₁-4 fibrils were longer than those in the 130 mM Na⁺ salt solution. However, for the P₁₁-8 fibrils, the opposite effect was observed, where the P₁₁-8 fibrils were longer in the 130 mM Na⁺ salt solution when compared to the P₁₁-8 fibrils in the 230 mM Na⁺ salt solution (Figure 47 and Figure 48). For P₁₁-12, the 2-way ANOVA revealed that only the GAG molar ratio had a significant effect ($p < 0.05$) on the length of the P₁₁-12 fibrils. The analysis also revealed that, Na⁺ ion concentration in the salt solution, GAG molar ratio and the combination of the latter all had a significant effect ($p < 0.05$) on the widths of the P₁₁-12 fibrils.

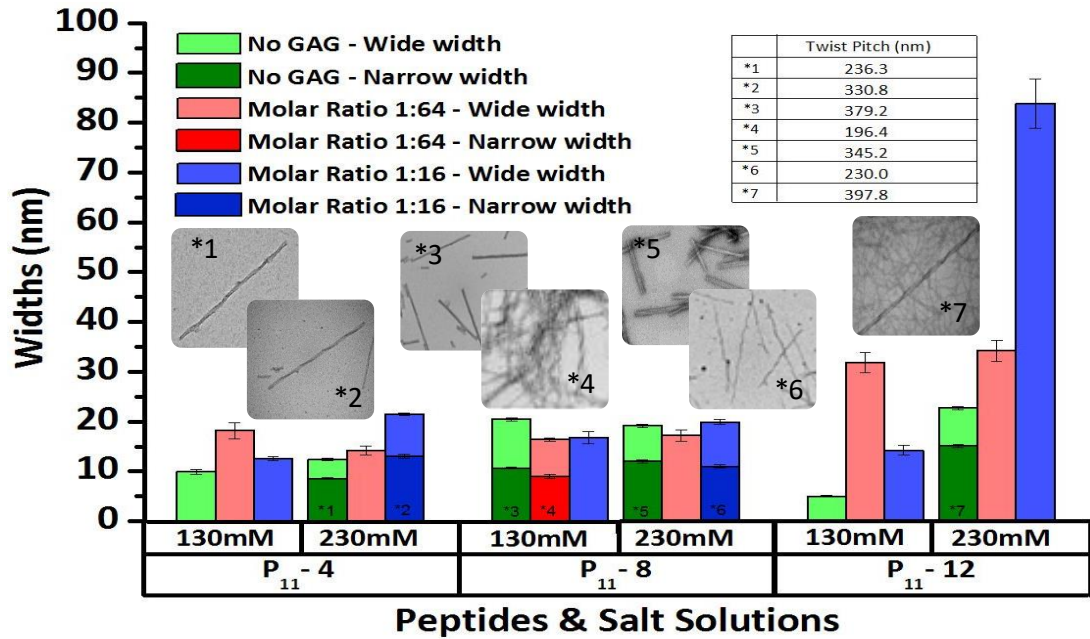


Figure 47: Widths of fibrils of all peptides in two different Na⁺ salt solutions at pH 7.4 at varying molar ratios of GAG. Widths of the fibrils were determined from TEM images at a magnification of 30,000 using the software imageJ. 20 fibrils were measured for each sample. The data is presented as the mean (n=20) ± 95% confidence intervals. Data was analysed using 2-way analysis of variance. This showed that the Na⁺ ion concentration in the salt solution, GAG molar ratio and their combined effects had a significant effect on the overall widths of the fibrils formed by all three peptides ($p < 0.05$).

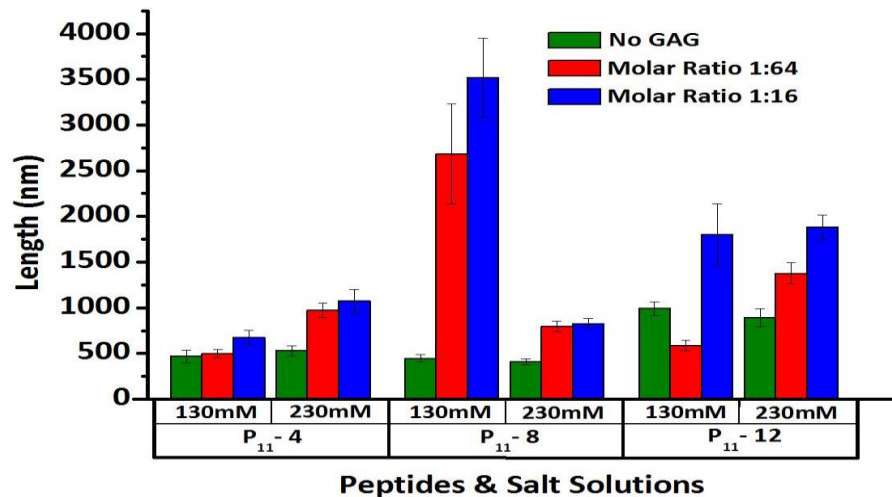


Figure 48: Lengths of fibrils of all peptides in two different Na⁺ salt solutions at pH 7.4 at varying molar ratios of GAG. Lengths of the fibrils were determined from TEM images at a magnification of 12,000 using the software imageJ. 20 fibrils were measured for each sample. The data is presented as the mean (n=20) ± 95% confidence intervals. Data was analysed using 2-way ANOVA and statistical significance was determined at $p < 0.05$. This showed that for P₁₁-4 and P₁₁-8 the Na⁺ ion concentration in the salt solution, GAG molar ratio and their combined effects all had a significant effect on the lengths of the fibres formed ($p < 0.05$). For P₁₁-12, the Na⁺ ion concentration had no significant effect on the lengths of the fibrils formed by P₁₁-12 ($p = 0.084$). However, the GAG molar ratio had a significant effect on the length of the fibrils formed by P₁₁-12 ($p < 0.05$). The combined effect of GAG molar ratio and Na⁺ ion concentration in the salt solution had a significant effect on the length of the fibrils formed by P₁₁-12 ($p = 0.049$).

3.4.3 Determination of elastic and viscous shear moduli of peptides and peptide-GAG mixtures at varying molar ratios in the presence of two different physiological Na⁺ salt solutions with varying Na⁺ ion concentrations using Rheology

All of the samples tested exhibited a higher G' than G'' value, which confirmed that all hydrogels exhibited viscous solid-like behaviour.

3.4.3.1 Shear modulus of peptides alone

Samples were prepared as described in Section 3.3.5.2.1. P₁₁-4 and P₁₁-8 in both Na⁺ salt solutions formed cloudy self-supporting gels, however P₁₁-12 formed a clear gel in the 130mM Na⁺ salt solution but in the 230mM Na⁺ salt solution it formed a cloudy gel, as shown in Figure 49.

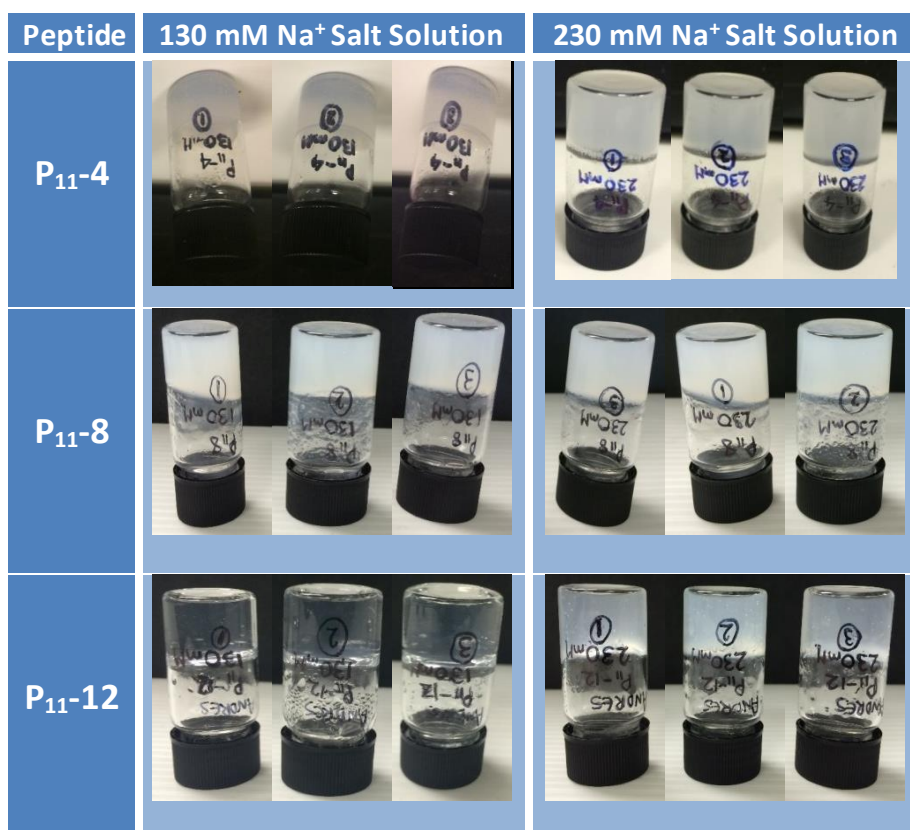


Figure 49: P₁₁-4, P₁₁-8 and P₁₁-12 self-supporting gels at 10 mg.ml⁻¹ in 130 mM and 230 mM Na⁺ salt solutions. Images captured 2 days after they were made before testing on the rheometer (n=3).

As shown in Figure 50, the LVER of the two amplitude sweeps run at 1 Hz and 20 Hz for each peptide, were used to calculate the shear strain value to run the frequency sweep. P₁₁-4 in the 130 mM and 230 mM Na⁺ salt solutions had a shear strain value of 0.1 % and 0.15 %, respectively. P₁₁-8 in the 130 mM and 230 mM Na⁺ salt solutions had a shear strain value of 0.3 %. P₁₁-12 in the 130 mM and 230 mM Na⁺ salt solutions had a shear strain value of 0.3 %

and 0.1 %, respectively. During the amplitude sweep tests, it was observed that the shear moduli of the P₁₁-12 gels were considerably lower than for the P₁₁-4 and P₁₁-8 gels in both Na⁺ salt solutions, which was concurrent with the weakness of the P₁₁-12 gel when it was handled and placed on the rheometer for testing. A slight tap of the vial caused shearing in the gel which did not recover as quickly as the P₁₁-4 and P₁₁-8 gels.

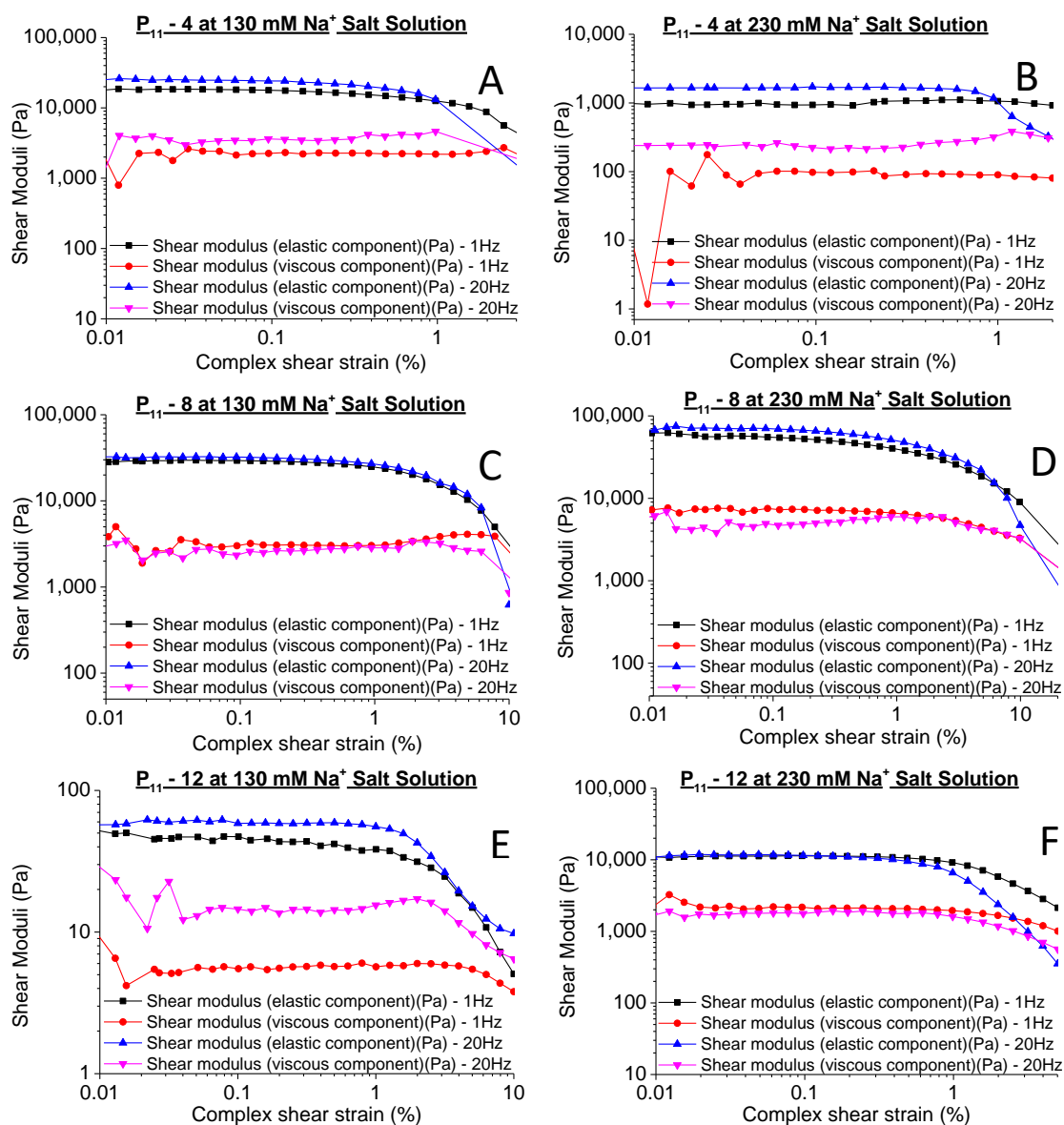


Figure 50: The amplitude sweeps (elastic and viscous modulus vs. shear strain) of P₁₁-4, P₁₁-8 and P₁₁-12 at 10 mg.ml⁻¹ in 130 mM and 230 mM Na⁺ salt solutions. Shear strain started at 0.01 % and ramped up to 100% at a temperature 37°C. Shear strain chosen within the LVER was: (A=0.1 %, B=0.15 %, C, D and E=0.3 % and F=0.1 %).

For the peptides alone, the shear moduli of P₁₁-4 and P₁₁-8 were higher than those of P₁₁-12 by two orders of magnitude, which indicated that there was variation between the glutamine based peptide gels and the serine based peptide gels in both Na⁺ salt solutions across the

frequency range studied (Figure 51A & B). Increasing the Na⁺ salt concentration increased the moduli of P₁₁-12, indicating that the positively charged serine based peptide was interacting positively with the increased concentration of Na⁺ ions in the higher ionic strength solution, hence increasing its mechanical stiffness three-fold (Figure 51C), which was concurrent with the FTIR analysis, as the β-sheet component also increased. A very slight increase in the shear moduli was noticed more so at the 130mM Na⁺ salt solution in the P₁₁-4 and P₁₁-8 samples, whereas this effect was not as apparent in the P₁₁-12 samples in either of the Na⁺ salt solutions, suggesting that as the frequency increased the P₁₁-4 and P₁₁-8 samples became stiffer (Figure 51A & B). Nevertheless, the frequency sweeps shown in Figure 51A & B were relatively flat indicating that the experiments were run near equilibrium state.

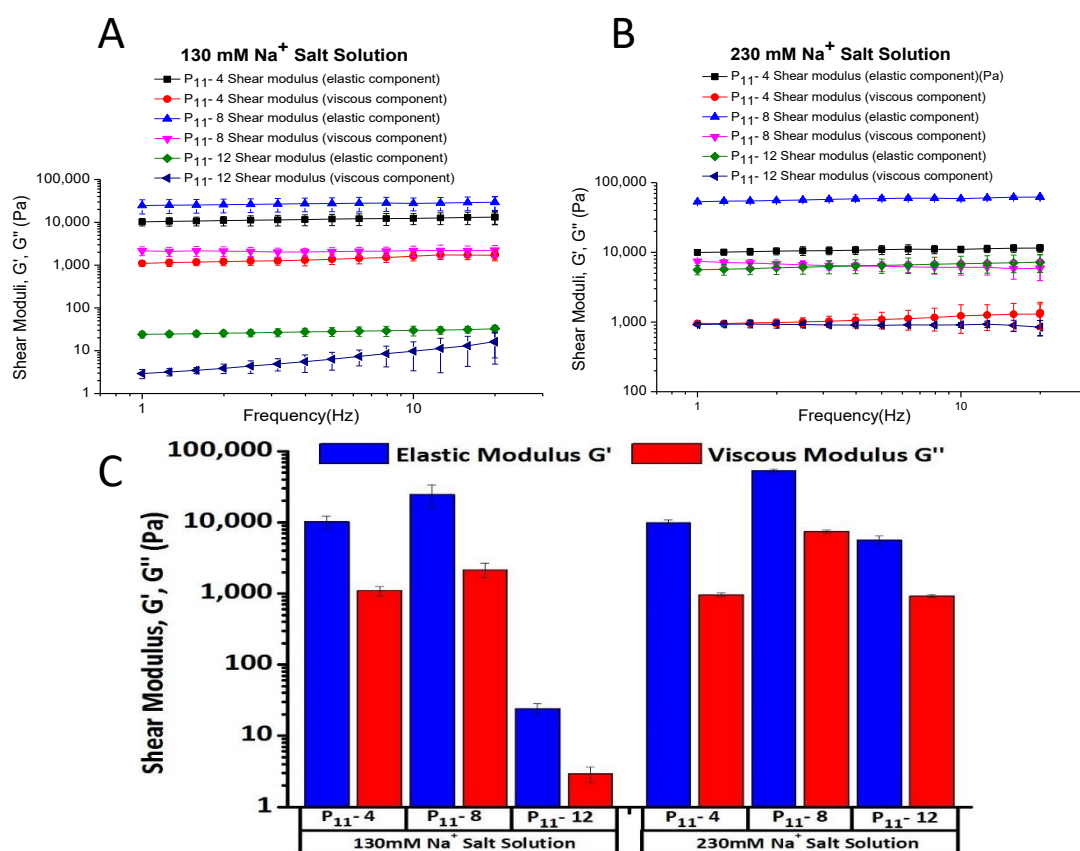


Figure 51: The effect of varying the Na⁺ ion concentration (130 mM or 230 mM) on the mechanical stiffness of the P₁₁-4, P₁₁-8 and P₁₁-12 gels, Strain 0.1 % and temperature 37°C: (A) Frequency sweep test between 1Hz and 20Hz for the P₁₁-4, P₁₁-8 and P₁₁-12 gels in the 130 mM Na⁺ salt solution, (B) Frequency sweep test between 1Hz and 20Hz for the P₁₁-4, P₁₁-8 and P₁₁-12 gels in the 230 mM Na⁺ salt solution, (C) Shear modulus extracted at 1Hz for the P₁₁-4, P₁₁-8 and P₁₁-12 gels in both 130 mM and 230 mM Na⁺ salt solutions. Data is presented as the mean (n=3) ± 95% confidence intervals. Individual samples were subject to an amplitude sweep before commencing the test, in order to identify the linear viscoelastic region (LVER). A strain value was then chosen within the middle region of the LVER and the shear moduli (elastic and viscous) were all calculated by running a frequency sweep test between 1Hz and 20Hz.

3.4.3.2 Shear modulus of peptide: GAG mixtures

In this study, the mixing of GAGs with the peptides in different ionic strength salt solutions and the effect on the rheological properties were investigated. It was hypothesised that the charged GAG chains would not only interact electrostatically with the charged peptides but also with the two ionic salt solutions.

Samples were prepared as described in Section 3.3.5.2.2. The P₁₁-4 and P₁₁-8: GAG mixtures in both Na⁺ salt solutions formed cloudy self-supporting gels, however P₁₁-12 in the 130 mM Na⁺ salt solution at both GAG molar ratios, even after vortexing, sonicating and heating, did not gel or form a viscous liquid as with other peptide-GAG mixtures. After allowing 48 hours for the P₁₁-12: GAG mixtures to reach equilibrium, a slight change in appearance of the gels was observed for the mixture at the higher molar ratio (1:16) of GAG. Some self-assembly was observed on the walls of the tube as well as some solid clumps within the runny liquid, however the mixture was still liquid in nature. The mixtures at the lower molar ratio (1:64) of GAG also had solid-clumps within the runny liquid but with no self-assembly on the walls of the tube. These observations were not obvious initially but became more apparent when loading samples onto the rheometer. The appearance of the gels is shown in Table 26. The addition of the GAG to P₁₁-12 in the 230mM Na⁺ salt solution had a similar effect. Upon mixing, the P₁₁-12: GAG mixture at the lower GAG molar ratio (1:64), showed self-assembly on the walls. After vortexing, sonicating and heating small clumps of solid aggregates were present in the viscous liquid suspension, which remained after the 48 hours prior to testing (Table 26). Similarly, the P₁₁-12: GAG mixture at the higher GAG molar ratio (1:16), exhibited the same phenomenon however it formed a very weak gel after 48 hours just prior to testing. This gel sheared easily upon inverting and loading onto the rheometer, as shown in Table 26, in particular the 3rd sample. The addition of the GAG to P₁₁-8 led to much faster gelation, with self-supporting gels forming almost instantly on the addition of the GAG (Table 26); even before they had been sonicated, vortexed or heated. This behaviour had not been observed previously with any other of the peptides alone. Gels were very hard to shear once they had been made which made the measurement of pH after 24 hours very difficult.

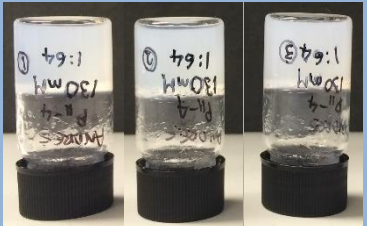
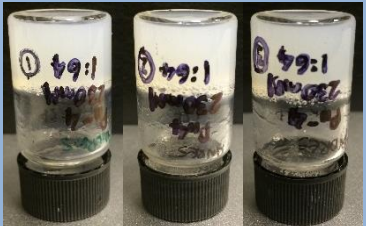
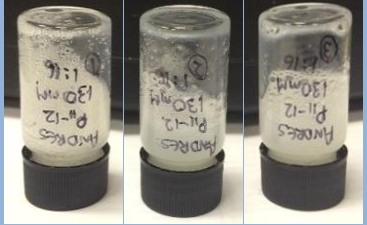
Peptide	GAG Molar Ratio	130 mM Na ⁺ Salt Solution	230 mM Na ⁺ Salt Solution
P ₁₁ -4	1:64		
	1:16		
P ₁₁ -8	1:64		
	1:16		
P ₁₁ -12	1:64		
	1:16		

Figure 52: P₁₁-4, P₁₁-8 and P₁₁-12 self-supporting gels at 10 mg.ml⁻¹ at two different GAG molar ratios (1:64 & 1:16) in 130 mM and 230 mM Na⁺ salt solutions. Images captured 2 days after they were made before testing on the rheometer (n=3).

The LVER of the two amplitude sweeps run at 1 Hz and 20 Hz for each peptide: GAG mixture, which were used to calculate the shear strain value that the frequency sweep would be run at are shown in Figure 53. P₁₁-4 at both GAG molar ratios and in both the 130 mM and 230

mM Na⁺ salt solutions had a shear strain value of 0.15 %. P₁₁-8 at GAG molar ratio 1:64 in the 130 mM and 230 mM Na⁺ salt solution had a shear strain value of 0.17 % and 0.15 %, respectively. P₁₁-8 at GAG molar ratio 1:16 in the 130 mM and 230 mM Na⁺ salt solutions had a shear strain value of 0.1 % and 0.3 %, respectively. P₁₁-12 at both GAG molar ratios and in both the 130 mM and 230 mM Na⁺ salt solutions had a shear strain value of 0.15 %. The amplitude sweep test again showed that the shear moduli of the P₁₁-12 gels were considerably lower than the P₁₁-4 and P₁₁-8 gels in both Na⁺ salt solutions, which was concurrent with the weakness of the P₁₁-12 gel when it was handled and placed on the rheometer for testing.

The frequency sweeps shown in Figure 54A-F, showed that the elastic moduli for all the peptide: GAG mixtures were higher than the viscous modulus, indicating that the samples exhibited a solid-like behaviour. Their overall flatness of the data lines was indicative that the test runs were near the equilibrium state of the hydrogels. For P₁₁-4, the addition/presence of more of GAG (1:16) in both the 130 mM and 230 mM Na⁺ salt solutions, led to a slight decrease in the shear moduli of P₁₁-4. P₁₁-4: GAG mixtures in the 230 mM Na⁺ salt solution were the stiffest hydrogels when compared to those in the 130 mM Na⁺ salt solution regardless of the GAG molar ratio. P₁₁-8 in the presence of GAG molar ratios 1:16 and 1:64, were also investigated. The observations of the gelation properties of these gels were reflected in the rheological properties of P₁₁-8, where the highest shear moduli of all the peptide: GAG mixtures investigated were seen in P₁₁-8 at GAG molar ratio of 1:64 in both of the Na⁺ salt solutions. However similarly to P₁₁-4 the addition of more GAG (1:16) to P₁₁-8 led to a reduced stiffness compared to P₁₁-8 at the 1:64 GAG molar ratio. Despite their liquid like appearance, P₁₁-12 samples tested demonstrated solid-like behaviour as the samples tested were biphasic (i.e. fluid and flocculated peptide). The P₁₁-12 gels in the 130mM Na⁺ salt solution were stiffer at the higher GAG molar ratio (1:16) when compared to those at the lower GAG molar ratio.

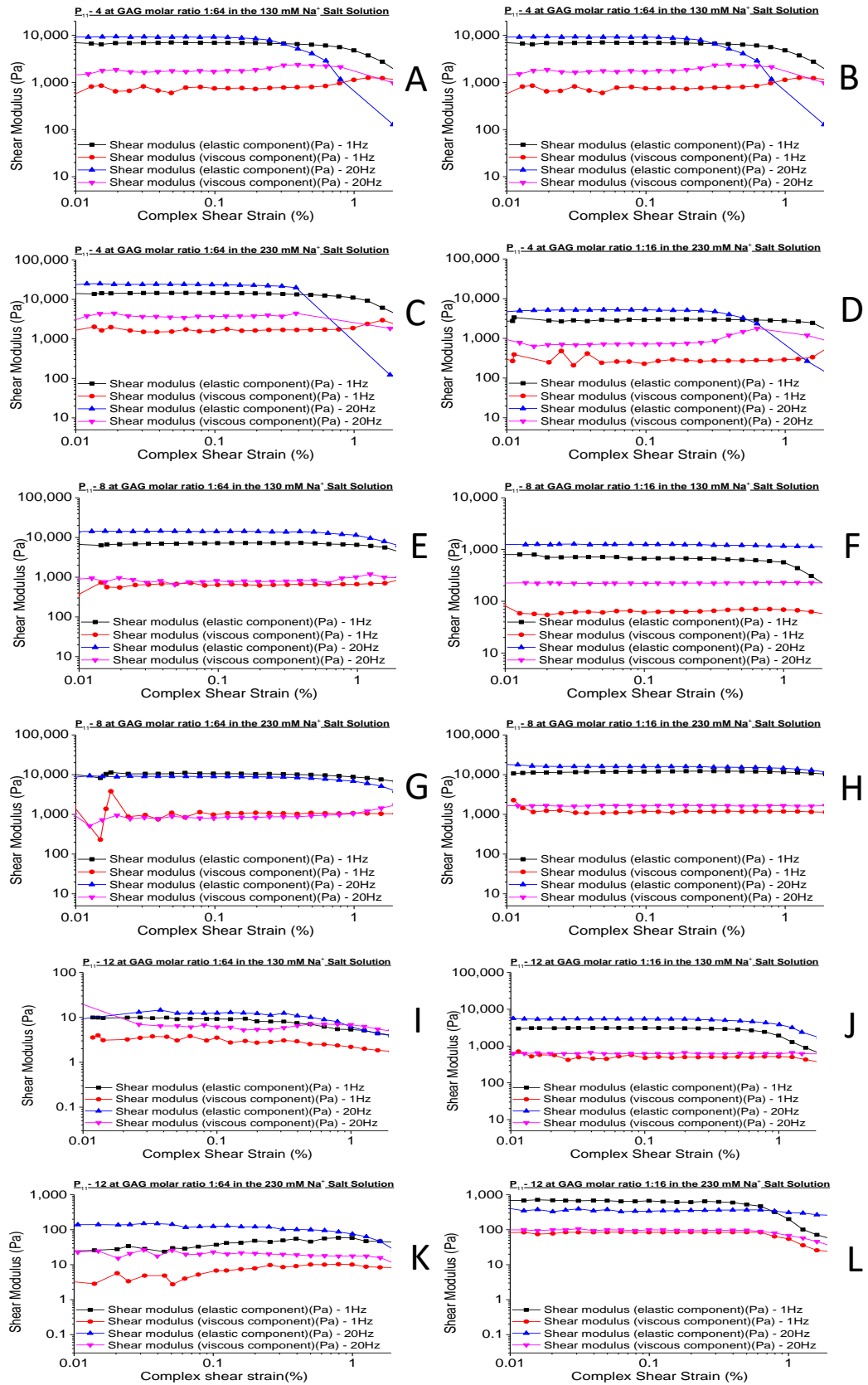


Figure 53: The amplitude sweeps (elastic and viscous modulus vs. shear strain) of P₁₁-4, P₁₁-8 and P₁₁-12: GAG mixtures at 10 mg.ml⁻¹ in 130 mM and 230 mM Na⁺ salt solutions. Shear strain started at 0.01 % and ramped up to 100% at a temperature 37°C. Shear strain chosen within the LVER was: (A, B, C & D=0.15 %, E=0.17 %, F=0.1 %, G=0.15 %, H=0.3 %, I, J, K & L=0.15 %).

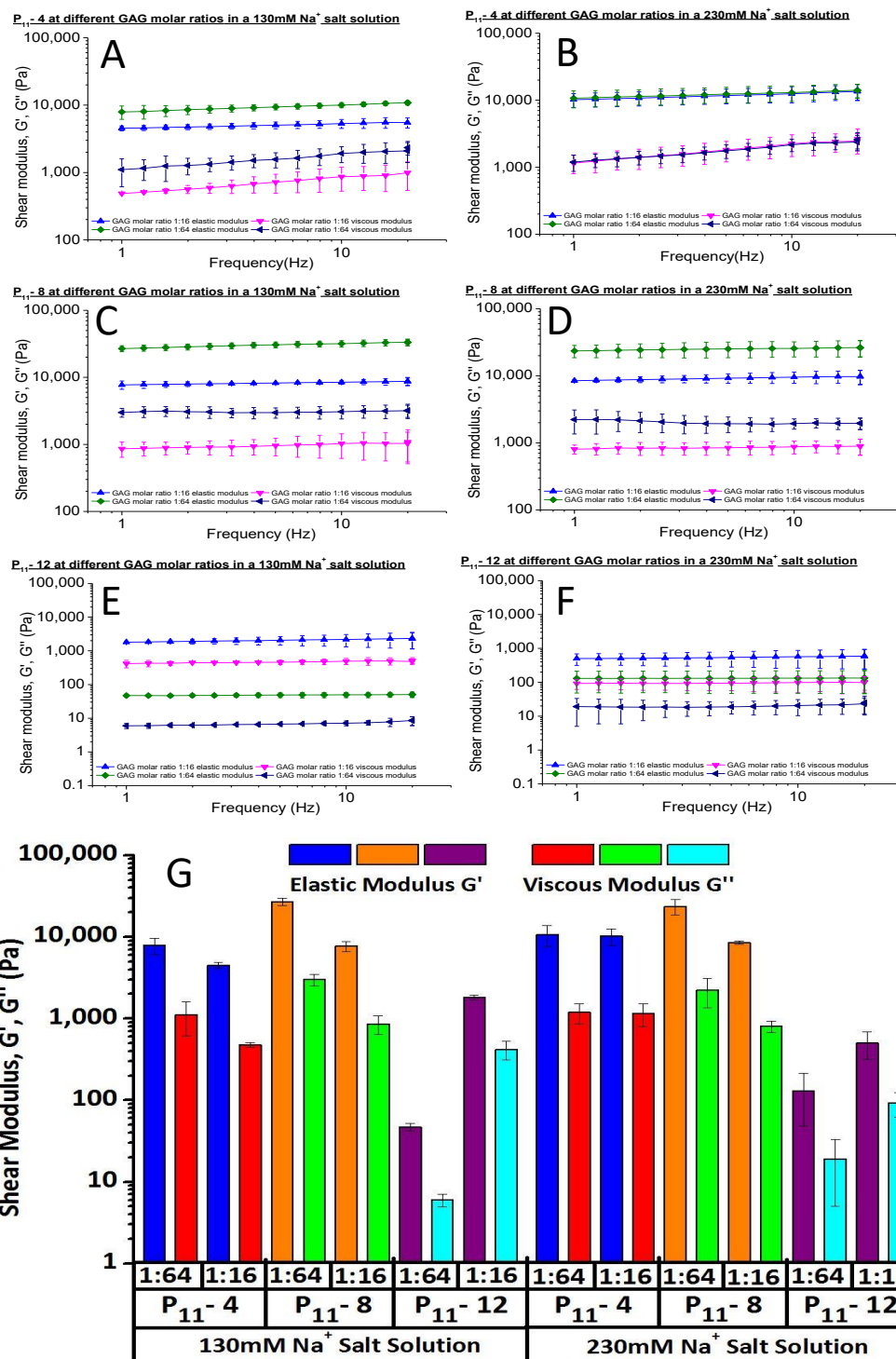


Figure 54: The effect of varying the Na⁺ ion concentration (130 mM or 230 mM) and GAG molar ratio (1:16 and 1:64) on the mechanical stiffness of the P₁₁-4, P₁₁-8 and P₁₁-12: GAG mixtures. Temperature 37°C. Frequency sweep tests between 1Hz and 20Hz for the P₁₁-4, P₁₁-8 and P₁₁-12 at GAG molar ratio of 1:16 and 1:64 in the: (A, C & E) 130 mM Na⁺ salt solution & (B, D & F) in the 230 mM Na⁺ salt solution, (G) Shear modulus extracted 1Hz for the P₁₁-4, P₁₁-8 and P₁₁-12 at GAG molar ratio of 1:16 and 1:64 in both 130 mM and 230 mM Na⁺ salt solution. Data is presented as the mean (n=3) ± 95% confidence intervals. Individual samples were subject to an amplitude sweep before commencing the test, in order to identify the linear viscoelastic region (LVER). A strain value was then chosen within the middle region of the LVER and the shear moduli (elastic and viscous) were all calculated by running a frequency sweep test between 1Hz & 20Hz.

3.4.3.3 Shear modulus of chondroitin sulfate alone

In order to understand the effect of the GAG, rheological studies of chondroitin sulfate alone in both 130mM and 230mM Na⁺ salt solutions were carried out. The lowest (4.85 mg.ml⁻¹) and highest (22.1 mg.ml⁻¹) concentrations of chondroitin sulfate were used (see Table 14). These concentrations were deemed as a good starting point to determine whether the GAGs alone had any mechanical properties. All samples were made up as described in Section 3.3.5.2.3. All the GAG solutions regardless of their concentration or the Na⁺ salt solution they were in, formed clear runny liquids as shown in Figure 55.

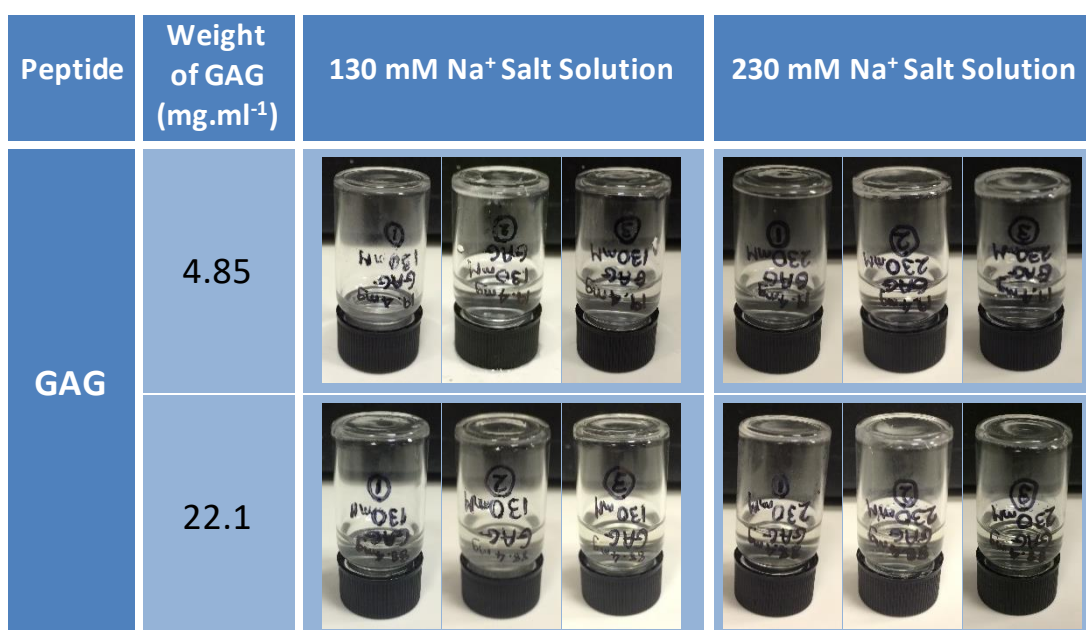


Figure 55: Varying concentrations of chondroitin sulfate (4.85 mg.ml⁻¹ and 22.1 mg.ml⁻¹) in 130 mM & 230 mM Na⁺ salt solutions. Images captured 2 days after the solutions were prepared before testing on the rheometer (n=3).

The amplitude sweep in both the 130 mM and 230 mM Na⁺ salt solutions (Figure 56A - D), showed that chondroitin sulfate at both the highest (22.1 mg.ml⁻¹) and lowest (4.85 mg.ml⁻¹) concentration had a very large LVER. This indicated that the gels could undergo higher strains before there was a breakdown in the molecular structure. However, the shear moduli values were among the lowest in this study, hence the stiffness of these liquids was very low. A strain value of 10% was chosen to carry out the frequency sweeps for all samples (Figure 57A & B). The shear moduli in the frequency sweep spectrum varied drastically across the frequency range (1Hz to 20Hz). This behaviour was observed across both chondroitin sulfate concentrations in both Na⁺ salt solutions, in which the viscous moduli and the elastic moduli crossed over at various points, eventually converged or in most cases the viscous moduli were higher than the elastic moduli, indicating that the suspensions formed had a more liquid nature than solid. This agreed with the physical properties (Figure 55) of the suspensions made, which were all liquid.

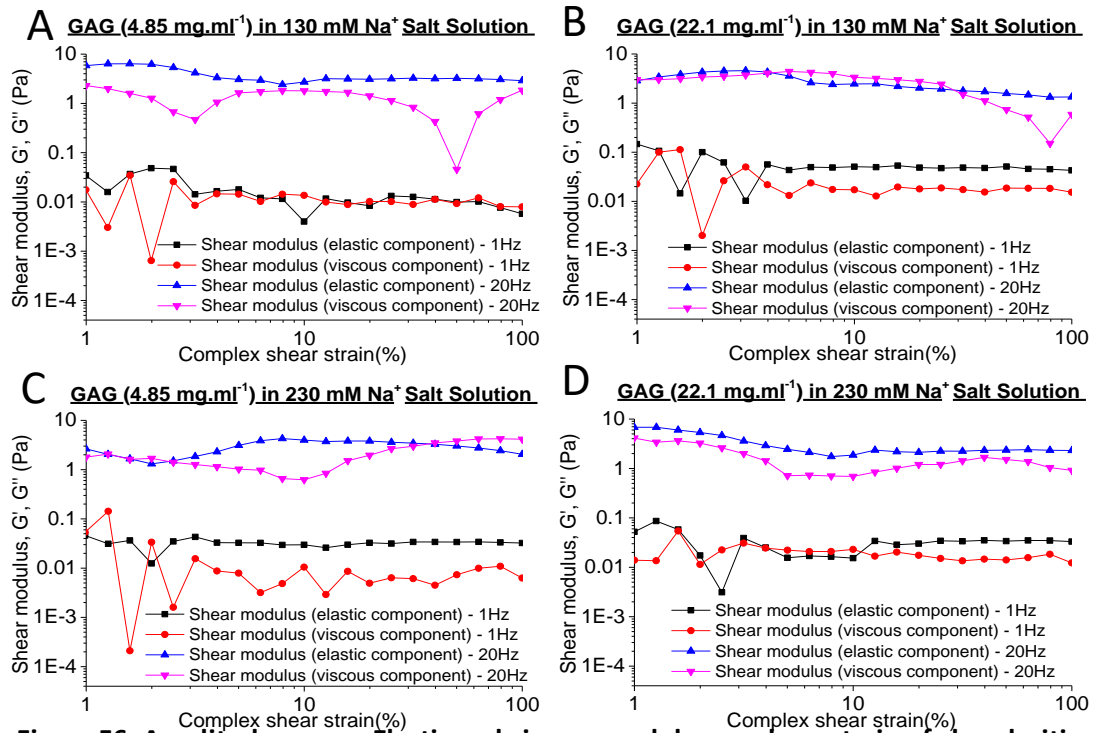


Figure 56: Amplitude sweep: Elastic and viscous modulus vs. shear strain of chondroitin sulfate in both the 130 mM and 230 mM Na⁺ salt solutions at concentrations of 4.85 and 22.1 mg.ml⁻¹. Starting shear strain: 0.01%, end shear strain: 100%, Temperature 37°C. Shear strain chosen within the LVER for frequency sweep was 10% for all samples. Data presented as the mean (n=3) ± 95% confidence intervals.

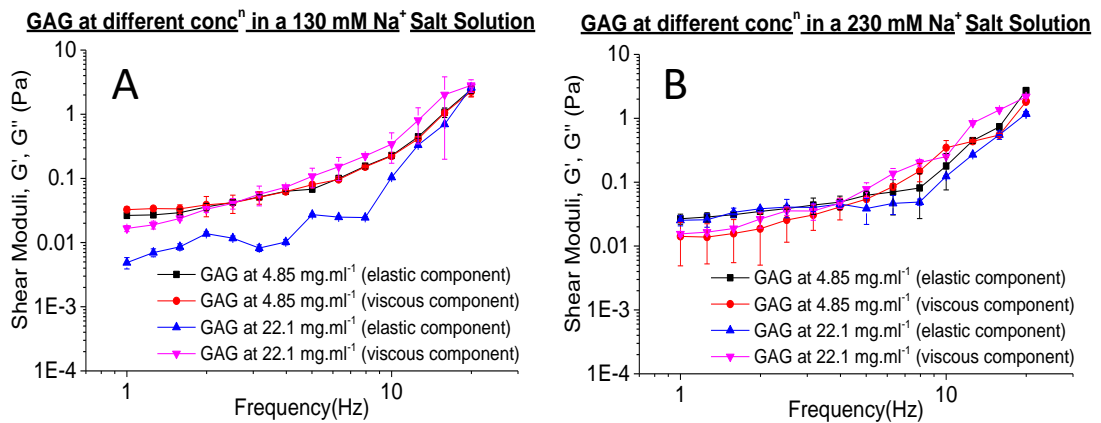


Figure 57: Frequency sweep: Elastic and viscous modulus vs. frequency of chondroitin sulfate in both the 130 mM and 230 mM Na⁺ salt solutions at a concentration of 4.85 and 22.1 mg.ml⁻¹. Starting frequency: 1Hz, end frequency: 20Hz, Shear strain: 10%, Temperature 37°C. Data presented as the mean (n=3) ± 95% confidence intervals.

3.4.4 Summary of the effect of GAG molar ratio and Na⁺ salt solution on the elastic shear modulus (G') of the peptide and PEP: GAG mixtures.

A summary of the effects of two GAG molar ratios (1:16 and 1:64) and two Na⁺ salt solutions (130 mM and 230 mM) on the elastic shear modulus of the peptides alone and the peptide: GAG mixtures at 1 Hz, is presented in Table 27. The data clearly showed that P₁₁-4, P₁₁-8 and their PEP: GAG mixtures had the stiffest gels.

Table 27: Summary table of the elastic shear modulus (G') of the peptides alone and the PEP: GAG mixtures at 1 Hz.

	Elastic shear modulus (G') (Pa)					
	Peptide alone		1:16 GAG		1:64 GAG	
	130 mM	230 mM	130 mM	230 mM	130 mM	230 mM
P ₁₁ -4	10,282 ± 2,047	9,951 ± 880	4,480 ± 377	10,190 ± 2,385	7,930 ± 1,774	10,720 ± 3,032
P ₁₁ -8	24,604 ± 8,943	53,173 ± 2,398	7,722 ± 1,087	8,468 ± 404	26,854 ± 2,737	23,515 ± 4,891
P ₁₁ -12	24 ± 4	5,608 ± 867	1,813 ± 124	502 ± 186	47 ± 5	130 ± 82

The data is presented as the mean (n=3) ± 95% confidence intervals.

3.5 Discussion

A peptide-hydrogel biomaterial for use in the regeneration of osteoarthritic cartilage should be able to form self-supporting gels in a physiological environment, show characteristic morphology similar to that of proteoglycan structures found in native cartilage and be strong enough to remain in the area to which it is applied. In this study, it was hypothesised that GAG chains at different molar ratios would not only interact electrostatically with the charged self-assembling peptides but also with the two ionic salt solutions. To gain a better understanding of whether such interactions were possible, the rheological data from this study was considered alongside the data from the studies of the self-assembly of the peptide-GAG mixtures using FTIR, and the morphological assessment of the peptide-GAG mixtures using TEM.

Initial experiments of the peptides alone in two different Na⁺ salt solutions (130 mM Na⁺ salt solution and 230 mM Na⁺ salt solution); gave an insight of how the three peptides would behave under normal physiological conditions and also within the environment of the surface layer of articular cartilage. Despite the difference in the percentages of β-sheet formation between the peptides, they all exhibited characteristic networks of entangled fibrils, which were indicative of self-sustaining gels as supported by the TEM images. Increasing the ionic strength of the Na⁺ salt solution had different effects on the three peptides. Decreases in the percentage of β-sheet formed in P₁₁-4, at increased ionic strength

could have been due to the monovalent cation interaction in the unassembled (monomeric) state. The monovalent cations could have interacted with the negatively charged peptide, forming an electric layer around the negatively charged monomer; which in turn would have increased the translational (ϵ_{trans}) energy barrier, preventing self-assembly. Similarly, increases in the β -sheet formed for P₁₁-8 and P₁₁-12 at higher ionic strength, could be attributed to the net positive charge of these monomeric peptides; which could have caused local repulsion of the monovalent cations, thus, not incurring an increase in the translation energy barrier. This study highlighted the potential effects of the surrounding ionic environment on the biochemical properties of the peptides.

A similar study carried out by Carrick *et al.*, showed the effect that ionic strength had on the self-assembly, morphology and gelation of pH responsive β -sheet tape-forming peptides (Carrick *et al.*, 2007). This study emphasised the effect that the physiological-like conditions (130mM NaCl in D₂O – no other salts added), had on the transition from fluid solutions with monomeric random coil, to gels with an anti-parallel β -sheet structure. The shifts in the transitions experienced by P₁₁-4, P₁₁-8, & P₁₁-12 (Figure 58), as a result of an increase in the ionic strength, were attributed to the screening of electrostatic repulsions between the positive and negative side chains of the individual peptides; rather than a change of the deprotonation behaviour of the amino acid side chains or the net peptide charge.

This can be quantified by the DLVO theory, which predicts that the addition of salts will screen charged groups from each other and therefore decrease the Debye length of the solvent (Caplan *et al.*, 2000; Caplan *et al.*, 2002). The behaviour of this P₁₁-X series of peptides is consistent with this theory, however, the effects of different concentrations of salts or different types of counter ions was not studied by Carrick *et al.* (2007). They did comment that the use of ions with a greater charge (usually divalent ions), which have a larger Debye radius (divalent ion vs univalent ions), allow the divalent ions to screen the electrostatic interactions over a larger range. Possibly affecting the overall self-assembly mechanism, which could explain the results presented here.

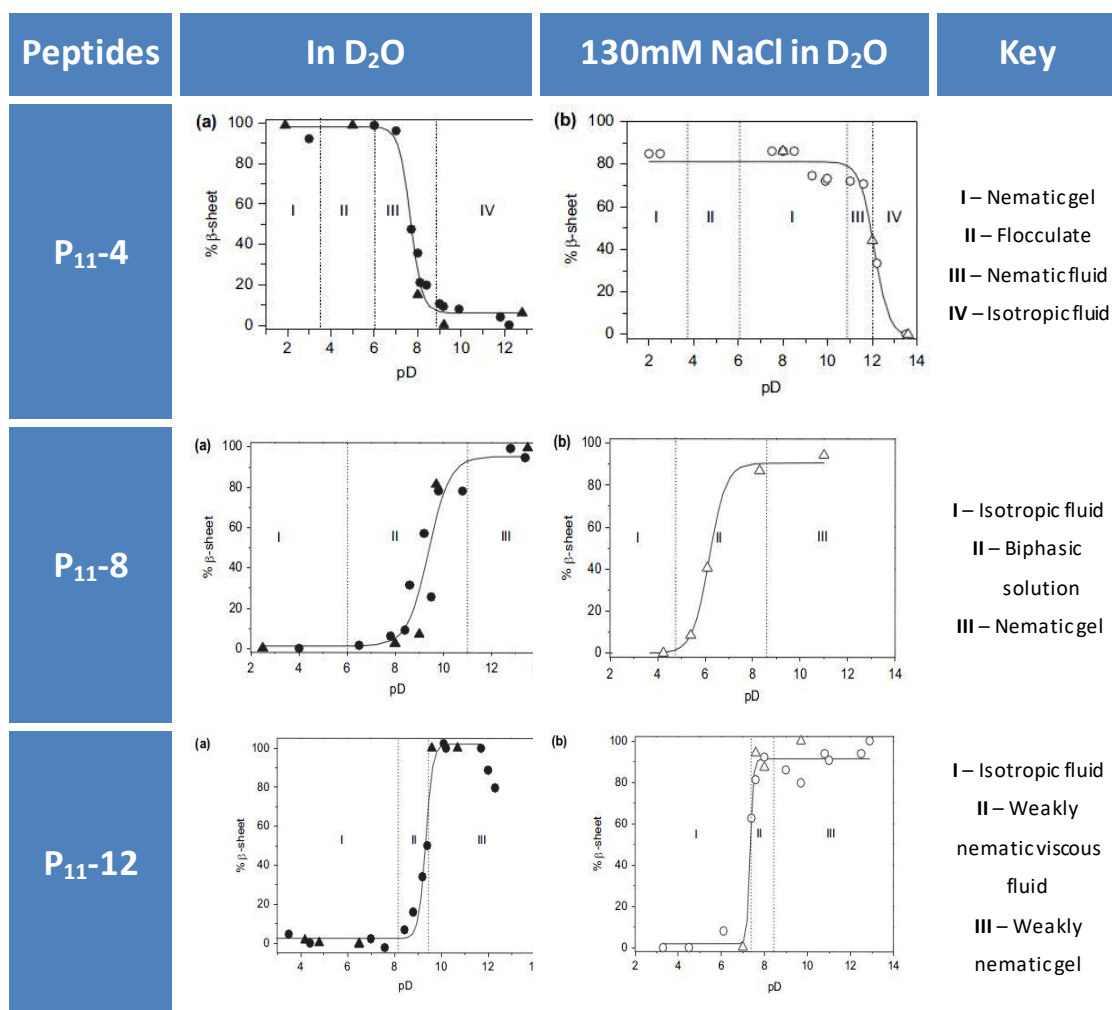


Figure 58: Self-assembly behaviour of P₁₁-4, P₁₁-8 and P₁₁-12 in 130 mM Na⁺ salt solution with no other salts. (a) Percentage of β -sheet of the peptides determined by FTIR (●) and NMR (▲) as a function of pD in D₂O. (b) Percentage of β -sheet of the peptides determined by FTIR (○) and NMR (△) as a function of pD in 130mM NaCl in D₂O, adapted from (Carrick et al., 2007).

Although initial studies showed promising results, in terms of peptide ability to form self-supporting gels in two different Na⁺ salt solutions; the aim was to mix the peptides with chondroitin sulfate (GAGs) with the goal of restoring the biomechanical properties of OA cartilage. These highly negatively charged molecules could potentially interfere with peptide self-assembly and therefore this required investigation.

The FTIR data showed that a small addition of GAG, could either increase or decrease the β -sheet percentage and also, in some instances disrupt the ability of the peptides to self-assemble. In the case of P₁₁-4 in 130 mM Na⁺ salt solution, the decrease in β -sheet, after a small addition of GAG (1:64), could be explained by the interaction of the highly negatively charged GAG molecules with the negatively charged peptide, increasing the translation energy required, hence limiting the self-assembly. However, in the 230 mM Na⁺ salt solution a similar effect was observed, which could be explained by the screening of electrostatic repulsion between the positive and negative side chains of P₁₁-4 with the increasing

concentration of Na⁺ ions. Nevertheless, the addition of increased amounts of GAG seemed to drive the assembly further.

Similarly, in the case of P₁₁-8, the addition of the higher GAG molar ratio (1:16) not only increased β -sheet formation but also formed self-sustaining hydrogels, which was not the case with P₁₁-12. This behaviour could be explained by the inherent design of the peptide amino acid sequence. P₁₁-4 and P₁₁-8 each contain four glutamine residues, which means they contain four hydrogen acceptor sites and four hydrogen donor sites each (Figure 59). Therefore, they can form eight intermolecular hydrogen bonds which have favourable enthalpy. This is termed the polar zipper effect. P₁₁-12 has four serine residues, which only have two hydrogen acceptor sites and two hydrogen donor sites (Figure 59), therefore, P₁₁-12 can only form four intermolecular bonds, which has less favourable enthalpy. In addition, the hydroxyl functional group of serine, also has a high affinity to hydrogen bond with deuterium oxide (another form of water). This results in deuterium oxide competing for hydrogen bond interactions with the peptides containing serine residues, in turn causing self-assembly to be less favourable. The latter could explain why the P₁₁-12: GAG mixture, had such low β -sheet formation, lacked fibrillary morphology and did not form self-sustaining hydrogels.

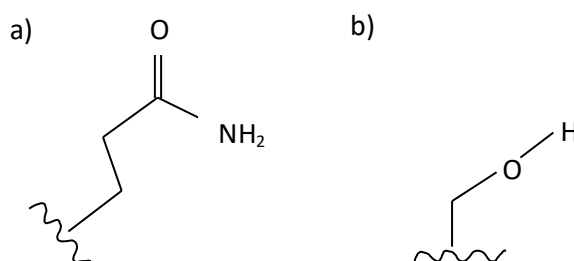


Figure 59: Amino acid residues: a) Glutamine residue b) Serine residue.

A study by Miles *et al.*, also looked at the percentage of β -sheet content within P₁₁-4, P₁₁-8 and P₁₁-12 in the presence of GAGs. The commented that the addition of larger amounts of GAG did not inhibit the P₁₁ peptides self-assembly, which is somewhat contrary to what was found in this study. However, it is very important to note that Miles *et al.*, tested the peptides in only a 130 mM NaCl in D₂O, whereas in our study we investigated two salt solutions containing varying amounts of physiological salts as well as two GAG molar ratios. Therefore, difference seen between the two studies are attributed to the difference in physiological solutions used to reconstitute the peptides.

As with all techniques, FTIR has its limitations especially when used to analyse peptide hydrogels (Kubelka and Keiderling, 2001) as these biomaterials are very sensitive to the way

they are treated. The biphasic solutions/gels analysed in the FTIR can dissociate upon the application of mechanical force between the CaF₂ discs, resulting in sheer thinning, therefore leading to a disproportionate amount of gel and fluid between the IR discs, which could lead to inaccurate determination of β -sheet content. However, every effort was made to reduce this with the use of a known path length of 0.25mm. Nevertheless, due to the concentration regime and aqueous salt conditions used, FTIR was the only available means to assess the conformation of the system studied. Despite the possible limitations of the technique, FTIR analysis clearly highlighted that two of the three SAPs (P₁₁-4 and P₁₁-8) demonstrated a greater percentage of β -sheet in the presence of the GAG at 130mM and 230mM Na⁺ salt concentrations, when compared to P₁₁-12. This higher percentage of β -sheet, demonstrated that self-assembly had taken place under physiological conditions, making P₁₁-4 and P₁₁-8, good candidates to take forward into biological studies, depending on their fibril morphology and biomechanical properties. The formation of peptide gels is subject to a difference in the kinetics of self-assembly which can be influenced by the surrounding conditions and the molar ratio of GAG. Therefore, the values of β -sheet percentage presented in this study may not be indicative of values that the peptide and peptide-GAG mixtures may have achieved, if they had been left to reach a full equilibrium state.

When considering the overall morphology of the SAPs and SAP-GAG mixtures, it was observed that generally those peptides and peptide-GAG mixtures that exhibited higher β -sheet formation tended to exhibit denser networks of fibrils and fibres, with a greater proportion of junction points. The presence of these nanofibrillar networks with interwoven morphology indicated the formation of self-supporting hydrogels. However, this was not the case for P₁₁-12 at both GAG molar ratios and in both Na⁺ salt solutions. This peptide precipitated out of solution and formed solid white flocculates, some of which were observed in the TEM images for P₁₁-12. These clumps appeared to interact with each other to form bundles and small networks as was the case in the other gels. The low percentage of β -sheet formation exhibited in the FTIR analysis could be linked to the irregular fibril morphology and this may have been due to the unexpected formation of nanotubes, although these were not widely observed.

The changes seen in β -sheet percentage and morphology; as a result of increasing the Na⁺ ion concentration could have been due to the increased amount of positively charged sodium ions present in the salt solutions. This could have been as a result of the interactions with the differently charged peptide residues, which in theory could have inhibited or promoted the formation of β -sheet secondary structure as well as fibril formation. Moreover, the presence of other cations and anions, present within these Na⁺ salt solutions could also have

played a role in the interaction with the differently charged peptide residues and also have had positive or negative impacts on the peptide self-assembly and fibril morphology.

It is important to consider that the variations and trends observed in the widths and lengths of the SAPs and SAP-GAG mixtures, may not have been directly related to the concentration of GAGs and Na⁺ ions present in the salt solutions; due to the nature by which the peptides were processed for imaging. Peptide and peptide-GAG samples were left to dry before TEM analysis and therefore it is possible that the drying process could have had an effect on the fibril/fibre formation and/or association and hence affected the fibril widths and lengths.

Nevertheless, the TEM images showed that P₁₁-4 and P₁₁-8 alone and with GAG, demonstrated a characteristic network of entangled fibres/fibrils; an indicator that the SAPs had undergone hierarchical self-assembly to form these structures. Despite having some of the longest and thickest fibrils, P₁₁-12, did not demonstrate this characteristic network and hence would not be considered a good candidate for future studies as when coupled with the FTIR analysis, it would appear that the GAGs affected the self-assembly and morphology of P₁₁-12, which was not desirable for the intended application.

Previous studies with the same peptides have shown that the addition of GAG molecules, also enhanced the thermodynamic stability of the aggregates, increased β -sheet content and also acted as a trigger for peptide gelation, especially with the positively charged peptides (P₁₁-8 and P₁₁-12) (Miles et al., 2016). Miles *et al.* commented that electrostatic interactions could not be the sole reason to explain why there were favourable peptide-GAG interactions. The authors discussed the potential of other interactions, such as hydrogen bonding between the GAGs and peptides, which helped explain how the GAGs also enabled the self-assembly of like-charged anionic peptides (P₁₁-4). The authors were able to support their theory through the testing of polyethylene glycol (PEG) polymers with different molar ratios of GAG. There were no comparable improvements in the gelation kinetics when compared to the P₁₁-X, peptides, therefore it was concluded that the GAG must also be interacting directly with the peptide *via* physical bonds to enhance the gelation kinetics, which could explain the trends observed in the study presented here.

The P₁₁-x peptides were studied in two different GAG molar ratios (1:64 and 1:16) and Na⁺ salt solutions (130mM and 230mM Na⁺ salt solution). Each solution contained a different concentration of Na⁺ ions, as well as other salts found in cartilage tissue (Urban, 1994), as these particular conditions had not been studied previously. The FTIR and TEM analyses showed the combined effects that the ionic Na⁺ salt solutions and the negatively charged GAG had on the self-assembly and morphology (fibril formation) of the P₁₁-x peptides. It was

hypothesised that these changes in microscopic structures, would lead to changes in the bulk mechanical properties of these peptide hydrogels and hence a rheological study was able to determine these differences in mechanical properties. Peptide only and GAG only controls were also tested in order to determine the effect that the addition of GAG and different Na⁺ salt solution had on the shear moduli.

The rheological studies were not only able to identify the molar ratio of SAP-GAG that gave favourable biomechanical properties, but also showed the effect that the presence of GAG chains had on the mechanical stiffness of the SAP hydrogels as a function of GAG concentration. Perusal of the data revealed the combined effect of the three variables (peptide, GAG molar ratio and Na⁺ salt concentration) had an effect on the overall shear modulus at 1Hz. It is also important to comment on the data for the GAG controls where it was confirmed that, regardless of the concentration of GAG added to the 130 mM and 230 mM Na⁺ salt solutions, the samples exhibited no mechanical strength. Therefore, the GAG on its own had negligible stiffness, when compared to the peptide on its own and the peptide-GAG mixtures. This supported previous hypotheses that the mechanical properties observed for the peptide-GAG mixtures were due to interactions between the negatively charged GAG and the positively/negatively charged peptides as well as their interaction with the surrounding ionic Na⁺ salt solution. Given the two physiological environments that these peptides were tested under, it was clear that the addition of the GAG allowed for the mechanical properties of the peptide hydrogels to be tuned over a range of up to four orders of magnitude (Table 27). In all peptide samples tested, the elastic component was found to be greater than the viscous component, demonstrating solid-like behaviour of these hydrogels and in some cases, even exhibiting shear thinning characteristics that may be advantageous for their future uses in cartilage regeneration. Of the three SAP-GAG mixtures, it was clear that two of the peptide hydrogels were more favourable, P₁₁4 and P₁₁-8, of which P₁₁-8 was the stiffest. Overall when comparing the behaviour of P₁₁-8 in both cases (Case 1: In both 130 mM and 230 mM Na⁺ salt solutions, with Case 2: In both 130 mM and 230 mM Na⁺ salt solutions with the addition of two GAG molar ratios); the addition of the GAG had a very different effect depending on the ionic strength of Na⁺ salt solution that the peptide was in. In the 130 mM Na⁺ salt solution, P₁₁-8 at the lower molar ratio of GAG (1:64) had a positive effect on the moduli. Whereas, at the higher molar ratio of the GAG (1:16), it seemed to have a detrimental effect on the moduli. The latter was also true for both molar ratios of GAG in the 230 mM Na⁺ salt solution. Nevertheless, P₁₁-8 in both the 130 mM and 230 mM Na⁺ salt solutions at the lowest GAG molar ratio exhibited an elastic modulus of around +23,000 Pa; which was relatively high for a gel made of soft matter. The bundles of aggregates captured

in the TEM images of P₁₁-8 in both Na⁺ salt solutions (130 mM and 230 mM) at a GAG molar ratio of 1:64, showed areas of denser bundles of fibrillar networks, indicating that there that there were higher number of junction points. This observation supported the results of the rheological study.

The mechanical properties of the SAP-GAG mixtures were influenced by the ionic interactions between the negatively charged GAGs and the positively/negatively charged peptides as well as their interaction with the surrounding ionic Na⁺ salt solution. This study showed that the addition of another charged bio-polymer and the change in the ionic strength of the surrounding solution had a large effect on the stiffness of the individual peptide hydrogels by either promoting a greater number of entanglements in particular peptides or by inhibiting the peptides ability to form entanglements and junction points. The addition of the GAG not only provided the high charge found in native tissue, which contributes to the hydration and function of cartilage, but at certain molar ratios, it improved the rheological properties of some of the resulting gels. Increasing the Na⁺ ion concentration (as found in the surface of cartilage), allowed for the investigation of how the peptides would behave in *in vivo* conditions and also the effect that this had on the rheological properties of the resulting gels. Overall in this study, higher concentrations of GAG (1:16) decreased the gel stiffness of the glutamine-based peptides (P₁₁-4 and P₁₁-8). However, at lower GAG concentrations (1:64) the stiffness of the P₁₁-4 gels was slightly improved, but more so in P₁₁-8 gels. Nevertheless, the corresponding peptides alone were generally mechanically stiffer. By contrast, for the serine-based peptide (P₁₁-12) gel stiffness was increased at high GAG concentrations, but the stiffness values were still much lower than the glutamine based peptides.

A similar study carried by Miles *et al.* at the University of Leeds, also showed that the GAG can have a great effect on the shear modulus of the peptides (Miles et al., 2016). Although the solution used was made up in differently to the one in this study, the authors also commented that at higher GAG concentrations the shear modulus of the peptides decreased, when compared to the peptides with lower GAG concentrations. The authors also commented on how the presence of the GAGs not only affects the peptide interaction but also has an effect on their microscopic structure. Specifically concluding that the shear modulus of the peptide gels was related to the thickness of the fibrils and/or the number of junction points between the interacting fibrils, which in turn is dependent on the density of the chains, their width and length and cross-linking affinity at the junction points. A conclusion which strongly agreed with the findings in this study.

The equilibrium shear modulus of cartilage has been quoted to be in the range of 0.05 to 0.25 MPa (Athanasίου et al., 2009). Our strongest peptide and peptide: GAG gel was P₁₁-8 (1:64 GAG molar ratio), with an elastic shear modulus of approximately 0.027 MPa, which doesn't put it far off the shear modulus of healthy cartilage. Bearing in mind that the gels are made of soft matter and have only been tested in an environment that is meant to mimic the internal environment of the knee, these peptide: GAG gels have a potential to improve the biomechanical properties of GAG depleted condylar cartilage.

New SAP-GAG hybrid materials have been developed with adjustable mechanical properties. Their ability to self-assemble and the incorporation of chondroitin sulfate, at the correct molar ratio makes them feasible candidates for a minimally invasive therapy to aid in the restoration of mechanical properties to early stage osteoarthritic cartilage. FTIR and TEM studies have highlighted the SAP-GAG combinations that were able to form characteristic self-supporting gels able to produce characteristic entangled fibrillary networks similar to those found in native cartilage. Alongside this, the rheological studies at (1Hz) determined that P₁₁-4 and P₁₁-8 peptide-GAG combinations, were among the stiffest.

The combination of these studies has identified that two of the three SAPs demonstrate all of the three favourable properties: high β -sheet percentage, characteristic entangled fibrillar networks and a high stiffness coefficient.

In conclusion, the data presented in this study indicates that P₁₁-4 and P₁₁-8-chondroitin sulfate mixtures have properties which make them suitable candidates for further investigation for their capacity to restore the biomechanical properties of GAG depleted tissues, such as early stage OA cartilage.

Chapter 4 Development of GAG depleted cartilage models

4.1 Introduction

In order to be able to test the ability of the peptide and peptide-GAG mixtures to restore the mechanical properties of GAG depleted cartilage, it was necessary to develop an osteoarthritic-like cartilage model. Several studies have used GAG-depleting enzymes, such as chondroitinase ABC (CaseABC) to selectively degrade specific proteoglycans of articular cartilage to study their role in the biomechanical responses of the tissue and also to create osteoarthritic-like cartilage models, to test novel cartilage regeneration therapies (Schmidt et al., 1990; Chen et al., 1997; Pickard et al., 1998; Basalo et al., 2004; Basalo et al., 2005; Sasada et al., 2005; Katta et al., 2008). Chondroitinase ABC (Case ABC) at pH 8 has been shown to degrade chondroitin sulfate A, B and C at greater rates than chondroitin and hyaluronic acid. It does not breakdown other GAGs such as heparin, keratan sulfate or heparan sulfate (Yamagata et al., 1968). Other studies have shown that the use of SDS within decellularisation processes can also severely deplete the levels of GAGs within porcine cartilage tissues (Stapleton et al., 2008; Kheir et al., 2011). The number of sodium dodecyl sulfate (SDS) washes and the concentration of SDS determine the levels of GAGs removed, however the use of high concentrations of SDS (1.0-2.0% w/v) can also lead to disruption of matrix proteins and collagen fibres (Samouillan et al., 2000; Elder et al., 2010; Kheir et al., 2011). These damaging effects can be minimised by using low concentration SDS (0.1% w/v; Stapleton et al., 2008; Kheir et al., 2011). Therefore, the use of chondroitinase ABC and low concentration SDS were investigated for the development of GAG depleted cartilage models in this study.

4.2 Aims and objectives

The aim of the research described in this chapter was to create a GAG depleted cartilage model and characterise the model biochemically and histologically.

4.2.1 Objectives

- 1) To develop a procedure that would consistently remove GAGs from native porcine femoral condylar cartilage to create femoral condyles with GAG depleted cartilage.
- 2) To determine the GAG content of native porcine femoral cartilage and GAG depleted porcine femoral cartilage.

- 3) To characterise the GAG depleted porcine femoral cartilage using histology and to compare the histological features to those of native porcine femoral cartilage.

4.3 Experimental Methods

4.3.1 Acquisition of porcine femoral condyles

Porcine femoral condyles were acquired, dissected and stored as described in Chapter 2; Section 2.2.2.2 to 2.2.2.4.

4.3.2 Treatment of porcine femoral cartilage with chondroitinase ABC.

The enzyme chondroitinase ABC was used throughout this thesis for the depletion of GAGs from porcine femoral cartilage, unless otherwise stated.

As recommended by the supplier, chondroitinase ABC (Case ABC from *Proteus vulgaris*, Sigma) was made at the required concentration with an aseptically prepared buffer solution at pH 8, with the addition of antibiotic solution to inhibit microbial growth and a proteinase inhibitor, aprotinin, to prevent autolysis of the ECM proteins. The effect of the CaseABC treatment on the GAG content of the femoral condylar cartilage was determined using the dimethylmethylene blue assay (DMB assay), outlined in Chapter 2; Section 2.2.5.3.1.

4.3.2.1 GAG depletion of cartilage tissue

Reagents:

- Bovine serum albumin (BSA) 2% (w/v) solution. BSA (10 mg) was dissolved in 0.5 ml of distilled water (dH₂O).
- BSA solution 0.01% (w/v). BSA (10 mg) was dissolved in 100 ml of dH₂O.
- Buffer solution (pH8) Trizma base (0.61 g; Sigma) and 0.49 g of sodium acetate (Thermo Fisher) were dissolved in 50 ml of dH₂O. The pH was adjusted to 8 by adding 6M HCL or 6M NaOH drop-wise.
- Antibiotic solution: (*Working concentration: nystatin [250 U.ml⁻¹], gentamicin [20 U.ml⁻¹], Polymixin B [200 µg.ml⁻¹], vancomycin [50 µg.ml⁻¹], Primixin I.V [200 µg.ml⁻¹], amphotericin B [25 µg.ml⁻¹], aprotonin [10 KIU.ml⁻¹]*). Gentamicin (1 mg), 10 mg Polymixin B, 2.5 mg of vancomycin and 10 mg of Primixin I.V were dissolved in 1250 µl of nystatin, 10 µl of aprotonin, 5 ml of amphotericin B and 0.5 ml of 2% (w/v) BSA solution. The final solution was aliquoted into 0.7 ml volumes into sterile Eppendorf tubes.

- Hank's balanced salt solution (HBSS) with 1 mM Zn²⁺ and penicillin/streptomycin 100 µg.ml⁻¹. ZnCl₂ (78.3 g) was dissolved in 28 ml of sterile HBSS. This solution (25 ml) was filter sterilised and 10 ml of penicillin/streptomycin (neat as supplied by the manufacturer) was added. This was carried out aseptically in a class II cabinet.

The Case ABC (10 U) was reconstituted by adding 0.5 ml of 0.01% (w/v) BSA solution. The reconstituted solution was transferred into a universal container and the volume was made up to 5 ml using the 0.01% (w/v) BSA solution. The CaseABC (0.1 U.ml⁻¹) solution was aliquoted in volumes of 0.25 ml into Eppendorf tubes. Aliquots were stored at -20 °C until needed (max storage: 6 months).

4.3.2.2 Enzymatic painting of CaseABC agarose gel onto porcine femoral cartilage – Model 1

The CaseABC (0.1 U.ml⁻¹) was mixed with an agarose gel to allow the painting of the Case ABC solution onto the surface of the porcine condyle. A control containing just the antibiotic solution in the agarose gel was also used. Three porcine femoral condyles (both medial and lateral condyles) were used for the application of the CaseABC solution and another 3 for the application of the control solution.

Agarose (15 mg) was dissolved in 4 ml of Case ABC buffer to make a 0.3 % (w/v) solution. The solution was placed in the microwave for approximately 30-45 seconds to dissolve the agarose. The solution was allowed to cool to 37°C before adding 1 aliquot (0.68 ml) of the antibiotic solution followed by 1 aliquot (0.25 ml) of the CaseABC solution. The mixture was then vortexed gently to ensure thorough mixing of contents and eventual gelling (viscous liquid). The sol-gel was kept at 37°C until time of application. The control gel was prepared in the same way except the Case ABC solution was replaced with 0.25 ml of 0.01 % (w/v) BSA solution.

Porcine femoral condyles were transferred to a sterile class II cabinet and placed into a sterile pot. An area of interest was marked out by a permanent marker and, using a paint brush, the CaseABC gel (or control gel) was generously applied to this area (Figure 60). Condyles were returned to their sterile containers and incubated at 37°C for 2 hours.



Figure 60: Sterile condyles showing the area of interest marked out in permanent marker, Case ABC gel was applied to this area to allow the depletion of GAGs.

After the 2 hours, another CaseABC agarose gel (or control gel) was prepared as described above and re-applied to the femoral condyles in the area of interest and incubated at 37°C for a further 2 hours. The process was repeated again and after the 3rd application of the CaseABC agarose gel (or control gel), the condyles were incubated at 37°C overnight. CaseABC enzyme is inhibited by Zn²⁺ ions, therefore the following day, the condyles were transferred into sterile 250 ml pots and washed twice for 30 min in 200 ml of HBSS Zn²⁺ solution on an orbital shaker at room temperature with agitation of 240 rpm.

Cartilage condyles were then transferred to a sterile dissection table. Condyles were clamped and two plugs were aseptically removed from each condyle as described in Chapter 2; Section 2.2.2.3. Cartilage was removed from the bone in both plugs. One plug was used for histological analysis (Safranin O staining) and the other for GAG analysis.

4.3.2.3 Injection of CaseABC solution into porcine femoral cartilage – Model 2

This method of GAG depletion used the same reagents described in Section 4.3.2. For Model 2 the enzyme was administered using a 30G needle and syringe to a pre-determined area (Figure 61). A control containing just the enzyme buffer solution and antibiotic solution was also used. Three porcine femoral condyles (both medial and lateral condyles) were used for the injection of the CaseABC solution and another three for the injection of the control solution.

Firstly, 8.1 ml of enzyme buffer was dispensed into a glass universal container and placed in a water bath at 37°C. Whilst warming, 2 aliquots (1.4 ml) of antibiotic solution were added, followed by 2 aliquots (0.5 ml) of CaseABC solution. The solution was vortexed gently to ensure thorough mixing of the contents and kept at 37°C until use. For the control solution, CaseABC solution was replaced with 0.5 ml of 0.01 % (w/v) BSA solution.

Condyles were transferred to a class II cabinet and placed onto a sterile surface. An area of interest was marked out by a permanent marker (Figure 61). Using a 30G needle-syringe the femoral cartilage was injected with the CaseABC mixture (or control solution) at 20 locations in the pattern shown in Figure 61. Approximately 0.1 ml of the solution was injected at each site, holding the syringe perpendicular to the cartilage surface. Injection of the CaseABC mixture (or control solution) was carried out slowly into the cartilage, applying a small amount of force to the syringe plunger and occasionally pulling in and out simultaneously to ensure deposition of the enzyme.

Treated condyles were then returned to their 250 ml sterile containers and incubated at 37°C overnight. The following day condyles were washed twice for 30 min in 200 ml of HBSS Zn²⁺ solution on an orbital shaker at room temperature with agitation of 240 rpm.

Two plugs were removed from each condyle as described in Chapter 2; Section 2.2.2.3. Cartilage was removed from the bone in both plugs. One plug was used for histological analysis (Safranin O staining) and the other for GAG analysis (Figure 61).

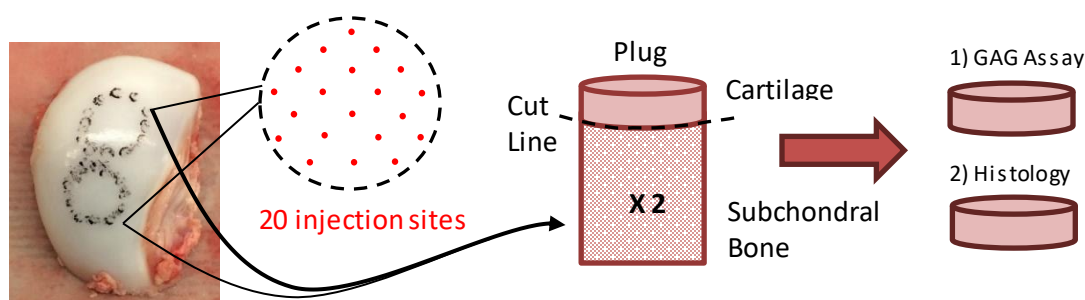


Figure 61: Porcine femoral condyle showing the area of interest marked out in permanent marker. Schematic to the right shows the pattern in which the CaseABC solution (or control solution) was injected to this area to allow the depletion of GAGs. Twenty injections were made in each site. 9 mm plugs were taken from each site for histological analysis. One plug was used for Safranin O and the other plug was used to GAG quantification.

4.3.3 SDS and PBS washes of porcine condylar cartilage – Model 3

A series of SDS and PBS washes were carried out in order to deplete femoral condylar cartilage of its GAGs. Four methods were developed in model 3. The duration in which the femoral condylar cartilage remained in either SDS or PBS changed in each method. Three porcine femoral condyles (both medial and lateral condyles) were used for each method in this study. Three untreated native porcine femoral condyles (both medial and lateral condyles) were used as the control in this study.

Reagents:

- Sodium dodecyl sulfate (SDS) solution (0.1% w/v). SDS (2 g; Sigma) was dissolved in 2 L of dH₂O and 2 ml of aprotinin (Nordic pharma, 10 KIU.ml⁻¹) was then added.
- Phosphate buffered saline (PBS): PBS tablets (20; Sigma) were added to 2 L of dH₂O. The pH was adjusted to between 7.2-7.4, by adding 6M HCL or 6M NaOH dropwise. The solution was then autoclaved and 2 ml of aprotinin (10 KIU.ml⁻¹) was added.
- Salt solution (130 mM Na⁺; as outlined in Chapter 3; Section 3.3.1.3). KCl, (1.04 g), 1.11 g of CaCl₂, 10.29 g of NaCl, 7.06 g of NaHCO₃ were dissolved in 2 L of dH₂O.

The method was carried out over four days as described below:

Day 1: porcine femoral condyles (medial and lateral) were placed into 250 ml plastic sterile containers and 200 ml of 0.1% (w/v) SDS was added. Containers were then secured onto an orbital shaker using tape. The shaker was placed in an incubator at 37°C and agitated at 240 rpm. The condyles were incubated overnight.

Day 2: the SDS solution was replaced with 200 ml of fresh sterile 0.1% (w/v) SDS and the samples were returned to the 37°C incubator and agitated at 240 rpm overnight.

Day 3: the 0.1% (w/v) SDS solution was replaced with 200 ml of fresh PBS containing aprotinin. The samples were returned to the incubator at 37°C and agitated at 240 rpm for three hours. This step was repeated, followed by a final 24 hour incubation in fresh PBS.

Day 4: the PBS was replaced with the 130 mM Na⁺ salt solution and left to soak overnight at 4 °C with no agitation.

Two plugs were removed from each condyle as described in Chapter 2; Section 2.2.2.3. Cartilage was removed from the bone in both plugs. One plug was used for histological analysis (Safranin O staining) and the other for GAG analysis.

4.3.4 Histological Characterisation

In order to allow visualisation of any GAG removal from the cartilage as a result of the methods applied in models (1) to (3), histological analysis was performed. This analysis was also carried out using native cartilage to observe any differences in GAG distribution. Femoral condylar cartilage plugs were extracted from the GAG depleted condyles and native cartilage as outlined above. Cartilage tissues were fixed in zinc fixative, processed and sectioned as described in Chapter 2; Sections 2.2.3.1 to 2.2.3.3. Sections were placed on slides and were stained with Safranin O and fast green.

4.3.5 GAG Quantification

The GAG content remaining in the GAG depleted tissue from models (1) to (3) was measured using a DMB assay, to quantify the amount of sulfated sugars remaining within the tissue, as described in Chapter 2; Section 2.2.5.3.1. The GAG content of native cartilage samples was also determined for a comparison to be made. There were 3 porcine femoral condyles (both medial and lateral condyles) for each GAG depleted model and 3 native cartilage samples. One plug from each condyle (medial and lateral condyle; GAG depleted and native cartilage) was used for the GAG analysis. Samples were weighed 3 times before lyophilisation (wet weight) and 3 times after (dry weight) and an average was recorded for the calculation of percentage GAG per tissue wet and dry weight, as described in Chapter 2; Section 2.2.5.2.

4.3.6 SDS Quantification in GAG depleted cartilage (Model 3)

The SDS concentration within the GAG depleted porcine femoral condylar cartilage was measured at four different stages of the process for GAG depletion used in model 3. This was carried out to determine the amount of SDS remaining at the end of each process within the GAG depleted femoral condylar cartilage. This was important because it was thought that residual SDS in the cartilage might affect the self-assembly of the peptides and peptide-GAG mixtures. The analysis was performed on solutions that the femoral condylar cartilage was immersed in. In addition to reagents listed in Section 4.3.3, the following reagents were used.

Reagents:

- Stains-all stock solution (1.8 mM, Sigma E9379, Lot no#BCBM9845V). Stains-all (10 mg) was dissolved in 10 ml of 50 % (v/v) isopropanol in dH₂O. This was then wrapped in foil and stored at 4°C.
- Stains-all working solution (90 µM) was made by mixing 1 ml of the stains-all stock solution, 1 ml of formamide and 18 ml of dH₂O. This was wrapped in foil and stored at 4°C.

SDS was dissolved in three different solvents (SDS 0.1% w/v, PBS and 130 mM Na⁺ salt solution) at 2 mg.ml⁻¹. These solutions were then serially diluted in the appropriate solvent to produce a range of standards from 2 to 2000 µg.ml⁻¹ and a standard curve was produced.

A clear flat-bottomed 96-well plate was used for the assay, 200 µl of stains-all working solution was added to each well and 10 µl of each standard was added in triplicates. The following samples were analysed: (1) the last SDS wash; (2) the two three hour PBS washes; (3) the one 24 hour PBS wash and 4) the 130 mM soak. One microliter was taken from each

solution and added into the 96-well plate in triplicates. The plate was shaken for 2 min and the absorbance of each well was measured using a microplate spectrophotometer at 447 nm. A graph of SDS concentration against absorbance at 447 nm was plotted using the standard solutions. A linear regression analysis was performed and used to interpolate the concentration of SDS in the test samples.

4.4 Results

4.4.1 Evaluation of native and GAG depleted porcine femoral condyles

Three different methods for producing GAG depleted cartilage were investigated. Images of sections of native porcine condylar cartilage and porcine condylar cartilage that had been subject to the three different GAG depletion techniques stained with Safranin O are presented in Figure 62, Figure 64, Figure 66 and Figure 67. The GAG content in native porcine condylar cartilage and porcine condylar cartilage that had been subject to the three different GAG depletion techniques is presented in Figure 63, Figure 65 and Figure 68; with the statistical analysis of the data shown in Figure 70.

4.4.1.1 Model 1

Images of sections of porcine condylar cartilage that had been painted with CaseABC agarose gel and a control agarose-gel without CaseABC; stained with Safranin O are presented in Figure 62A & B, respectively. The control cartilage tissue showed characteristic cartilage architecture and cell organisation, throughout the depth of the cartilage tissue, when compared with native porcine cartilage tissue. Porcine cartilage that had been treated with the CaseABC showed similar histo-architecture compared to the control cartilage tissue and native porcine cartilage. It was, however clear from the Safranin O stain distribution that the CaseABC treatment had removed some of the GAGs from the surface of the cartilage.

Measurement of the depth of GAG depletion in all samples (n=3 for porcine condylar cartilage painted with CaseABC and n=3 for the control cartilage, painted without CaseABC), across 6 different points along the top surface of the cartilage, showed that the average depth of GAG depletion was approximately 163 μm from the surface of the cartilage in the CaseABC treated cartilage; compared to 8 μm in the control porcine condylar cartilage, which had not been treated with CaseABC. The latter was attributed to the lower levels of GAGs in the superficial layer of cartilage compared to the mid-zone. The data (depth of the GAG depleted surface layer) was analysed using Student's t-test to test the null hypothesis that applying the agarose CaseABC gel did not affect the depth of GAG depletion of porcine

condylar cartilage when compared to the cartilage control tissue, treated with only an antibiotic agarose-gel. This showed that the depth of GAG depletion was significantly greater in the CaseABC treated samples than in the control samples ($p=5.3 \times 10^{-6}$).

The GAG concentration per cartilage dry weight of the porcine condylar cartilage painted with a CaseABC agarose gel, the control (without CaseABC) and the untreated native porcine condylar cartilage, are shown in Figure 63. The native porcine cartilage had the highest average GAG content at 225 ug.mg^{-1} . The average GAG content of the porcine condylar cartilage that had been painted with CaseABC (model 1 - 137 ug.mg^{-1}), was lower than the GAG content seen in the porcine condylar cartilage that had not been painted with CaseABC, (control - 218 ug.mg^{-1}).

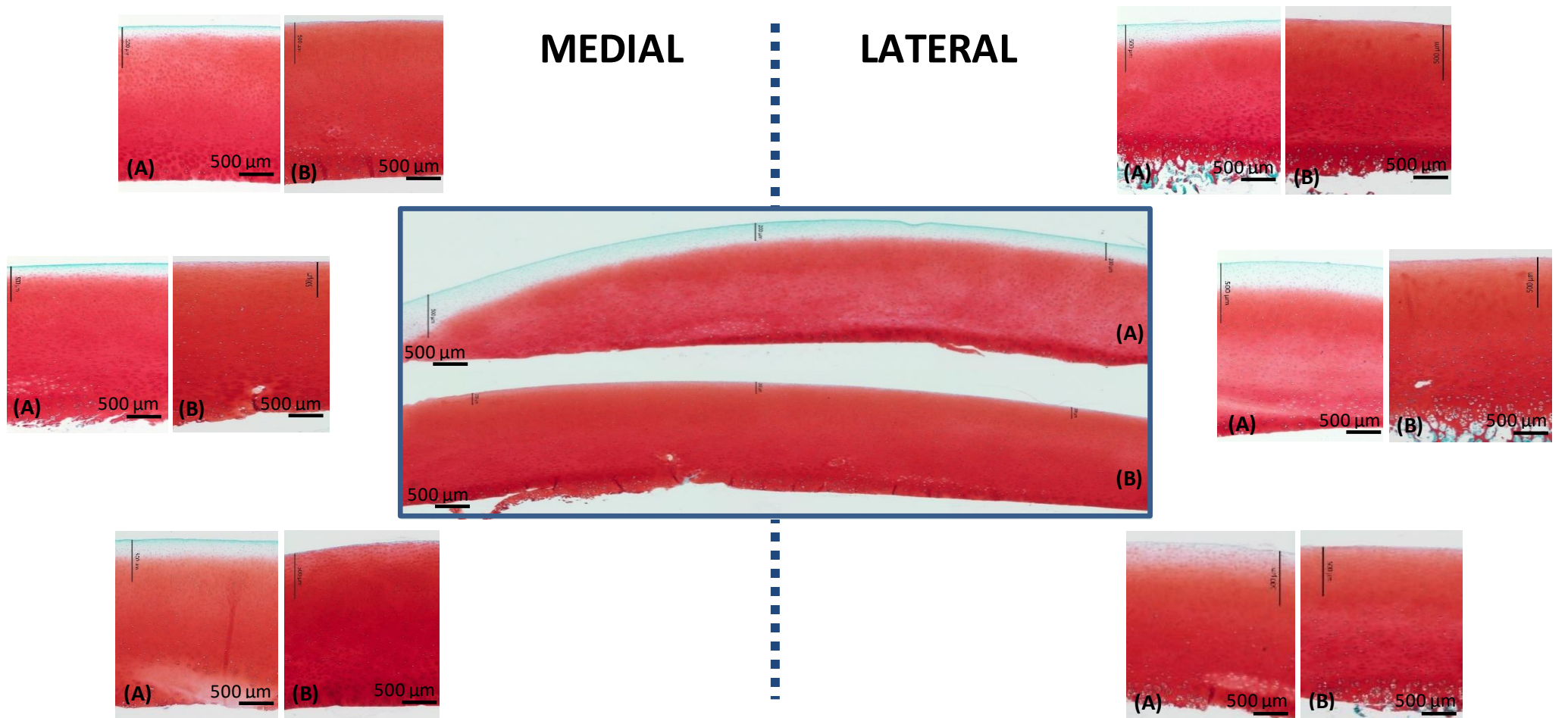


Figure 62: Safranin O stained sections of GAG depleted porcine condylar cartilage treated with an agarose gel containing CaseABC and antibiotic/aprotinin solution (model 1) and a porcine condylar cartilage treated with an agarose gel containing only antibiotic/aprotinin solution (control). (A) GAG depleted cartilage, (B) Control sample. Images to the left were medial condyles sectioned perpendicular to the cartilage surface and images to the right were lateral condyles sectioned perpendicular to the cartilage surface. The middle picture is representative images of perpendicular cross-sections of porcine cartilage plugs, that have been GAG depleted and one that has not: (A) GAG depleted, lateral porcine cartilage plug. (B) Control, medial porcine cartilage plug. Scale bars are drawn on in individual images so that the depth of GAG depletion could be quantified.

The data showed that the method used in model 1 of painting agarose gel containing antibiotic solution and CaseABC, onto the porcine condylar cartilage surface, reduced the average GAG content when compared to the control (without CaseABC) and native porcine condylar cartilage, by circa 40 %.

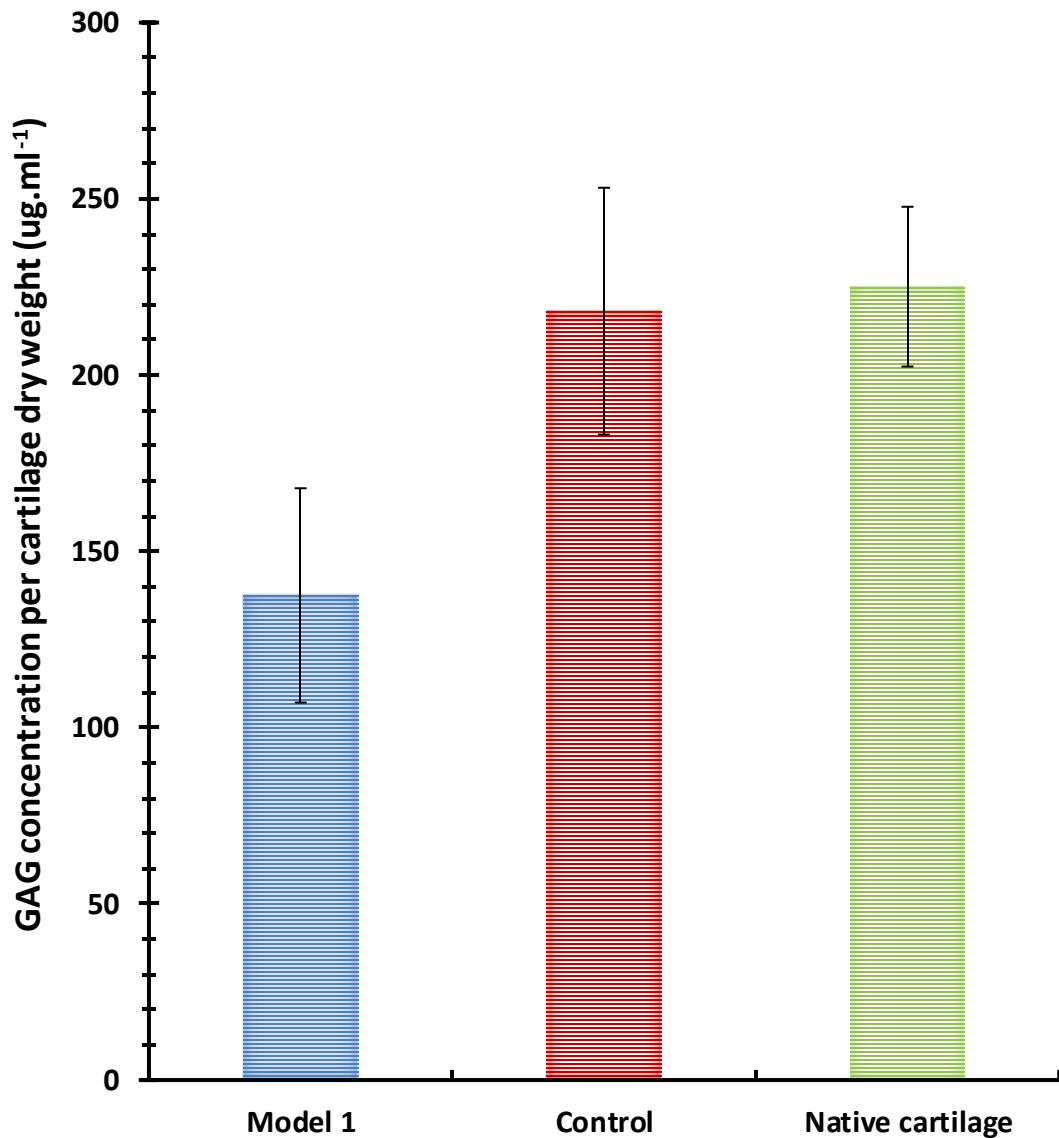


Figure 63: GAG content of cartilage from GAG depleted porcine condylar cartilage in model 1 compared to the control sample and untreated native porcine condylar cartilage. Model 1 consists of porcine condylar cartilage painted with CaseABC enzyme containing antibiotic/aprotinin in an agarose gel. The control porcine condylar cartilage was painted with buffer containing antibiotic/aprotinin in an agarose gel (without CaseABC). Data is expressed as the mean (n=6) \pm 95 % confidence limits and is the average of the medial and lateral condyles.

4.4.1.2 Model 2

Images of sections of porcine cartilage tissue subjected to injection of CaseABC containing antibiotic/ aprotinin solution and porcine cartilage tissue subjected to injection of antibiotic/ aprotinin solution (control), stained with Safranin O are presented in Figure 64A & B, respectively. Porcine cartilage tissue treated with both injection techniques showed that there was removal of GAG in both groups. It was observed that the sections of the cartilage that had been injected with the CaseABC enzyme tended to have a brighter Fast Green stain (blue stain) than the sections of the cartilage injected with just the antibiotic/ aprotinin solution. The GAG content was measured using the DMB assay.

The GAG concentration per cartilage dry weight of the porcine condylar cartilage injected with CaseABC containing antibiotic/ aprotinin solution, antibiotic/ aprotinin solution injected only and untreated native porcine condylar cartilage, are shown in Figure 65. The native porcine cartilage had the highest average GAG content at 225 ug.mg^{-1} . The average GAG content of the porcine condylar cartilage that had been injected with CaseABC (model 2 - 174 ug.mg^{-1}), was lower than the GAG content seen in the porcine condylar cartilage that had not been injected with CaseABC, (control - 201 ug.mg^{-1}). The data showed that the method used in model 2 of injecting an antibiotic solution containing CaseABC into porcine condylar cartilage, reduced the average GAG content when compared to the control (without CaseABC) and native porcine condylar cartilage, by circa 14 % and 23 %, respectively.

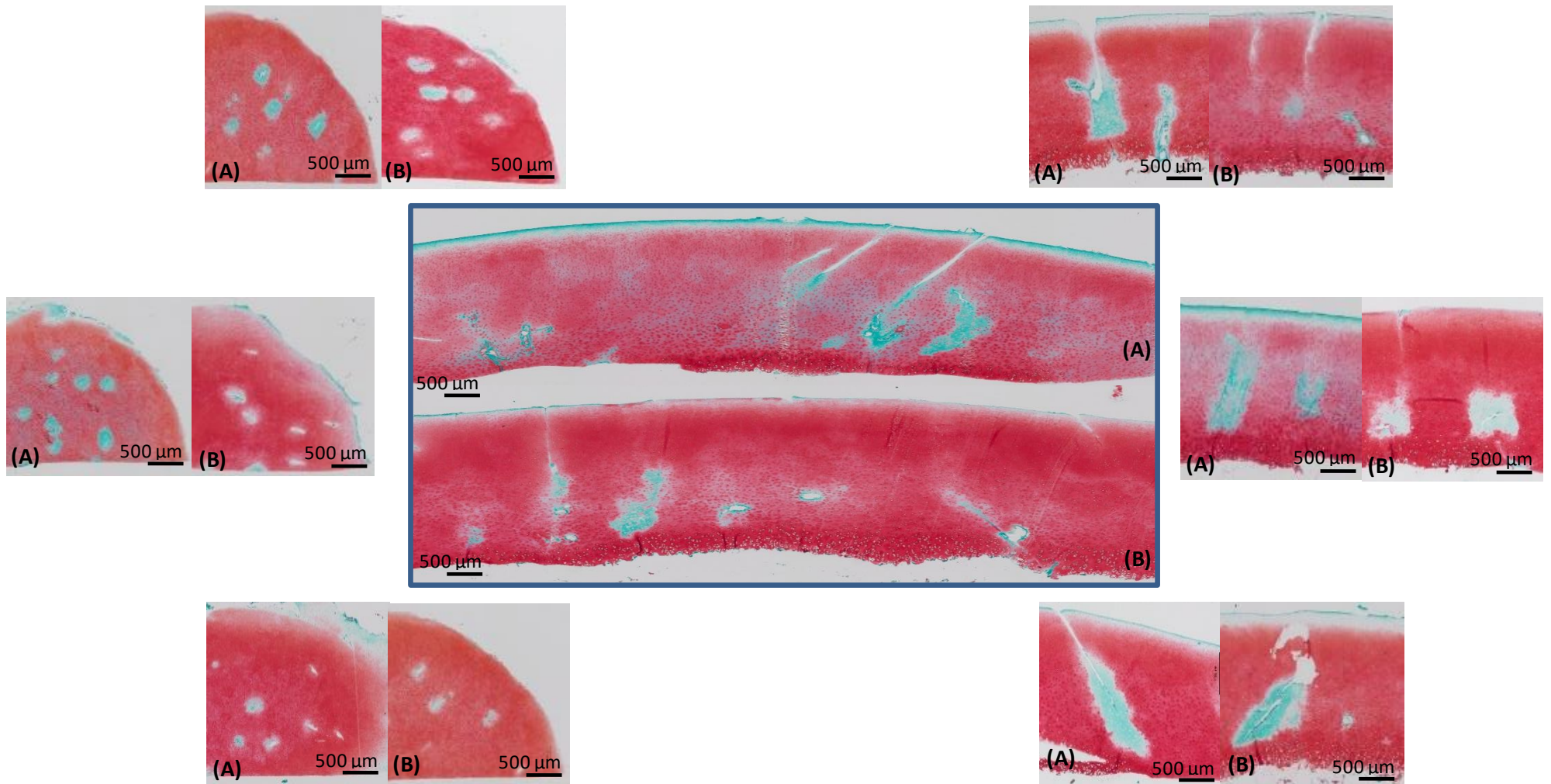


Figure 64: Safranin O stained sections of GAG depleted porcine condylar cartilage treated with injections of CaseABC containing antibiotic/aprotinin solution (model 2) and porcine condylar cartilage treated with injections of antibiotic/ aprotinin solution alone (control). (A) GAG depleted cartilage with CaseABC, (B) Control samples. Images to the left were lateral condyles sectioned parallel to the cartilage surface and images to the right were lateral condyles sectioned perpendicular to the cartilage surface. The middle picture is representative images of perpendicular cross-sections of porcine cartilage plugs that have been injected with CaseABC and the other with an antibiotic/aprotinin solution: (A) GAG depleted, medial porcine cartilage plug. (B) Control, medial porcine cartilage plug.

Scale bars are drawn on individual images so that the depth of GAG depletion could be quantified.

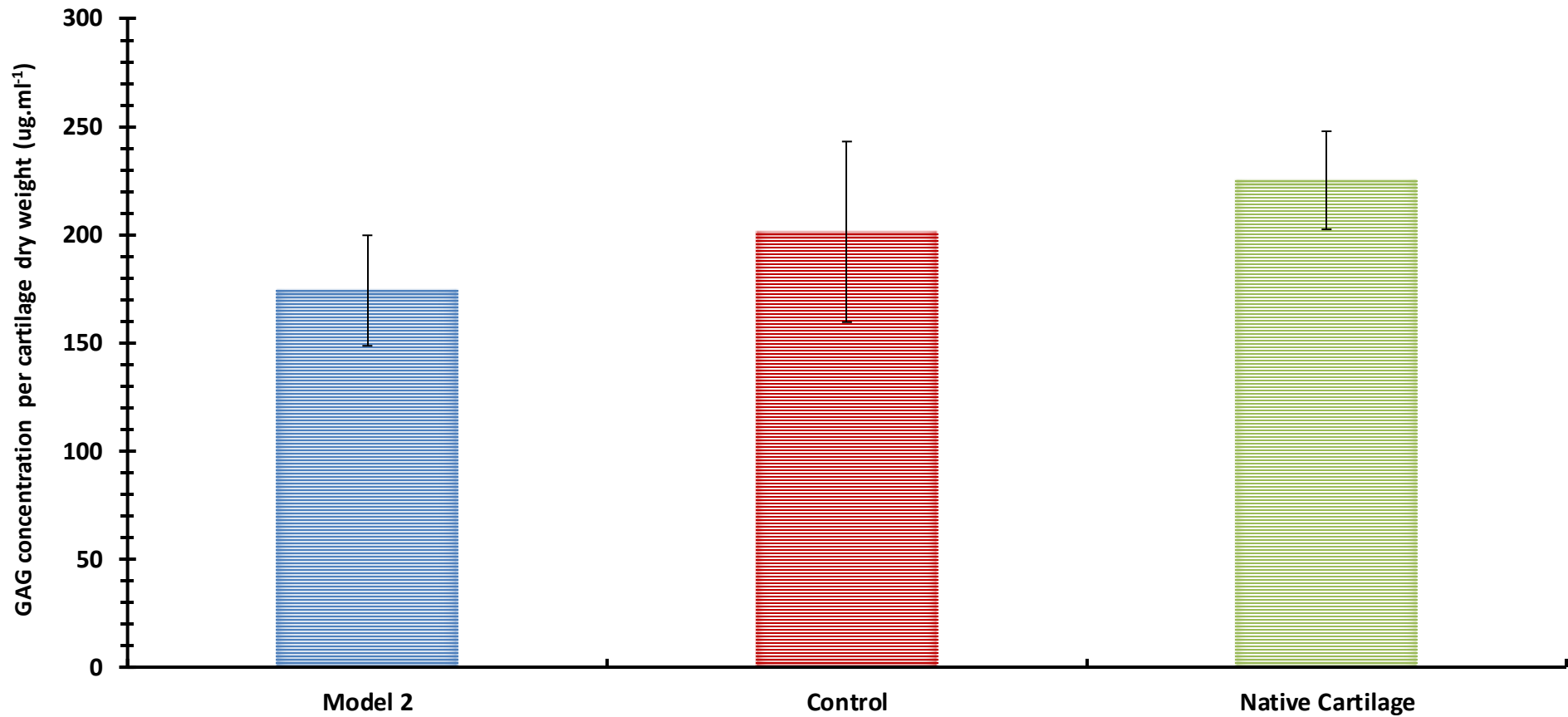


Figure 65: GAG content of cartilage from GAG depleted porcine condylar cartilage in models 2 compared to the control sample and untreated native porcine condylar cartilage. Model 2 consists of porcine condylar cartilage injected with CaseABC enzyme containing antibiotic/aprotinin solution. The control porcine condylar cartilage was injected with buffer containing antibiotic/aprotinin solution (without CaseABC). Data is expressed as the mean (n=6) \pm 95 % confidence limits and is the average of the medial and lateral condyles.

4.4.1.3 Model 3

Method Development

This model underwent some development during which the porcine femoral condyles were subject to various cycles of SDS and PBS washes, until the required removal of GAG was obtained. The methods applied during the development of the process are shown below:

Method 1): One 24 hour wash in SDS and two 24 hour washes in PBS containing aprotinin.

Method 2): Two 24 hour washes in SDS and two 24 hour washes in PBS containing aprotinin.

Method 3): Two 24 hour SDS washes and three 24 hour washes in PBS containing aprotinin.

Method 4) Two 24 hour SDS washes followed by two three hour washes in PBS containing aprotinin and ending with one 24 hour wash in PBS containing aprotinin.

Images of sections of porcine condylar cartilage, stained with Safranin O that has been subjected to method 1 and method 4 are presented in Figure 66 and Figure 67, respectively. Untreated, native porcine condylar cartilage was used as the control. Images of porcine condylar cartilage treated with method 1 showed that there was partial removal of GAGs, mostly in the top layer of cartilage. However, method 1 showed inconsistency in the amount of GAG that was removed. On the other hand, images of porcine condylar cartilage that had been treated with method 4 showed to have removed the majority of the GAGs throughout the depth of the cartilage and seemed to be consistent within the replicates. It was observed that the sections of the cartilage that had been subjected to the treatment in method 4, tended to have a brighter Fast Green stain (blue stain) than the sections of the cartilage that has been subjected to the treatment in method 1. The images of the native porcine condylar cartilage showed a consistent red stain throughout the depth of the cartilage, indicating that there had been no removal of GAGs.

The GAG content was measured using the DMB assay. The GAG concentration per cartilage dry weight of the porcine condylar cartilage subjected to treatment in methods 1-4 and untreated native porcine condylar cartilage, are shown in Figure 68. The average GAG content of the porcine condylar cartilage subjected to treatments in methods 1-4 was 58.6, 58.2, 57.4 and 56.1 $\mu\text{g}\cdot\text{mg}^{-1}$, respectively. This was lower than the average GAG content seen in the untreated native porcine cartilage control, 225.1 $\mu\text{g}\cdot\text{mg}^{-1}$. The data showed that the treatments used in methods 1 -4 reduced the GAG content of porcine condylar cartilage by circa 74 % on average, when compared to the untreated native porcine condylar cartilage (control).

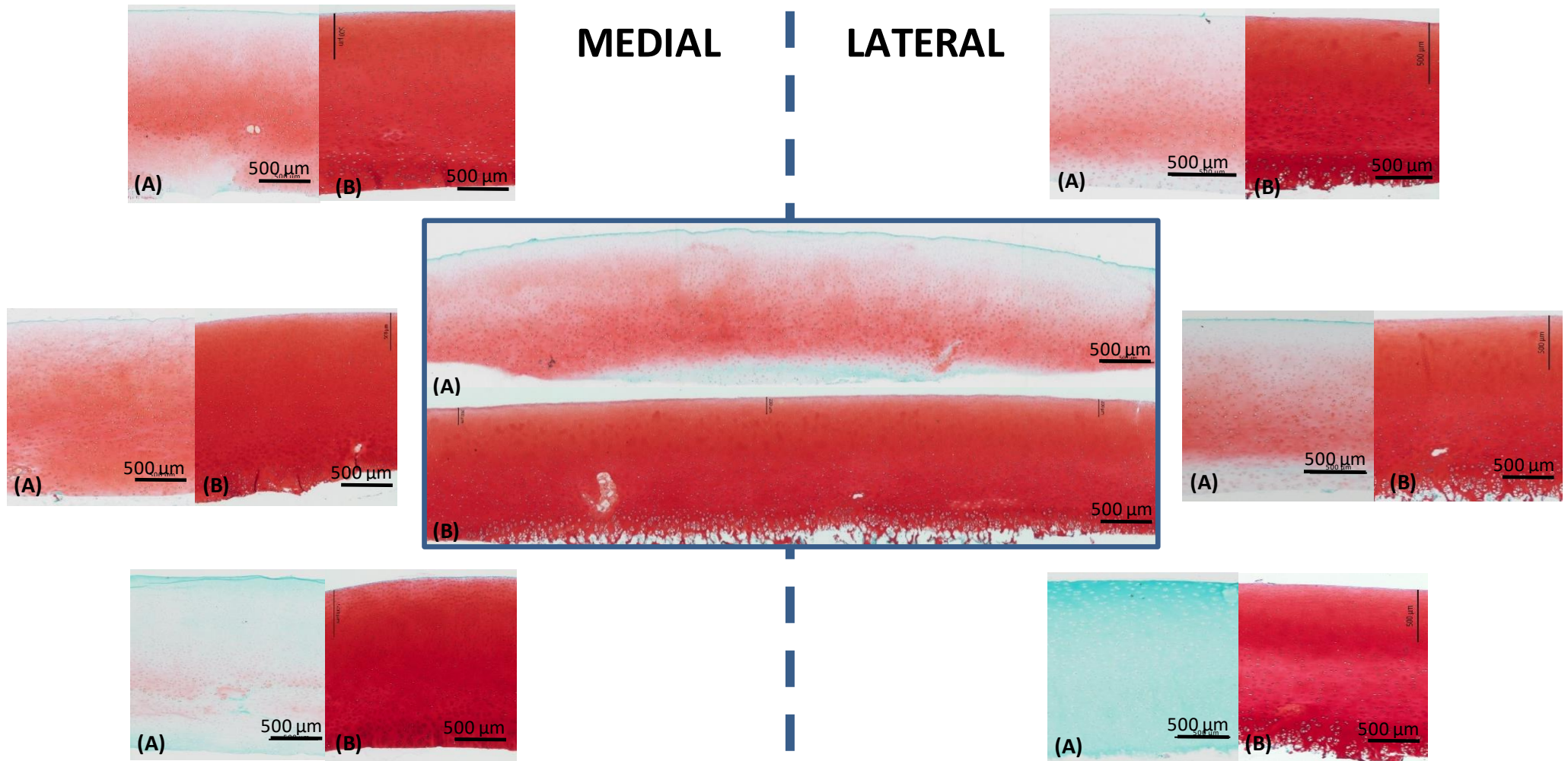


Figure 66: Safranin O stained sections of GAG depleted porcine condylar cartilage and untreated native porcine condylar cartilage control from model 3. (A) GAG depleted porcine condylar cartilage; model 3 – treatment method 1: treated with one 24 hour wash of 0.1 % SDS and two 24 hour washes of PBS+ aprotinin, (B) Untreated native porcine condylar cartilage (control). Images to the left were medial condyles sectioned perpendicular to the cartilage surface and images to the right were lateral condyles sectioned perpendicular to the cartilage surface. The middle picture is representative images of perpendicular cross-sections of porcine cartilage plugs, that have been GAG depleted and one that has not: (A) GAG depleted, lateral porcine cartilage plug. (B) Control, lateral porcine cartilage plug. Scale bars are drawn on individual images so that the depth of GAG depletion could be quantified.

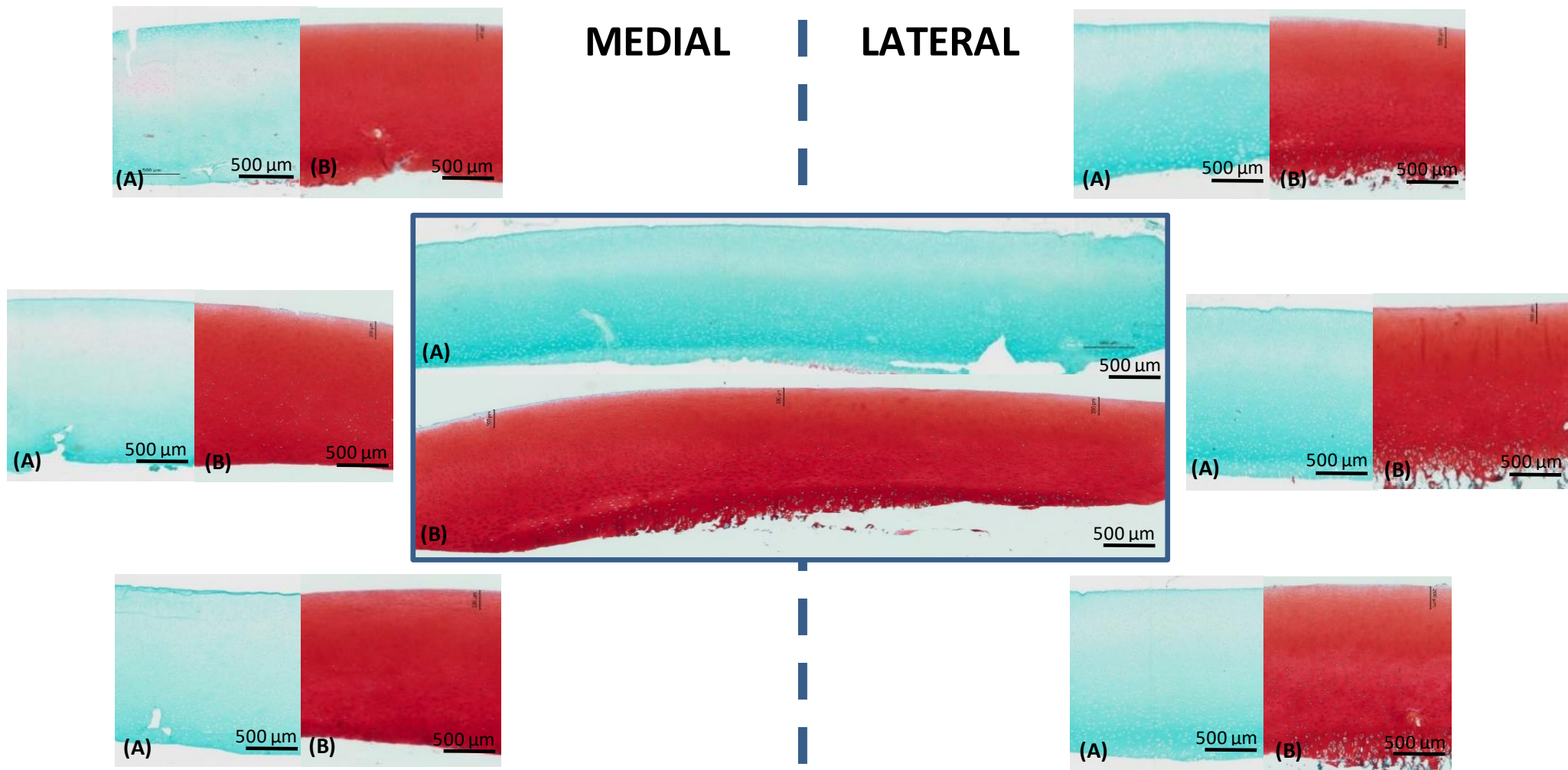


Figure 67: Safranin O stained sections of GAG depleted porcine condylar cartilage and untreated native porcine condylar cartilage control from model 3. (A) GAG depleted porcine condylar cartilage; model 3 – treatment method 4: treated with two 24 hour washes of 0.1 % SDS, followed by two three hour washes in PBS + aprotinin and ending with one 24 hour wash in PBS + aprotinin, (B) Untreated native porcine condylar cartilage (control). Images to the left were medial condyles sectioned perpendicular to the cartilage surface and images to the right were lateral condyles sectioned perpendicular to the cartilage surface. The middle picture is representative images of perpendicular cross-sections of porcine cartilage plugs, that have been GAG depleted and one that has not: (A) GAG depleted, lateral porcine cartilage plug. (B) Control, lateral porcine cartilage plug. Scale bars are drawn on individual images so that the depth of GAG depletion could be quantified.

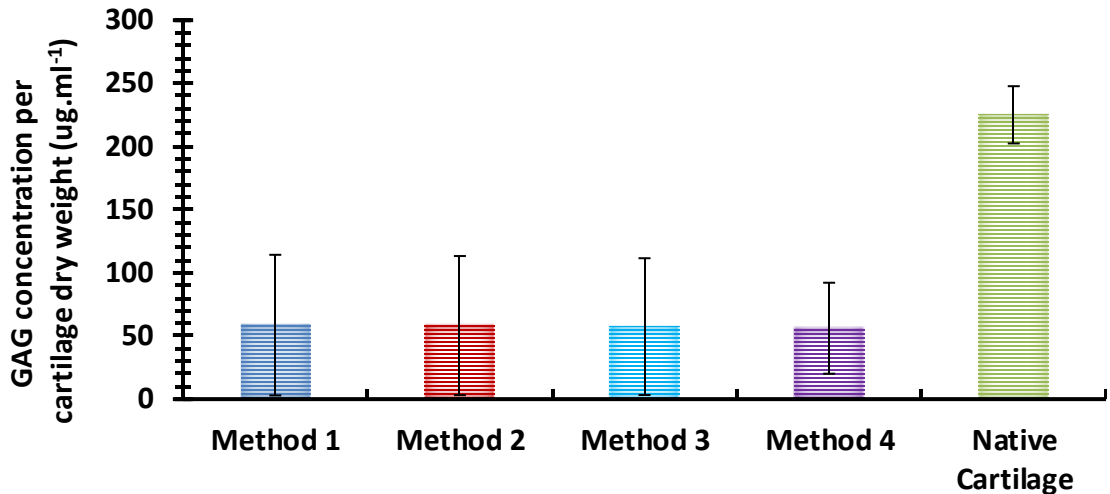


Figure 68: GAG content of cartilage from GAG depleted porcine cartilage in model 3. Samples tested consisted of porcine condylar cartilage washed using method 1, 2, 3 and 4, and untreated native porcine condylar cartilage as a control. Data is expressed as the mean (n=6) \pm 95 % confidence limits and is the average of the medial and lateral condyles.

It was hypothesised that residual SDS might affect the self-assembly of the peptides and peptide-GAG mixtures; and so its removal would be beneficial to the development of model 3. Therefore, a study was carried out to investigate SDS concentrations in the solution after each wash, in the four methods developed as described in section 4.3.6 and the results are presented in Figure 69.

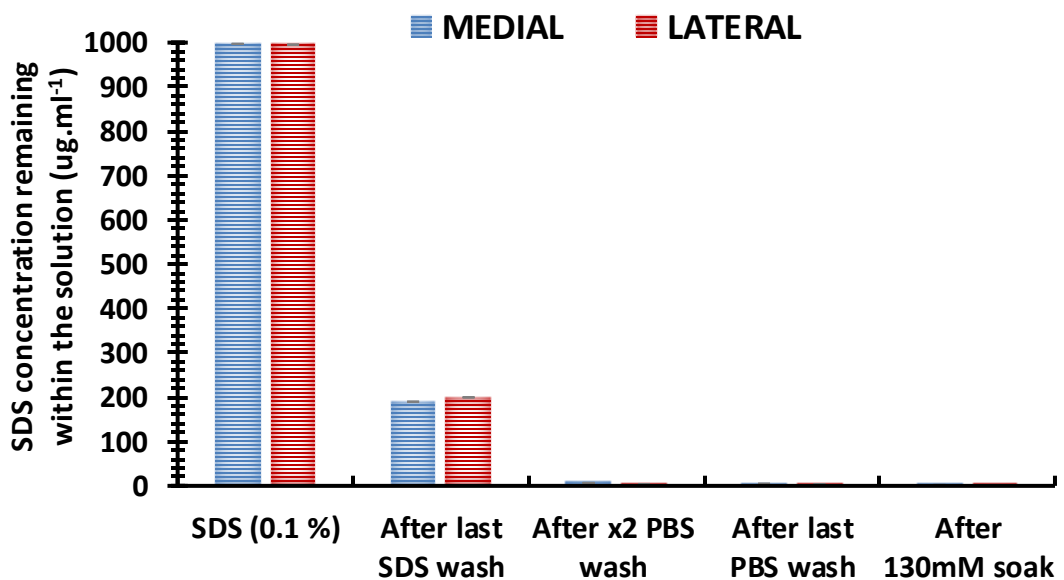


Figure 69: SDS concentration (ug.ml⁻¹) after given SDS and PBS washes in model 3, method 4. Readings were taken from the solutions at the end of: 1) the last SDS wash, 2) two three-hour PBS washes, 3) one 24 hour PBS wash and 4) 130 mM soak. Data is expressed as the mean (n=3) \pm 95 % confidence limits.

The data showed that the SDS concentration lowered each time a new solution was introduced into the wash cycles. After the last two 24-hour SDS washes, also applicable to

methods 2-4, the SDS concentration remaining within the solution was reduced by circa 80 %. After the last two 24-hour PBS washes, also applicable to method 3, the SDS concentration remaining within the solution had been further reduced by circa 99.3 %. After the final 130 mM Na⁺ salt solution soak the concentration of SDS remaining in the solution had been reduced to 99.8 %. The repetitive wash cycles in SDS and PBS used in this study, were an effective way of reducing the amount of residual SDS found within the cartilage tissue.

4.4.2 GAG quantification of native and GAG depleted porcine femoral cartilage

The GAG concentration ($\mu\text{g}\cdot\text{mg}^{-1}$ dry weight) of the untreated native cartilage samples was compared to the GAG concentration in the GAG depleted cartilage (model 1, model 2 and model 3 (method 4)) to determine which of the three models had significantly reduced GAG concentrations. The data is shown in Figure 70. The data was analysed by one-way ANOVA followed by post-hoc analysis (Tukey Kramer; $p < 0.05$) to determine differences between group means. This showed that the GAG concentrations in GAG depleted cartilage produced in models 1, 2 and 3 had significantly lower GAG concentration when compared to the untreated native cartilage control. The GAG depleted cartilage produced using model 3 had significantly reduced GAG concentration compared to the GAG depleted cartilage produced using model 1 and model 2 but there was no significant difference between the GAG concentrations in GAG depleted cartilage produced using models 1 and 2.

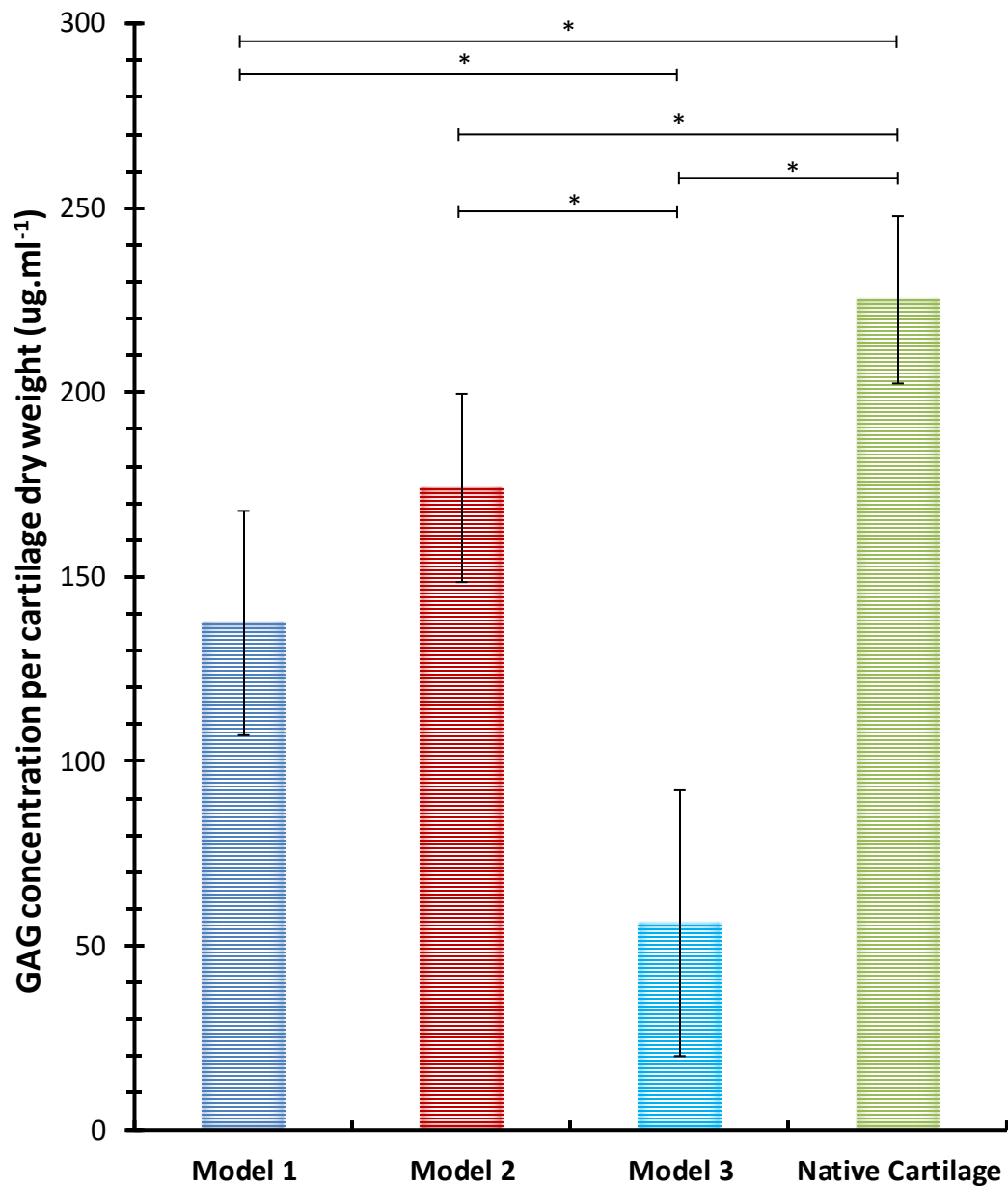


Figure 70: GAG content of cartilage from GAG depleted porcine cartilage in Models 1 - 3 vs. native porcine cartilage. Model 1 consisted of porcine condylar cartilage painted with CaseABC containing antibiotic in an agarose gel. Model 2 consisted of porcine condylar cartilage injected with CaseABC containing antibiotic solution and model 3 consisted of porcine condylar cartilage treated with two 24 hour washes of SDS containing aprotinin, two 3 hour PBS washes containing aprotinin, one 24 hour PBS wash containing aprotinin and a 24-hour soak in 130 mM Na⁺ salt solution. Data is expressed as the mean (n=6) ± 95 % confidence limits. Data was analysed by one-way analysis of variance followed by a Tukey Kramer post-hoc analysis to determine differences between group means. *indicates p<0.05.

4.5 Discussion

The aims of the studies described in this chapter were to investigate methods for depleting the GAG content of porcine femoral condylar cartilage; in order to create a model for the testing of SAP: GAG mixtures. The studies investigated the biological and biochemical properties of three GAG depleted cartilage models compared to native porcine cartilage. It was clear that after treatment model 3 - method 4 produced a severe GAG depleted cartilage model, model 2 produced a moderate GAG depleted cartilage model and model 1 produced a mild GAG depleted cartilage model.

To assess the amount of GAG removed, the GAG content of each cartilage model was assessed qualitatively with Safranin O staining of tissue sections and quantitatively using a colorimetric assay with DMB dye. Qualitatively, all models showed characteristic zonal distribution of proteoglycans. However, in model 1, the technique of painting the CaseABC enzyme onto the cartilage surface, to deplete the GAGs, only removed the GAGs in the top superficial tangential zone (~163 μm). It is thought that the CaseABC enzyme acted through diffusion removing only the GAGs in the surface layer. A study by Leddy and Guilak (2003) showed that zonal differences in diffusion coefficients of articular cartilage are due to the molecular interaction with the ECM molecules, which act as barriers to diffusion. Although, the study by Leddy and Guilak (2003), stated that proteoglycans do slow the diffusion of larger molecules (>40 kDa), the cartilage's relatively low diffusion coefficient in the surface zone suggested that other matrix macro molecules such as collagen, may also hinder a molecules motion into deeper zones of cartilage (Leddy and Guilak, 2003). Our findings corroborate with the latter study as CaseABC has a known molecular weight of 120 kDa, which explains why only the top layer (surface zone) of cartilage was affected by the enzyme. This theory could also be applied to the effects seen in model 2 whereby the injected enzyme appeared to have only diffused locally around the areas into which it had been injected. It is likely that diffusion of the CaseABC, was hindered by the molecular interactions with the surrounding proteoglycan and collagen network.

Initially the aim was to create models with varying levels of GAG depletion, so that the SAPs and SAP: GAG mixtures could be tested at "various stages of OA". After optimisation, model 1 achieved a partial/mild depletion of GAGs in the surface layer of cartilage; which was somewhat inconsistent. Nevertheless, this approach provided a model that could be comparable to cartilage at the very early stages of OA and hence could be a good model to test the SAPs and SAP: GAG mixtures in future studies. Model 2, although it did not create cartilage with a significantly lower GAG content than model 1, it was attributed a moderate

model of GAG depletion; since the GAGs were clearly depleted in areas of the mid-zone of the cartilage, as indicated by the histological analysis. The levels of GAG depletion in model 3 (circa 90 % loss of GAGs) throughout the whole depth of the cartilage were severe. Therefore, the methodology used for model 3 was considered the appropriate approach for creating a reproducible cartilage depleted model, for the future testing of the SAP: GAG mixtures. It was hypothesised that if the majority of the GAGs were removed, the biomechanical properties of the cartilage would be significantly affected and therefore when the SAPs or SAP: GAG mixtures were injected into this model, changes to the biomechanical properties would be measurable.

Removal of residual SDS after treatment in model 3, was a very important factor in the development of the model; as it was thought that any residual SDS could hinder the self-assembly of the SAP: GAG mixtures in future testing. Hence, it was important to optimise the washing process following SDS treatment in model 3. An SDS assay was performed on the solutions used to wash the cartilage samples. The majority of the previous studies using stains-all to measure SDS, reported measured absorbance of SDS at 510 nm (Campbell et al., 1983; Arand et al., 1992; Rusconi et al., 2001). However, Wilshaw (2006) found that measuring the absorbance at 447 nm gave better correlation between the absorbance and the concentration of SDS, when producing the standard curve. After the last SDS wash, the concentration of SDS in solution was reduced by ~80 % (193.8 ug.ml^{-1}). This would have been applicable to methods 2-4. In method 4, after the two 3 hour PBS washes and a 24-hour PBS wash (which would have been comparable to the three PBS washes in method 3); the amount (ug.ml^{-1}) of SDS in the wash solution was reduced by ~99 %. A further 24 hour 130 mM Na^+ salt solution soak, reduced the amount (ug.ml^{-1}) of SDS in solution by 99.8 %, indicating that by the end of all the washes there was only 0.2 % (2.1 ug.ml^{-1}) of SDS remaining in the tissue. The additional 130 mM Na^+ salt solution soak in method 4 was to ensure that any essential ions, that may have been lost over the continuous washes in SDS and PBS, were replenished. Therefore, the GAG depleted cartilage would have a more physiologically relevant environment, as changes in the ionic composition of the cartilage could lead to changes in the self-assembly of the SAP and SAP: GAG mixtures in future studies.

The use of pig legs sourced from the local abattoirs meant that all tissue used in this whole study came from food chain sources. The all parts of the porcine legs were used, from ligaments to tiny blood vessels, as well as whole joints such as the knee and ankle. This approach to our research tried to encompass the 3R's approach. Each experiment was carefully thought out and all the tissue was used so that none of it went to waste. An example

of this was the cartilage plugs taken for histology, whereby from each plug two histological evaluations could be carried out reducing the amount of tissue required, which compares the three aspects of the 3R principles (replacement, reduction and refinement).

4.6 Conclusion

Model 1 (painting of the cartilage surface with CaseABC), showed a mean reduction in GAGs of 39 %, when compared to native porcine cartilage; however, the GAGs were only removed from the cartilage surface. Nevertheless, a significant reduction in the GAG concentration was observed between the test and control cartilage. Model 2 (injection of CaseABC into the cartilage), showed a mean reduction in GAGs of 23 % compared to native porcine cartilage; however, GAGs were only depleted from the areas in which the CaseABC had been injected. Again, there was a significant reduction in GAG concentration between the test and control group. Model 3 (washing in SDS and PBS), showed a 75% reduction in GAG concentration compared to native porcine cartilage, without any histological evidence of damage to the cartilage.

Based on the findings in this study, model 3 was identified as the most suitable model to take forwards for testing whether the SAPs and SAP: GAG mixtures could restore the biomechanical properties of GAG depleted porcine condylar cartilage. The next stage of the study, was to develop an appropriate methodology for measuring the biomechanical properties of the native and GAG depleted porcine condylar cartilage.

Chapter 5 Development of methods for the determination of the biomechanical properties of native and GAG depleted cartilage.

5.1 Introduction

In Chapter 4, different methods were investigated for producing GAG depleted models of porcine femoral cartilage. It was found that treatment with SDS was the most appropriate method for producing porcine femoral cartilage which was severely (circa 75%) depleted of GAGs. The next stage in the investigations was to determine the effects of GAG removal using SDS on the biomechanical properties of the cartilage.

In order to do this, it was necessary to develop a suitable method for the indentation testing of the cartilage which would enable differences in the mechanical properties between the native and GAG depleted cartilage to be determined. Indentation tests have been used as an analysis tool to determine the displacement of a material such as cartilage to investigate its biomechanical properties, specifically creep behaviour under a given load. Indentation tests are straight forward to perform experimentally with minimal sample preparation. This has made indentation testing a popular technique for the determination of the biomechanical properties of cartilage (Kempson et al., 1971; Mak et al., 1987; Mow et al., 1989; Swann and Seedhom, 1989; Forster and Fisher, 1996; Pickard et al., 1998; Jin et al., 2000; Rieppo et al., 2003; Boschetti et al., 2004; Lu et al., 2004) (Stolz et al., 2004; Kleemann et al., 2005; Katta et al., 2008; Hall et al., 2009; Abdelgaied et al., 2015). A constant compressive load applied to the cartilage surface via an indenter, results in an initial elastic deformation followed by a creep deformation, due to the exudation of the interstitial fluid. Initially this exudation occurs rapidly, which leads to high rates of deformation, but this decreases gradually as the flow of interstitial fluid ceases. Once equilibrium is reached there is no more fluid flow, and the applied load is borne mostly by the solid collagen-proteoglycan matrix, with some being taken by the interstitial fluid (Mow et al., 1980). As the rate of creep is governed by fluid exudation, permeability of the cartilage tissue can be determined. The modulus of the solid matrix of cartilage at equilibrium, can also be measured when there is no longer any fluid flow, which occurs at the final equilibrium deformation. This type of displacement analysis was therefore chosen for this study because GAGs are known to increase the stiffness of cartilage and hence resistance to deformation when under load. It was hypothesised that removal of the GAGs from porcine condylar cartilage would reduce the compressive stiffness of the cartilage tissue, resulting in increased displacement, which could be evaluated using indentation testing.

Linear biphasic poroelastic finite element models have been developed to simulate creep indentation tests. These models have been used to determine the biphasic properties of cartilage by sequentially tuning these properties until the model outputs match those of the experimental outputs, for example the model used by Abdelgaied et al. (Abdelgaied et al., 2015). This finite element model was derived from supplementary mathematical models (Mak et al., 1987; Mow et al., 1989), which were developed so that the permeability and equilibrium elastic modulus of cartilage tissues could be calculated. Therefore, this finite element model was implemented in this study to determine the equilibrium elastic modulus and permeability of native and GAG depleted porcine condylar cartilages.

Previous studies have used a range of contact stresses ranging from as low as 0.01 MPa to as high as 0.28 MPa (Katta et al., 2007; Abdelgaied et al., 2015) as nominal values to study the effect of load on the biomechanical properties of cartilage. In this study, it was decided to adopt a systematic approach of testing different loads to determine the load that, when applied during indentation testing, would result in a significant difference between the deformation of the native and GAG depleted cartilages and also reveal differences between the equilibrium elastic modulus and permeability. This was important because it was the intention to treat the GAG depleted cartilage with SAP: GAGs and investigate the capacity of the SAP: GAGs to restore the biomechanical properties to values that were similar to native cartilage. The limitations of the experimental indentation test equipment used in this study, meant that the highest load that could be applied to the rig was 0.51 N. This load generated a contact stress of 0.1 MPa, using a 2.5 mm diameter stainless steel pin; which was only half of that used in previous studies. This was primarily due to the space available to insert the weights and the weights which were available, which would fit onto the top of the indenter. With the weights available, contact stresses of 0.02, 0.06, 0.1 MPa were achieved in this study; corresponding to the three loads (0.11, 0.31, & 0.51 N). Therefore, based on the previous studies carried out in the Institute of Medical and Biological Engineering at the University of Leeds and the limitations to the experimental set-up and equipment; a contact stress of 0.1 MPa was chosen initially as a starting point, to investigate the effect of load variation on native and GAG depleted porcine condylar cartilage. Although, the contact stress levels were at the lower end of the *in vivo* joint loading spectrum (Brown and Shaw, 1983; Mow and Ateshian, 1997; Mow and Hayes, 1997; Rolfe et al., 2006), the low stress levels ensured that the tissue deformation remained small with equilibrium strain magnitudes <15 %. Deformation should be kept to minimum as the model uses a linear biphasic model, which assumes permeability is constant with deformation, but this assumption is only valid for

small deformation. Furthermore, the computational simulation cannot converge for high levels of deformation as some elements will end up with zero volume due to the high deformation, therefore giving us an error message in the simulation model.

5.2 Aims and objectives

The aim of this chapter was to investigate the effect of load variation during indentation testing of native porcine condylar cartilage and porcine condylar cartilage in which the GAGs had been depleted using SDS; in order to identify a suitable load for detection of a significant difference in the deformation, equilibrium elastic modulus and permeability between the native and GAG depleted porcine condylar cartilages.

5.2.1 Objectives

- 1) To systematically test three different loads: low (0.11 N), medium (0.31 N) and high (0.51 N) during creep indentation testing of native and GAG depleted porcine condylar cartilage to evaluate the deformation of the cartilages under the specified loads over 60 min.
- 2) To determine the thickness of the native and GAG depleted porcine condylar cartilage using a needle indentation method.
- 3) To use finite element analysis to derive the equilibrium elastic modulus and permeability of the native and GAG depleted porcine condylar cartilages from the deformation under load and cartilage thickness measurement data under three different loads.

5.3 Experimental methods

5.3.1 Acquisition of porcine femoral condyles

Porcine femoral condyles were dissected and stored as described in Chapter 2; Section 2.2.2.2 to 2.2.2.4.

5.3.2 GAG depletion of porcine femoral condylar cartilage

GAG depleted porcine condylar cartilages were produced using treatment with SDS (method 4) following the procedure outlined in Chapter 4; Section 4.3.3.

5.3.3 Biomechanical characterisation of porcine femoral cartilage

5.3.3.1 Indentation testing - sample and equipment preparation

Native and GAG depleted samples of porcine femoral condyles were first fixed in PMMA as outlined in Chapter 2; Section 2.2.6.1. The deformation over time of the native and GAG depleted cartilages were determined using indentation test methods as described in Chapter

2; Section 2.2.6.2. Three porcine condyles (medial and lateral) were used for each test group. Indentation testing was carried out under three different loads as described below.

5.3.3.1.1 Low load - 0.11 N

The samples were mounted onto the indentation rig as outlined in Chapter 2; Section 2.2.6.1. The weight of the shaft (11.69 g) was the only load (0.11 N) acting on the specimens. The samples were allowed to equilibrate in PBS for 10 min and the indentation tip (2.5 mm flat indenter) was located on the flattest surface of the femoral condyle. The lock holding the indenter tip was released and the cartilage was indented with a load of 0.11 N over 1 h as described in Chapter 2; Section 2.2.6.2.

5.3.3.1.2 Medium load - 0.31 N

An extra weight of 20.2 g (two small discs of 10.1 g) was added to the top of the indenter shaft giving a total weight of 31.89 g. The total load applied to the porcine femoral condyle specimens equated to 0.31 N. Tests were carried out as described in Chapter 2; Section 2.2.6.2.

5.3.3.1.3 High load - 0.51 N

An extra weight of 40.4 g (two small discs of 10.1 g and one 20.2 g disc) was added to the top of the indenter shaft, giving a total weight of 52.09 g. The total load applied to the porcine femoral condyle specimens equated to 0.51 N. Tests were carried out as described in Chapter 2; Section 2.2.6.2.

5.3.3.2 Cartilage thickness measurements

Cartilage thickness of the native and GAG depleted cartilage samples was measured using an Instron material testing machine and measurements were always taken after indentation, as outlined in Chapter 2; Section 2.2.6.4. Samples were allowed to recover in a sealed Tupperware box moistened with PBS tissue, which was kept at 4°C overnight.

5.3.3.3 Finite element method for derivation of biomaterial properties of porcine condylar cartilage.

The deformation data obtained from the indentation testing of the GAG depleted and native porcine condylar cartilage over time with varying loads, together with the cartilage thickness data, were used to derive the equilibrium elastic modulus and permeability of the cartilages, as described in Chapter 2; Section 2.2.6.5.

5.4 Results

5.4.1 Cartilage thickness measurements

For each cartilage group (GAG depleted and native) indented with different loads, the cartilage thickness was measured for both medial and lateral condyles. Cartilage thickness data for low, medium and high load experiments are presented in Figure 71, Figure 72 and Figure 73, respectively. On the whole, no differences were observed in the thickness of the cartilage from the medial condyles of the native and GAG depleted samples within each load experiment. Similar trends were observed for the thickness of the cartilage from the lateral condyles.

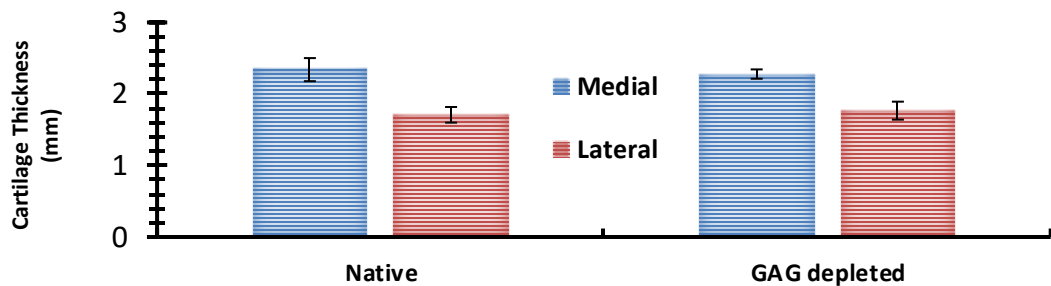


Figure 71: Low Load (0.11 N) - Cartilage thickness measurement for native and GAG depleted cartilage (n=5). Samples were measured six times in the area of interest after indentation. Data is expressed as the mean (n=5) \pm 95 % confidence limits.

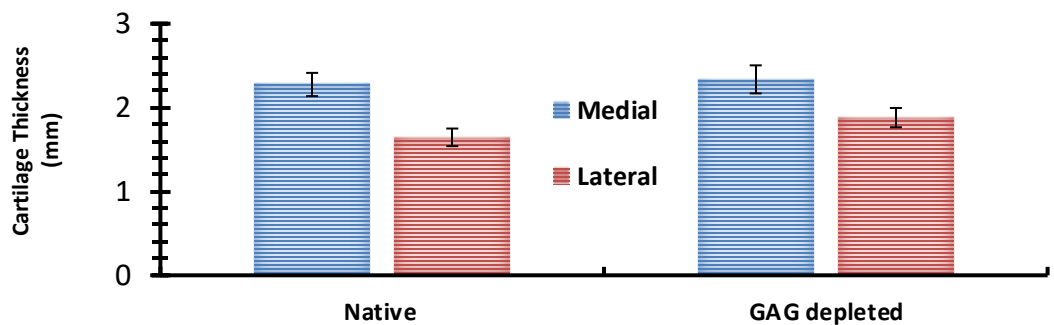


Figure 72: Medium Load (0.31 N) - Cartilage thickness measurement for native and GAG depleted cartilage (n=6). Samples were measured six times in the area of interest after indentation. Data is expressed as the mean (n=6) \pm 95 % confidence limits.

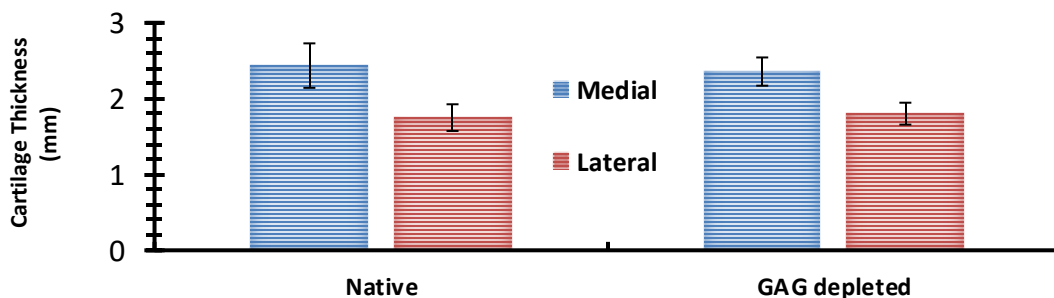


Figure 73: High Load (0.51 N) - Cartilage thickness measurement for native and GAG depleted cartilage (n=3). Samples were measured six times in the area of interest after indentation. Data is expressed as the mean (n=3) \pm 95 % confidence limits.

5.4.2 Percentage deformation

5.4.2.1 Low load – 0.11 N

Deformation properties of the GAG depleted and native cartilages (medial and lateral porcine condyles) under a load of 0.11 N are shown in Figure 74 and Figure 75. Deformation under load over a period of 1 hour is shown in Figure 74 and the final percentage deformation at 1 hour is shown in Figure 75, for both medial and lateral condyles.

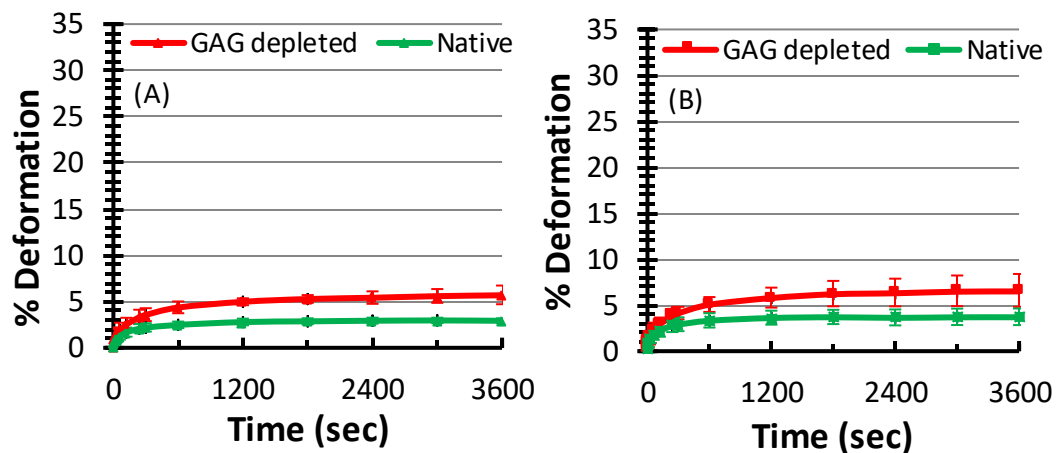


Figure 74: Percentage deformation of native and GAG depleted cartilage over the duration of 1 hour with a load of 0.11 N: (A) Medial condyle (B) Lateral condyle. Data was subject to arcsine transformation prior to calculation of the mean and 95 % confidence limits. Data is expressed as the back transformed mean (n=5) \pm 95 % confidence limits.

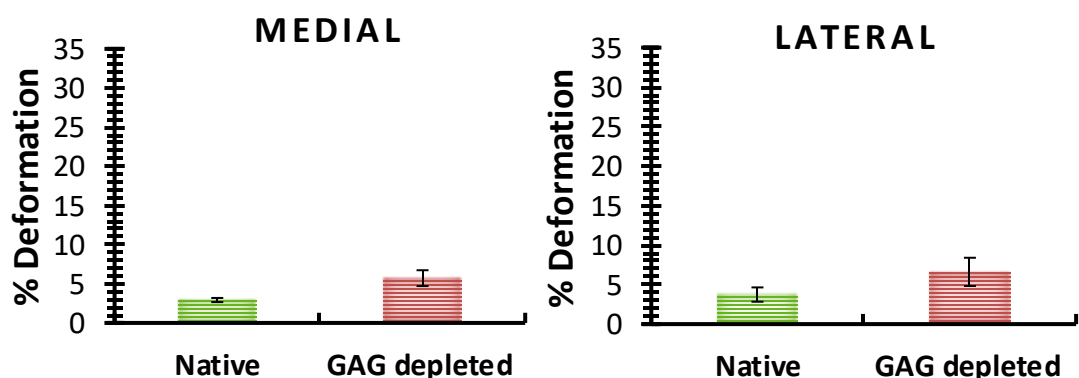


Figure 75: Final percentage deformation of native and GAG depleted cartilage at 1 hour with a load of 0.11 N. Data was subject to arcsine transformation prior to calculation of the mean and 95 % confidence limits. Data is expressed as the back transformed mean (n=5) \pm 95 % confidence limits.

The deformation curves over the duration of 1 hour showed that the GAG depleted medial and lateral condylar cartilage deformed more than the native condylar cartilage. The rate of initial deformation (0-600 seconds) for the native medial and lateral condylar cartilage was slow and steady and reached equilibrium after approximately 1200 seconds. However, the rate of initial deformation (0-600 seconds) for the GAG depleted medial and lateral condylar

cartilage was slightly quicker and reached equilibrium after approximately 1800 seconds. The equilibrium deformation at 1 hour for the native and GAG depleted medial condylar cartilage was 2.9 % and 5.7 %, respectively and for the native and GAG depleted lateral condylar cartilage it was 3.7 % and 6.5 %, respectively. None of the cartilages tested exceeded 15 % deformation.

In order to compare the percentage deformation of the native and GAG depleted cartilage at one hour, the data for the medial and lateral condyles tested at a load of 0.11 N was arcsin transformed. The trend seen in the data indicated that the percentage deformation of the GAG depleted cartilage was greater than the percentage deformation of the native cartilage for both the medial and lateral condyles.

5.4.2.2 Medium load – 0.31 N

Deformation properties of the native and GAG depleted cartilages under a load of 0.31 N; from both medial and lateral porcine condyles are shown in Figure 76 and Figure 77. Deformation under load over a period of 1 hour is shown in Figure 76 and final percentage deformation is shown in Figure 77, for both medial and lateral condyles.

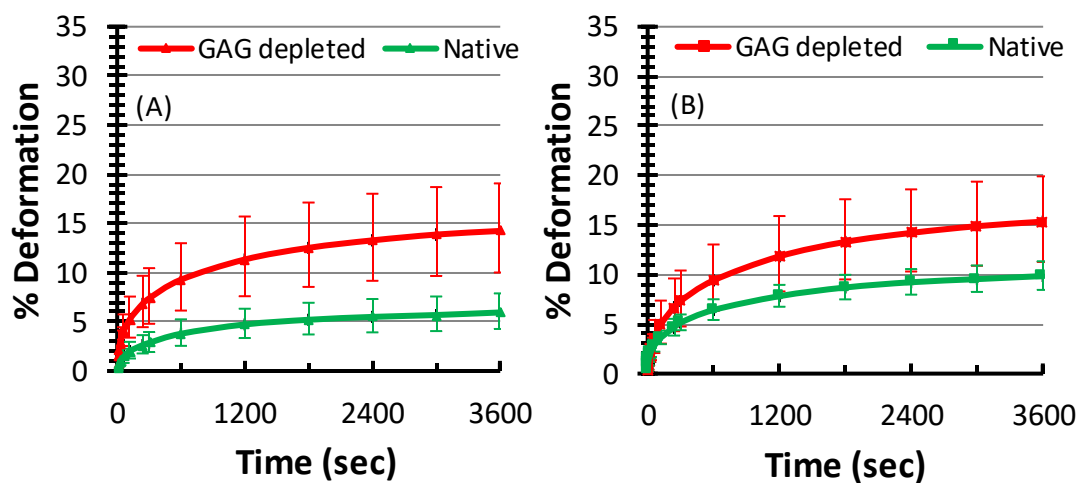


Figure 76: Percentage deformation of native and GAG depleted cartilage over the duration of 1 hour with a load of 0.31 N: (A) Medial condyle (B) Lateral condyle. Data was subject to arcsine transformation prior to calculation of the mean and 95 % confidence limits. Data is expressed as the back transformed mean (n=6) ± 95 % confidence limits.

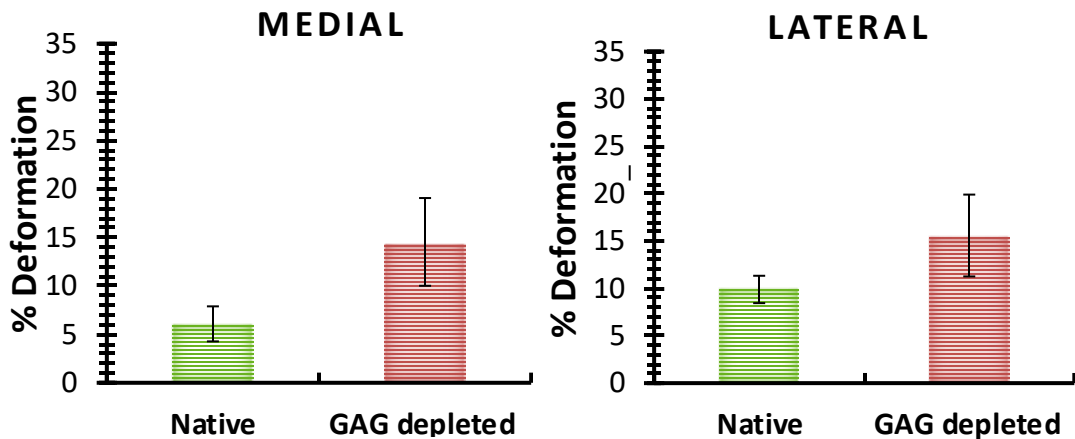


Figure 77: Final percentage deformation of native and GAG depleted cartilage at 1 hour with a load of 0.31 N. Data was subject to arcsine transformation prior to calculation of the mean and 95 % confidence limits. Data is expressed as the back transformed mean (n=6) \pm 95 % confidence limits.

When tested using a load of 0.31 N, the deformation curves over the duration of 1 hour showed that the GAG depleted condylar cartilage deformed more than the native condylar cartilage in both medial and lateral condyles. The rate of initial deformation (0-600 seconds) for the native medial condylar cartilage was steady and reached equilibrium after approximately 1800 seconds. However, the rate of initial deformation (0-600 seconds) for the native lateral condylar cartilage was slightly quicker and reached equilibrium after approximately 2400 seconds. The rate of initial deformation (0-600 seconds) for the GAG depleted medial and lateral condylar cartilage was quicker than in the native condylar cartilage. The equilibrium deformation at 1 hour for the native and GAG depleted medial condylar cartilage was 6 % and 14.2 %, respectively and for the native and GAG depleted lateral condylar cartilage it was 9.8 % and 15.3 %, respectively.

In order to compare the percentage deformation of the native and GAG depleted cartilage at one hour, the data for the medial and lateral condyles tested at a load of 0.31 N was arc sin transformed. The trend seen in the data indicated that the percentage deformation of the GAG depleted cartilage was greater than the percentage deformation of the native cartilage for both the medial and lateral condyles.

5.4.2.3 High load – 0.51 N

Deformation properties of the native and GAG depleted cartilages under a load of 0.51 N; from both medial and lateral porcine condyles are shown in Figure 78 and Figure 79. Deformation under load over a period of 1 hour is shown in Figure 78 and final percentage deformation is shown in Figure 79, for both medial and lateral condyles.

The deformation curves over the duration of 1 hour showed that the GAG depleted lateral condylar cartilage deformed more than the native lateral condylar cartilage, but this was not the case for the medial condyles. The rate of initial deformation (0-600 seconds) for the native and GAG depleted medial condylar cartilages was very similar and reached equilibrium after approximately 2400 seconds. However, the rate of initial deformation (0-600 seconds) for the native lateral condylar cartilage was slightly quicker than its medial counterpart. However, the rate of initial deformation (0-600 seconds) for the GAG depleted lateral condylar cartilage was the quickest. The equilibrium deformation at 1 hour for the native and GAG depleted medial condylar cartilage was 13.4 % and 13.5 %, respectively and for the native and GAG depleted lateral condylar cartilage it was 16.8 % and 21.1 %, respectively.

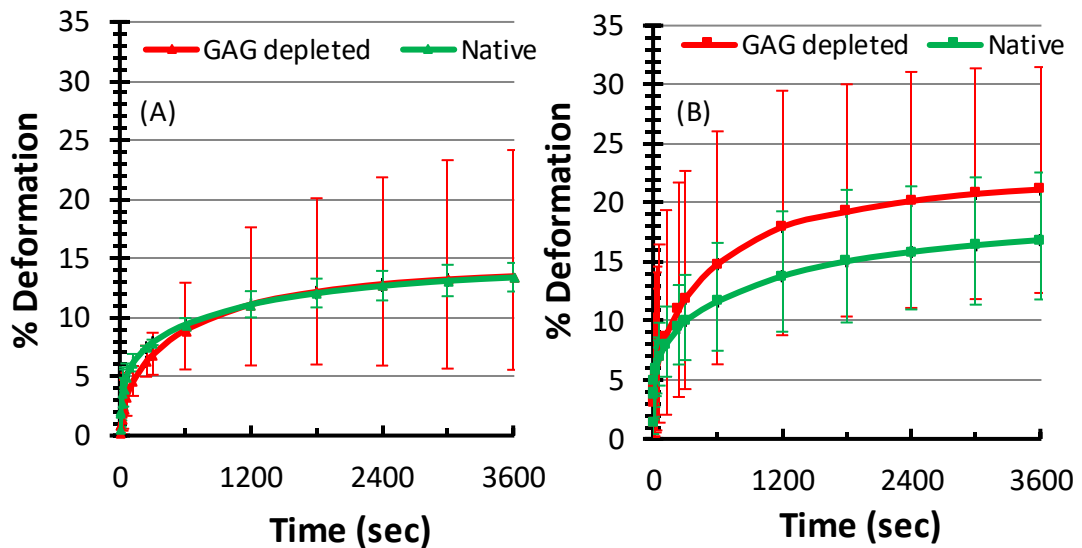


Figure 78: Percentage deformation of native and GAG depleted cartilage over the duration of 1 hour with a load of 0.51 N: (A) Medial condyle (B) Lateral condyle. Data was subject to arcsine transformation prior to calculation of the mean and 95 % confidence limits. Data is expressed as the back transformed mean (n=3) \pm 95 % confidence limits.

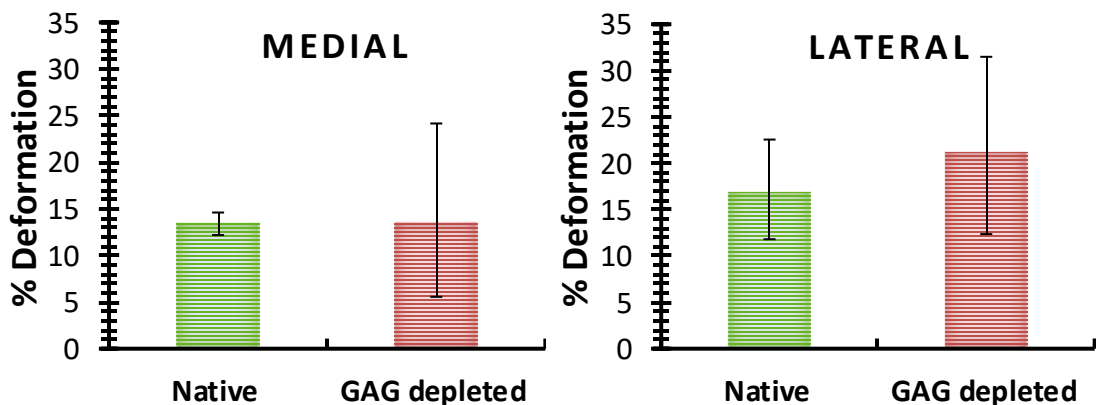


Figure 79: Final percentage deformation of native and GAG depleted cartilage at 1 hour with a load of 0.51 N. Data was subject to arcsine transformation prior to calculation of the mean and 95 % confidence limits. Data is expressed as the back transformed mean (n=3) \pm 95 % confidence limits.

As above, for the 0.11 N and 0.31 N loads the final percentage deformation data at 1 hour for the native and GAG depleted cartilage at a load of 0.51 N, was arc sin transformed. The trend seen was that there was no difference between the percentage deformation mean values between the native samples when compared to that of the GAG depleted samples in both medial and lateral condyles.

Overall, GAG depletion using SDS rendered the cartilage tissue soft, indicating a loss of compressive stiffness. This was evident, because unlike the native cartilage samples, after indentation prominent indentation marks were observed on the cartilage surface of the GAG depleted cartilage samples where the stainless steel indentation pin had been in contact with the femoral condylar cartilage tissue. These indentation marks became more prominent at higher loads.

5.4.3 Equilibrium elastic modulus and permeability

The FEA model was used to calculate the equilibrium elastic modulus and permeability using the data from only the medial condyles since the deformation curves at higher loads showed that the lateral condyles gave high creep deformation (creep deformation > 15% of the porcine condylar cartilage thickness). Hence the lateral condyle deformation data was excluded from being input into the FEA model, as high levels of deformation (from the lateral condyles) would lead to inaccurate predictions of the equilibrium elastic modulus and permeability.

Representative images of the deformation curve fitting for the native and GAG depleted medial condylar cartilage with a load of 0.31 N are shown in Figure 80. These curve fittings were used in the FEA model to calculate the equilibrium elastic modulus and permeability of the samples. Under the load of 0.31 N, perusal of the data showed that the GAG depleted samples showed greater deformation than the native cartilage samples and this was also the case across all loads applied to these two groups. However, the greatest difference in the deformation was observed between the native and GAG depleted cartilages under a load of 0.31 N (medium load).

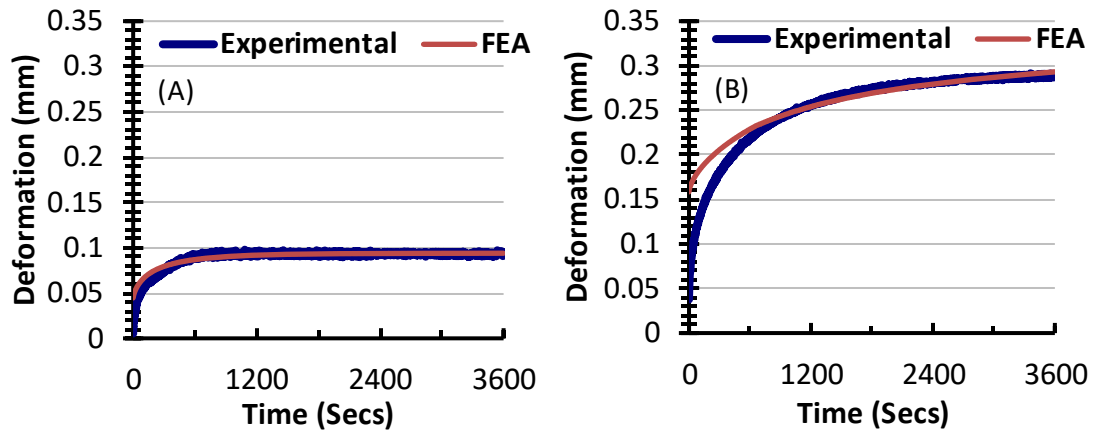


Figure 80: Representative graphs of indentation characteristics obtained experimentally and through FEA model curve fitting of a medial porcine condyle under a load of 0.31 N.
 (A): Curve fitting the deformation profile of a porcine medial condyle –Native (B): Curve fitting the deformation profile of a porcine medial condyle –GAG depleted.

The equilibrium elastic modulus and permeability for the native and GAG depleted medial condyles under loads of 0.11 N, 0.31 N and 0.51 N are shown in Figure 81, Figure 82 and Figure 83, respectively. The R^2 values presented in Figure 81, Figure 82 and Figure 83, represent how close the FE model curve fitting was to the last 70% of the experimental deformation curve. Only samples with an R^2 value greater than 75% were accepted as relevant and accurate enough for this study.

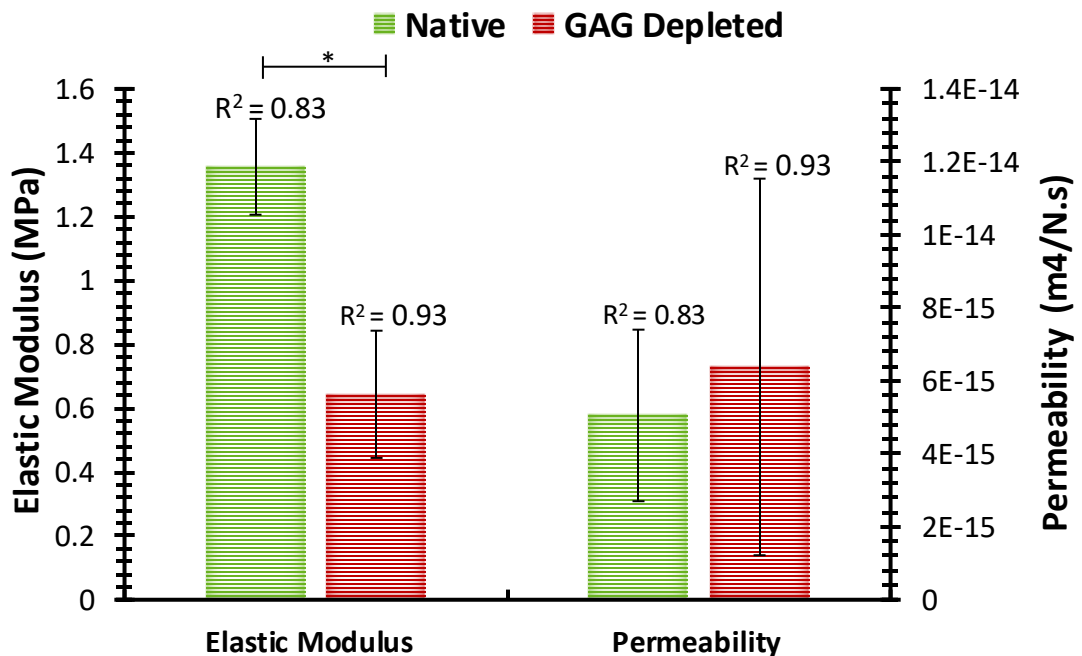


Figure 81: Equilibrium elastic modulus and permeability of native and GAG depleted medial condylar cartilage under a load of 0.11 N. Data is expressed as the mean ($n=5$) \pm 95 % confidence limits. The R^2 values define how close the FE model curve fitting was to the last 70% of the experimental deformation curve, the closer the R^2 value is to 1, the better the fit.

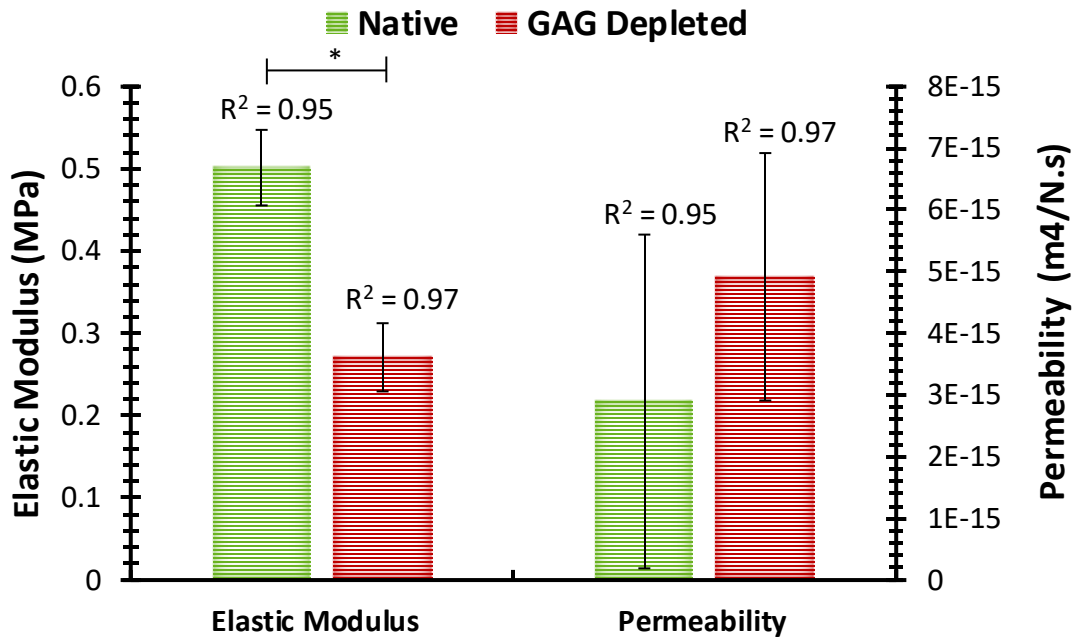


Figure 82: Equilibrium elastic modulus and permeability of native and GAG depleted medial condylar cartilage under a load of 0.31 N. Data is expressed as the mean (n=6) ± 95 % confidence limits. The R² values define how close the FE model curve fitting was to the last 70% of the experimental deformation curve, the closer the R² value is to 1, the better the fit.

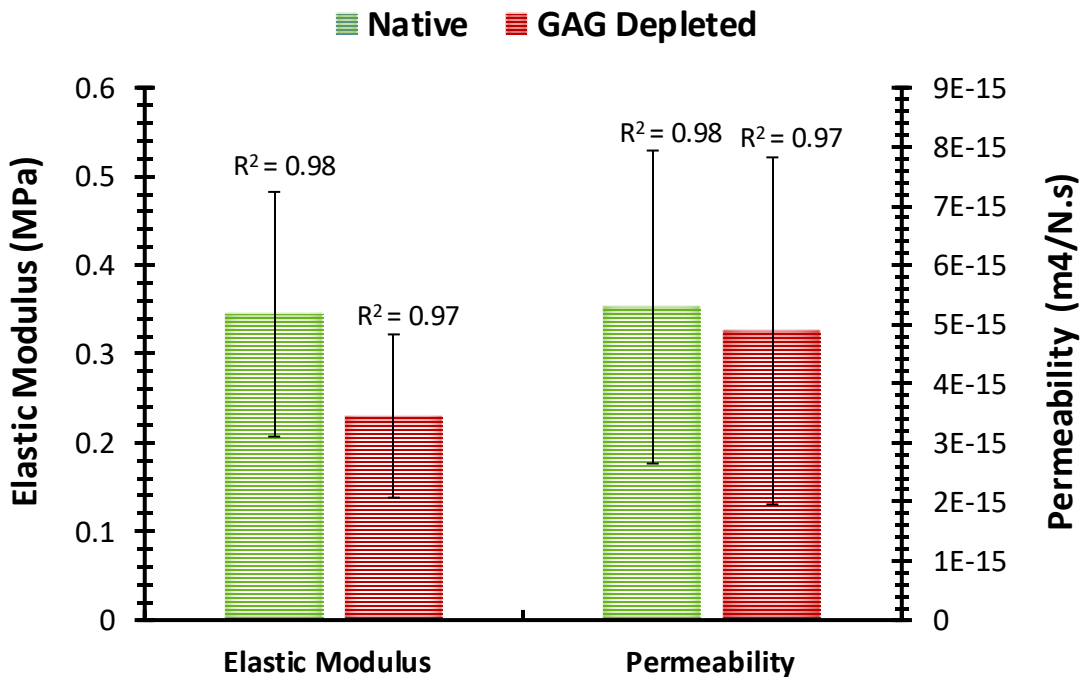


Figure 83: Equilibrium elastic modulus and permeability of native and GAG depleted medial condylar cartilage under a load of 0.51 N. Data is expressed as the mean (n=3) ± 95 % confidence limits. The R² values define how close the FE model curve fitting was to the last 70% of the experimental deformation curve, the closer the R² value is to 1, the better the fit.

Overall, the native porcine medial condylar cartilage exhibited a higher equilibrium elastic modulus compared to the GAG depleted porcine medial condylar cartilage when tested under the three different loads. The data for the native and GAG depleted groups under each load were compared using the Student's t-test. This revealed that the equilibrium elastic modulus of the native porcine medial cartilage was significantly greater than the GAG depleted porcine medial condylar cartilage when tested under the low (0.11N; $p = 4.65 \times 10^{-5}$) and medium (0.31N; $p = 2.35 \times 10^{-5}$) loads. However, this trend was not the case when tested under the high (0.51N; $p = 0.4$) load, further studies (i.e higher n value) are needed to verify the significance.

With regard to the average permeability values, there was a trend for these to be greater in the GAG depleted cartilage samples compared to the native cartilage samples when tested under the 0.11N and 0.31 N loads but not when tested under the 0.51 N load. Again, the data for the permeability of the native and GAG depleted medial porcine condylar cartilage under each load was compared using the Student's t-test which revealed no significant differences between the groups when tested under the three different loads. (0.11 N, $p = 0.5$; 0.31 N, $p = 0.2$ and 0.51 N, $p = 0.9$).

5.5 Discussion

The aim of this study was to investigate the effect that load variation had on the deformation, equilibrium elastic modulus and permeability of native and GAG depleted cartilages. The ideal load for future testing was the load that gave rise to a significant difference in percentage deformation, equilibrium elastic modulus and permeability between the native and GAG depleted cartilages. Therefore, from investigation of three different loads during indentation testing of porcine femoral condyle cartilage described here, it was clear, after indentation and FEA analysis, that the medium load (0.31 N, 31.89 g) was the test load that best showed a clear difference in the biomechanical properties between the native and GAG depleted porcine cartilages.

It was observed that there was no significant difference in the thickness of the cartilage in the native and GAG depleted medial condyles within each load experiment. Similarly, comparison of the thickness of the cartilage in the native and GAG depleted lateral condyles specimens was not significantly different within the experiments conducted at 0.11 N and 0.51 N; however, the thickness of the GAG depleted cartilage was significantly greater than the native cartilage in the lateral condyles in the experiments conducted at 0.31 N. The reason for this are unclear; however, it is possible that this was due to natural biological

variation in the cartilage of these particular samples. A radiographic and image analysis method developed by Wayne *et al.* (1998) for the measurement of articular cartilage showed that the thickness of the cartilage in porcine lateral condyles was between 1.1 mm – 1.9 mm. Similarly, another study measured porcine cartilage thickness from digital histological images and showed thicknesses of 1.2–2.4 mm and 1.2–1.6 mm for the medial and lateral condyles, respectively. Measured porcine femoral cartilage thicknesses in the current study (medial: 2.2 - 2.4 mm; lateral: 1.5 – 1.8 mm), showed good agreement with the ranges reported by Wayne *et al.* (1998) and Fermor (2013).

GAGs are attached to the protein core of proteoglycans, of which chondroitin sulfate is the most abundant and important. The highly electro-negatively charged groups on these GAGs (sulfate and carboxyl groups) control the osmotic swelling pressure that gives cartilage tissue its compressive mechanical properties. They are able to do this by trapping/restricting water and other small molecules in-between their chains. Therefore, water flow through the cartilage ECM is restricted by these GAGs, because of their hydrophilic nature and they therefore play an important role in the biomechanical properties and biphasic properties of cartilage (Mow *et al.*, 1980; Ateshian *et al.*, 1994; Forster and Fisher, 1996; Mow and Ateshian, 1997). When cartilage is initially loaded, the interstitial 'water phase' of cartilage bears most of the load and over time it is transferred to the solid matrix of the tissue (i.e. collagen); in order to reduce the load on the solid matrix. This interaction between GAGs, interstitial water and the collagen network of articular cartilage is considered to be vital for normal biomechanical function. Osteoarthritic cartilage is associated with a reduced number of proteoglycans as it is subject to matrix degeneration, which leads to changes in the biomechanical function of the tissue, rendering it to lose compressive stiffness.

Here, a GAG depleted model of cartilage, developed in Chapter 4, using SDS washes was used to represent osteoarthritic cartilage.

The effect of load variation on native and GAG depleted porcine condylar cartilage samples was carried out using a series of indentation tests, from which the deformation properties, equilibrium elastic modulus and permeability were calculated. Deformation curves for all loads studied showed that the GAG depleted porcine condylar cartilage exhibited higher deformation across a 1 hour time period, when compared to the native porcine condylar cartilage. This can be explained, as the low levels of GAGs in the GAG depleted cartilage were not able to aid in resisting the compression of the cartilage. Significant differences between the native and GAG depleted porcine condylar cartilage's in terms of percentage deformation (after it has been normalised for the thickness and arcsine transformed) were found when

the medial condyles were tested at low and medium loads, and in the lateral condyle when tested at low load. Similar trends were observed when the percentage deformation had reached equilibrium after 1 hour. The average deformation of the medial condyles at equilibrium (after 1 hour) for the native and GAG depleted cartilages, in the low load experiment was 2.9 % and 5.7 %, respectively and for the lateral condyles, 3.7 % and 6.5 %, respectively. In the medium load experiment the medial condyles average equilibrium deformation was 6% and 14.2 %, respectively.

When observing the data of the high load experiment, percentage deformation appeared to be higher in the GAG depleted cartilage in both the medial or lateral condyles, when compared to the native cartilage. Proteoglycans are responsible for the restriction of fluid flow through the ECM of cartilage; however, increased fluid flow as a result of reduction/removal of proteoglycans leads to a reduced load supported by the fluid phase, hence tissue should show greater deformation. Therefore, GAG depleted cartilage samples were expected to have a much higher deformation than the native cartilage samples, as these samples had had 75% of their GAGs removed prior to indentation. However, in the indentation tests conducted at high load (0.51 N), this was not the case, especially in the medial condylar cartilage samples. It is thought that this could be because the load applied to both the native and GAG depleted samples was too high, for a difference in the deformation to be demonstrated between the two groups. This was further clarified when the deformation data was back transformed and plotted as a percentage deformation of the cartilage thickness.

The native and GAG depleted cartilage of the lateral condyles in the high load experiment and the GAG depleted cartilage of the lateral condyles in the medium load experiment; showed to have a percentage deformation greater than 15%, which meant that the derived data for the equilibrium elastic modulus and permeability would not be accurate; as deformation should be kept to a minimum (<15%) to abide by the linear biphasic model used in this study, which assumes permeability is constant with deformation. However, this is only valid for small deformations up to 15% (Mow et al., 1989; Proctor et al., 1989; Athanasiou et al., 1991). The higher percentage deformation seen in the lateral condylar cartilage compared to the medial condylar cartilage, was thought to be because the cartilage in the lateral condyles was thinner than their medial counterpart. The thinner the cartilage, the fewer macro and micro structures there are to resist the compressive loads as well as less fluid to resist the compressive loads applied. This becomes exacerbated in the samples that have had the GAGs removed, hence explaining why the GAG depleted cartilage in the lateral

condyles generally had a slightly higher deformation. Therefore, it was decided to only analyse the deformation data from the indentation testing of native and GAG depleted medial condylar cartilage in the FE model, for calculation of the equilibrium elastic modulus and permeability.

An axisymmetric poroelastic FE model used by Abdelgaied *et al.* (2015) was used to curve fit the experimental deformation to determine the effect that load variation had on the equilibrium elastic modulus and permeability of native and GAG depleted porcine cartilages.

As the load was increased, the equilibrium elastic modulus decreased for both native and GAG depleted cartilages. The cartilages' ability to resist compression diminishes the greater the load, hence its elastic modulus will decrease naturally. It is important to note that when cartilage is subject to indentation tests, the rate of deformation is typically controlled by the permeability of the sample, whereas the equilibrium deformation (deformation at the end, usually the last 70% of the experiment, where the deformation stays constant) is the outcome of the elastic modulus of the sample (Mak *et al.*, 1987; Mow *et al.*, 1989).

The equilibrium elastic modulus was greater in the native cartilage samples when compared to the GAG depleted samples, regardless of the load being added. This can be explained because the GAG depleted cartilage exhibited a reduced compressive stiffness due to the loss of GAGs and hence a lower elastic modulus; and was less able to resist compression when compared to the native cartilage. Comparable changes in the softness of cartilage, equilibrium percentage deformation, and decrease in equilibrium elastic modulus (due to removal of GAGs); have been reported in the literature with similar indentation tests of articular cartilage by Bonassar *et al.* (1995), Reippo *et al.* (2003), Han *et al.* (2007) and Katta *et al.* (2007).

It was hypothesised that the mean permeability of the GAG depleted cartilage would be higher than native cartilage; as the removal of water binding GAGs would allow the interstitial fluid to move more freely within the remaining collagen network, as the matrix would be more porous. However, this was not the case across all load experiments. No significant differences were observed between the GAG depleted and native cartilage samples.

However, at the high (0.51N) load, the permeability of the native cartilage was slightly higher than the GAG depleted cartilage. It is also worth noting that at this higher load, the mean elastic modulus, tended to be higher in the native cartilage more so than the GAG depleted cartilage and this same trend was also observed in the deformation data of the native and

GAG depleted cartilage under the high load. However, one cannot comment on the significance of these trends as the sample size was too small ($n=3$). Nevertheless, the reason for the trend seen in the percentage deformation between the native and GAG depleted cartilage in the high load, could be explained by the fact that the larger loads may have a governing effect on the ability of the tissue to control the deformation, regardless of the amount of GAGs present in both native and GAG depleted cartilages. It was for this reason that the higher load (0.51 N) was not chosen for future studies.

A limitation of the experimental indentation testing methodology, was the low contact stresses that were inherent in the setup of the equipment used in this study. A way around this could have been to use a smaller stainless-steel pin to increase the contact stress, but such a set up becomes physiologically irrelevant as in the natural joint, loads are dispersed over large contact areas. Conversely, changing the stainless-steel pin to a standard 9 mm cartilage pin would have been more beneficial but it was not possible to attach such a pin in the rig used in this study. Furthermore, if this were possible, the load could not have been increased further to compensate for the now even lower contact stress that would have been possible with a 9 mm cartilage pin.

Therefore, the experimental set up used in this study, was acceptable to achieve the aims of this study, which were to: investigate the effect of load variation on native and GAG depleted porcine condylar cartilage and to identify which load would give rise to a significant difference in the deformation, elastic modulus and permeability between the native and GAG depleted porcine condylar cartilages.

5.6 Conclusion

The current study, while evaluating the effect of load variation on the deformation, equilibrium elastic modulus and permeability of native and GAG depleted porcine condylar cartilage, also addressed the importance of GAGs in the biomechanical properties of articular cartilage. The loss of compressive stiffness in the GAG depleted porcine condylar cartilage physically manifested in the form of noticeable deformation marks visible to the naked eye in the contact zones at the end of indentation tests. Whereas, deformation marks were not evident in native porcine condylar cartilage samples. This phenomenon can be simply explained in terms of load supported by the fluid and solid phase. GAG depleted porcine condylar cartilage had decreased fluid phase load support. This depletion of GAGs which are intrinsic to the mechanical properties of cartilage caused a relatively higher proportion of the load to be transferred to the solid phase of articular cartilage, which lead to higher

deformation when compared to native porcine condylar cartilage samples, that were able to support most of the load in the fluid phase before transferring it solid phase, at a much slower rate.

The medium and low loads both showed significant difference in the deformation as well as in the equilibrium elastic modulus ($p < 0.05$) between the native and GAG depleted medial porcine condylar cartilage samples; which was not so apparent in the high load experiment. However, the medium load measured the biggest significant differences in the deformation between native and GAG depleted porcine cartilage models. Therefore, this load was adopted in the following chapter to evaluate the deformation and mechanical properties of GAG depleted porcine condylar cartilage treated with peptide and PEP: GAG mixtures, which have been designed to treat GAG depleted articular cartilage tissue and improve its biomechanical properties.

Chapter 6 Investigation of the effects of injection of peptide-GAG mixtures to GAG depleted cartilage.

6.1 Introduction

The biomechanical properties of articular cartilage are compromised by the loss of GAGs, which is due to the onset and natural progression of osteoarthritis and other joint diseases (Lohmander et al., 1989; Arden and Nevitt, 2006; Lorenz and Richter, 2006; Pitsillides and Beier, 2011; Clarkin et al., 2011; Ashkavand et al., 2013; Lee et al., 2013). The loss of GAGs reduces the cartilage's ability to withstand compressive forces (Mankin and Lippiell, 1971; Dudhia, 2005; Otsuki et al., 2008; Katta et al., 2008). It has been suggested that restoring GAGs, in particular chondroitin sulfate (CS), to GAG depleted cartilage may be beneficial to the biomechanical and frictional properties of articular cartilage (Katta, 2007). The hypothesis that SAPs in combination with GAGs can be an effective treatment to improve the biomechanical properties of osteoarthritic cartilage was therefore tested *in vitro*.

Previous chapters have highlighted the favourable properties of P₁₁₋₄ and P₁₁₋₈ in combination with GAGs. Therefore, the next stage of the study was to determine the effect of the peptides and PEP: GAG mixtures of P₁₁₋₄ and P₁₁₋₈, on the deformation and biomechanical properties of GAG depleted porcine condylar cartilage, when compared to native porcine condylar cartilage using indentation testing. The *in vitro* GAG depleted porcine condylar cartilage model developed in Chapter 4 – (model 3: method 4) and the load for indentation testing determined in Chapter 5 – (medium load 0.31 N), were used to evaluate the utility of P₁₁₋₄ and P₁₁₋₈ and their PEP: GAG mixtures, as a minimally invasive treatment for GAG depleted porcine condylar cartilage. The FE model applied in Chapter 5 was used to determine whether the peptides and PEP: GAG mixtures improved the biomechanical properties of GAG depleted porcine condylar cartilage. All PEP: GAG mixtures tested were at the lower GAG molar ratio of 1:64, as it was hypothesised that any effect on the deformation and biomechanical properties of the GAG depleted cartilage at the lower GAG molar ratio, would be magnified at a higher GAG molar ratio. Only medial porcine condyles were used in FE analysis, as previous studies showed that lateral porcine condyles demonstrated high creep deformation (creep deformation > 15% of the porcine condylar cartilage thickness), which would lead to inaccurate predictions of the equilibrium elastic modulus and permeability.

Fluorescence recovery after photobleaching (FRAP) is a quantitative technique that takes advantage of particular properties of fluorophores, in which fluorophores are excited at a certain wavelength and emit a fluorescent light. Originally, it was developed in 1970s by Axelrod *et al.* as a technique to study the dynamics of molecular mobility in tissues or cells, by measuring the rate of fluorescent recovery of organic dyes, such as fluorescein, in a previously bleached area (Axelrod *et al.*, 1976; Koppel *et al.*, 1976). FRAP was used in this study to determine whether the peptides and PEP: GAG mixtures that had been fluorescently tagged with fluorescein; were able to remain in a self-assembled state after injection into GAG depleted condylar cartilage and indentation testing. It was hypothesised that the samples that were completely self-assembled would show little or no fluorescence recovery after photobleaching. The gel like structure of the peptide or PEP: GAG mixtures would prevent the fluorescein molecules in the non-bleached areas from diffusing to the area that had been bleached

6.2 Aims and objectives

The aim of this chapter was to investigate whether P₁₁-4 and P₁₁-8 and their PEP: GAG mixtures were able restore the biomechanical properties of GAG depleted porcine condylar cartilage.

6.2.1 Objectives

- 1) To evaluate the deformation and biomechanical properties of native and GAG depleted porcine condylar cartilage and GAG depleted porcine condylar cartilage injected with peptides (P₁₁-4 and P₁₁-8) and PEP: GAG mixtures (P₁₁-4 and P₁₁-8 at a GAG molar ratio of 1:64), using indentation testing and FEA.
- 2) To determine the thickness of the native, GAG depleted and injected (peptide / PEP: GAG mixtures) porcine condylar cartilage, using a needle indentation method.
- 3) To determine whether, after indentation testing, the peptides (P₁₁-4 and P₁₁-8) and PEP: GAG mixtures (P₁₁-4 and P₁₁-8 at a GAG molar ratio of 1:64) injected into GAG depleted porcine condylar cartilage remained in a self-assembled state within the cartilage, using fluorescence recovery after photobleaching (FRAP) analysis.

6.3 Experimental Design

The experimental design in this study was to determine the effects of injecting GAG depleted condylar cartilage with: peptide alone (P₁₁-4 only, P₁₁-8 only), PEP: GAG mixtures (P₁₁-4: GAG injection, P₁₁-8: GAG injection) and chondroitin sulfate alone (CS injection only) on deformation properties when compared to GAG depleted condylar cartilage (negative

control) and native condylar cartilage (positive control). The three test groups determined the individual effects that either the peptide, chondroitin sulfate or the combination of the two, had on the deformation properties of GAG depleted condylar cartilage.

Since testing the effects of the peptides and PEP: GAG mixtures involved physically injecting the solutions into the cartilage, it was also important to determine the effects of injection of a pressurized fluid as well as any physical damage caused to the cartilage through the needle injection. Therefore, initial studies were carried out to compare the deformation properties of native condylar cartilage; native condylar cartilage injected with distilled water (native water injection) and native condylar cartilage injected with a needle only with no fluid (native injection only). These two control experiments were carried out, because the effect of injecting fluid or piercing the cartilage surface on the deformation properties, would be better demonstrated in native cartilage, that had not had the GAGs removed, hence isolating any effects. These test groups determined the effects that: a) the injection of pressurised water and b) the piercing of the cartilage surface had on the deformation properties of native condylar cartilage.

6.4 Experimental Methods

6.4.1 Acquisition of porcine femoral condyles

Porcine femoral condyles were acquired, dissected and stored as described in Chapter 2; Section 2.2.2.2 to 2.2.2.4. Native porcine condyles were mounted in PMMA as outlined in Chapter 2; Section 2.2.6.1.

6.4.2 GAG depletion of porcine femoral condylar cartilage

Three (medial and lateral) GAG depleted porcine condyles were produced using the procedure outlined in Chapter 4; Section 4.3.3. The GAG depleted porcine condyles were mounted in PMMA as outlined in Chapter 2; Section 2.2.6.1.

6.4.3 Preparation of peptides, peptide: GAG mixtures and chondroitin sulfate GAG control.

The concentration of peptides was the same for all experiments (10 mg.ml^{-1} , $\sim 6 \text{ mM}$) and the molar ratio of chondroitin sulfate (GAG) used in the PEP: GAG mixtures was 1:64. In this study, the peptides used (P_{11-4} and P_{11-8}) were doped with fluorescein tagged- P_{11-4} and P_{11-8} purchased from commercial suppliers (PolyPeptide Group, Sweden). The molar ratio of fluorescein tagged- P_{11-4} and P_{11-8} to non-tagged P_{11-4} and P_{11-8} was 1:150. The chondroitin

sulfate GAG control was doped with a fluorescein stock solution (7.8 mM), in order to visualise the mobility of the fluorescein and fluorescein-tagged peptides in subsequent FRAP experiments.

The peptide, PEP: GAG mixture and chondroitin sulfate GAG control were weighed as outlined in Table 28.

Table 28: Masses of peptide and chondroitin sulfate (GAG) weighed out for the different injection experiments.

	Peptide alone	PEP: GAG mixture		CS alone
		GAG	Peptide	
P ₁₁ -4	10.53 mg	4.85 mg	10.53 mg	4.94 mg
P ₁₁ -8	12.65 mg	4.94 mg	12.65 mg	

Concentration of the peptide was 10 mg.ml⁻¹. GAG molar ratio for the PEP: GAG mixture was 1:64. All samples were made up to a total volume of 1 ml.

6.4.3.1 Preparation of peptides for studies of injection of peptide alone.

Corresponding weights of peptide (Table 28) were weighed into a glass vial. Buffer (developed by James Warren PhD student; School of Mechanical Engineering) was added (1 ml) into each vial containing the peptide to maintain the peptide in a monomeric state. Sodium acetate buffer (1 M) at pH 4 was used for P₁₁-8 samples and sodium phosphate buffer (1 M) at pH 10 was used for P₁₁-4 samples. Samples were vortexed for 30 seconds and sonicated for 5 mins. Monomerised peptide samples were frozen in liquid nitrogen (-196 °C) and then lyophilised. Once fully lyophilised, samples were stored at 4 °C in the dark until used for injection into the porcine condylar cartilage.

6.4.3.2 Preparation of peptides and chondroitin sulfate for studies of peptide: GAG mixture injections.

Corresponding weights of peptide and GAG (Table 28) were weighed into individual glass vials. The P₁₁-4 sample was monomerised with 500 µl of 1 M sodium phosphate buffer at pH 10 and the P₁₁-8 sample was monomerised with 1 M sodium acetate buffer at pH 4. The corresponding monomerising buffer (500 µl) was added to the corresponding vials containing the GAG. The reconstituted GAG solution was then added to its corresponding peptide solution. Samples were vortexed for 30 seconds and then sonicated for 5 mins. The monomerised PEP: GAG mixtures were frozen in liquid nitrogen (-196 °C) and then lyophilised. Once fully lyophilised, samples were stored at 4 °C in the dark until required.

6.4.3.3 Preparation of chondroitin sulfate for studies of GAG only injections.

The highest weight of GAG (Table 28), was selected as a control and weighed into a glass vial. Fluorescein stock solution 7.8 mM was diluted (5 µl stock + 995 µl buffer) to a concentration

of 38 μM using a physiological buffer (130mM Na^+ salt solution at $\sim\text{pH}$ 7.4 – Chapter 3; Section 3.3.1.3). The weighed-out GAG was added to this diluted fluorescein solution and then lyophilised. The lyophilised powder was stored at 4 $^{\circ}\text{C}$ in the dark until required for testing.

6.4.4 Injection of peptides, PEP: GAG mixtures and chondroitin sulfate (GAG) into GAG depleted porcine condylar cartilage.

After the GAG depleted porcine femoral condyles had been mounted in PMMA; lyophilised peptide, PEP: GAG and GAG were reconstituted in 1 ml of distilled water. A needle and 1 ml syringe, were used to draw up 1 ml of the corresponding monomeric peptide, PEP: GAG mixture or chondroitin sulfate solution into the syringe, ready for injection into the GAG depleted porcine condylar cartilage (Figure 84). Three porcine femoral condyles (both medial and lateral condyles) were used for all groups in this study.

6.4.4.1 Injection of native porcine condylar cartilage with and without water.

A preliminary study was carried out to determine the effects of injecting native condylar cartilage with water and just a needle. Control injections of distilled water (1 ml), and a control of just the injection were performed on native porcine condylar cartilage. Three porcine femoral condyles (both medial and lateral condyles) were used for all control groups in this study.



Figure 84: Hydrated monomeric peptide being drawn up into a 1 ml syringe, ready for injection into the GAG depleted porcine condylar cartilage.

The flattest region of interest (ROI) of the condyle was chosen by eye, as the injection site. The injection technique used to inject the porcine condylar cartilage is illustrated in Figure 85. The highlighted area was injected 20 times around the circumference of the prescribed ROI. In total 1ml of the peptide, PEP: GAG mixture, water or chondroitin sulfate solution was deposited across these 20 injection sites, approximately 50 μl at each injection site. The needle was tilted at *circa* 45 $^{\circ}$, so that the peptide, PEP: GAG mixture, water or GAG solution could be deposited under the ROI, as demonstrated in Figure 85.

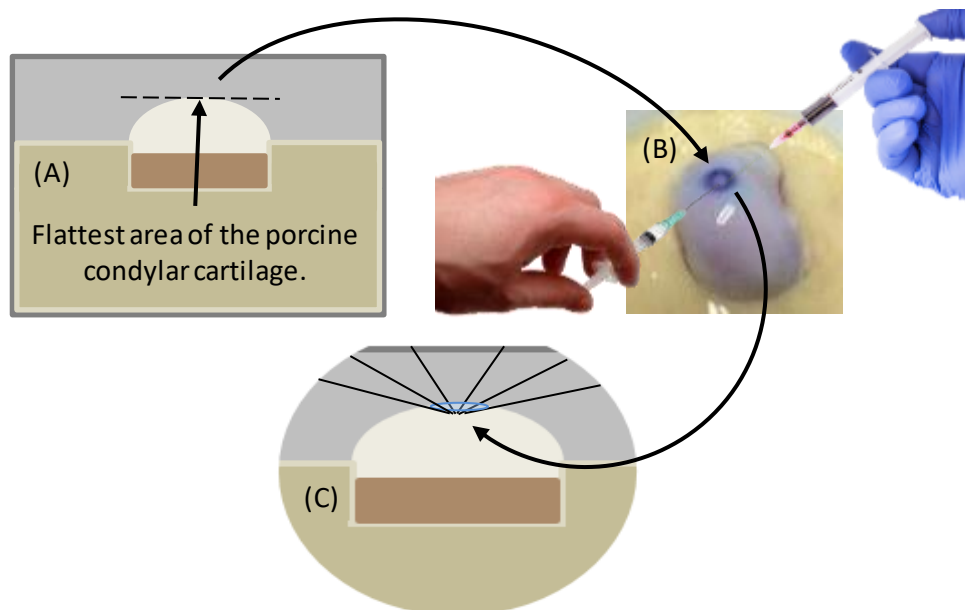


Figure 85: Schematic showing (A) the identification of the flattest region of interest (ROI) of the GAG depleted porcine condylar cartilage. (B) The injection of the peptide, PEP: GAG mixture, water or chondroitin sulfate solution to the ROI and (C) the orientation of how the needle was inserted into the femoral condylar cartilage.

The needle was retracted very slowly in stages, depositing approximately 50 μ l of the solution into the cavity created in the GAG depleted porcine condylar cartilage until the needle tip reached the surface of the cartilage. The GAG depleted porcine condylar cartilage samples injected with peptide and PEP: GAG mixtures were left to equilibrate for one day, in a moist environment at 4 $^{\circ}$ C in the dark, before indentation testing. All controls (native porcine condylar cartilage, native porcine condylar cartilage injected with water, native porcine condylar cartilage injected only and GAG depleted porcine condylar cartilage samples injected with chondroitin sulfate doped with fluorescein) were also stored in a moist environment at 4 $^{\circ}$ C in the dark for one day, before indentation testing.

6.4.5 Biomechanical characterisation of porcine femoral condylar cartilage

6.4.5.1 Indentation testing - sample and equipment preparation

After the samples had been injected with the peptide, PEP: GAG mixture, water or chondroitin sulfate and left to equilibrate (Section 6.4.4), the percentage deformation of the treated GAG depleted and native cartilages was determined using the indentation method described in Chapter 2; Section 2.2.6.2. The medium load (0.31 N) established as the appropriate load in the previous chapter, was applied. PBS was added into the cup holder, containing the PMMA fixed cartilage condyle, as described in Chapter 2; Section 2.2.6.2.

However, in this study the whole condyle was not completely submerged, instead PBS was filled to just before the area where the porcine cartilage had been injected.

6.4.5.2 Cartilage thickness measurements

The thickness of the cartilage in all of the experimental and control groups was measured using an Instron material testing machine and the measurements were always taken after indentation testing, as outlined in Chapter 2; Section 2.2.6.4. Injected samples were allowed to recover in a sealed Tupperware box moistened with PBS tissue, kept in the dark at 4°C overnight prior to thickness measurement.

6.4.5.3 Finite element method for derivation of material properties of porcine condylar cartilage

Deformation data of the treated GAG depleted and native porcine condylar cartilage, along with its cartilage thickness data were input into the FE model, which was used to derive the equilibrium elastic modulus and permeability, as described in Chapter 2; Section 2.2.6.5.

6.4.6 Determination of self-assembly of peptides and PEP: GAG mixtures *in situ* in GAG depleted porcine condylar cartilage.

6.4.6.1 Cryo-embedding

After the thickness of the cartilage in the treated samples had been measured, 9 mm plugs were removed from the porcine femoral condyles within the prescribed ROI, as described in Chapter 2; Section 2.2.2.3. Cartilage was removed from the bone and placed in cryo-plastic moulds. The cartilage was covered in OCT embedding medium and then placed flat into a freezer at -20 °C until set and required for sectioning.

Frozen cartilage tissue blocks embedded in OCT medium were removed from the freezer and placed into the cryostat, which had been set to -25 °C. Additional OCT embedding medium was applied to the back of the frozen cartilage block and pressed firmly onto a cryostat chuck. The chuck was then placed onto the super cooling stage inside the cryostat for 5 mins and a weight was applied to the top of the block until the frozen cartilage block had adhered evenly to the chuck. The chuck with the embedded frozen cartilage tissue was mounted into the chuck holder in the required orientation and the sample was fastened. The angle of the cutting blade was set to 4° and then moved towards the embedded samples. The section thickness was set to 100 µm. Cut sections were placed on Superfrost Plus⁺ slides by placing the slide just above the freshly cut cartilage tissue and allowing the section to self-adhere to

the slide. Twelve sections of each cartilage sample were cut (4 per slide; 3 slides for each sample).

Slides were then placed in 70 % alcohol (w/v) for one minute to remove the excess OCT medium and then left to air dry. Samples containing fluorescein were covered in tin foil and kept in the dark.

6.4.6.2 Fluorescence recovery after photobleaching (FRAP)

Slides containing sections of the GAG depleted porcine condylar cartilage injected with fluorescently tagged peptide, PEP: GAG mixtures or GAG, were placed into a Zeiss confocal microscope (LSM800 Inverted). Injection sites were first located, before a region of interest (ROI) was marked out next to the injection site, using the FRAP module tools on the Zeiss confocal microscope. A second ROI was also marked out, as a control, away from the injection site but in an area in which the fluorescently labelled peptide was visible. The ROI near the injection site was bleached for 10 seconds with a focused high-powered laser beam at a wavelength of 525 nm. The second ROI was not bleached, and was used as a control reference. Subsequently, the diffusion of the surrounding 'non-bleached' fluorescent molecules into the bleached area was recorded every 500 ms for 1 minute, until equilibrium was reached. Recovery of the fluorescent intensity of the bleached ROI was plotted against time to produce a recovery curve, which gave information on the mobility of the fluorescein within the: GAG and peptide only samples as well as the PEP: GAG gel samples. The FRAP analysis module on the Zeissconfocal microscope, was used to analyse the recovery curve to determine the diffusion constant of the fluorescein. Examples of different recovery profiles are shown in Figure 86 and were used to identify the self-assembly state of the peptides and PEP: GAG mixtures by classifying the mobility of the fluorescein that had been tagged to the peptide in the peptide samples and peptide in the PEP: GAG mixtures. Live screen shot images of the bleaching process were also recorded.

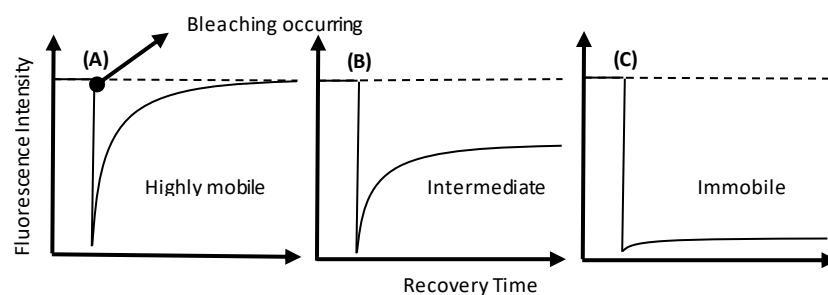


Figure 86: Diffusion profiles for the intensity of fluorescein over a period of time: (A) highly mobile (not self-assembled) (B) intermediately mobile and (C) immobile (self-assembled).

6.5 Results

In this study, there were several groups of native and GAG depleted porcine condylar cartilages into which different solutions were injected. The effects of injecting fluorescein-tagged peptide doped P₁₁-4 and P₁₁-8 alone and in combination with GAG, at a molar ratio of 1:64 on the deformation properties of GAG depleted porcine condylar cartilage were investigated. As a control, GAG depleted porcine condylar cartilage was injected with chondroitin sulfate doped with fluorescein. In addition, the effects of injecting native porcine condylar cartilage with water or just an injection with no solution were investigated. There were three porcine femoral condyles (medial - n=3; lateral - n=3) used in all groups.

6.5.1 Preliminary study to determine the effects of injecting water and just a needle (without water) on the deformation properties of native condylar cartilage.

6.5.1.1 Cartilage thickness measurements

For each cartilage group (native, native water injection and native injection only) indented with the medium load of 0.31 N; the cartilage thickness was measured for both medial (n=3) and lateral (n=3) condyles. Cartilage thickness data for the medial and lateral condyles of all groups is presented in Figure 87 and Figure 88, respectively. The data was analysed by one-way analysis of variance which revealed no significant variation in the thickness of the cartilage of the medial condyles of all the groups. However, in the lateral condyles the thickness of the cartilage in the native cartilage group was significantly greater ($p < 0.05$) than the thickness of the cartilage in the native injected only group.

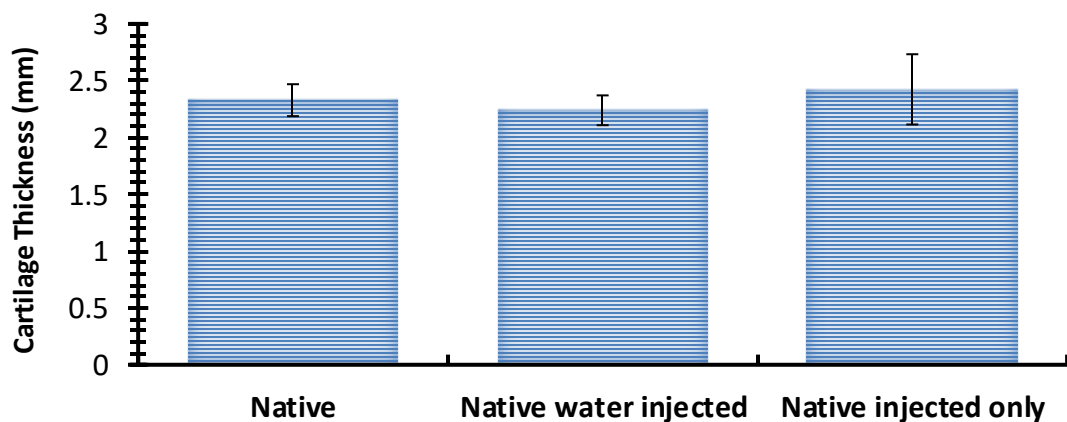


Figure 87: Cartilage thickness measurement of the medial condyles for the: native, native water injected and native injected only groups (n=3 for all groups). Samples were measured six times in the area of interest after indentation. Data is expressed as the mean (n=3) \pm 95 % confidence limits.

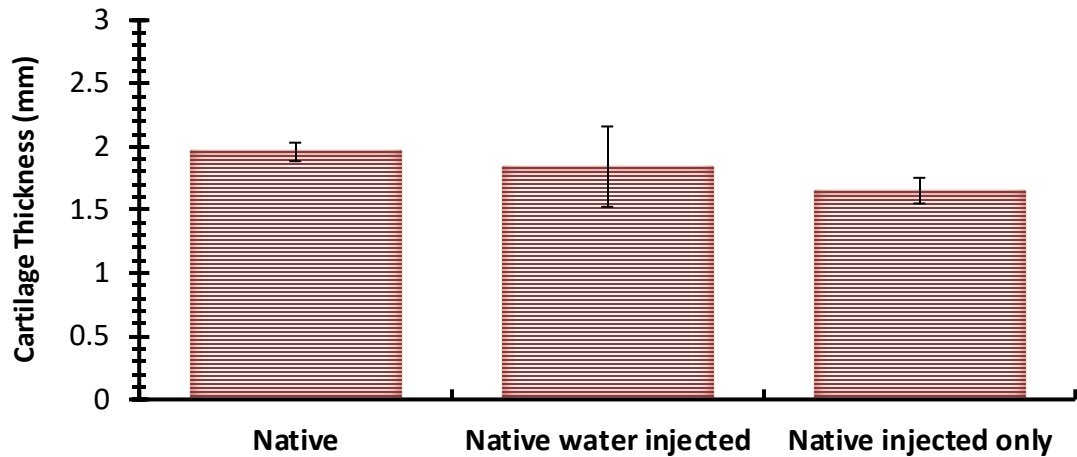


Figure 88: Cartilage thickness measurement of the lateral condyles for the: native, native water injected and native injected only groups (n=3 for all groups). Samples were measured six times in the area of interest after indentation. Data is expressed as the mean (n=3) \pm 95 % confidence limits.

6.5.1.2 Percentage deformation

Deformation properties of all three groups under a load of 0.31 N; for both medial and lateral porcine condyles are shown in Figure 89 to Figure 91. The percentage deformation of both the medial and lateral condyles under a load of 0.31 N, over a period of 1 hour, is shown in Figure 89 and Figure 90, respectively. The final percentage deformation (at 1 hour) of all the groups, for both medial and lateral condyles is shown in Figure 91.

The effect of injecting water and just an injection without water, on the percentage deformation of native condylar cartilage was determined by comparing the percentage deformation at 1 hour with that of the native porcine condylar cartilage for (a) the medial and (b) the lateral condyles. The data is presented in Figure 91.

The deformation curves of both medial and lateral condyles, over the duration of 1 hour showed that the native condylar cartilage deformed the least. The data also showed that the percentage deformation of the medial condylar cartilage samples of all groups had lower deformation properties when compared to the lateral condylar cartilage samples. It was observed that the native medial condylar cartilage injected with water reached equilibrium faster ($t = 1200$ secs), when compared to native medial condylar cartilage injected without water and the native medial condylar cartilage control.

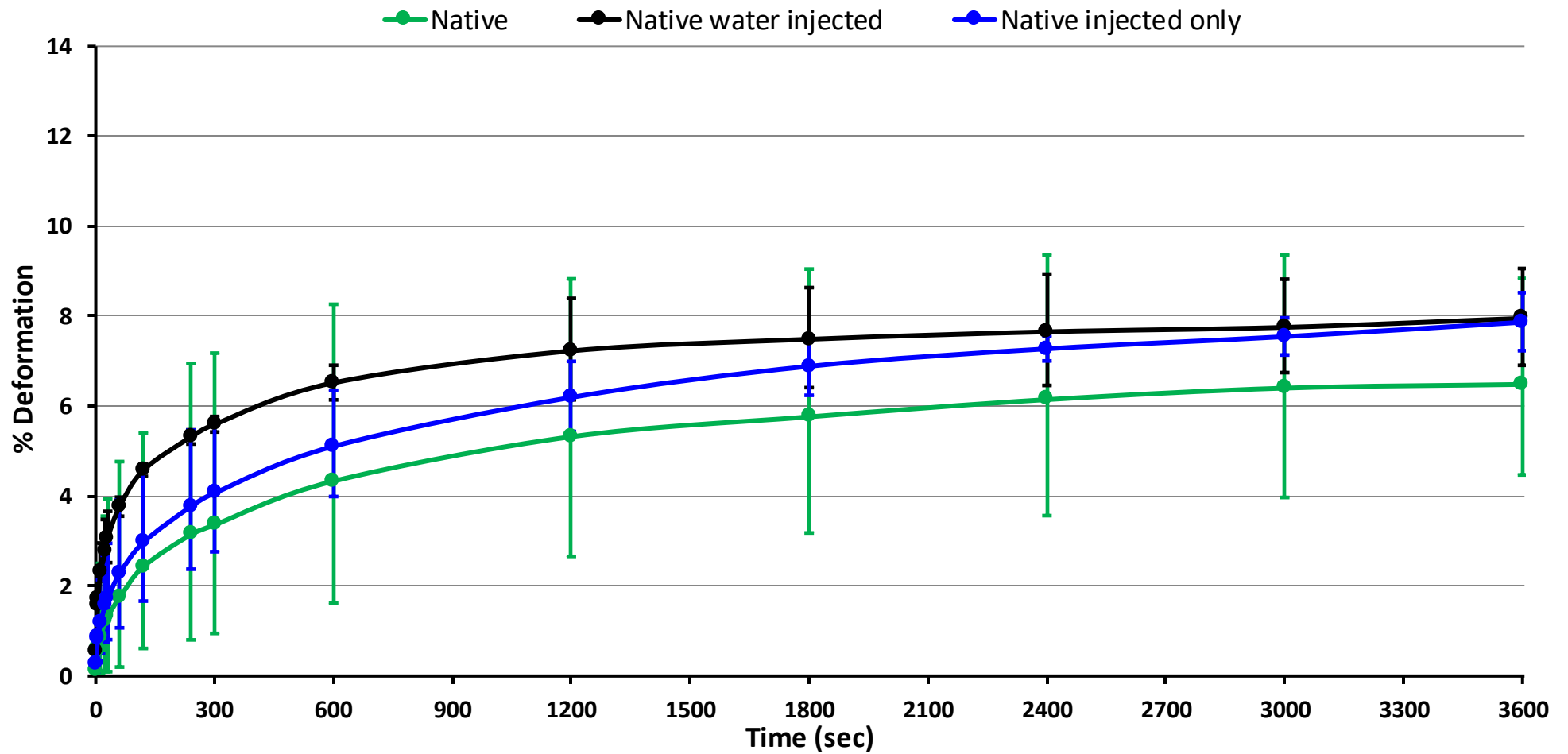


Figure 89: Percentage deformation of medial condyles from: native, native water injected and native injected only groups, over the duration of 1 hour with a load of 0.31 N. Data was subject to arcsine transformation prior to calculation of the mean and 95 % confidence limits. Data is expressed as the back transformed mean (n=3) \pm 95 % confidence limits.

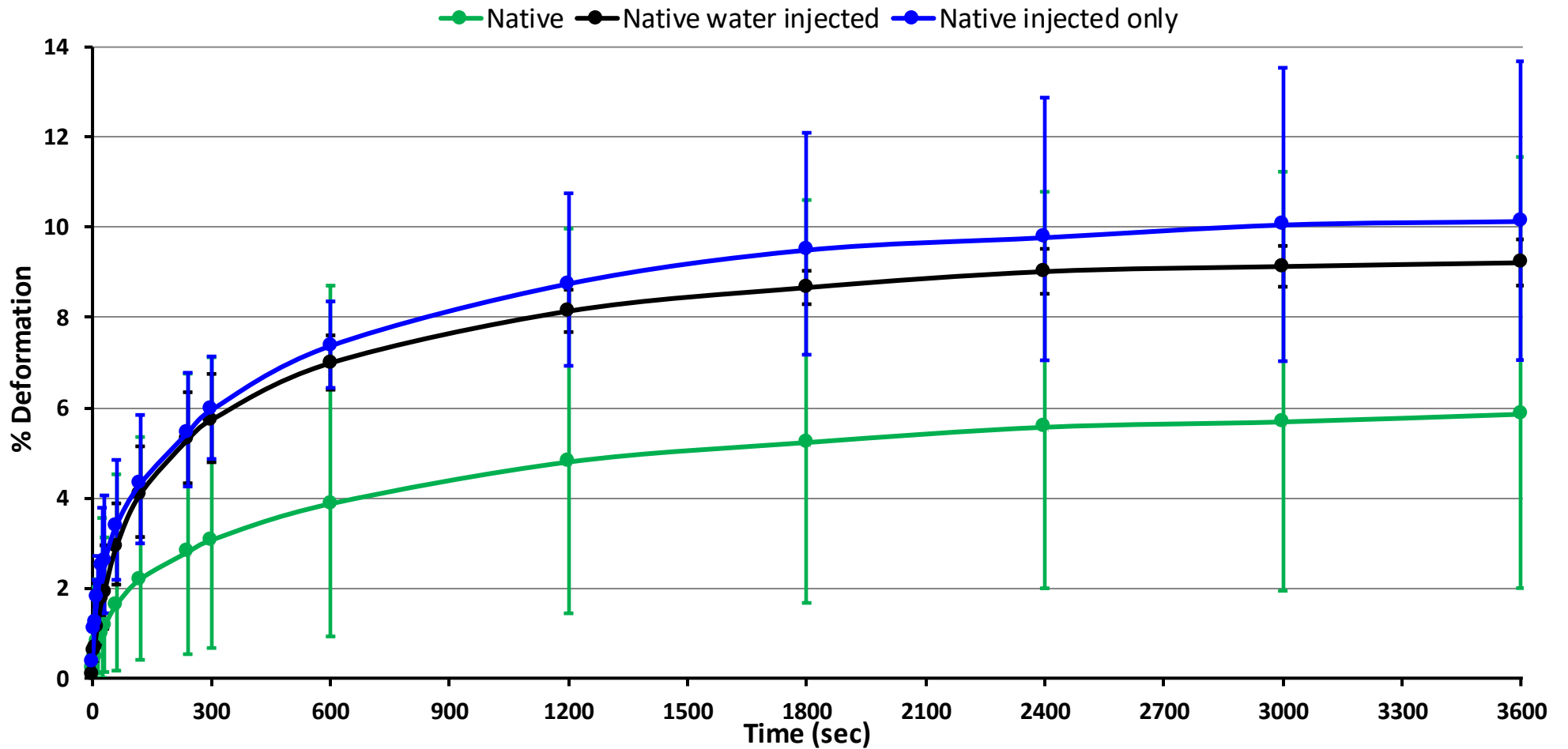


Figure 90: Percentage deformation of lateral condyles from: native, native water injected and native injected only groups, over the duration of 1 hour with a load of 0.31 N. Data was subject to arcsine transformation prior to calculation of the mean and 95 % confidence limits. Data is expressed as the back transformed mean (n=3) \pm 95 % confidence limits.

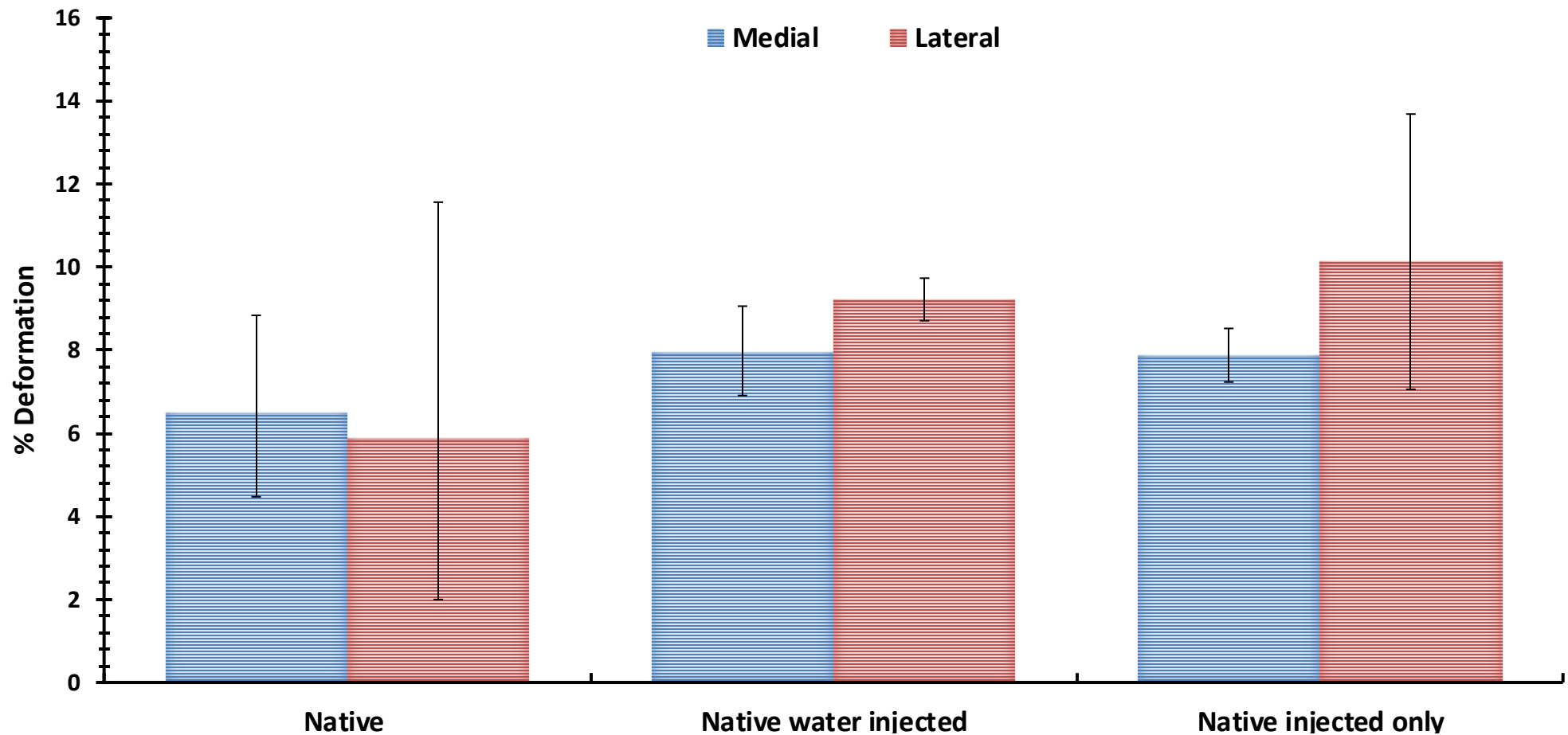


Figure 91: Final percentage deformation at 1 hour of: native, native water injected and native injected only groups, for the medial and lateral condyles, with a load of 0.31 N. Data was subject to arcsine transformation prior to calculation of the mean (n=3) and 95 % confidence limits. Data is expressed as the back transformed mean (n=3) \pm 95 % confidence limits.

The mean percentage deformation at 1 hour for the medial condyles of the native, native water injected and native injection only condylar cartilage were 6.5 %, 8 % and 7.9 %, respectively. For the lateral condyles, the mean percentage deformation was 5.9 %, 9.2 % and 10.1 % for the native, native water injected and native injection only condylar cartilage.

To determine if the injection of water or just injections without water, had an effect on the deformation properties of native porcine condylar cartilage, the percentage deformation data at 1 hour was compared (Figure 91). Due to the small sample size (n=3) the data was not subject to statistical analysis.

In the medial condyles the data showed that native medial condylar cartilage injected with water or just injection without water appeared to have a minimal effect to increase the deformation, only increasing the deformation by circa 1.5 % in both cases. For the lateral condyles, there appeared to be a greater effect with the mean deformation increasing from circa 6 % to 10 %, following the injection alone.

6.5.2 The effects of injecting P₁₁-4 and P₁₁-8 alone and in combination with GAG, at a molar ratio of 1:64 on the deformation properties of GAG depleted porcine condylar cartilage.

6.5.2.1 Cartilage thickness measurements

For each cartilage group (native, GAG depleted, GAG depleted chondroitin sulfate (CS) injected only, P₁₁-4: GAG injected, P₁₁-4 only injected, P₁₁-8: GAG injected and P₁₁-8 only injected) indented with the medium load of 0.31 N; the cartilage thickness was measured for both medial (n=3) and lateral (n=3) condyles. Cartilage thickness data for the medial and lateral condyles of all groups is presented in Figure 92 and Figure 93, respectively. Due to small sample size (n=3) the cartilage thickness data for the medial and lateral condyles was not subjected to statistical analysis. Nevertheless, the data for the medial condyles showed that there was minimal variation in the cartilage thickness across all groups. In the lateral condyles, there appeared to be one group (native, 1.9 mm) that had a slightly higher cartilage thickness when compared to the rest of the groups which had an average thickness of around 1.7 mm.

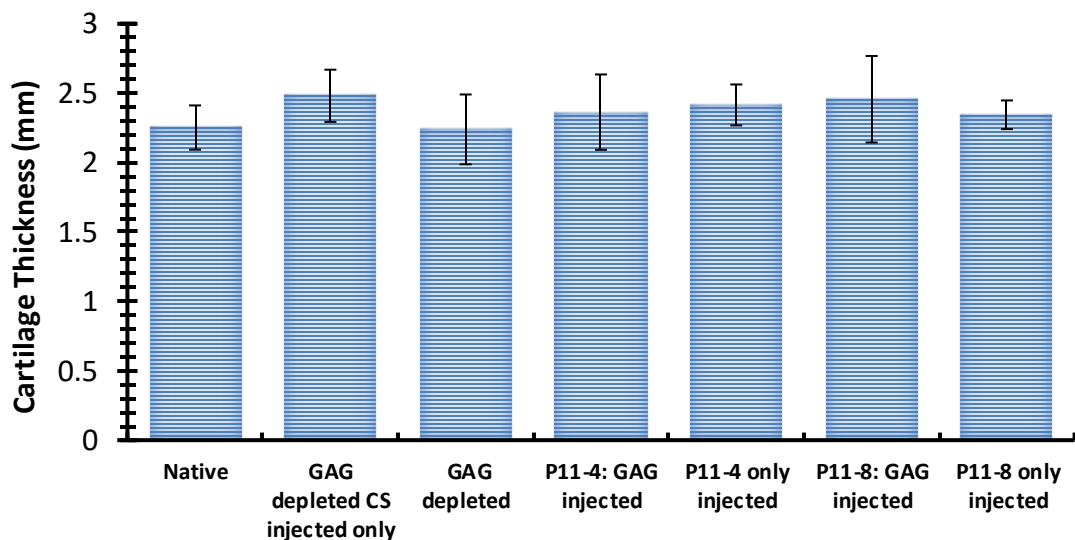


Figure 92: Cartilage thickness measurement of the medial condyles for the: native, GAG depleted chondroitin sulfate (CS) injected only, GAG depleted, P₁₁-4: GAG injected, P₁₁-4 only injected, P₁₁-8: GAG injected and P₁₁-8 only injected groups (n=3 for all groups).
Samples were measured six times in the area of interest after indentation. Data is expressed as the mean (n=3) ± 95 % confidence limits.

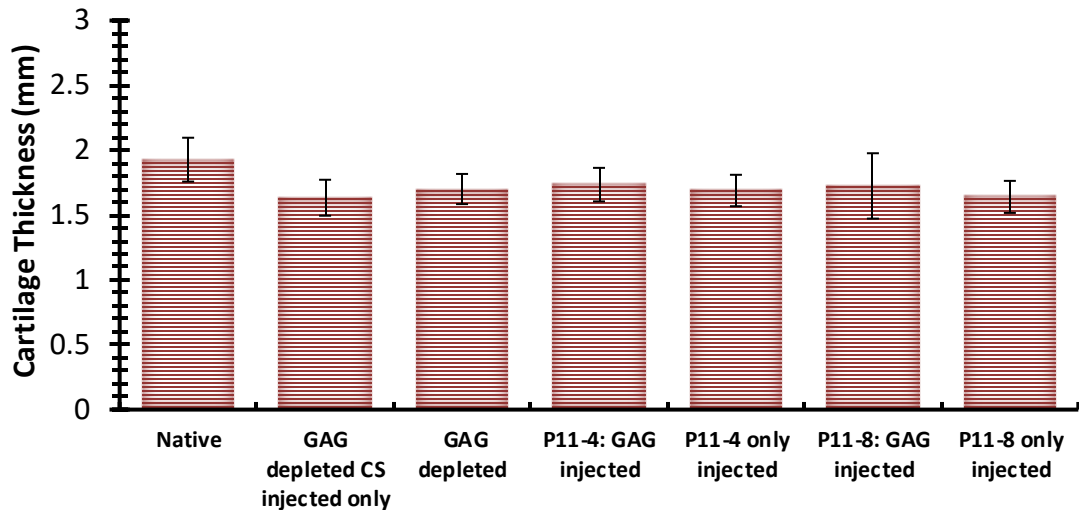


Figure 93: Cartilage thickness measurement of the lateral condyles for the: native, GAG depleted chondroitin sulfate (CS) injected only, GAG depleted, P₁₁₋₄: GAG injected, P₁₁₋₄ only injected, P₁₁₋₈: GAG injected and P₁₁₋₈ only injected groups (n=3 for all groups). Samples were measured six times in the area of interest after indentation. Data is expressed as the mean (n=3) ± 95 % confidence limits.

6.5.2.2 Percentage deformation

Deformation properties of all groups under a load of 0.31 N; for both medial and lateral porcine condyles are shown in Figure 94 - Figure 98. The percentage deformation of the medial and lateral condyles under a load of 0.31 N, over a period of 1 hour, is shown in Figure 94 and Figure 95, respectively. The final percentage deformation (at 1 hour) of all the groups and the corresponding controls, for both medial and lateral condyles is shown in Figure 96.

The effect of injecting the peptides P₁₁₋₄ and P₁₁₋₈, and the PEP: GAG mixtures, on the percentage deformation of GAG depleted condylar cartilage was determined by comparing the percentage deformation at 1 hour with the GAG depleted and native porcine condylar cartilage. The data is presented in Figure 97 and Figure 98, for the medial and lateral condyles respectively.

The deformation curves of both medial and lateral condyles, over the duration of 1 hour showed that the native condylar cartilage deformed the least and that the GAG depleted CS injected condylar cartilage deformed the most. The data also showed that medial condylar cartilage samples injected with P₁₁₋₄: GAG and P₁₁₋₈: GAG mixtures had lower deformation properties compared to the GAG depleted condylar cartilage and in the lateral condylar cartilage samples; injections of P₁₁₋₄: GAG, P₁₁₋₈: GAG and P₁₁₋₈ also reduced the deformation compared to the GAG depleted condylar cartilage samples.

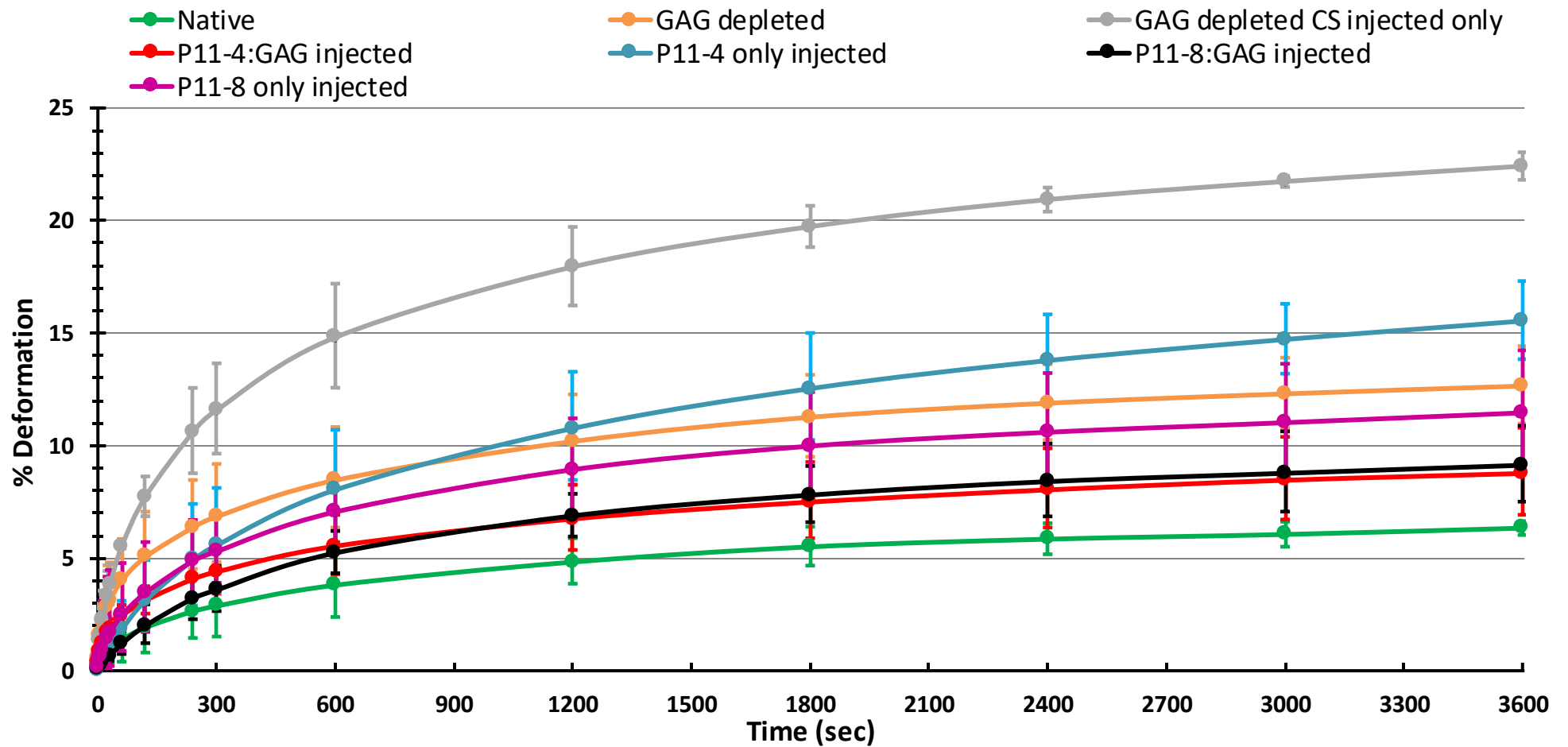


Figure 94: Percentage deformation of medial condyles from: native, GAG depleted chondroitin sulfate (CS) injected only, GAG depleted, P₁₁-4: GAG injected, P₁₁-4 only injected, P₁₁-8: GAG injected, P₁₁-8 only injected groups, over the duration of 1 hour with a load of 0.31 N. Data was subject to arcsine transformation prior to calculation of the mean and 95 % confidence limits. Data is expressed as the back transformed mean (n=3) ± 95 % confidence limits.

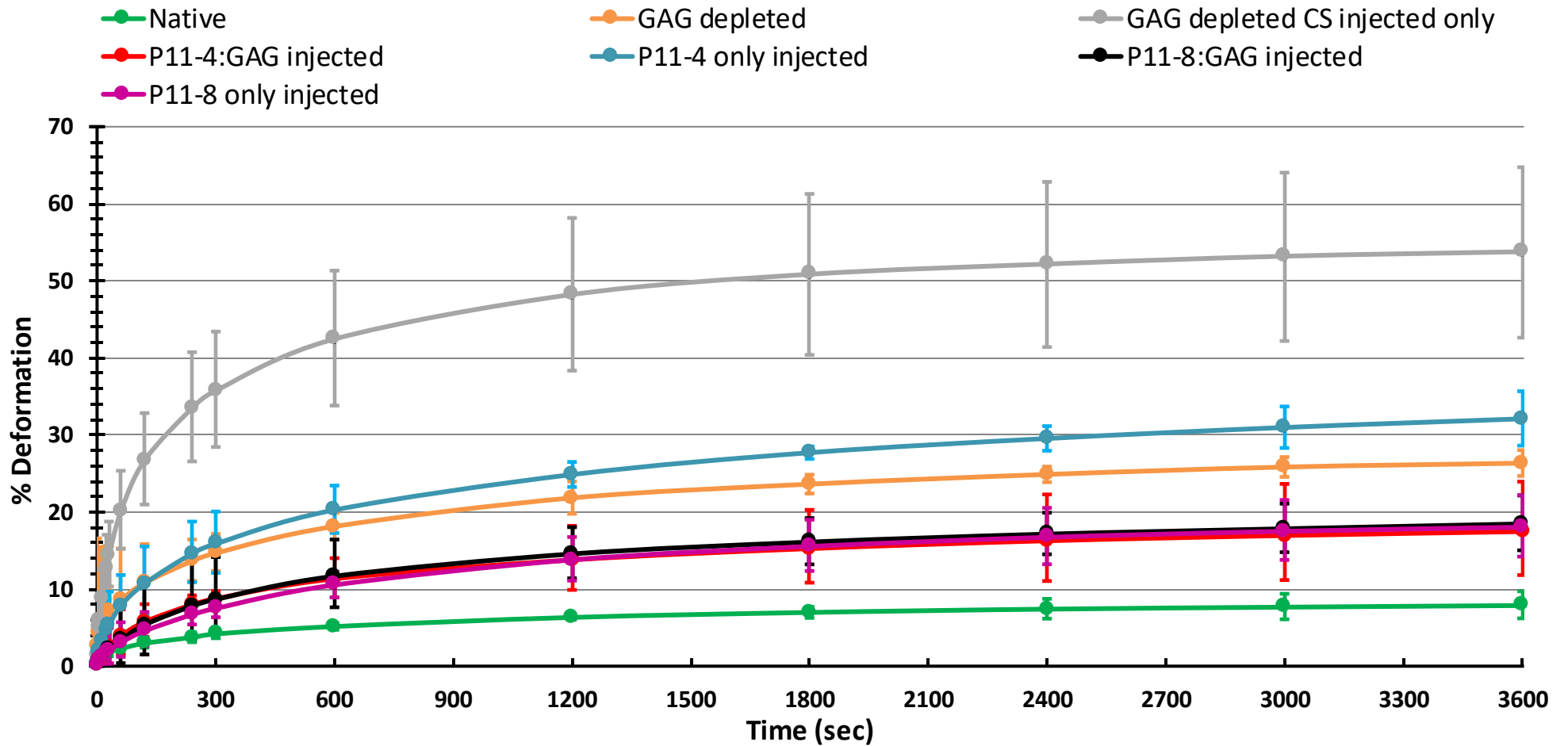


Figure 95: Percentage deformation of lateral condyles from: native, GAG depleted chondroitin sulfate (CS) injected only, GAG depleted, P₁₁-4: GAG injected, P₁₁-4 only injected, P₁₁-8: GAG injected, P₁₁-8 only injected groups, over the duration of 1 hour with a load of 0.31 N. Data was subject to arcsine transformation prior to calculation of the mean and 95 % confidence limits. Data is expressed as the back transformed mean (n=3) ± 95 % confidence limits.

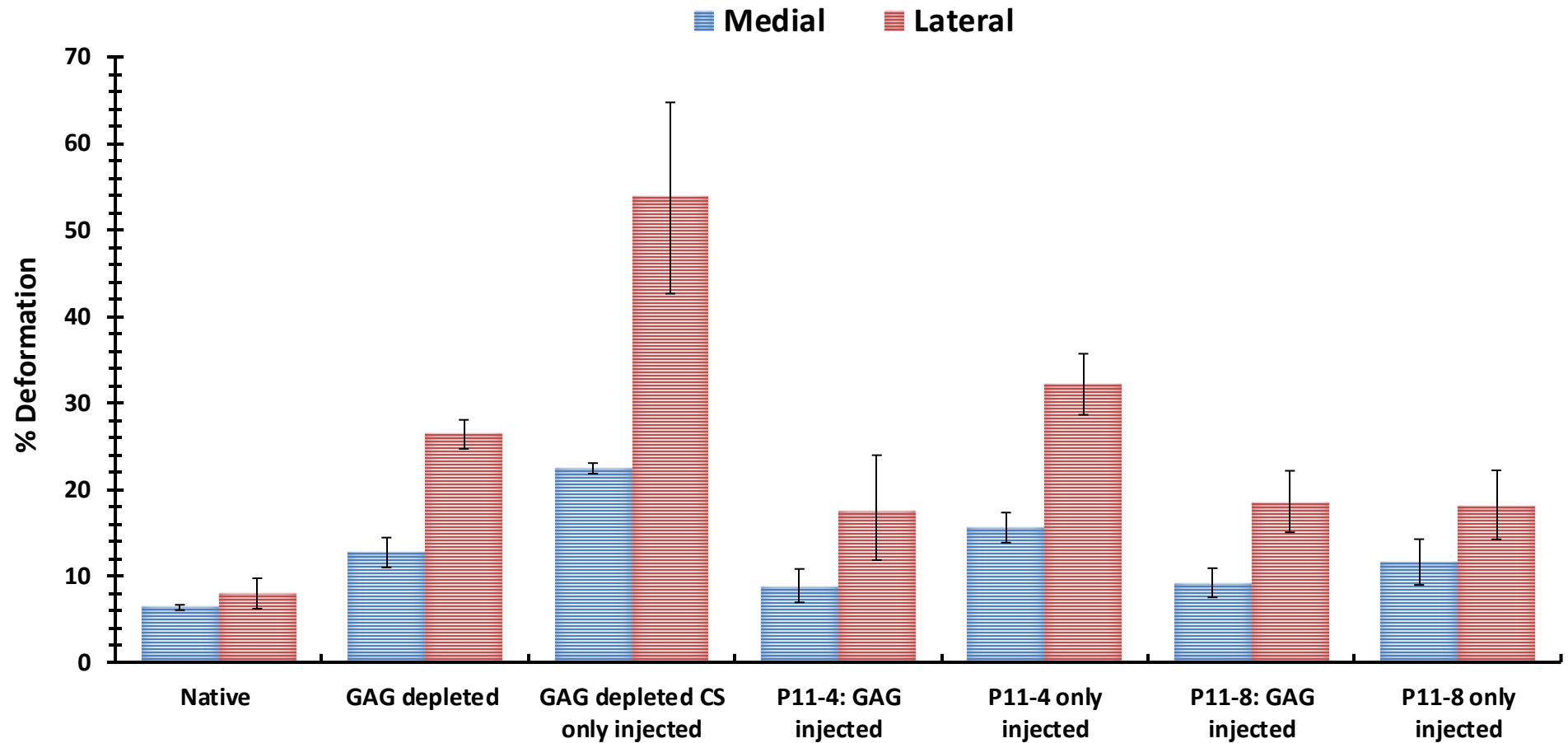


Figure 96: Final percentage deformation at 1 hour of all groups: native, GAG depleted chondroitin sulfate (CS) injected only, GAG depleted, P₁₁-4: GAG injected, P₁₁-4 only injected, P₁₁-8: GAG injected, P₁₁-8 only injected, for the medial and lateral condyles, with a load of 0.31 N. Data was subject to arcsine transformation prior to calculation of the mean (n=3) and 95 % confidence limits. Data is expressed as the back transformed mean (n=3) ± 95 % confidence limits.

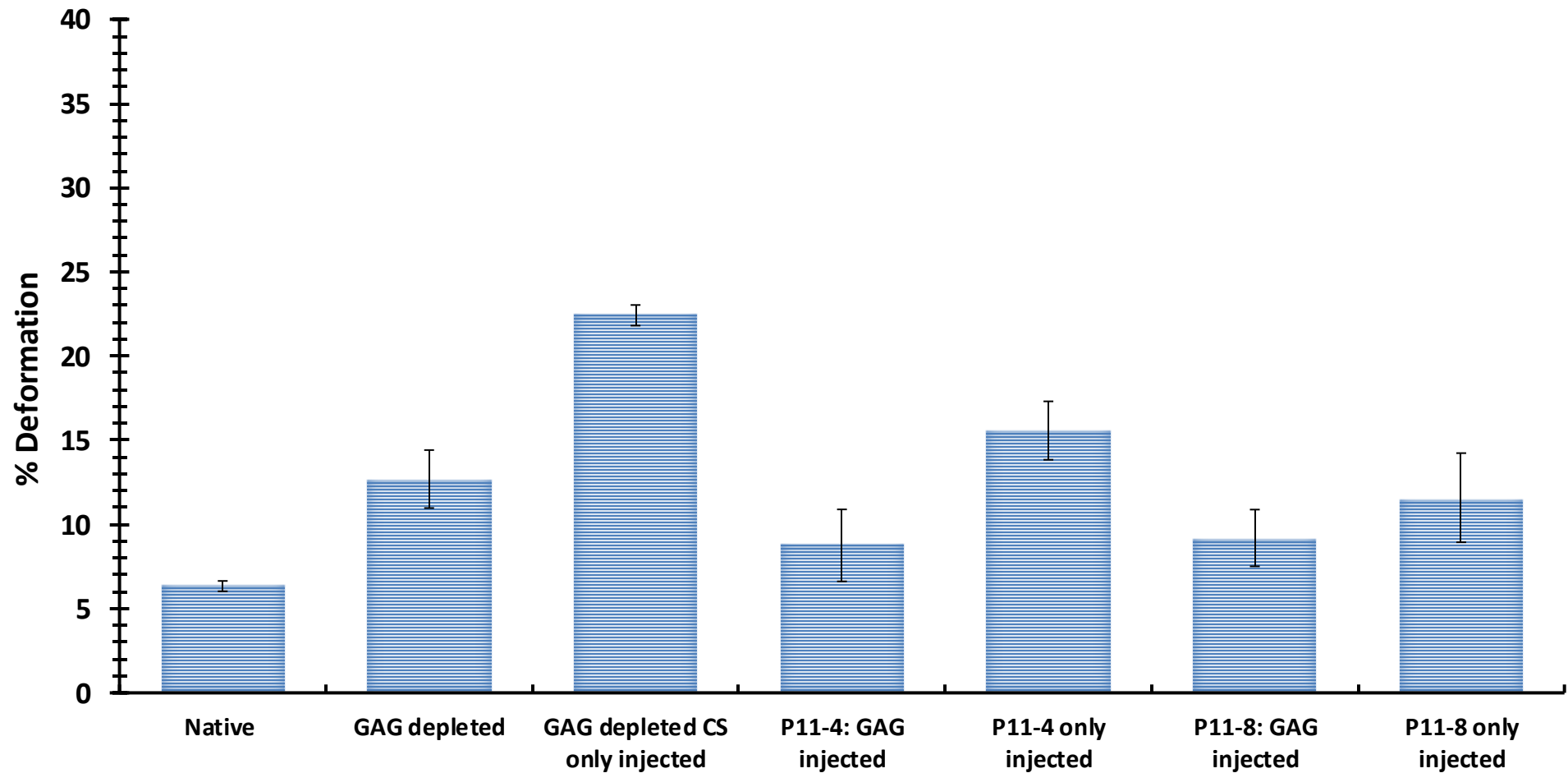


Figure 97: Final percentage deformation at 1 hour of medial condyles from: native, GAG depleted, GAG depleted chondroitin sulfate (CS) injected only, P₁₁-4: GAG injected, P₁₁-4 only injected, P₁₁-8: GAG injected, P₁₁-8 only injected, with a load of 0.31 N. Data was subject to arcsine transformation prior to calculation of the mean and 95 % confidence limits and statistical analysis. Data is expressed as the back transformed mean (n=3) ± 95 % confidence limits.

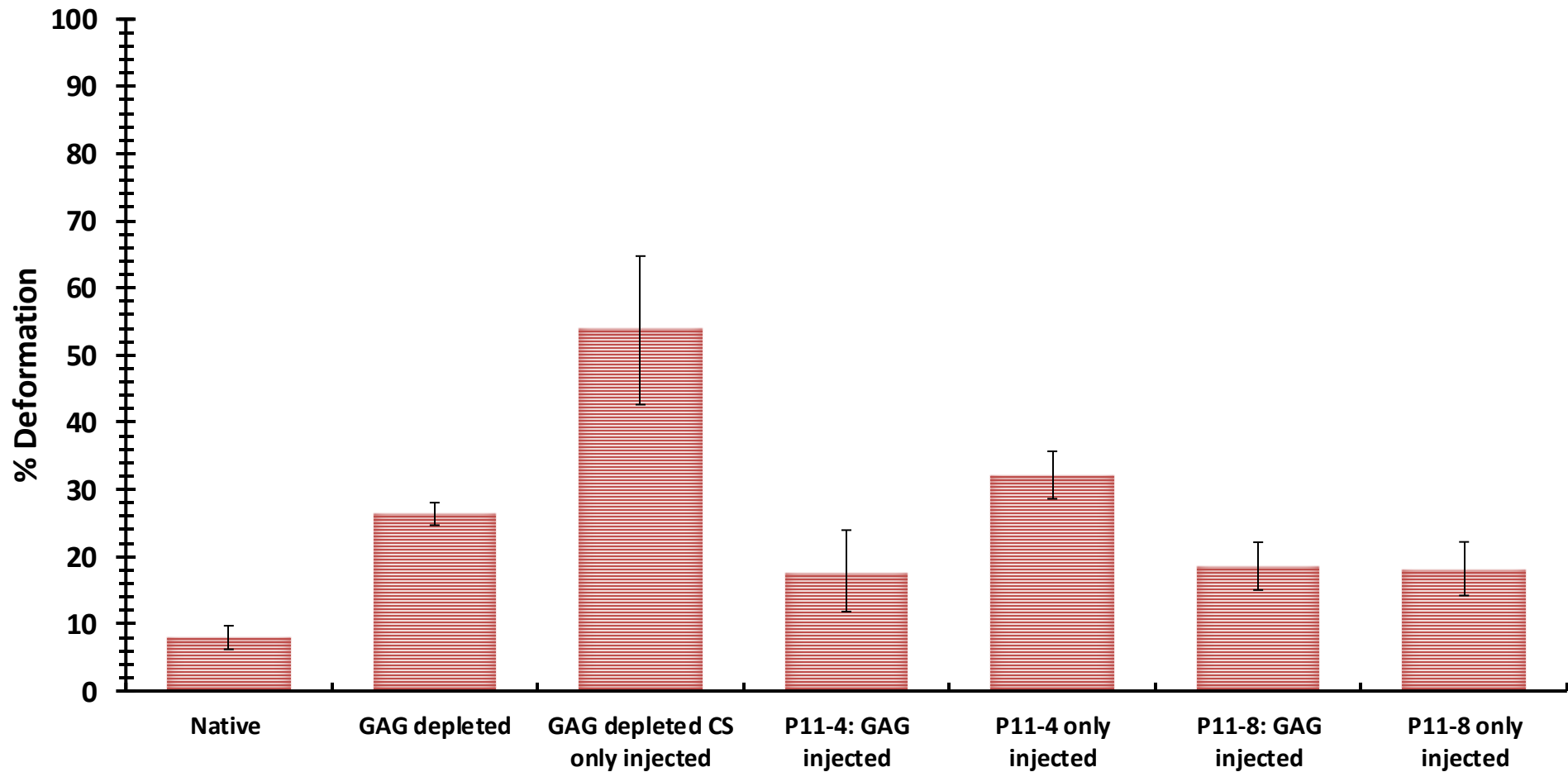


Figure 98: Final percentage deformation at 1 hour of lateral condyles from: native, GAG depleted, GAG depleted chondroitin sulfate (CS) injected only, P₁₁-4: GAG injected, P₁₁-4 only injected, P₁₁-8: GAG injected, P₁₁-8 only injected, with a load of 0.31 N. Data was subject to arcsine transformation prior to calculation of the mean and 95 % confidence limits and statistical analysis. Data is expressed as the back transformed mean (n=3) ± 95 % confidence limits.

The injection of chondroitin sulfate into the GAG depleted porcine condylar cartilage had a negative effect on the percentage deformation of the porcine condylar cartilage. An increase in the percentage deformation of 43.6 % in the medial and 51 % in the lateral condyles was observed when compared to the GAG depleted porcine condylar cartilage control. To determine if the peptides P₁₁-4 or P₁₁-8, or PEP: GAG mixtures improved the deformation properties of GAG depleted porcine condylar cartilage, the percentage deformation data at 1 hour between the PEP: GAG injected samples and the GAG depleted condylar cartilage, was compared. Due to the small sample size (n=3) the data was not subject to statistical analysis.

In the medial condyles, the data showed that injection of the GAG depleted condylar cartilage with P₁₁-4: GAG and P₁₁-8: GAG, reduced the percentage deformation by 30.7 % and 27.8 % respectively, when compared to the GAG depleted condylar cartilage control. However, when comparing the percentage deformation of GAG depleted porcine condylar cartilage injected with P₁₁-4: GAG and P₁₁-8: GAG, minimal differences were seen between the two, suggesting that neither of these two PEP: GAG mixtures were better than the other at reducing the percentage deformation of the GAG depleted condylar cartilage. GAG depleted condylar cartilage injected with P₁₁-4 and chondroitin sulfate only both appeared to increase the percentage deformation of GAG depleted condylar cartilage.

In the lateral condyles, the data showed that injection of the GAG depleted condylar cartilage with P₁₁-4: GAG, P₁₁-8: GAG and P₁₁-8 only, reduced the percentage deformation by 33.7 %, 30 % and 31.5 % respectively, when compared to the GAG depleted condylar cartilage control. However, when comparing the percentage deformation of the GAG depleted condylar cartilage injected with P₁₁-4: GAG, P₁₁-8: GAG and P₁₁-8 only, minimal differences were seen, which again indicated that neither of the two PEP: GAG mixtures nor the peptide only injection were significantly better than the others at reducing the percentage deformation of the GAG depleted condylar cartilage. Nevertheless, the PEP: GAG mixtures appeared to improve the deformation properties of GAG depleted lateral condylar cartilage, which was not the case for the GAG depleted condylar cartilage samples injected with P₁₁-4 and chondroitin sulfate only.

The percentage deformation data for the medial condyles showed that the GAG depleted condylar cartilage injected with P₁₁-4 only, P₁₁-8 only, P₁₁-8: GAG and chondroitin sulfate only all appeared to have a higher percentage deformation (15.5, 11.5 and 9.1 %, respectively) compared to the native condylar cartilage control (6.3 %). Although the GAG depleted condylar cartilage injected with P₁₁-4: GAG had a higher percentage deformation (8.7 %) than

the native condylar cartilage control, the difference between the two was less when compared to the latter groups. This indicated that the P₁₁-4: GAG mixture may be able to restore the deformation properties of GAG depleted porcine medial condylar cartilage to those of the native porcine medial condylar cartilage. However, the percentage deformation data of the lateral condyles for all the groups showed that the mean percentage deformations were higher than the native lateral condylar cartilage control.

6.5.3 Equilibrium elastic modulus and permeability

An FE model was used to calculate the equilibrium elastic modulus and permeability using the data from only the medial condyles, since the deformation curves in the lateral condyles gave high creep deformation (creep deformation > 15 % of the porcine condylar cartilage thickness). Hence the lateral condyle deformation data was excluded from being input into the FE model, as high levels of deformation would lead to inaccurate predictions of the equilibrium elastic modulus and permeability. The GAG depleted condylar cartilage samples injected with chondroitin sulfate only, were also excluded from the FE model for the same reasons.

Representative images of the deformation curve fittings for the GAG depleted porcine medial condylar cartilage injected with P₁₁-4: GAG, P₁₁-4 only, P₁₁-8: GAG and P₁₁-8 only are shown in Figure 99A-D. These curve fittings were used to calculate the equilibrium elastic modulus and permeability of the samples.

Perusal of the data showed that the GAG depleted condylar cartilage injected with the PEP: GAG (both P₁₁-4 and P₁₁-8) had lower deformation than the GAG depleted condylar cartilage injected with the peptides alone. The curve fittings shown in Figure 99A-D, show how close the FE model curve fitting was to the last 70% of the experimental deformation curve and this was confirmed by the R² values for the above graphs, which were: P₁₁-4: GAG = 0.953; P₁₁-4 only = 0.954; P₁₁-8: GAG = 0.951; P₁₁-8 only = 0.954. The higher the value of R² the closer the fit between the experimental and FE model curves. Only samples with an R² value greater than 75% were accepted as relevant and accurate enough for this study.

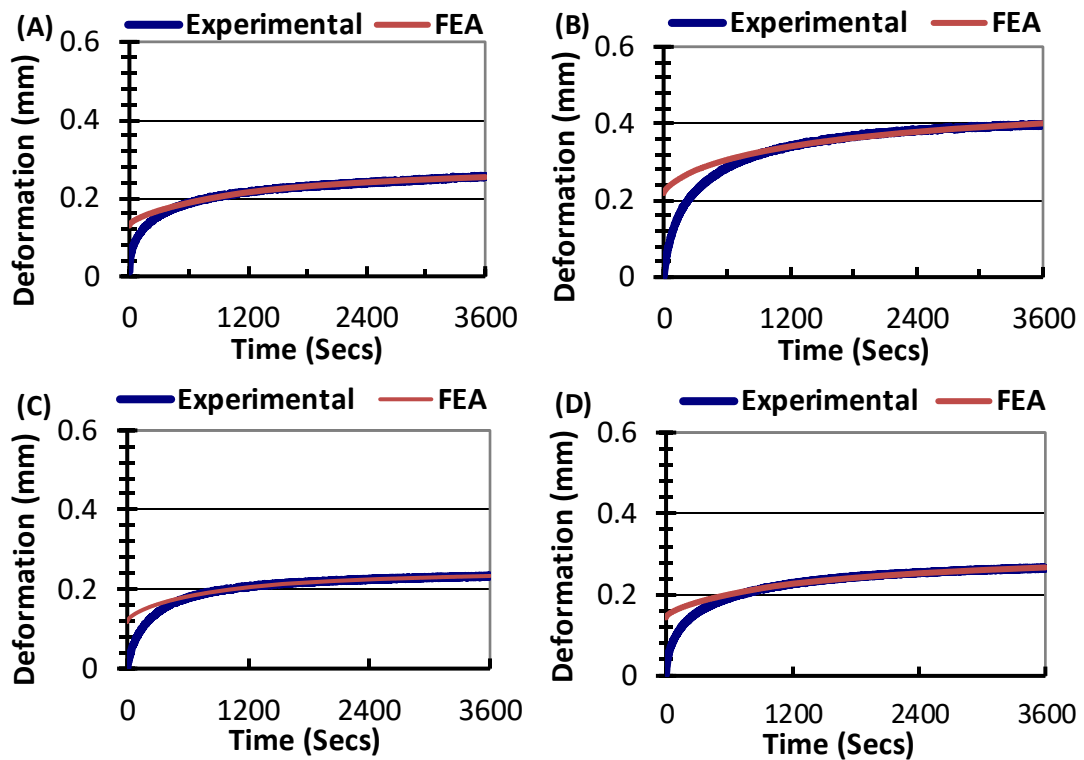


Figure 99: Representative graphs of indentation characteristics obtained experimentally and through FEA model curve fitting of a medial porcine condyle under a load of 0.31 N.

(A): Curve fitting the deformation profile of a GAG depleted porcine medial condyle injected with P11-4: GAG (B): Curve fitting the deformation profile of a GAG depleted porcine medial condyle injected with P11-4 only (C): Curve fitting the deformation profile of a GAG depleted porcine medial condyle injected with P11-8: GAG (D): Curve fitting the deformation profile of a GAG depleted porcine medial condyle injected with P11-8 only.

The equilibrium elastic modulus and permeability values for the medial condyles of the GAG depleted cartilage injected with P₁₁-4: GAG, P₁₁-8: GAG, P₁₁-4 only, P₁₁-8 only and their corresponding native and GAG depleted condylar cartilage are shown in Figure 100. The data was compared to determine differences between group means. This showed that the native condylar cartilage exhibited a higher average equilibrium elastic modulus when compared to the GAG depleted condylar cartilage injected with P₁₁-8: GAG, P₁₁-4 only, P₁₁-8 only as well as the GAG depleted condylar cartilage control. However, the data showed that the injection of P₁₁-4: GAG to the GAG depleted condylar cartilage had minimal effect on the mean elastic modulus (0.43 MPa) when compared to the native condylar cartilage control (0.5 MPa). It was also observed that the addition of the GAG to the P₁₁-4 peptide, appeared to substantially increase the equilibrium elastic modulus, hence stiffness, of the GAG depleted condylar cartilage, which was not the case in the samples injected with the P₁₁-8 peptide. Nevertheless, both the PEP: GAG mixtures (P₁₁-4: GAG and P₁₁-8: GAG) appeared to be stiffer than GAG depleted condylar cartilage control.

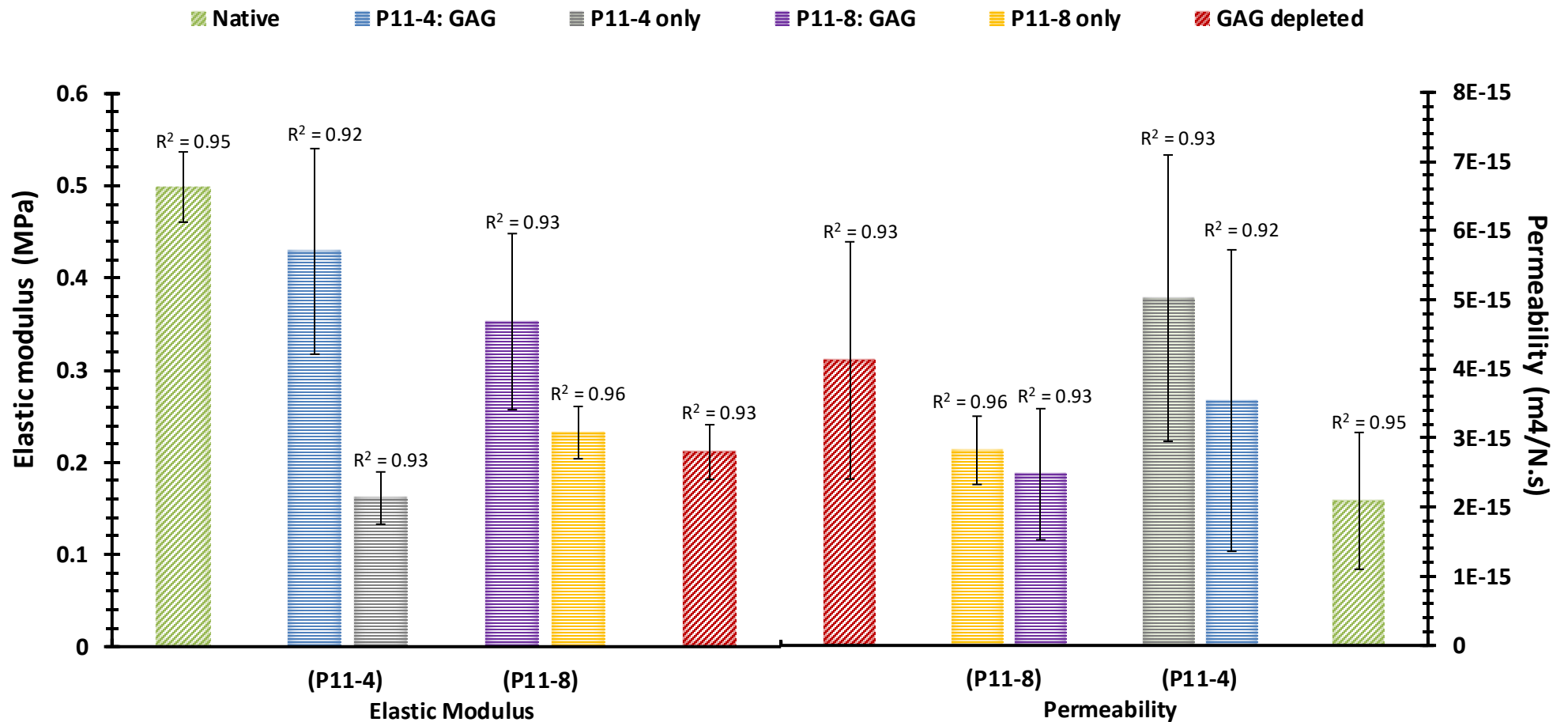


Figure 100: Elastic modulus and permeability of GAG depleted porcine medial condylar cartilage injected with P₁₁₋₄: GAG, P₁₁₋₄ only, P₁₁₋₈: GAG, P₁₁₋₈ only and their corresponding native and GAG depleted condylar cartilage controls, under a load of 0.31 N. Data is expressed as the mean (n=3) ± 95 % confidence limits. The R² values define how close the FE model curve fitting was to the last 70% of the experimental deformation curve, the closer the R² value is to 1, the better the fit.

6.5.4 Summary of the effects of injecting GAG-depleted porcine medial condylar cartilage with peptides and PEP: GAG mixtures on the percentage deformation, elastic modulus and permeability values for all groups tested.

A summary of the effects of injecting GAG depleted medial porcine condylar cartilage with P₁₁-4: GAG, P₁₁-4 only, P₁₁-8: GAG and P₁₁-8 only when compared to native and GAG depleted medial porcine condylar cartilage is presented in Table 29. The study suggests that the injection of the P₁₁-4: GAG mixture may be able to restore the biomechanical properties of the GAG-depleted porcine medial condylar cartilage to levels that were not too different to native porcine medial condylar cartilage.

Table 29: Summary table of the percentage deformation, elastic modulus and permeability and the difference between the GAG depleted medial porcine condylar cartilage sample injected with P₁₁-4: GAG, P₁₁-4 only, P₁₁-8: GAG and P₁₁-8 only and the native and GAG depleted medial porcine condylar cartilage.

		P ₁₁ -4 alone	P ₁₁ -4:GAG	P ₁₁ -8 alone	P ₁₁ -8:GAG
Percentage deformation	Vs GAG depleted	ND	↓	ND	↓
	Vs Native	↑	ND	↑	↑
Permeability	Vs GAG depleted	ND	ND	ND	ND
	Vs Native	ND	ND	ND	ND
Elastic modulus	Vs GAG depleted	ND	↑	ND	↑
	Vs Native	↓	ND	↓	↓

Key: (↑) = higher; (↓) = lower; (ND) = no difference.

6.5.5 Fluorescence recovery after photobleaching (FRAP) analysis to determine self-assembly of injected fluorescein-doped P₁₁-4 and P₁₁-8 and fluorescein-doped PEP: GAG mixtures in GAG depleted condylar cartilage.

Representative images of GAG depleted porcine medial condylar cartilage injected with fluorescein-tagged peptide doped P₁₁-4: GAG and P₁₁-4 only, and fluorescein-tagged peptide-doped P₁₁-8: GAG and P₁₁-8 only, are presented in Figure 101, Figure 102, Figure 103 and Figure 104, respectively. Images of GAG depleted cartilage injected with chondroitin sulfate only, native and GAG depleted cartilage controls are presented in Figure 105, Figure 106 and Figure 107, respectively. All images were captured after indentation testing had been performed. Sections of the cartilage presented in these images were taken parallel to the cartilage surface. Images of the injected cartilage samples were captured using both

transmitted light and with the fluorescein filter. For each cartilage sample that had been injected with the fluorescein-tagged peptide, PEP: GAG mixture or fluorescein doped chondroitin sulfate; images were taken before photobleaching ($t=1$ sec), immediately after bleaching ($t=6$ secs) and after 1 min of recovery. A recovery curve was also recorded, which showed the fluorescence intensity of the ROI that had been photobleached (red line/circle) and the fluorescence intensity of the control ROI (green line/circle), over a period of 1 min.

6.5.5.1 GAG depleted porcine medial condylar cartilage injected with fluorescein-tagged peptide-doped P₁₁-4: GAG and fluorescein-tagged peptide-doped P₁₁-4 alone.

Images of GAG depleted condylar cartilage injected with fluorescein-tagged peptide-doped P₁₁-4: GAG, are presented in Figure 101. The injection sites of GAG depleted cartilage that were injected with fluorescein-tagged peptide doped P₁₁-4: GAG are shown in Figure 101 (A) to (D). The green fluorescence present around the injection sites and surrounding areas was due to the diffusion of the fluorescein-tagged P₁₁-4: GAG throughout the thickness of the cartilage. The bleached ROI outlined by the red circle in Figure 101 (B) was much darker, when compared to the same ROI in Figure 101 (A), in which the GAG depleted cartilage sample had not been bleached. GAG depleted cartilage samples injected with fluorescein-tagged peptide-doped P₁₁-4: GAG demonstrated no fluorescence recovery, which was confirmed by the recovery curve shown in Figure 101 (F). The initial fluorescence intensity of the bleached ROI and the control ROI was 100 and 106, respectively. After bleaching ($t=6$ s), the fluorescence intensity of the bleached ROI was reduced to 79, and it recovered by 2% to 81 and remained at this intensity for the duration of the test (1 minute). However, the fluorescence intensity of the control ROI steadily decreased over the duration of the experiment, which was due to the inherent photo-bleaching of imaging the sample, over a period of time. Nevertheless, the fluorescence intensity of the control ROI remained relatively constant.

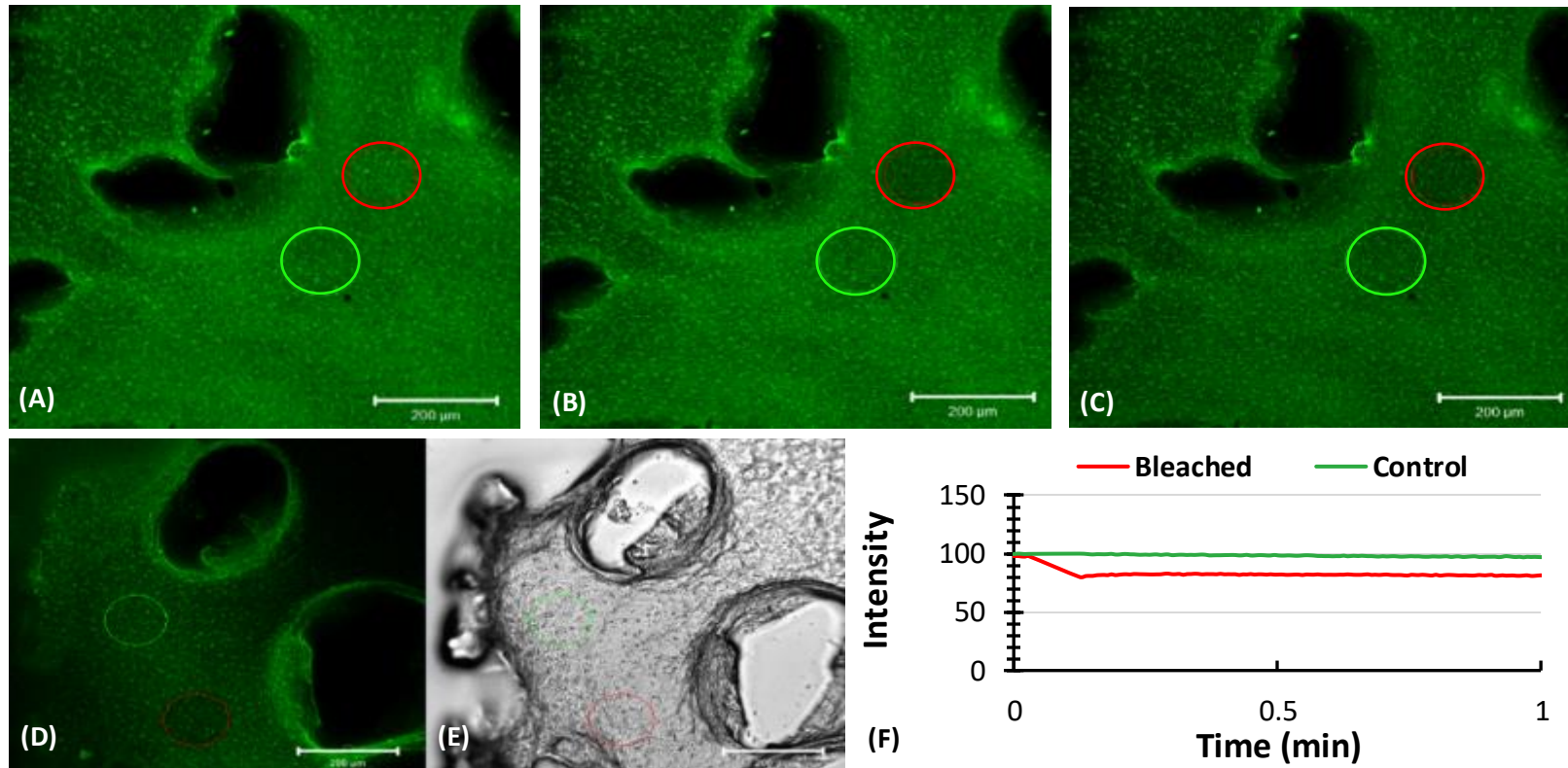


Figure 101: Representative FRAP images of GAG depleted porcine condylar cartilage injected with fluorescein-tagged peptide-doped P₁₁-4: GAG. Red lines/circles highlight the ROIs that were bleached in each sample and the green lines/circles highlight the ROIs that were used as control areas in each sample. (A) Image of a GAG depleted condylar cartilage sample injected with fluorescein-tagged peptide-doped P₁₁-4: GAG prior to bleaching (t=1 s), (B) Image of a GAG depleted condylar cartilage sample injected with fluorescein-tagged peptide-doped P₁₁-4: GAG immediately after bleaching (t=6 s), (C) Image of a GAG depleted condylar cartilage sample injected with fluorescein-tagged peptide-doped P₁₁-4: GAG after recovery (t=60 s). (D) GAG depleted condylar cartilage injected with fluorescein-tagged peptide-doped P₁₁-4: GAG, imaged with a fluorescein filter compared to (E) the same sample imaged in transmitted light. (F) Recovery curve for a GAG depleted medial condylar cartilage sample injected with fluorescein-tagged peptide-doped P₁₁-4: GAG, which revealed no recovery in the bleached area. All images were captured from sections of medial condyles.

Images of GAG depleted condylar cartilage injected with fluorescein-tagged peptide-doped P_{11-4} on its own, are presented in Figure 102. The injection sites of GAG depleted cartilage that were injected with fluorescein-tagged peptide-doped P_{11-4} alone are shown in Figure 102 (A) to (D). The green fluorescence present around the injection sites and surrounding areas was due to the diffusion of the fluorescein-tagged P_{11-4} throughout the thickness of the cartilage. The bleached ROI outlined by the red circle in Figure 102 (B) was much darker, when compared to the same ROI in Figure 102 (A), in which the GAG depleted cartilage sample had not been photobleached. GAG depleted cartilage samples injected with fluorescein-tagged peptide-doped P_{11-4} alone, demonstrated no fluorescence recovery, which was confirmed by the recovery curve in shown in Figure 102 (F). The initial fluorescence intensity for both bleached ROI and the control ROI was 120. After bleaching ($t=6$ s), the fluorescent intensity of the bleached ROI reduced to ~ 92 , where it recovered by 0.7 % to ~ 93 and remained at this intensity for the duration of the test (1 minute). The fluorescence intensity of the control ROI remained constant throughout the test.

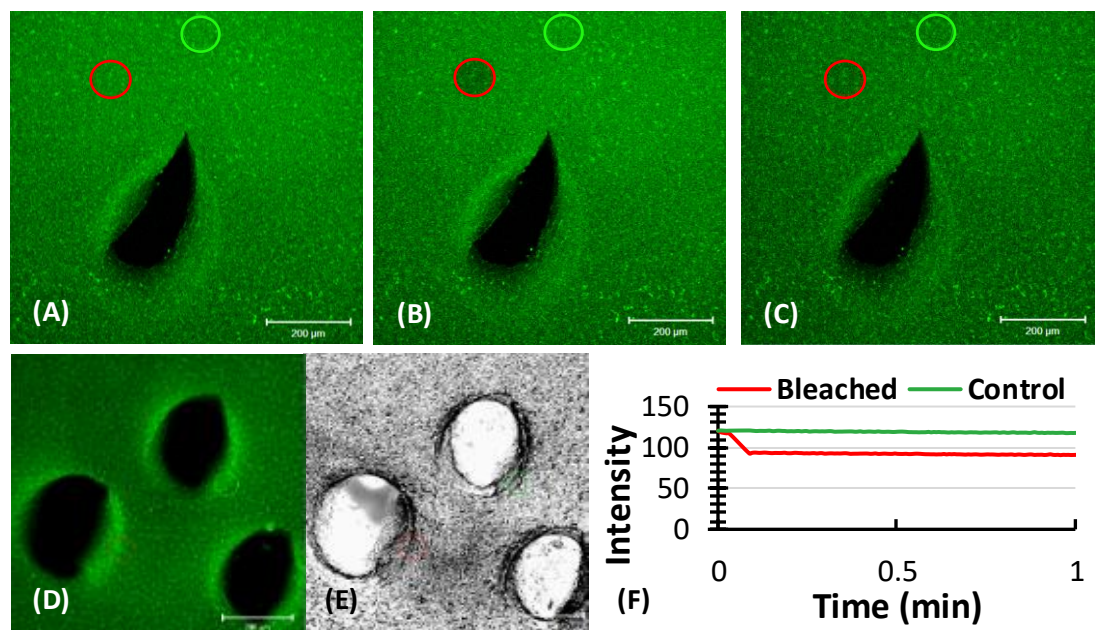


Figure 102: Representative FRAP images of porcine GAG depleted condylar cartilage injected with fluorescein-tagged peptide-doped P_{11-4} alone. Red lines/circles highlight the ROIs that were bleached in each sample and the green lines/circles highlight the ROIs that were used as control areas in each sample. (A) Image of a GAG depleted condylar cartilage sample injected with fluorescein-tagged peptide-doped P_{11-4} alone prior to bleaching ($t=1$ s), (B) Image of a GAG depleted condylar cartilage sample injected with fluorescein-tagged peptide-doped P_{11-4} alone immediately after photobleaching ($t=6$ s), (C) Image of a GAG depleted condylar cartilage sample injected with fluorescein-tagged peptide-doped P_{11-4} alone after recovery ($t=60$ s). (D) GAG depleted condylar cartilage injected with fluorescein-tagged peptide-doped P_{11-4} alone, imaged with a fluorescent filter compared to (E) the same sample imaged in transmitted light. (F) Recovery curve for a GAG depleted condylar cartilage sample injected with fluorescein-tagged peptide-doped P_{11-4} alone, which revealed no recovery in the bleached area. All images were captured from sections of medial condyles.

6.5.5.2 GAG depleted condylar cartilage injected with fluorescein-tagged peptide-doped P₁₁₋₈: GAG and fluorescein-tagged peptide-doped P₁₁₋₈ alone.

Images of GAG depleted condylar cartilage injected with fluorescein-tagged peptide-doped P₁₁₋₈: GAG are presented in Figure 103. Figure 103 (A) to (D) show the injection sites of GAG depleted cartilage that was injected with fluorescein-tagged peptide-doped P₁₁₋₈: GAG. The green fluorescence seen around the injection sites and surrounding areas was due to the diffusion of the fluorescein-tagged peptide-doped P₁₁₋₈: GAG throughout the thickness of the cartilage. The bleached ROI outlined by the red circle in Figure 103 (B) was much darker due to the bleaching, when compared to the same ROI in Figure 103 (A), where the GAG depleted cartilage sample had not been bleached. GAG depleted cartilage samples injected with fluorescein-tagged peptide-doped P₁₁₋₈: GAG demonstrated no fluorescence recovery, which was confirmed by the recovery curve in Figure 103 (F). The initial fluorescence intensity of both the bleached ROI and the control ROI was 108. After bleaching (t=6 s), the fluorescence intensity of the bleached ROI reduced to ~89, where it recovered by 0.3 % to ~90 and remained at this intensity for the duration of the test (1 minute). The fluorescence intensity of control ROI stayed constant over the duration of the experiment.

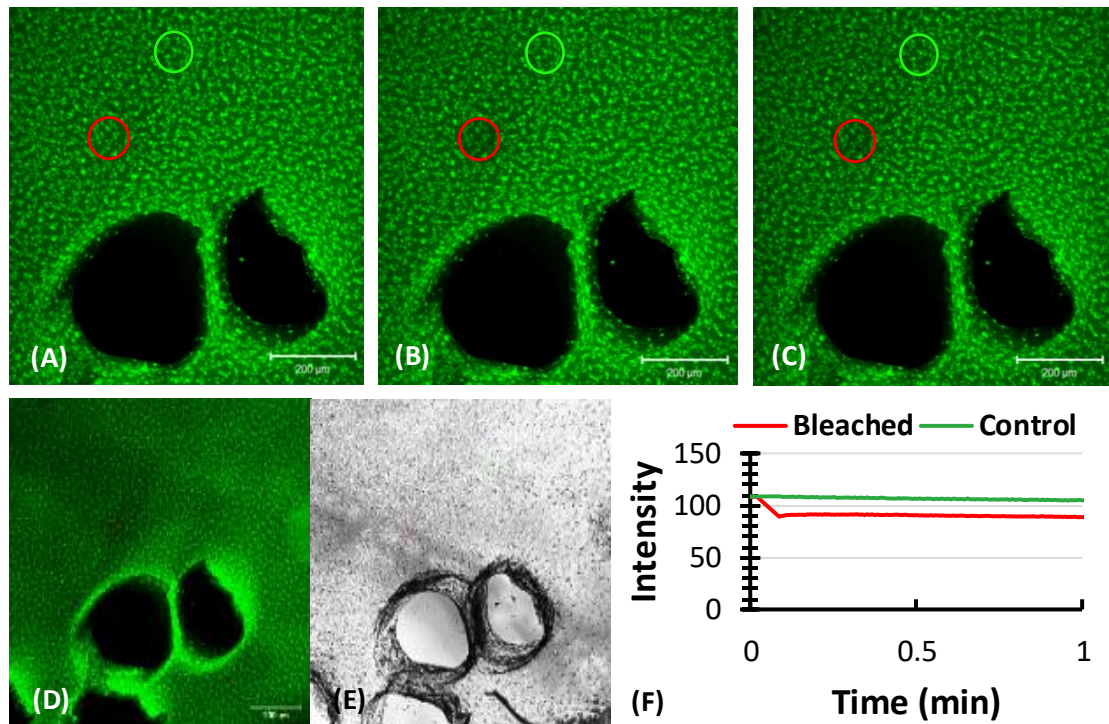


Figure 103: Representative FRAP images of porcine GAG depleted condylar cartilage injected with fluorescein-tagged peptide-doped P₁₁-8: GAG. Red lines/circles highlight the ROIs that were bleached in each sample and the green lines/circles highlight the ROIs that were used as control areas in each sample. (A) Image of a GAG depleted condylar cartilage sample injected with fluorescein-tagged peptide-doped P₁₁-8: GAG prior to bleaching (t=1s), (B) Image of a GAG depleted condylar cartilage sample injected with fluorescein-tagged peptide-doped P₁₁-8: GAG straight after bleaching (t=6s), (C) Image of a GAG depleted condylar cartilage sample injected with fluorescein-tagged peptide-doped P₁₁-8: GAG after recovery (t=60s). (D) GAG depleted condylar cartilage injected with fluorescein-tagged peptide-doped P₁₁-8: GAG, imaged with a fluorescein filter compared to (E) the same sample imaged in transmitted light. (F) Recovery curve for a GAG depleted condylar cartilage sample injected with fluorescein-tagged peptide-doped P₁₁-8: GAG, which revealed no recovery in the bleached area. All images were captured from sections of medial condyles.

Images of GAG depleted condylar cartilage injected with fluorescein-tagged peptide-doped P₁₁-8 on its own, are presented in Figure 104. Figure 104 (A) to (D) show the injection sites of GAG depleted cartilage that was injected with fluorescein-tagged peptide-doped P₁₁-8. The bleached ROI outlined by the red circle in Figure 104 (B) was much darker, when compared to the same ROI in Figure 104 (A), where the GAG depleted cartilage sample had not been bleached. GAG depleted cartilage samples injected with fluorescein-tagged peptide-doped P₁₁-8 on its own, demonstrated no fluorescence recovery, which was confirmed by the recovery curve in Figure 104 (F). The starting fluorescent intensity for the bleached ROI and the control ROI was ~ 80 and ~ 82, respectively. After bleaching (t=6 s), the fluorescent intensity of the bleached ROI as reduced to ~ 58, subsequently no fluorescence recovery was

observed for the remainder of the test (1 minute). The fluorescent intensity of the control ROI stayed constant throughout the test.

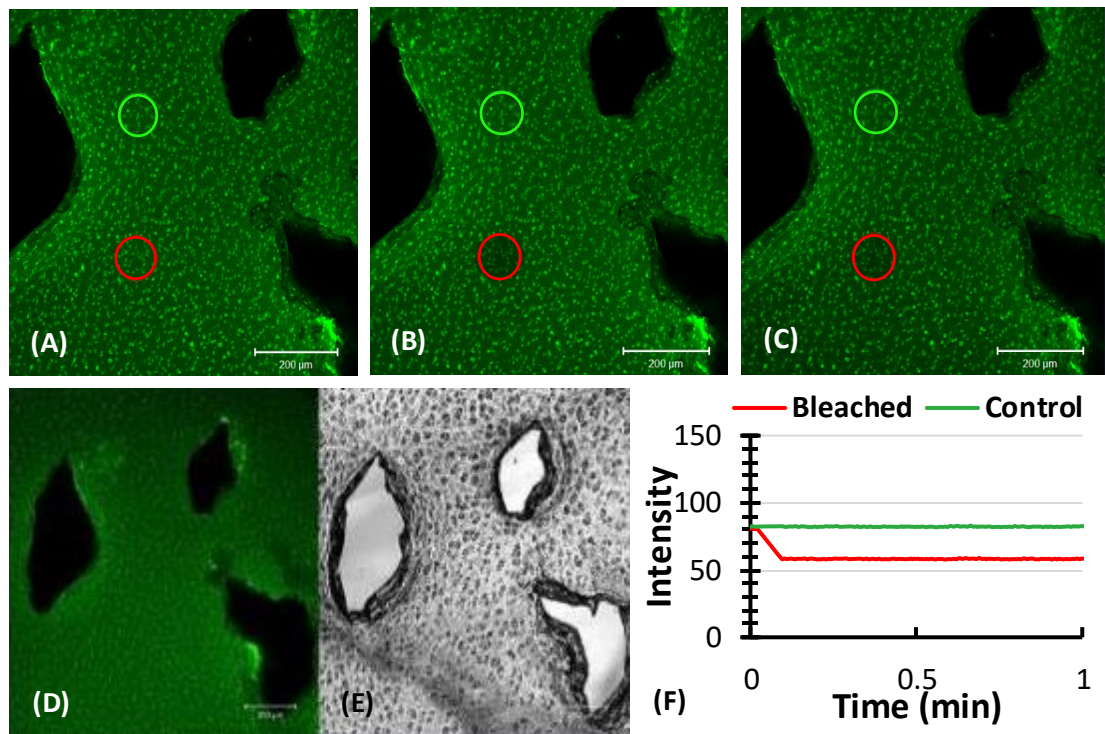


Figure 104: Representative FRAP images of porcine GAG depleted condylar cartilage injected with fluorescein-tagged peptide-doped P₁₁-8 only. Red lines/circles highlight ROI that were bleached in each sample and the green lines/circles highlight ROI that were used as control areas in each sample. (A) Image of a GAG depleted condylar cartilage sample injected with fluorescein-tagged peptide-doped P₁₁-8 only prior to bleaching (t=1 s), (B) Image of a GAG depleted condylar cartilage sample injected with fluorescein-tagged peptide-doped immediately after bleaching (t=6 s), (C) Image of a GAG depleted condylar cartilage sample injected with fluorescein-tagged peptide-doped P₁₁-8 only after recovery (t=60 s). (D) GAG depleted condylar cartilage injected with fluorescein-tagged peptide-doped P₁₁-8 only, imaged with a fluorescent filter compared to (E) the same sample imaged in transmitted light. (F) Recovery curve for a GAG depleted condylar cartilage sample injected with fluorescein-tagged peptide-doped P₁₁-8 only, which revealed no recovery in the bleached area. All images were taken from sections of medial condyles.

6.5.5.3 GAG depleted condylar cartilage injected with fluorescein-tagged CS alone.

Images of GAG depleted condylar cartilage injected with fluorescein-tagged chondroitin sulfate, are presented in Figure 105. Figure 105 (A) to (D) show the injection sites of GAG depleted cartilage that was injected with fluorescein-tagged chondroitin sulfate. The green fluorescence surrounding the injection site was slightly more intense in these particular samples, which could have been due to the increased mobility of the fluorescein-tagged chondroitin sulfate without the peptide that allowed it to move more freely throughout the thickness of the GAG depleted cartilage. The bleached ROI outlined by the red circle in Figure 105 (B) was darker, when compared to the same ROI in Figure 105 (A), in which the GAG

depleted cartilage sample had not been bleached. GAG depleted cartilage samples injected with fluorescein-tagged chondroitin sulfate, demonstrated fluorescence recovery. The initial fluorescence intensity for the bleached ROI and the control ROI was ~ 137 and ~ 139 , respectively. After bleaching ($t=6s$), the fluorescence intensity of the bleached ROI reduced to ~ 91 . However, after 1 minute the sample had recovered by 88 % and after 2 minutes it had fully recovered to its original fluorescence intensity. This was confirmed by Figure 105 (C), in which the bleached ROI (red circle) was no longer darkened and had returned to its original shade of green. The fluorescence intensity of the control ROI stayed constant throughout the test.

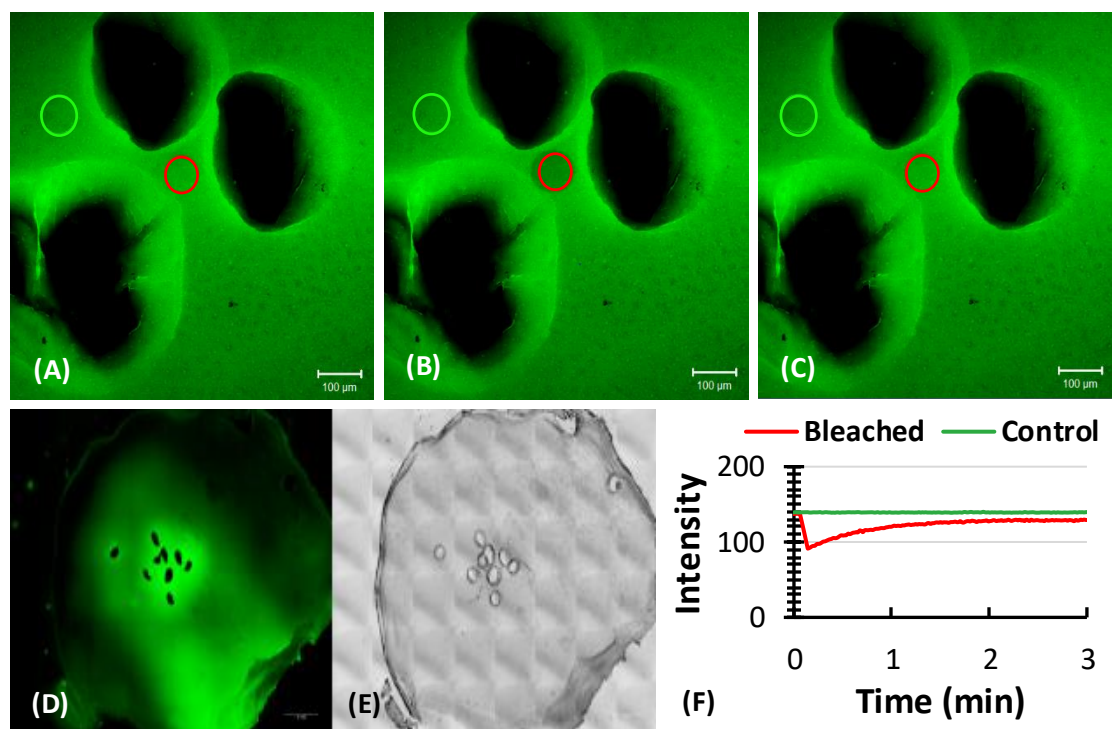


Figure 105: Representative FRAP images of porcine GAG depleted condylar cartilage injected with fluorescein-tagged chondroitin sulfate (CS). Red lines/circles highlight the ROIs that were bleached in each sample and the green lines/circles highlight the ROIs that were used as control areas in each sample. (A) Image of a GAG depleted condylar cartilage sample injected with fluorescein-tagged CS prior to bleaching ($t=1s$), (B) Image of a GAG depleted condylar cartilage sample injected with fluorescein-tagged CS straight after bleaching ($t=6s$), (C) Image of a GAG depleted condylar cartilage sample injected with fluorescein-tagged CS after recovery ($t=60s$). (D) GAG depleted condylar cartilage injected with fluorescein-tagged CS, imaged with a fluorescent filter compared to (E) the same sample imaged in transmitted light. (F) Recovery curve for a GAG depleted condylar cartilage sample injected with fluorescein-tagged CS, which revealed recovery in the bleached area. All images were taken from sections of medial condyles.

6.5.5.4 Native condylar cartilage.

Images of untreated native condylar cartilage after indentation testing, are presented in Figure 106. Tiled images of native cartilage sections cut perpendicular to the surface of cartilage, viewed under transmitted light and a fluorescein filter are shown in Figure 106 (A) and Figure 106 (B), respectively. No fluorescence was observed, in Figure 106 (B), as the native condylar cartilage had not been exposed or injected with any fluorescent fluorophore, prior to viewing it. Figure 106 (C) and (D) are zoomed in images (Mag x 25) of Figure 106 (A) and (B) which also showed no fluorescence.

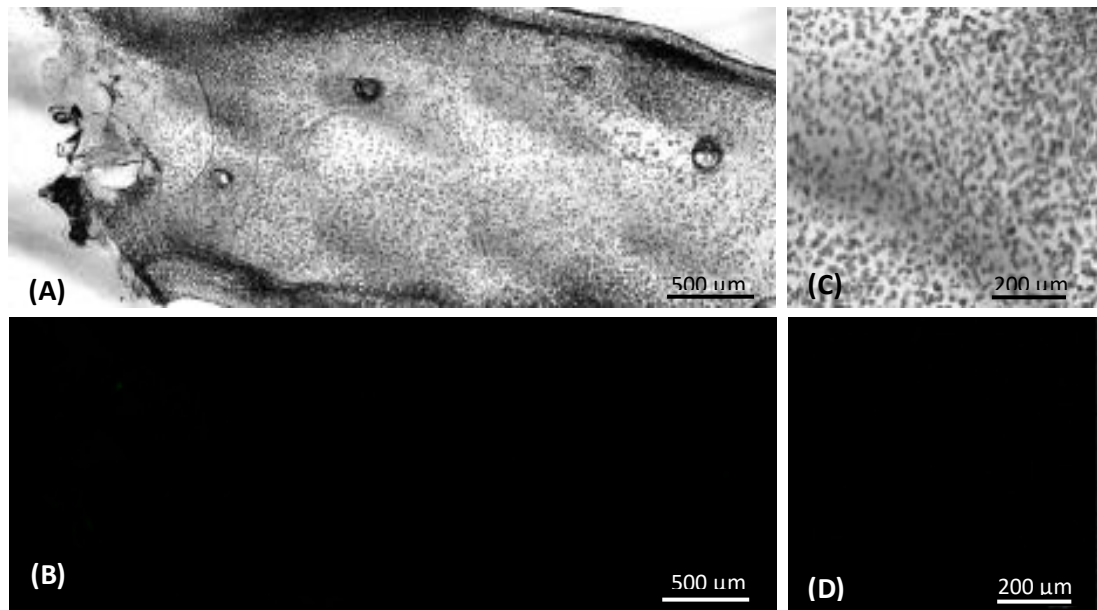


Figure 106: Representative images of native porcine condylar cartilage viewed under a fluorescein filter and transmitted light. (A) Tiled image of a native condylar cartilage sample viewed under transmitted light and (B) a fluorescein filter, which showed no fluorescence. (C) Magnified image (x 25) of a native condylar cartilage sample viewed under transmitted light and (D) a fluorescein filter, which showed no fluorescence. All images were taken from sections of medial condyles.

6.5.5.5 GAG depleted condylar cartilage.

Images of untreated GAG depleted condylar cartilage after indentation testing, are presented in Figure 107. Tiled images of a GAG depleted cartilage section cut perpendicular to the surface of cartilage, viewed under transmitted light and a fluorescein filter are shown in Figure 107 (A) and Figure 107 (B), respectively. No fluorescence was observed, in Figure 107 (B), as the GAG depleted condylar cartilage had not been exposed or injected with any fluorescent fluorophore, prior to viewing it. Figure 107 (C) and (D) are zoomed in images (Mag x 25) of Figure 107 (A) and (B) which also showed no fluorescence.

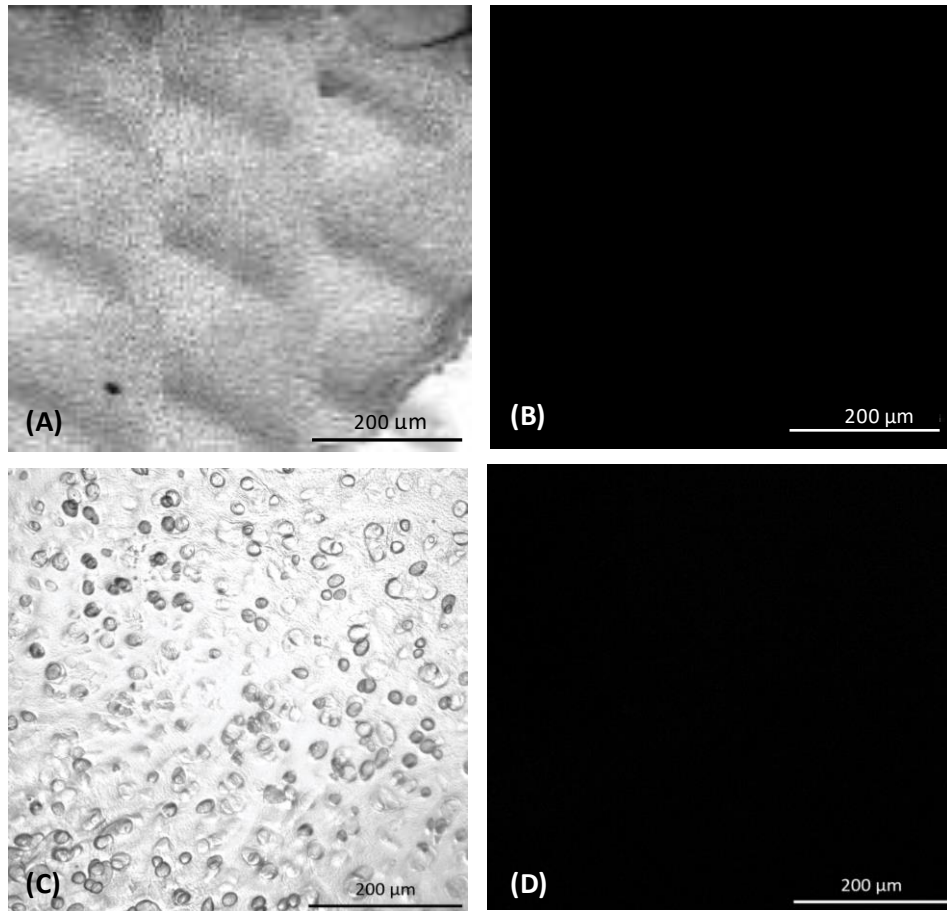


Figure 107: Representative images of porcine GAG depleted condylar cartilage viewed under a fluorescein filter and transmitted light. (A) Tiled image of a GAG depleted condylar cartilage sample viewed under transmitted light and (B) a fluorescein filter, which showed no fluorescence. (C) Magnified image (x 25) of a GAG depleted condylar cartilage sample viewed under transmitted light and (D) a fluorescein filter, which showed no fluorescence. All images were taken from sections of medial condyles.

6.6 Discussion

The aim of this study was to investigate the effect of injecting PEP: GAG mixtures and peptide alone (P_{11-4} and P_{11-8}) on the deformation, elastic modulus and permeability of GAG depleted porcine condylar cartilage. The ideal PEP: GAG mixture or peptide alone would give rise to a significant decrease in the percentage deformation, a significant increase in the equilibrium elastic modulus and a significant decrease in permeability between the treated GAG depleted porcine condylar cartilage and the GAG depleted porcine condylar cartilage control. Furthermore, the treated GAG depleted porcine condylar cartilage mixture would have a percentage deformation, equilibrium elastic modulus and permeability that was not significantly different to the native condylar cartilage. From the studies carried out in this chapter, there was clear evidence that injection of the P_{11-4} : GAG mixture restored the deformation and equilibrium elastic modulus of GAG depleted porcine medial condylar

cartilage to levels that were not significantly different to those of native porcine medial condylar cartilage, whilst remaining self-assembled *in situ*. Injection of the P₁₁-8: GAG mixture; however, restored the deformation properties of GAG depleted porcine medial condylar cartilage but not the equilibrium elastic modulus. The P₁₁-8: GAG mixture also remained self-assembled *in situ*. Conclusions regarding the difference in the permeability values could not be drawn, as the permeability values between the native and GAG depleted porcine condylar cartilage controls were not significantly different.

It was observed that there was no significant difference in the cartilage thicknesses between any of the medial condylar cartilage tested samples. No significant differences in the thicknesses of the lateral condylar cartilage was observed in the majority of the groups. However, the thickness of the native lateral condylar cartilage was significantly greater than the GAG depleted lateral condylar cartilage injected with: CS only, P₁₁-8 and the native condylar cartilage injected with no fluid. The reasons for this are unclear, however it is possible that this was due to natural biological variation in the cartilage of these particular porcine cartilage samples. Nonetheless, the porcine condylar cartilage thicknesses measured in this study (medial: 2.2 - 2.4 mm; lateral: 1.6 – 1.9 mm) showed good agreement with the ranges reported by Wayne et al. (1998), Fermor (2013) and the previous study carried out in Chapter 5.

The effect of injecting P₁₁-4: GAG and P₁₁-8: GAG on the biomechanical properties of GAG depleted condylar cartilage was investigated using indentation testing with a load of 0.31 N, followed by FE analysis, from which the deformation, equilibrium elastic modulus and permeability were calculated. Deformation curves for both medial and lateral condyles showed that the native condylar cartilage exhibited the lowest deformation over a 1 hour time period, when compared to all other groups. The GAG depleted condylar cartilage injected with chondroitin sulfate only exhibited the highest deformation. The deformation behaviour of the native porcine cartilage in this study remained the lowest of all groups and was similar to the behaviour of native condylar cartilage reported in the literature (Katta et al., 2008; Katta et al., 2009; Abdelgaied et al., 2015; Fermor et al., 2015), which may have been due to the presence of GAGs within the tissue. However, the deformation behaviour of GAG depleted condylar cartilage injected with chondroitin sulfate alone, was somewhat strange, and it was not easily explained why injection of chondroitin sulfate alone caused the percentage deformation of the GAG depleted cartilage to increase by such an extent (43.6% in the medial and 51% in the lateral condyles), when compared to the GAG depleted cartilage control. A possible explanation was the GAG depleted condylar cartilage may have had some

GAGs present/remaining (circa 50 $\mu\text{g. mg}^{-1}$; Chapter 4); which were likely not bound in large aggregated molecules to hyaluronic acid chains as a result of the SDS treatment. The injection of the highly negatively charged chondroitin sulfate; may have caused repulsion with the remaining GAG molecules and/or negative cations, which could have contributed to the increase in percentage deformation observed in both the medial and lateral condylar cartilage. Similar to the previous study in Chapter 5, the deformation curve for the GAG depleted porcine condylar cartilage exhibited higher deformation across the 1 hour time period when compared to the native porcine condylar cartilage for both the medial and lateral condyles. This was due to the reduced levels of aggregated GAGs in the GAG depleted cartilage. Only GAGs attached to aggrecan which are linked to hyaluronic acid via a link protein, contribute to the compressive resistance of cartilage (Muir, 1978; Han et al., 2011). However, the treatment with SDS to produce the GAG depleted condylar cartilage model, would have disrupted the link protein interaction with the hyaluronic acid, making any remaining GAGs much more mobile and hence ineffective, which was why the GAG depleted condylar cartilage exhibited higher deformation.

The effect of injecting native condylar cartilage with water and the effect of injecting without any fluid were also investigated. It was found that these treatments did not affect the final percentage deformation of native condylar cartilage, as no significant difference in the percentage deformation were observed. Therefore, any effects observed from the GAG depleted condylar cartilage samples injected with peptide, PEP: GAG or just GAG; were considered to be due to the treatment with the substances themselves and not due to the injection process.

Significant differences in the percentage deformation (after it had reached equilibrium, at 1 hour) were found between the GAG depleted porcine medial condylar cartilage and the GAG depleted porcine medial condylar cartilage injected with P₁₁-4: GAG and P₁₁-8: GAG. Injection of both PEP: GAG mixtures into medial and lateral GAG depleted condylar cartilage samples significantly reduced the percentage deformation compared to the GAG depleted condylar cartilage control. Furthermore, no significant difference in the percentage deformation was found between the native porcine medial condylar cartilage and the GAG depleted porcine medial condylar cartilage injected with P₁₁-4: GAG, which was not the case for the GAG depleted porcine condylar cartilage injected with P₁₁-8: GAG. Therefore, injection of P₁₁-4: GAG restored the deformation properties of GAG depleted porcine condylar cartilage to a level that was similar to and not significantly different to native porcine condylar cartilage.

The percentage deformation (after 1 hour) of GAG depleted porcine condylar cartilage injected with P₁₁-4 alone, in the lateral condyles, was significantly higher when compared to the GAG depleted porcine lateral condylar cartilage control. Whereas, injection of P₁₁-8 on its own into GAG depleted porcine condylar cartilage, significantly reduced the percentage deformation (after 1 hour) of the lateral condyle when compared to the GAG depleted porcine lateral condylar cartilage control. However, this was not the case in the medial condyles where no significant effect of treatment with P₁₁-4 or P₁₁-8 alone was observed.

GAG depleted porcine condylar cartilage injected with P₁₁-4: GAG had significantly lower percentage deformation (after 1 hour) when compared to the GAG depleted porcine condylar cartilage injected with P₁₁-4 on its own, in both the medial and lateral condyles. Conversely, no significant difference in the percentage deformation was observed between the GAG depleted porcine condylar cartilage samples injected with P₁₁-8: GAG and P₁₁-8 on its own, in either the medial and lateral condyles.

Analysis of the percentage deformation data for both medial and lateral condyles, showed that injection of the PEP: GAG mixtures into GAG depleted porcine condylar cartilage, was better at restoring the deformation properties of GAG depleted porcine condylar cartilage when compared to the peptides on their own. The majority of lateral condyles group tested, were shown to have a percentage deformation greater than 15 %, which meant that any derived data for the equilibrium elastic modulus and permeability would not be accurate and therefore were excluded from the FE analysis. The higher percentage deformation seen in the lateral condyles compared to the medial condyles was assumed to be due to differences in thicknesses between the medial and lateral condyles.

An axisymmetric poroelastic FE model (described in Chapter 5), was used to curve fit the experimental deformation data to determine the effect that injecting P₁₁-4: GAG, P₁₁-4 only; P₁₁-8: GAG and P₁₁-8 only, had on the equilibrium elastic modulus and permeability of GAG depleted porcine condylar cartilage.

The equilibrium elastic modulus was significantly greater in the native cartilage samples when compared to all the other groups, with the exception of the GAG depleted porcine condylar cartilage samples injected with P₁₁-4: GAG. The finding that injection of P₁₁-4: GAG was able to restore the equilibrium elastic modulus of GAG depleted medial condylar cartilage to a level similar to that of native cartilage, indicated that this PEP: GAG mixture had the desired effect of restoring the biomechanical properties of GAG depleted porcine medial condylar cartilage. On the other hand, injection of GAG depleted condylar cartilage with P₁₁-4 peptide on its own, significantly lowered the equilibrium elastic modulus when

compared to the GAG depleted porcine condylar cartilage control. It was therefore concluded that the GAGs in the P₁₁₋₄: GAG mixture contributed to improving the compressive stiffness of the GAG depleted medial condylar cartilage, possibly by improving the gelation properties of the peptide but also by providing increased osmotic swelling pressure.

Injection of the GAG depleted porcine medial condylar cartilage with P₁₁₋₈: GAG also significantly increased the elastic modulus of the GAG depleted porcine condylar cartilage. However, P₁₁₋₈: GAG was not able to restore the compressive stiffness of the GAG depleted porcine condylar cartilage to the same or similar level as the native porcine condylar cartilage. The average equilibrium elastic modulus of the P₁₁₋₄: GAG injected GAG depleted condylar cartilage had a trend towards higher compressive stiffness than the samples injected with P₁₁₋₈: GAG, although this was not significantly different. This trend could have been due to the net charge difference of these two peptides. P₁₁₋₄ is negatively charged and P₁₁₋₈ is positively charged. The combination of these peptides with a highly negatively charged GAG, chondroitin sulfate, could explain the difference seen in the compressive stiffness of GAG depleted condylar cartilage. The combination of two negatively charged substances (P₁₁₋₄ and CS) could have caused high repulsive forces between the two substances, hence contributing to the increase in compressive stiffness of the GAG depleted condylar cartilage. This highly negatively charged PEP: GAG hydrogel could also have interacted electrostatically with the naturally occurring ions present within the GAG depleted condylar cartilage model. These ions were replaced in the GAG depleted model, at the end of its GAG depletion process (Chapter 4; Section 4.3.3)); where they had been left to soak in a 130 mM Na⁺ salt solution, containing all essential salts present in native cartilage, as described by Urban (1994)). This interaction with the surrounding cations and anions, may have provided the GAG depleted condylar cartilage injected with P₁₁₋₄: GAG with resistance to compression, by increasing the fluid phase load support that would be very low in cartilage with GAGs depleted. It may be hypothesised that the P₁₁₋₄: GAG hydrogel acted as a better damper, during the fluid phase load support of the GAG depleted condylar cartilage by retaining excess water within the cartilage tissue matrix; which is why its average equilibrium elastic modulus, hence compressive stiffness was higher.

It was hypothesised that, due to the removal of GAGs from the GAG depleted condylar cartilage, the permeability of the GAG depleted porcine condylar cartilage control would be significantly higher than native cartilage. Similarly, as explained in Chapter 5, this was not supported by the data obtained and no significant differences in the permeability between any of the groups tested in this study was observed.

The relationship between the equilibrium elastic modulus and permeability values in this study was that the higher the equilibrium elastic modulus, the lower the permeability value. This can be explained by the cartilage's ability to resist compressive forces. In native condylar cartilage, which has all of its matrix components, the flow of interstitial fluid through the matrix is restricted and controlled, hence it is less permeable to fluid and better able to withstand compressive loads. However, cartilage in which the micro and macro structure has been altered/removed, no longer has the ability to restrict or control the flow of interstitial fluid, hence is more permeable and less able to resist compressive forces (Maroudas et al., 1968; Maroudas et al., 1973; Maroudas and Venn, 1977; Muir, 1978; Buckwalter et al., 2005; Franke et al., 2007; Wilson et al., 2007 ; Han et al., 2011).

It was important to determine whether the peptides and peptide GAG mixtures injected into the GAG depleted condylar cartilage samples were self-assembled. In order to explore this, FRAP analysis was used. The FRAP images captured over the duration of 1 minute and the recovery curves, showed that the peptide and PEP: GAG mixtures remained self-assembled in-situ, even after the cartilage samples had been indented with a load of 0.31 N. All the GAG depleted condylar cartilage samples injected with peptide alone (P₁₁-4 and P₁₁-8) and PEP: GAG mixtures (P₁₁-4: GAG and P₁₁-8: GAG) that had been bleached; demonstrated no significant fluorescence recovery in the bleached ROI. The final images captured in the FRAP experiments (t = 60s) for samples injected with peptide and PEP: GAG mixtures, showed that the bleached ROI remained darker than the image pre-bleach (t=0s). Hence, the fluorophore was not able to diffuse back from the non-bleached areas into the bleached areas, as the fluorophore had been trapped within the self-assembled peptide or PEP: GAG gels. These experiments confirmed that the fluorescently tagged peptides and PEP: GAG mixtures were able to remain self-assembled within the cartilage tissue.

Bleached fluorophore molecules, that are not restricted and are able to move freely, are replaced by non-bleached fluorophore molecules over time, resulting in a recovery in fluorescent intensity of the bleached ROI, visualised in the recovery curve (Swift and Trinkle-Mulcahy, 2004). The GAG depleted porcine condylar cartilage injected with the CS doped fluorescein, demonstrated such behaviour. When the ROI in this sample was bleached at t=6 seconds, the fluorophore's fluorescence intensity became much lower (darker) than the pre-bleached ROI (t=0 seconds). However, the fluorescence intensity of the bleached ROI fully recovered after t=60 seconds, which highlighted the high mobility of the fluorescein-tagged CS within the cartilage sample. The fast recovery of the fluorescence intensity seen in

samples injected with fluorescein-tagged CS, supported the conclusions that the samples injected with fluorescently tagged peptide and PEP: GAG, remained self-assembled in-situ. Native and GAG depleted porcine condylar cartilage controls were also imaged under the same fluorescein filter as well as transmitted light. This was carried out to demonstrate that the fluorescence seen in the GAG depleted condylar cartilage injected with fluorescein-tagged peptides P₁₁-4: GAG, P₁₁-4 only, P₁₁-8: GAG and P₁₁-8 only; could be solely attributed to the fluorescence from the fluorescein used to tag the peptide and PEP: GAG mixtures and not any auto-fluorescence that may have been present in the cartilage samples. The images of the native and GAG depleted condylar cartilage controls, showed no fluorescence under the fluorescein filter, confirming the validity of the data.

6.7 Conclusion

The successful delivery of P₁₁-4 and P₁₁-8 peptides and PEP: GAG mixtures into GAG depleted condylar cartilage was demonstrated in this study. It was also shown that the minimally invasive injection of a PEP: GAG mixture comprising P₁₁-4 was able to restore the biomechanical properties of GAG depleted porcine condylar cartilage. All peptide and PEP: GAG mixtures injected remained self-assembled within the GAG depleted condylar cartilage, even after a load of 0.31 N was applied; which was indicative of the strength of the gels but also, the possible favourable interactions between the gels and surrounding cartilage matrix that allowed the peptide hydrogels to remain self-assembled. It was further demonstrated that the chondroitin sulfate GAG had an important role to play in the restoration of the biomechanical properties of the GAG depleted condylar cartilage. This was attributed to its highly negative charge and ability to regulate the osmotic pressure within the cartilage matrix. It is hypothesised that the restoration of GAGs, being held in place by the self-assembled P₁₁-4 peptide: GAG hydrogel within the GAG depleted condylar cartilage, was key to the improved compressive stiffness. It is important to note that the molar ratio of GAG chosen in this study was low (1:64). Therefore, it is hypothesised that these improvements could be amplified through the delivery of a higher GAG molar ratio (e.g. 1:16). Nevertheless, the data obtained in this study indicated that the P₁₁-4: GAG mixture, could be a suitable candidate for the future treatment of early stage osteoarthritic cartilage.

Chapter 7 Conclusions and Future Studies

The net depletion of glycosaminoglycan in osteoarthritic cartilage has been linked with a loss of biomechanical properties and function *in vitro* (Mankin and Lippiell, 1971; Otsuki et al., 2008) and is considered to be a major contributor to the progression of OA (Bell et al., 2006). Katta *et al.*, proposed an approach to repair early cartilage degeneration by restoring GAG levels in order to maintain the functional cartilage material properties. Chondroitin sulfate alone was, however not able to restore the biomechanical properties of GAG deficient articular cartilage (Katta, 2007). The aim of this study was to explore the use of a mixture of chondroitin sulfate and self-assembling peptides for the restoration of the biomechanical properties of GAG depleted cartilage; ideally to a level intrinsic to natural cartilage. It was hypothesised, that the combination of SAPs and GAGs, would improve the biomechanical properties of GAG depleted cartilage via the successful delivery and retention of the GAG molecules by the self-assembled peptide to the tissue.

The study followed a systematic approach in which the self-assembly, fibril morphology and biomechanical properties of different peptides and PEP: GAG mixtures were explored (Chapter 3), to select suitable candidates for further biological studies. A suitable *in vitro* GAG depleted porcine cartilage model for testing the selected peptides and PEP: GAG mixtures was then developed (Chapter 4), followed by the development of a method for biomechanical evaluation of this model (Chapter 5). Lastly, the injection of the peptides and PEP: GAG mixtures into GAG depleted porcine condylar cartilage was evaluated, through mechanical indentation testing and FEA analysis, in an attempt to restore the biomechanical properties (Chapter 6).

7.1 Major conclusions

In Chapter 3, three peptides (P₁₁-4, P₁₁-8 and P₁₁-12) were studied at two different GAG molar ratios (1:16 and 1:64) as well as in two ionic salt solutions (130mM and 230mM Na⁺ salt solution). The salt solutions each contained a different concentration of Na⁺ ions, as well as other salts found in cartilage tissue (Aggeli et al., 1997), which had not been previously studied with these peptides. This novel experimental design, gave insight regarding how the peptides and peptide: GAG mixtures would behave not only under normal physiological conditions, but also within the environment of the surface layer of articular cartilage. The FTIR and TEM studies identified that P₁₁-4 and P₁₁-8 peptides: along with their peptide: GAG mixtures; exhibited a high percentage of β -sheet formation. It was also shown that they were

able to form characteristic self-supporting gels, able to produce characteristic entangled fibrillar network morphology, similar to that of proteoglycan structures found in native cartilage (Hardingham and Muir, 1974; Poole, 1997; Mow and Ateshian, 1997). In addition, rheological studies revealed that the addition of chondroitin sulfate to the SAPS; as well as alteration in the ionic strength of the surrounding solution, allowed for the mechanical properties of the peptide-hydrogels to be tuned over a range of up to four orders of magnitude. Addition of chondroitin sulfate to the peptides promoted a greater number of fibrillar entanglements and junction points, rendering the P₁₁-4 and P₁₁-8 peptide-GAG mixtures the stiffest of the three peptides. The study identified that the P₁₁-4 and P₁₁-8 peptide-GAG mixtures, demonstrated all the favourable characteristics of hydrogels with potential ability to restore the biomechanical properties of GAG depleted cartilage.

A GAG depleted model of porcine femoral condylar cartilage was successfully developed in Chapter 4. Histological analysis and GAG quantification highlighted that the use of the chondroitinase ABC enzyme, painted onto the surface of porcine condylar cartilage produced a mild GAG depleted cartilage model (model 1). Injection of chondroitinase ABC into porcine condylar cartilage produced a moderate GAG depleted cartilage model (model 2). Washes in low concentrations of SDS (0.1 % (w/v)) alongside PBS washes, was shown to produce a severe GAG depleted cartilage model (model 3), in which a 75% reduction in GAG content of the cartilage was observed, when compared to native cartilage. The development of these models was novel and the models could be used to represent different stages of cartilage degeneration in future studies. Model 3 was chosen as the most suitable model to take forward for assessment of the effects of PEP: GAG mixtures, based on its low GAG content.

In Chapter 5, the focus was to develop an appropriate methodology for the indentation testing of cartilage, to study differences in the biomechanical properties between native and GAG depleted porcine condylar cartilage. The aim was to achieve a test method that gave significant differences in the percentage deformation, equilibrium elastic modulus and permeability between native and GAG depleted porcine condylar cartilages. The latter was important because the intention was to inject SAPs and SAP: GAG mixtures into the GAG depleted cartilage, to investigate the capacity of these injectable hydrogels to restore the biomechanical properties of the GAG depleted cartilage, to values that were similar to native porcine condylar cartilage. This study was unique, since previous indentation tests had only been performed on porcine condylar cartilage pins (Katta et al., 2007; Katta et al., 2008; Abdelgaied et al., 2015). The present study was undertaken on whole porcine femoral condyles, both medial and lateral, to avoid any cut surfaces to the cartilage into which the

SAP: GAGs were to be injected. Injection of the peptides and peptide: GAG mixtures into cartilage in which the collagen had been damaged by cutting; would likely have resulted in leakage from the cut surfaces prior to self-assembly. Of the three loads tested, significant differences in the deformation and equilibrium elastic modulus between the native and GAG depleted porcine condylar cartilage were achieved using 0.11N and 0.31N loads. However, the use of a 0.31 N load resulted in the greatest significant difference in the deformation between native and GAG depleted porcine cartilage models. Consequently, this load was used for future studies of the SAP: GAG mixtures, to assess their potential in restoring the biomechanical properties of GAG depleted condylar cartilage.

In Chapter 6, the aim was to evaluate whether the peptides P₁₁-4 and P₁₁-8 and their PEP: GAG mixtures at a molar ratio of 1:64, were able to restore the biomechanical properties of GAG depleted condylar cartilage. The peptides and peptide: GAG mixtures were successfully delivered into GAG depleted porcine condylar cartilage as visualised and confirmed by FRAP analysis. No fluorescence recovery after bleaching was observed in either the peptide or PEP: GAG injected samples, confirming the successful self-assembly of the SAPs. Histological analysis and GAG quantification techniques were not performed to assess whether the GAG had been successfully retained within the cartilage due to time constraints. However, the biomechanical test data indirectly indicated that the GAG delivered together with the peptides was retained. FRAP analysis of fluorescein-tagged chondroitin sulfate (GAG) injected samples, showed that the GAG alone was not retained at the injection sites within the cartilage and that it also reduced the deformation properties of GAG depleted porcine condylar cartilage.

Interestingly, a recent study by Miles *et al.*, demonstrated that injection of P₁₁-12: GAG hydrogels restored the biomechanical properties of denucleated bovine intervertebral discs (Miles *et al.*, 2016). The authors commented on the ability of the GAGs to enhance the biomechanical properties of the hybrid gels by accelerating gelation kinetics and providing favourable thermodynamic conditions for self-assembly, which supported the findings of the present study. The indentation tests performed in this study, showed that injections of P₁₁-4: GAG restored the deformation properties and equilibrium elastic modulus of GAG depleted porcine condylar cartilage, to levels that were not significantly different to those of native porcine condylar cartilage.

7.2 Future studies

Although the aims of the studies performed in this thesis were largely met, further work is required to gain a greater understanding of these novel peptide: GAG hydrogels, as a potential minimally invasive therapy for the repair of osteoarthritic cartilage. Further testing of higher GAG molar ratio combinations and additional models for testing the peptide: GAG hydrogels are desirable.

7.2.1 Histological and GAG quantification of PEP: GAG treated cartilage.

Histological analysis and GAG quantification techniques were not performed to assess whether the GAG had been successfully retained within the cartilage, due to time constraints. Therefore, additional histological imaging and GAG quantification of: GAG depleted condylar cartilage injected with PEP: GAG mixtures; GAG depleted condylar cartilage (negative control); native condylar cartilage (positive control) and GAG depleted condylar cartilage injected with chondroitin sulfate alone would be beneficial. These studies would determine whether: (a) the GAG had been successfully retained within the cartilage and where it was localised; and (b) if the net GAG content of the GAG depleted condylar cartilage injected with PEP: GAG mixtures and/or chondroitin sulfate alone, had increased. The data could then be compared to the native and GAG depleted condylar cartilage controls.

7.2.2 Testing of mild and moderate GAG depleted porcine cartilage models.

In Chapter 4, three different GAG depleted porcine condylar cartilage models were developed which showed varying levels of GAG content. These models provide potential models of earlier stages of osteoarthritis, that could be used to test future cartilage repair methods. However, due to time constraints it was not possible to determine the effects of the SAP: GAG mixtures on the biomechanical properties of the mild and moderate GAG depleted porcine condylar cartilage (models 1 and 2). It would be useful to determine the efficacy of the PEP: GAG mixtures in restoring the biomechanical properties of these mild and moderate GAG depleted models, representative of different stages of osteoarthritic cartilage degeneration.

7.2.3 Testing of higher GAG molar ratio of PEP: GAG mixtures – 1:16

The lower molar ratio of GAG (1:64) was used in the PEP: GAG mixtures studied in Chapter 6 to evaluate the initial hypothesis. It was the intention to carry out further studies of PEP: GAG mixtures with a higher molar ratio of chondroitin sulfate, however, this was not possible

due to time constraints. Given the improvements in the biomechanical properties of GAG depleted porcine condylar cartilage observed with the lower GAG molar ratio; it might be hypothesised that because of the role of the GAGs in the improved gelation kinetics and biomechanical properties of the SAP: GAG hydrogels; these improvements could be amplified through the delivery of a higher GAG molar ratio (e.g. 1:16). This could be tested in further studies using the methods developed in this thesis.

7.2.4 Development of friction test to study the bio-tribological properties of the PEP: GAG mixtures.

Regrettably, the development of an appropriate methodology for studying the biotribological properties of native and GAG depleted condylar cartilage was not undertaken. It has been reported in the literature that the coefficient of friction of cartilage increases with GAG depletion (Katta et al., 2008), which is likely due to reduced biphasic and boundary lubrication (Forster and Fisher, 1996; Mow and Ateshian, 1997). A study at the University of Leeds, carried out frictional tests using a pendulum friction simulator. The study showed elevated friction and wear of the medial compartmental bovine knee without a meniscus, when compared to the intact joint (McCann et al., 2009). Therefore, additional frictional test like the latter, which identify any difference in the frictional properties between GAG depleted and native condylar cartilages would have been beneficial. This in turn would, evaluate whether or not the SAP: GAG mixtures contributed to improvement in the biphasic and boundary lubrication regimes in GAG depleted condylar cartilage.

7.2.5 Use of natural whole joint GAG depleted models in knee simulator to investigate the effects of PEP: GAG mixtures on function.

Recent work at the University of Leeds, has led to the development and validation of a natural whole joint knee simulator. The tribological function and biomechanical properties of the natural porcine knee joint has been successfully evaluated using this simulator; which is currently being adapted for evaluation of natural human knee joints (Liu et al., 2015). The significance of this study is that this natural knee joint simulation model could be used as a tool to assess the future novel early stage cartilage and meniscus repair interventions. Therefore, future studies should aim to evaluate the tribological and biomechanical function of native, GAG depleted and GAG depleted porcine femoral cartilage treated with the PEP: GAG mixtures. Moreover, once adapted for use with human knee joints, the whole knee joint simulation model could be used to determine the efficacy of the PEP: GAG mixtures in restoring the biomechanical properties of human osteoarthritic cartilage.

7.2.6 Leakage study to assess the stability of the PEP: GAG gel over a prolonged time period.

The reversible properties of the P₁₁-X family of SAPs, is due to changes in the equilibrium environment, which has been reported in the literature (Aggeli et al., 2003; Carrick et al., 2007). These properties could cause the breakdown of the self-assembled hydrogels into monomeric components, thus, leading to the leakage of GAGs into the surrounding tissue. Hence, following injection of PEP: GAG mixtures into GAG depleted cartilage the biomechanical properties of the SAP: GAG treated GAG depleted cartilage may decrease over time. Therefore, it would be important to undertake a study to determine whether the GAG was lost from the PEP: GAG treated cartilage over time. This could be carried out in whole joint models, preferably under cyclic loading. The study should investigate GAG leakage into the surrounding lubricant, at different time points during and after friction and biomechanical tests. The study will show the ability of the SAP: GAG mixtures to retain the GAG within the GAG depleted cartilage under physiological conditions. Similarly, fluorescently labelled SAPs could be used to calculate the concentration of SAP leakage during these studies.

7.3 Potential for Clinical Translation

Self-assembling peptides have been widely used in tissue engineering and biomedical applications, as discussed in Chapter (1). Clinical translation of these materials, has been achieved. The peptide group at the University of Leeds demonstrated the utility of P₁₁-4 in enamel remineralisation of human teeth (Kirkham et al., 2007) and then tested the clinical safety of P₁₁-4 in patients with caries lesions (Brunton et al., 2013). The study showed no biocompatibility issues nor cytotoxic effects, which was confirmed in other studies (Wilshaw et al., 2008; Kyle et al., 2010; Maude et al., 2011). The studies of Kirkham et al. (2007) and Brunton et al. (2013) led to the successful commercialisation of P₁₁-4 for caries treatment by Credentis in Zurich, Switzerland. Hence, there is good evidence that biomedical applications of the P₁₁-X series of peptides can be translated for patient benefit. The present study has highlighted the potential of P₁₁-4: GAG mixtures as a potential minimally invasive injection for the treatment of early stages of osteoarthritic cartilage. However, substantial barriers remain that must be overcome to enable successful commercial/clinical translation.

7.3.1 Arthroscopic delivery system

Although in this study SAP: GAG mixtures were successfully delivered into GAG depleted condylar cartilage, efforts should be made to optimise the delivery of this therapeutic mixture to: (1) attain further diffusion of the SAP: GAG mixture within the cartilage and (2) cause less damage to the cartilage articular surface. This could be achieved through re-design of the needle tip used to inject these SAP: GAG mixtures, whereby the needle could have more than one orifice along the length of the needle. This would improve the area in which the SAP: GAG mixture was able to diffuse into, following injection. Another solution might be to investigate different injection entry points into the cartilage to reach the desired treatment location. Entry from non-loading bearing areas could be a starting point, with variation in the injection angle to determine the effects on the biomechanical properties of the treated area, after injection.

7.3.2 Pre-clinical studies in animal models of osteoarthritis.

Following successful pre-clinical laboratory studies in natural whole joint models (Section 7.2.5) it would be necessary to carry out pre-clinical studies in an appropriate large animal model, such as sheep, to predict the clinical performance of SAP: GAG treatment. Induced OA models in animals, either through surgical techniques or injection methods; which act to stimulate intra-articular inflammation, direct matrix damage, or chondrocyte toxicity are documented in the literature (Teeple et al., 2013; Kuyinu et al., 2016). Injection of the SAP: GAG mixtures into these large animal induced OA joint models will provide more accurate representation of the ability of this novel therapy to improve the biomechanical properties of OA cartilage. This could be evaluated through biotribological and biomechanical tests in whole joint simulators, following sacrifice of the animals. Subject to acceptable performance in these studies, the SAP: GAG mixture therapy could be taken forward to pre-market medical device clinical trials to assess their clinical safety and utility in humans.

7.4 Significance of the study

In conclusion, this study has produced relevant GAG depleted condylar cartilage models which can be used to evaluate the restorative potential future cartilage repair methods; whilst highlighting the efficacy of SAP: GAG mixtures in restoration of the biomechanical properties of GAG depleted cartilage. This study has shown that the use of P₁₁-4 in combination with chondroitin sulfate has future potential for development as a minimally invasive treatment for early stage osteoarthritis.

References

- Abdelgaied, A., Stanley, M., Galfe, M., Berry, H., Ingham, E., and Fisher, J. 2015. Comparison of the biomechanical tensile and compressive properties of decellularised and natural porcine meniscus. *Journal of Biomechanics*. **48**, pp.1389-96.
- Aggeli, A., Bell, M., Boden, N., Keen, J. N., McLeish, T. C. B. et al. 1997. Engineering of peptide β -sheet nanotapes. *Journal of Material Chemistry*. **7**(7), pp.1135-45.
- Aggeli, A., Bell, M., Carrick, L. M., Fishwick, C. W., Harding, R. et al. 2003. pH as a trigger of peptide β -sheet self-assembly and reversible switching between nematic and isotropic phases. *J Am Chem Soc*. **125**(32), pp.9619-9628.
- Aggeli, A., Nyrkova, I. A., Bell, M., Harding, R., Carrick, L. et al. 2001. Hierarchical self-assembly of chiral rod-like molecules as a model for peptide β -sheet tapes, ribbons, fibrils, and fibers. *Proc Natl Acad Sci USA*. **98**(21), pp.11857-62.
- Aggelli, A. 2000. *Lecture 8: 1D Self Assembly of peptides into β -sheet tapes*. Leeds: University of Leeds.
- Akizuki, S., Mow, V. C., Muller, F., Pita, J. C., and Howell, D. S. 1987. Tensile properties of human knee joint cartilage. II. Correlations between weight bearing and tissue pathology and the kinetics of swelling. *J Orthop Res*. **5**(2), pp.173 – 86.
- Akizuki, S., Mow, V. C., Muller, F., Pita, J. C., Howell, D. S., and Manicourt, D. H. 1986. Tensile properties of human knee joint cartilage: I. Influence of ionic conditions, weight bearing, and fibrillation on the tensile modulus. *Journal of Orthopaedic Research*. **4**(4), pp.379-92.
- Alberts, B., Bray, D., Lewis, J., Raff, M., Roberts, K., and Watson, J. 1994. *Molecular Biology of the cell*. United States: Taylor & Francis.
- Alberts, B., Bray, D., Lewis, J., Raff, M., Roberts, K., and Watson, J. D. 2002. The Extracellular Matrix of Animals: After Secretion, Fibrillar Procollagen Molecules Are Cleaved to Collagen Molecules, Which Assemble into Fibrils. In: *Molecular biology of the cell (4th edition)*, New York: Garland Science Publishing.
- Albrecht, C., Tichy, B., Nürnberger, S., Hosiner, S., Zak, L., Aldrian, S., and Marlovits, S. 2011. Gene expression and cell differentiation in matrix-associated chondrocyte transplantation grafts: a comparative study. *Osteoarthritis and Cartilage*. **19**(10), pp.1219-1227.
- Alcaraz, M. J., Megías, J., García-Aranda, I., Clérigues, V., and Guillén, M. I. 2010. New molecular targets for the treatment of osteoarthritis. *Biochem Pharmacol*. **80**(1), pp.13-21.
- Almeida, H. V., Eswaramoorthy, R., Cunniffe, G. M., Buckley, C. T., O'Brien, F. J., and Kelly, D. J. 2016. Fibrin hydrogels functionalized with cartilage extracellular matrix and incorporating freshly isolated stromal cells as an injectable for cartilage regeneration. *Acta Biomaterialia*. **36**, pp.55-62.
- Alsalamah, S., Mollenhauer, J., Hain, N., Stock, K. P., Kalden, J. R., and Burmester, G. R. 1990. Cellular immune response toward human articular chondrocytes. T cell reactivities against chondrocyte and fibroblast membranes in destructive joint diseases. *Arthritis Rheum*. **33**(10), pp.1477-1486.
- Altman, R. D., Akermark, C., Beaulieu, A. D., and Schnitzer, T. 2004. Efficacy and safety of a single intra-articular injection of non-animal stabilized hyaluronic acid (NASHA) in patients with osteoarthritis of the knee. *Osteoarthritis Cartilage*. **12**(8), pp.642-649.

- Altman, R. D., Hochberg, M., Murphy, W. A. Jr., Wolfe, F., and Lequesne, M. 1995. Atlas of individual radiographic features in osteoarthritis. *Osteoarthritis Cartilage*. **3**(A), pp.3-70.
- Anderson, C. E., Ludowieg, J., Harper, H. A., and Engleman, E. P. 1964. The Composition of the organic component of human articular cartilage: relationship to age and degenerative joint disease. *J Bone Joint Surg Am*. **46**(6), pp.1176–1183.
- Andriacchi, T. P. 1994. Dynamics of knee malalignment [Review]. *Orthop Clin North Am*. **25**(3), pp.395-403.
- Andriacchi, T. P., Koo, S., and Scanlan, S. F. 2009. Gait mechanics influence healthy cartilage morphology and osteoarthritis of the knee. *J Bone Joint Surg Am*. **91**(Suppl 1), pp.95-101.
- Anika Therapeutics. *Hyalograft C Autograft*. [online]. Available from World Wide Web: <<http://www.anikatherapeutics.com/products/jointhealth/hyalograft.html>>
- Arand, M., Friedberg, T., and Oesch, F. 1992. Colorimetric quantitation of trace amounts of sodium lauryl sulfate in the presence of nucleic acids and proteins. *Analytical Biochemistry*. **207**, pp.73-75.
- Arden, N. and Nevitt, M. C. 2006. Osteoarthritis: Epidemiology. *Best Pract Res Clin Rheumatol*. **20**(1), pp.3-25.
- Arrondo, J. L. R., Muga, A., Castresana, J., and Goni, F. M. 1993. Quantitative studies of the structure of proteins in solution by Fourier transform infrared spectroscopy. *Progress in Biophysics and Molecular Biology*. **59**, pp.23-56.
- Arthritis Research UK. 2013. *Osteoarthritis in General Practise: Data and perspectives*. Chesterfield: Arthritis Research UK.
- Ashkavand, Z., Malekinejad, H., and Vishwanath, B. S. 2013. The pathophysiology of osteoarthritis. *J Pharma Res*. **7**(1), pp.132-138.
- Ateshian, G. A. 1997. A theoretical formulation for boundary friction in articular cartilage. *J Biomech Eng*. **119**(1), pp.81-6.
- Ateshian, G. A., Lai, W. M., Zhu, W. B., and Mow, V. C. 1994. An asymptotic solution for the contact of two biphasic cartilage layers. *J Biomechanics*. **27**(11), pp.1347-1360.
- Ateshian, G. A., Soltz, M. A., Mauck, R. L., Basalo, I. M., Hung, C. T., and Lai, W. M. 2003. The role of osmotic pressure and tension-compression nonlinearity in the frictional response of articular cartilage. *Transport in Porous Media*. **50**(1), pp.5-33.
- Ateshian, G. A. and Wang, H. 1997. Rolling resistance of articular cartilage due to interstitial fluid flow. *Proc Inst Mech Eng H*. **211**(5), pp.419– 24.
- Athanasίου, K. A., Agarwal, A., and Dzida, F. J. 1994. Comparative study of the intrinsic mechanical properties of the human acetabular and femoral head cartilage. *J Orthop Res*. **12**(3), pp.340-9.
- Athanasίου, K., Darling, E. M., and Hu, J. C. 2009. *Articular Cartilage Tissue Engineering*. Morgan & Claypool.
- Athanasίου, K., Rosenwasser, M., Buckwalter, J., Malinin, T., and Mow, V. 1991. Interspecies Comparisons of in situ Intrinsic Mechanical Properties of Distal Femoral Cartilage. *Journal of Orthopaedic Research*. **9**, pp.330-340.
- Atkinson, H.D.E. 2017. The negatives of knee replacement surgery: complications and the dissatisfied patient. *Orthopaedics and Trauma*. **31**(1), pp.25-33.

- Axelrod, D., Koppel, D.E., Schlessinger, J., Elson, E., and Webb, W.W. 1976. Mobility measurement by analysis of fluorescence photobleaching recovery kinetics. *Biophys. J.* **16**, pp.1055-1069.
- Ayral, X., Pickering, E. H., woodworth, T. G., Mackillop, N., and Dougados, M. 2005. Synovitis a potential predictive factor of structural progression of medial tibiofemoral knee osteoarthritis - results of a 1 year longitudinal arthroscopic study in 422 patients. *Osteoarthritis Cartilage.* **13**(5), pp.361-67.
- Bach, V. L. J. and Hunter, D. J. 2014. The epidemiology of osteoarthritis. *Best Practice & Research Clinical Rheumatology.* **28**(1), pp.5-15.
- Balakrishnan, B., Joshi, N., Jayakrishnan, A., and Banerjee, R. 2014. Self-crosslinked oxidized alginate/gelatin hydrogel as injectable, adhesive biomimetic scaffolds for cartilage regeneration. *Acta Biomaterialia.* **10**, pp.3650-3663.
- Barnes, H. A. 2000. *A handbook of elementary rheology.* Aberystwyth: The University of Wales, Institute of Non-Newtonian Fluid Mechanics, Department of Mathematics.
- Barnes Baili. 2011. *Histo Connective Tissue 2.* [online]. Available from World Wide Web: <<http://www.studyblue.com/notes/n/histo-connective-tissue-2/deck/995003>>
- Barth, A. 2000. The infrared absorption of amino acid side chains. *Progress in Biophysics & Molecular Biology.* **74**, pp.141-173.
- Barth, A. 2007. Infrared spectroscopy of proteins. *Biochimica et Biophysica Acta (BBA) - Bioenergetics.* **1767**(9), pp.1073-1101.
- Bartlett, W., Skinner, J. A., Gooding, C. R., Carrington, R. W., Flanagan, A. M., Briggs, T. W., and Bentley, G. 2005. Autologous chondrocyte implantation versus matrix-induced autologous chondrocyte implantation for osteochondral defects of the knee: a prospective, randomised study. *J Bone Joint Surg Br.* **87**(5), pp.640-645.
- Basalo, I. M., Mauck, R. L., Kelly, T.-A. N., Nicoll, S. B., Chen, F. H., Hung, C. T., and Ateshian, G. A. 2004. Cartilage interstitial fluid load support in unconfined compression following enzymatic digestion. *J. Biomech. Engng.* **126**(6), pp.779-786.
- Basalo, I. M., Raj, D., Krishnan, R., Chen, F. H., Hung, C. T., and Ateshian, G. A. 2005. Effects of enzymatic degradation on the frictional response of articular cartilage in stress relaxation. *J. Biomechanics.* **38**(6), pp.1343-1349.
- Bassani, R. and Piccigallo, B. 1992. *Hydrostatic Lubrication.* Italy: Elsevier Science.
- Bastard, J. P., Jardel, C., Bruckert, E., Blondy, P., Capeau, J. et al. 2008. Elevated levels of interleukin 6 are reduced in serum and subcutaneous adipose tissue of obese women after weight loss. *J Clin Endocrinol Metab.* **85**(9), pp.3338-42.
- Bayliss, M. T., Osborne, D., Woodhouse, S., and Davidson, C. 1999. Sulfation of Chondroitin Sulfate in Human Articular Cartilage: the effect of age, topographical position and zone of cartilage on tissue composition. *J Biol Chem.* **274**(22), pp.15892-15900.
- Beane, O. S. and Darling, E. M. 2012. Isolation, Characterization, and Differentiation of Stem Cells for Cartilage Regeneration. *Annals of Biomedical Engineering.* **40**(10), pp.2079-2097.
- Bell, C. J., Carrick, L. M., Katta, J., Jin, Z., Ingham, E. et al. 2006. Self-assembling peptides as injectable lubricants for osteoarthritis. *J Biomed Mater Res A.* **78**(2), pp.236-46.
- Bell, C. J., Ingham, E., and Fisher, J. 2006. Influence of hyaluronic acid on the time dependent friction response of articular cartilage under different conditions. *Proc Inst Mech Eng H.* **220**(1), pp.23-31.

- Benito, M. J., Veale, D. J., FitzGerald, O., Van den Berg, W. B., and Bresnihan, B. 2005. Synovial tissue inflammation in early and late osteoarthritis. *Ann Rheum Dis*. **64**(9), pp.1263-67.
- Bentley, G., Biant, L. C., Carrington, R. W. J., Akmal, M., Goldberg, A. et al. 2003. A prospective, randomised comparison of autologous chondrocyte implantation versus mosaicplasty for osteochondral defects in the knee. *J Bone Joint Surg Br*. **85**(2), pp.223-30.
- Bentley, G., Biant, L. C., Vijayan, S., Macmull, S., Skinner, J. A., and Carrington, R. W. J. 2012. Minimum ten-year results of a prospective randomised study of autologous chondrocyte implantation versus mosaicplasty for symptomatic articular cartilage lesions of the knee. *J Bone Joint Surg Br*. **94**(4), pp.504-509.
- Berenbaum, F. 2013. Osteoarthritis as an inflammatory disease (osteoarthritis is not osteoarthrosis!). *Osteoarthritis Cartilage*. **21**(1), pp.16-21.
- Bergschmidt, P., Ellenrieder, M., Bader, R., Kluess, D., Finze, S., Schwemmer, B., and Mittelmeier, W. 2016. Prospective comparative clinical study of ceramic and metallic femoral components for total knee arthroplasty over a five-year follow-up period. *The Knee*. **23**(5), pp.871-876.
- Berg, J. M., Tymoczko, J. L., and Stryer, L. 2002. *Biochemistry (5th edition)*. New York: Freeman, W. H.
- Bhattacharjee, M., Coburn, J., Centola, M., Murab, S., Barbero, A. et al. 2015. Tissue engineering strategies to study cartilage development, degeneration and regeneration. *Advanced Drug Delivery Reviews*. **84**, pp.107-122.
- BioTissue* - *BIOSEED*[®]-C. [online]. Available from World Wide Web: <<http://www.biotissue.de/news/25092016/>>
- BioTissue* - *BIOSEED*[®]-C. [online]. Available from World Wide Web: <<http://www.biotissue.de/bioseed/patients/bioseed-c/treatment-with-bioseed-c/>>
- Blom, A. B., van Lent, P. L., Holthuysen, A. E., van der Kraan, P. M., Roth, J., van Rooijen, N., and van den Berg, W. B. 2004. Synovial lining macrophages mediate osteophyte formation during experimental osteoarthritis. *Osteoarthritis Cartilage*. **12**(8), pp.627-35.
- Blom, A. B., van Lent, P. L., Libregts, S., Holthuysen, A. E., van der Kraan, P. M., van Rooijen, N., and van den Berg, W. B. 2007. Crucial role of macrophages in matrix metalloproteinase-mediated cartilage destruction during experimental osteoarthritis: involvement of matrix metalloproteinase 3. *Arthritis Rheum*. **56**(1), pp.147-157.
- Bluteau, G., Conrozier, T., Mathieu, P., Vignon, E., Herbage, D., and Mallein-Gerin, F. 2001. Matrix metalloproteinase 1, 3, 13 and aggrecanase 1 and 2 are differentially expressed in experimental osteoarthritis. *Biochim Biophys Acta*. **1526**(2), pp.147-58.
- Bock, H. C., Michaeli, P., Browne, C., Schultz, W., Kresse, H., Herken, R., and Miosge, N. 2001. The small proteoglycans decorin and biglycan in human articular cartilage of late-stage osteoarthritis. *Osteoarthritis Cartilage*. **9**(7), pp.654-63.
- Bonassar, L. J., Grodzinsky, A. J., Srinivasan, A., Davila, S. G., and Trippel, S. B. 2000. Mechanical and physicochemical regulation of the action of insulin-like growth factor-I on articular cartilage. *Arch Biochem Biophys*. **379**(1), pp.57-63.
- Bondeson, J., Wainwright, S. D., Lauder, S., Amos, N., and Hughes, C. E. 2006. The role of synovial macrophages and macrophage-produced cytokines in driving aggrecanases, matrix metalloproteinases, and other destructive and inflammatory responses in osteoarthritis. *Arthritis Res Ther*. **8**(6), p.R187.

- Borrás-Verdera, A., Calcedo-Bernal, V., Ojeda-Levenfeld, J., and Clavel-Sainz, C. 2013. Efficacy and safety of a single intra-articular injection of 2% hyaluronic acid plus mannitol injection in knee osteoarthritis over a 6-month period. *Rev Esp Cir Ortop Traumatol.* **56**(4), pp.274-280.
- Boschetti, F., Pennati, G., Gervaso, F., Peretti, G. M., and Dubini, G. 2004. Biomechanical properties of human articular cartilage under compressive loads. *Biorheology.* **41**(3-4), pp.159-66.
- Bradley, M. 2007. *Curve Fitting in Raman and IR Spectroscopy: Basic Theory of Line Shapes and Applications.* Thermo Fisher Scientific.
- Branden, C. and Tooze, J. 1999. *Introduction to protein structure.* New York: Garland Pub.
- Brandt, K. D., Myers, S. L., Burr, D., and Albrecht, M. 1991. Osteoarthritic changes in canine articular cartilage, subchondral bone, and synovium fifty-four months after transection of the anterior cruciate ligament. *Arthritis Rheum.* **34**(12), pp.1560-70.
- Brinker, M. R. and Miller, M. D. 1999. *Fundamentals of orthopaedics.* Philadelphia: WB Saunders.
- Brittberg, M., Lindahl, A., Nilsson, A., Ohlsson, C., Isaksson, O., and Peterson, L. 1994. Treatment of deep cartilage defects in the knee with autologous chondrocyte transplantation. *N Engl J Med.* **331**(14), pp.889-95.
- Brown, T. D. and Shaw, T. D. 1983. In vitro contact stress distributions in the natural human hip. *Biomech.* **16**(6), pp.373-84.
- Brunton, P. A., Davies, R. P., Burke, J. L., Smith, A., Aggeli, A., Brookes, S. J., and Kirkham, J. 2013. Treatment of early caries lesions using biomimetic self-assembling peptides - A clinical safety trial. *Br Dent J.* **215**(4), p.E6.
- Buckland-Wright, C. 2004. Subchondral bone changes in hand and knee osteoarthritis detected by radiography. *Osteoarthritis Cartilage.* **12**(Suppl A), pp.S10-19.
- Buckwalter, J.A., Mankin, H. J., and Grodzinsky, A. J. 2005. Articular Cartilage and Osteoarthritis. *Instr Course Lect.* **54**, pp.465-480.
- Bullough, P. G. 2004. The role of joint architecture in the etiology of arthritis. *Osteoarthritis Cartilage.* **12**(Suppl A), pp.S2-9.
- Burnett, S., Hart, D. J., Cooper, C., and Spector, T. D. 1994. *A Radiographic Atlas of Osteoarthritis.* London: Springer.
- Burr, D. B. 2004. Anatomy and physiology of the mineralized tissues: role in the pathogenesis of osteoarthrosis. *Osteoarthritis Cartilage.* **12**(Suppl A), pp.S20-30.
- Cai, S. and Singh, B. R. 2004. A Distinct Utility of Amide III Infrared Band for Secondary Structure Estimation of Aqueous Protein Solutions Using Partial Least Square Methods. *Biochemistry.* **43**, pp.2541-2549.
- Calo, E. and Khutoryanskiy, V. V. 2016. Biomedical applications of hydrogels: A review of patents and commercial products. *European Polymer Journal.* **65**, pp.252-267.
- Campbell, K. P., MacLennan, D.H., and Jorgensen, A. O. 1983. Staining of the Ca²⁺-binding proteins, calsequestrin, calmodulin, troponin C, and S-100, with the cationic carbocyanine dye "Stains-all." *Journal of Biological Chemistry.* **68**, pp.11267-11273.
- Campoccia, D., Doherty, P., Radice, M., Brun, P., Abatangelo, G., and Williams, D. F. 1998. Semisynthetic resorbable materials from hyaluronan esterification. *Biomaterials.* **19**, pp.2101-2127.

- Cancedda, R., Dozin, B., Giannoni, P., and Quarto, R. 2003. Tissue engineering and cell therapy of cartilage and bone. *Matrix Biol.* **22**(1), pp.81-91.
- Caplan, M. R., Moore, P. N., Zhang, S. G., Kamm, R. D., and Lauffenburger, D. A. 2000. Self assembly of beta sheet protein governed by relief of electrostatic repulsion relative to van de Waals attraction. *Biomacromolecules.* **1**, pp.627-631.
- Caplan, M. R., Schwartzfarb, E. M., Zhang, S. G., Kamm, R. D., and Lauffenburger, D. A. 2002. Control of self-assembling oligopeptide matrix formation through systematic variation of amino acid sequence. *Biomaterials.* **23**, pp.219-227.
- Carrick, L. M., Aggeli, A., Boden, N., Fisher, J., Ingham, E., and Waigh, T. A. 2007. Effect of ionic strength on the self-assembly, morphology and gelation of pH responsive β -sheet tape-forming peptides. *Tetrahedron.* **63**, pp.7457-7467.
- Carter, D. R., Beaupre, G. S., Wong, M., Smith, R. L., Andriacchi, T. P., and Schurman, D. J. 2004. The mechanobiology of articular cartilage development and degeneration. *Clin Orthop Relat Res.* **427**, pp.569-77.
- Chadjichristos, C., Ghayor, C., Kypriotou, M., Martin, G., Renard, E. et al. 2003. Sp1 and Sp3 transcription factors mediate interleukin-1 β down-regulation of human type II collagen gene expression in articular chondrocytes. *J Biol Chem.* **278**(41), pp.39762-39772.
- Chahal, J., Gross, A. E., Gross, C., Mall, N., Dwyer, T. et al. 2013. Outcomes of Osteochondral Allgraft Transplantation in the Knee. *Arthroscopy.* **29**(3), pp.575-588.
- Chang, K. V., Hsiao, M. Y., Chen, W. S., Wang, T. G., and Chien, K. L. 2013. Effectiveness of Intra-Articular Hyaluronic Acid for Ankle Osteoarthritis Treatment: A Systematic Review and Meta-Analysis. *Arch Phys Med Rehabil.* **94**(5), pp.951-60.
- Chan, S. M., Neu, C. P., Duraine, G., Komvopoulos, K., and Reddi, A. H. 2010. Atomic force microscope investigation of the boundary-lubricant layer in articular cartilage. *Osteoarthritis Cartilage.* **18**(7), pp.956-63.
- Chaudhari, A. M., Briant, P. L., Beville, S. L., Koo, S., and Andriacchi, T. P. 2008. Knee kinematics, cartilage morphology, and osteoarthritis after ACL injury. *Med Sci Sports Exerc.* **40**(2), pp.215-222.
- Chauffier, K., Liguillon, M. C., Bougault, C., Gosset, M., Priam, S. et al. 2012. Induction of the chemokine IL-8/Kc by the articular cartilage: possible influence on osteoarthritis. *Joint Bone Spine.* **79**(6), pp.604-9.
- Chee, A., Shi, P., Cha, T., Kao, T. H., Yand, A. H. et al. 2016. Cell Therapy with Human Dermal Fibroblasts Enhances Intervertebral Disk Repair and Decreases Inflammation in the Rabbit Model. *Global Spine Journal.* **6**, pp.771-779.
- Chen, A. C., Nguyen, T. T., and Sah, R. L. 1997. Streaming potentials during the confined compression creep test of normal and proteoglycan-depleted cartilage. *Ann. Biomed. Engng.* **25**(2), pp.269-277.
- Chen, J., Wang, C., Lü, S., Wu, J., Guo, X. et al. 2005. In vivo chondrogenesis of adult bone-marrow-derived autologous mesenchymal stem cells. *Cell and Tissue Research.* **319**, pp.429-438.
- Cherubino, P., Grassi, F. A., and Bulgheroni, P. 2003. Autologous chondrocyte implantation using a bilayer collagen membrane a preliminary report. *J Orthop Surg (Hong Kong).* **11**(1), pp.10-15.
- Chevalier, X., Jerosch, J., Goupille, P., van Dijk, N., Luyten, F. P. et al. 2010. Single, intra-articular treatment with 6 ml hylan G-F 20 in patients with symptomatic primary

- osteoarthritis of the knee: a randomised, multicentre, double-blind, placebo controlled trial. *Ann Rheum Dis.* **69**(1), pp.113-119.
- Chirgadze, Y. N., Fedorov, O. V., and Trushina, N. P. 1975. Estimation of amino acid residue side-chain absorption in the infrared spectra of protein solutions in heavy water. *Biopolymers.* **14**, pp.679-694.
- Chung, C. and Burdick, J. A. 2008. Engineering cartilage tissue. *Adv Drug Deliv Rev.* **60**(2), pp.243-262.
- Chung, C., Mesa, J., Miller, G. J., Randolph, M. A., Gill, T. J., and Burdick, J. A. 2006. Effects of auricular chondrocyte expansion on neocartilage formation in photocrosslinked hyaluronic acid networks. *Tissue Eng.* **12**(9), pp.2665-2673.
- Clarkin, C. E., Allen, S., J., Kuiper N., T., Wheeler B, P., Wheeler-Jones C., and A., Pitsillides A. 2011. Regulation of UDP-glucose dehydrogenase is sufficient to modulate hyaluronan production and release, control sulfated GAG synthesis, and promote chondrogenesis. *Journal of Cell Physiology.* **226**, pp.749-761.
- Coles, J. M., Chang, D. P., and Zauscher, S. 2010. Molecular mechanisms of aqueous boundary lubrication by mucinous glycoproteins. *Current Opinion in Colloid & Interface Science.* **15**(6), pp.406-416.
- Collin, E. C., Grad, S., Zeugolis, D. I., Vinatier, C. S., Clouet, J. R. et al. 2011. An injectable vehicle for nucleus pulposus cell-based therapy. *Biomaterials.* **32**(11), pp.2862-70.
- Cooper, C., Egger, P., Coggon, D., Hart, D. J., Masud, T., and Cicuttini, F. 1996. Generalized osteoarthritis in women: pattern of joint involvement and approaches to definition for epidemiological studies. *Journal of Rheumatology.* **23**, pp.1938-42.
- Cornish, J., Callon, K., Lin, C., Xiao, C., Mulvey, T, Cooper, G., and Reid, I. 1999. Trifluoroacetate, a contaminant in purified proteins, inhibits proliferation of osteoblasts and chondrocytes. *American Journal of Physiology - Endocrinology And Metabolism.* **277**, pp.E779-E783.
- Correa, D. and Lietman, S. A. 2017. Articular cartilage repair: Current needs, methods and research directions. *Seminars in Cell & Developmental Biology.* **62**, pp.67-77.
- Cremer, M. A., Rosloniec, E. F., and Kang, A. H. 1998. The cartilage collagens: a review of their structure, organization, and role in the pathogenesis of experimental arthritis in animals and in human rheumatic disease. *J Mol Med.* **76**(3-4), pp.275-288.
- Crockett, R., Grubelnic, A., Roos, S., Dora, C., Born, W., and Troxler, H. 2007. Biochemical composition of the superficial layer of articular cartilage. *J Biomed Mater Res A.* **82**(4), pp.958-64.
- Danion, F., Varraine, E., Bonnard, M., and Pailhous, J. 2003. Stride variability in human gait: the effect of stride frequency and stride length. *Gait Posture.* **18**(1), pp.69-77.
- Das, U. N. 2001. Is obesity an inflammatory condition? *Nutrition.* **17**(11-12), pp.953-66.
- Deschamps, A. A., Grijpma, D. W., and Feijen, J. 2001. Poly(ethylene oxide)/poly(butylene terephthalate) segmented block copolymers: the effect of copolymer composition on physical properties and degradation behavior. *Polymer.* **42**(23), pp.9335-9345.
- Detterline, A. J., Goldberg, S., Bach, B. R. Jr., and Cole, B. J. 2005. Treatment Options for Articular Cartilage Defects of the Knee. *Orthop Nurs.* **24**(5), pp.361-366.
- Dowson, D. 1995. Elastohydrodynamic and micro-elastohydrodynamic lubrication. *Wear.* **190**(2), pp.125-138.

- Dudhia, J. 2005. Aggrecan, aging and assembly in articular cartilage. *Cell Mol Life Sci.* **62**(19-20), pp.2241-56.
- Duffy, J. 2015. *Rheology - More than just viscosity*. Malvern.
- Duffy, J. 2016. *A basic introduction to rheology*. Worcestershire: Malvern Instruments Limited.
- Dumond, H., Presle, N., Pottie, P., Pacquelet, S., Terlain, B. et al. 2004. Site specific changes in gene expression and cartilage metabolism during early experimental osteoarthritis. *Osteoarthritis Cartilage.* **12**(4), pp.284-95.
- Du, W. J., Reppel, L., Leger, L., Schenowitz, C., Huselstein, C. et al. 2016. Mesenchymal Stem Cells Derived from Human Bone Marrow and Adipose Tissue Maintain Their Immunosuppressive Properties After Chondrogenic Differentiation: Role of HLA-G. *Stem Cells Dev.* **25**(19), pp.1454-1469.
- Dury, J. L. and Mooney, D. J. 2003. Hydrogels for tissue engineering: scaffold design variables and applications. *Biomaterials.* **24**(24), pp.4337-4351.
- El Sayed, K., Haisch, A., John, T., Marzahn, U., Lohan, A. et al. 2010. Heterotopic autologous chondrocyte transplantation-a realistic approach to support articular cartilage repair? *Tissue Eng Part B Rev.* **16**(6), pp.603-616.
- El Sayed, K., Marzahn, U., John, T., Hoyer, M., Zreiqat, H. et al. 2013. PGA-associated heterotopic chondrocyte cocultures: implications of nasoseptal and auricular chondrocytes in articular cartilage repair. *J Tissue Eng Regen Med.* **7**(1), pp.61-72.
- Elder, B.D., Kim, D.H., and Athanasiou, K.A. 2010. Developing an articular cartilage decellularisation process toward facet joint cartilage replacement. *Neurosurgery.* **66**, pp.722-727.
- Emans, P. J., Jansen, E. J., van Iersel, D., Welting, T. J., Woodfield, T. B. et al. 2012. Tissue-engineered constructs: the effect of scaffold architecture in osteochondral repair. *Journal of Tissue Engineering and Regenerative Medicine.* **7**(9), pp.751-6.
- Erggelet, C., Sittinger, M., and Lahm, A. 2003. The arthroscopic implantation of autologous chondrocytes for the treatment of fullthickness cartilage defects of the knee joint. *Arthroscopy.* **19**(1), pp.108-110.
- Erickson, G., Gimble, J. M., Franklin, D. M., Rice, H. E., Awad, H., and Guilak, F. 2002. Chondrogenic potential of adipose tissue-derived stromal cells in vitro and in vivo. *Biochemical and Biophysical Research Communications.* **290**, pp.763-769.
- Facchini, A., Lisignoli, G., Cristino, S., Roseti, L., De Franceschi, L., Marconi, E., and Grigolo, B. 2006. Human chondrocytes and Mesenchymal stem cells grown onto engineered scaffold. *Biorheology.* **43**(3-4), pp.471-480.
- Farahat, M. N., Yanni, G., Poston, R., and Panayi, G. S. 1993. Cytokine expression in synovial membranes of patients with rheumatoid arthritis and osteoarthritis. *Ann Rheum Dis.* **52**(12), pp.870-875.
- Farndale, R. W., Sayers, C. A., and Barrett, A. J. 1982. A direct spectrophotometric microassay for sulfated glycosaminoglycans in cartilage cultures. *Connective Tissue Research.* **9**(4), pp.247-8.
- Farquhar, T., Xia, Y., Mann, K., Bertram, J., Burton-Wurster, N., Jelinski, L., and Lust, G. 1996. Swelling and Fibronectin accumulation in articular cartilage explants after cyclical impact. *J Orthop Res.* **14**(3), pp.417-423.

- Fellah, B. H., Weiss, P., Gauthier, O., Rouillon, T., Pilet, P., Daculsi, G., and Layrolle, P. 2006. Bone repair using a new injectable self-crosslinkable bone substitute. *J Orthop Res.* **24**(4), pp.628-35.
- Felson, D. 1993. The course of osteoarthritis and factors that affect it. *Rheum Dis Clin North Am.* **19**, pp.607-15.
- Felson, D.T., Lawrence, R.C., Dieppe, P.A., Hirsch, R., Helmick, C.G. et al. 2000. Osteoarthritis: new insights. Part 1: the disease and its risk factors. *Ann Intern Med.* **133**(8), pp.635– 46.
- Felson, D. T., Zhang, Y., Anthony, J. M., Naimark, A., and Anderson, J. J. 1992. Weight loss reduces the risk for symptomatic knee osteoarthritis in women. *Ann Intern Med.* **116**(7), pp.535-9.
- Fermor, H. L., Russel, S. L., Williams, S., Fisher, J., and Ingham, I. 2015. Development and characterisation of a decellularised bovine osteochondral biomaterial for cartilage repair. *J Mater Sci: Mater Med.* **26**(5), p.186.
- Fernandes, J. C., Martel-Pelletier, J., Lascau-Coman, V., Moldovan, F., Jovanovic, D., and Raynauld, J. P. 2002. Collagenase-1 and collagenase-3 synthesis in normal and early experimental osteoarthritic canine cartilage: an immunohistochemical study. *J Rheumatol.* **10**(9), pp.722-33.
- Fernandes, J. C., Martel-Pelletier, J., and Pelletier, J. P. 2003. The role of cytokines in osteoarthritis pathophysiology. *Biorheology.* **39**(1-2), pp.237-46.
- Firth, A., Aggeli, A., Burke, J. L., Yang, X., and Kirkham, J. 2006. Biomimetic self-assembling peptides as injectable scaffolds for hard tissue engineering. *Nanomedicine.* **1**(2), pp.189-199.
- Fishwick, C. W. G., Beevers, A. J., Carrick, L. M., Whitehouse, C. D., Aggeli, A., and Boden, N. 2003. Structures of Helical β -Tapes and Twisted Ribbons: The Role of Side-Chain Interactions on Twist and Bend Behavior. *Nano Letters.* **3**(11), pp.1475-1479.
- Fontan, F. R., Piuze, N. S., Chahla, J., Payne, K. A., LaPrade, R. F., Muschler, G. F., and Garrido, P. G. 2017. Stem and Progenitor Cells for Cartilage Repair: Source, Safety, Evidence, and Efficacy. *Operative Techniques in Sports Medicine.* **25**(1), pp.25-33.
- Forster, H. and Fisher, J. 1996. The influence of loading time and lubricant on the friction of articular cartilage. *Proc Inst Mech Eng H.* **210**(2), pp.109-119.
- Franke, O., Durst, K., Maier, V., Göken, M., Birkholz, T. et al. 2007. Mechanical properties of hyaline and repair cartilage studied by nanoindentation. *Acta Biomaterialia.* **3**, pp.873-881.
- French, M. M., Rose, S., Canseco, J., and Athanasiou, K. A. 2004. Chondrogenic differentiation of adult dermal fibroblasts. *Annals of Biomedical Engineering.* **32**, pp.50-56.
- Furuzawa-Carballeda, J. and Alcocer-varela, J. 1999. Interleukin-8, interleukin-10, intercellular adhesion molecule-1 and vascular cell adhesion molecule-1 expression levels are higher in synovial tissue from patients with rheumatoid arthritis than in osteoarthritis. *Scand J Immunol.* **50**(2), pp.215-222.
- Galler, K. M., Cavender, A., Yuwono, V., Dong, H., Shi, S. et al. 2008. Self-assembling peptide amphiphile nanofibers as a scaffold for dental stem cells. *Tissue Eng Part A.* **14**(12), pp.2051-8.
- Galler, K. M., Hartgerink, J. D., Cavender, A. C., Schmalz, G., and D'Souza, R. N. 2012. A customized self-assembling peptide hydrogel for dental pulp tissue engineering. *Tissue Eng Part A.* **18**(1-2), pp.176-84.
- Gibson, A. J., McDonnell, S. M., and Price, A. J. 2006. Matrix-Induced Autologous Chondrocyte Implantation. *Oper Tech Orthop.* **16**(4), pp.262-265.

- Gibson, J. N., White, M. D., Chapman, V. M., and Strachan, R. K. 1992. Arthroscopic lavage and debridement for osteoarthritis of the knee. *J Bone Joint Surg Br.* **74**(4), pp.534-7.
- Glasoe, P. K. and Long, F. A. 1960. Use of glass electrodes to measure acidities in deuterium oxide. *The Journal of Physical Chemistry.* **64**, pp.188-9.
- Gleghorn, J.P. and Bonassar, L. J. 2008. Lubrication mode analysis of articular cartilage using Stribeck surfaces. *J Biomech.* **41**(9), pp.1910-8.
- Gobbi, A., Kon, E., Berruto, M., Filardo, G., Delcogliano, M. et al. 2009. Patellofemoral Full-Thickness Chondral Defects Treated With Second-Generation Autologous Chondrocyte Implantation. *Am J Sports Med.* **37**(6), pp.1083-92.
- Goldring, M. B. and Goldring, S. R. 2010. Articular cartilage and subchondral bone in the pathogenesis of osteoarthritis. *Ann NY Acad Sci.* **1192**, pp.230-37.
- Goldring, M. B. and Marcu, K. B. 2009. Cartilage homeostasis in healthy and rheumatic diseases. *Arthritis Res Ther.* **11**, p.224.
- Goldwasser, M., Astley, T., van der Rest, M., and Glorieux, F. H. 1982. Analysis of the type of collagen present in osteoarthritic human cartilage. *Clin Orthop Relat Res.* **167**, pp.296-302.
- Gooding, C. R., Bartlett, W., Bentley, G., Skinner, J. A., Carrington, R., and Flanagan, A. 2006. A prospective, randomised study comparing two techniques of autologous chondrocyte implantation for osteochondral defects in the knee: Periosteum covered versus type I/III collagen covered. *Knee.* **13**(3), pp.203-210.
- Gosset, M., Berenbaum, F., Levy, A., Pigenet, A., Thirion, S., Saffar, J. L., and Jacques, C. 2006. Prostaglandin E2 synthesis in cartilage explants under compression: mPGES-1 is a mechanosensitive gene. *Arthritis Res Ther.* **8**(4), p.R135.
- Gouze, J. N., Bordji, K., Gulberti, S., Terlain, B., Netter, P. et al. 2001. Interleukin-1 β down-regulates the expression of glucuronosyltransferase I, a key enzyme priming glycosaminoglycan biosynthesis: influence of glucosamine on interleukin-1 β -mediated effects in rat chondrocytes. *Arthritis Rheum.* **44**(2), pp.351-360.
- Greene, G. W., Banquy, X., Lee, D. W., Lowrey, D. D., Yu, J., and Israelachvili, J. N. 2011. Adaptive mechanically controlled lubrication mechanism found in articular joints. *Proc Natl Acad Sci.* **108**(3), pp.5255-5259.
- Grigolo, B., Lisignoli, G., Piacentini, A., Fiorini, M., Gobbi, P. et al. 2002. Evidence for redifferentiation of human chondrocytes grown on a hyaluronan-based biomaterial (HYAFF 11): molecular, immunohistochemical and ultrastructural analysis. *Biomaterials.* **23**(4), pp.1187-95.
- Grigolo, B., Roseti, L., Fiorini, M., Fini, M., Giavaresi, G. et al. 2001. Transplantation of chondrocytes seeded on a hyaluronan derivative (HYAFF[®] 11) into cartilage defects in rabbits. *Biomaterials.* **22**(17), pp.2417-2424.
- Groh, M. M. and Herrera, J. 2009. A comprehensive review of hip labral tears. *Curr Rev Musculoskelet Med.* **2**(2), pp.105-117.
- Guilak, F. 2011. Biomechanical factors in osteoarthritis. *Best Pract Res Clin Rheumatol.* **25**(6), pp.815-23.
- Guilak, F., Meyer, B. C., Ratcliffe, A., and Mow, V. C. 1994. The effects of matrix compression on proteoglycan metabolism in articular cartilage explants. *Osteoarthritis Cartilage.* **2**(2), pp.91-101.

- Guilak, F., Setton, L. A., and Kraus, V. B. 2000. Structure and function of articular cartilage. *In: et al W.E. GARRETT, (ed). Principles And Practice Of Orthopaedic Sports Medicine*, Philadelphia: Lippincott Williams & Wilkins.
- Gullbrand, S. E., Schaer, T. P., Agarwal, P., Bendigo, J. R., Dodge, G. R. et al. 2017. Translation of an injectable triple-interpenetrating-network hydrogel for intervertebral disc regeneration in a goat model. *Acta Biomaterialia*. **60**, pp.201-209.
- Haene, R., Qamirani, E., Story, R. A., Pinsker, E., and Daniels, T. R. 2012. Intermediate outcomes of fresh talar osteochondral allografts for treatment of large osteochondral lesions of the talus. *Am J Bone Joint Surg*. **94**(12), pp.1105-10.
- Hall, M.L., Krawczak, D.A., Simha, N.K., and Lewis, K.L. 2009. Effect of Dermatan Sulfate on the indentation and Tensile Properties of Articular Cartilage. *Osteoarthritis Cartilage*. **17**(5), pp.655-661.
- Halloran, J.P., Sibole, S., van Donkelaar, C.C., van Turnhout, M.C., Oomens, C.W. et al. 2012. Multiscale mechanics of articular cartilage: Potentials and challenges of coupling musculoskeletal, joint and microscale computational models. *Ann Biomed Eng*. **40**, pp.2456-2474.
- Han, E., Chen, S. S., Klisch, S. M., and Sah, R. L. 2011. Contribution of Proteoglycan Osmotic Swelling Pressure to the Compressive Properties of Articular Cartilage. *Biophysical Journal*. **101**, pp.916-924.
- Hardingham, T. E. and Muir, H. 1974. Hyaluronic acid in cartilage and proteoglycan aggregation. *Biochem J*. **139**(3), pp.565-581.
- Harris, P. I. and Chapman, D. 1995. The conformational analysis of peptides using fourier transform IR spectroscopy. *Biopolymers*. **37**(4), pp.251-263.
- Harris, J. D., Siston, R. A., Brophy, R. H., Lattermann, C., Carey, J. L., and Flanigan, D. C. 2011. Failures, re-operations, and complications after autologous chondrocyte implantation. *Osteoarthritis Cartilage*. **19**(7), pp.779-791.
- Hart, D. J., Spector, T.D., Brown, P., Wilson, P., Doyle, D. V., and Silman, A. J. 1991. Clinical signs of early osteoarthritis: reproducibility and relation to x ray changes in 541 women in the general population. *Annals of Rheumatology*. **50**, pp.467-70.
- Hayami, T., Funaki, H., Yaoeda, K., Mitui, K., Yamagiwa, H. et al. 2003. Expression of the cartilage derived anti-angiogenic factor chondromodulin-I decreases in the early stage of experimental osteoarthritis. *J Rheumatol*. **30**(10), pp.2207-17.
- Hayes, W. C. and Mockros, L. F. 1971. Viscoelastic properties of human articular cartilage. *J Appl Physiol*. **31**(4), pp.562-8.
- Hendriks, J., Guidoux, J., Verdonk, P., and Slynarski, K. 2013. First clinical experience with INSTRUCT – a single surgery, autologous cell based technology for cartilage repair. *In: Conference: ICRS 2013*. Izmir.
- Hendriks, J. A. A., Moroni, L., Riesle, J., Wijn, J. R., and Blitterswijk, C. A. 2013. The effect of scaffold-cell entrapment capacity and physico-chemical properties on cartilage regeneration. *Biomaterials*. **34**(17), pp.4259-4265.
- He, B., Yuan, X., Zhou, A., Zhang, H., and Jiang, D. 2014. Designer functionalised self-assembling peptide nanofibre scaffolds for cartilage tissue engineering. *Expert Rev Mol Med*. **16**, p.e12.
- Hickery, M. S., Bayliss, M. T., Dudhia, J., Lewthwaite, J. C., Edwards, J. C., and Pitsillides, A. A. 2003. Age-related changes in the response of human articular cartilage to IL-1 α and

transforming growth factor- β (TGF- β): chondrocytes exhibit a diminished sensitivity to TGF- β . *Journal of Biological Chemistry*. **278**(52), pp.53063–53071.

Holland, T. A and Mikos, A. G. 2006. Biodegradable polymeric scaffolds- Improvements in bone tissue engineering through controlled drug delivery. *Adv Biochem Eng Biotechnol*. **102**, pp.161-185.

Hooper, K. A., Macon, N. D., and Kohn, J. 1998. Comparative histological evaluation of new tyrosine-derived polymers and poly (L-lactic acid) as a function of polymer degradation. *J Biomed Mater Res*. **41**(3), pp.443-54.

Hosseinkhani, H., Hong, P. D., and Yu, D. S. 2013. Self-Assembled Proteins and Peptides for Regenerative Medicine. *Chem Rev*. **113**(7), pp.4837-4861.

Howell, D. S. 1986. Pathogenesis of osteoarthritis. *Am J Med*. **80**, pp.24-8.

Hrabchak, C., Roulette, J., Moss, I., Woodhouse, K., Akens, M. et al. 2010. Assessment of biocompatibility and initial evaluation of genipin crosslinked elastin-like polypeptides in the treatment of an osteochondral knee defect in rabbits. *Acta Biomaterialia*. **6**(6), pp.2108-2115.

Huang, B. J., Hu, J. C., and Athanasiou, K. A. 2016. Cell-based tissue engineering strategies used in the clinical repair of articular cartilage. *Biomaterials*. **98**, pp.1-22.

Huang, J. I., Zuk, P. A., Jones, N. F., Zhu, M., Lorenz, H. P., Hedrick, M. H., and Benhaim, P. 2004. Chondrogenic potential of multipotential cells from human adipose tissue. *Plastic and Reconstructive Surgery*. **113**, pp.585-594.

Huebner, J. L., Otterness, I. G., Freund, E. M., Caterson, B., and Kraus, V. B. 1998. Collagenase 1 and collagenase 3 expression in a guinea pig model of osteoarthritis. *Arthritis Rheum*. **41**(5), pp.877-90.

Hunter, D. J. 2011. Osteoarthritis. *Best Pract Res Clin Rheumatol*. **25**(6), pp.801-814.

Hunter, D. J. and Matthews, G. 2011. Emerging drugs for osteoarthritis. *Expert Opin Emerg Drugs*. **16**(3), pp.479-491.

Hunziker, E. B. and Kapfinger, E. 1998. Removal of proteoglycans from the surface of defects in articular cartilage transiently enhances coverage by repair cells. *J Bone Joint Surg Br*. **80**(1), pp.144-50.

Hwang, N. S., Kim, M. S., Sampattavanich, S., Baek, J. H., Zhang, Z., and Elisseeff, J. 2006. Effects of three-dimensional culture and growth factors on the chondrogenic differentiation of murine embryonic stem cells. *Stem Cells*. **24**, pp.284-291.

Ishibashi, M., Hikita, A., Fujihara, Y., Takato, T., and Hoshi, K. 2017. Human auricular chondrocytes with high proliferation rate show high production of cartilage. *Regenerative Therapy*. **6**, pp.21-28.

Israelachvil, J. N. 1992. *Intermolecular and surface forces*. London: Academic Press.

Issa, R. I. and Griffin, T. M. 2012. Pathobiology of obesity and osteoarthritis: integrating biomechanics and inflammation. *Pathobiol Aging Age Relat Dis*. **9**(2), p.17470.

Jackson, M. and Mantsch, H. H. 1995. The Use and Misuse of FTIR Spectroscopy in the Determination of Protein Structure. *Critical Reviews in Biochemistry and Molecular Biology*. **30**, pp.95-120.

Jackson, D. W., Simon, T. M., and Aberman, H. M. 2001. Symptomatic articular cartilage degeneration: the impact of the new milenium. *Clin Orthop Relat Res*. **391 Suppl**, pp.S14-25.

- Jaffe, F. F., Mankin, H. J., Weiss, C., and Zarins, A. 1974. Water binding in the articular cartilage of rabbits. *J Bone Joint Surg Am*, Vol. **56**(5), pp.1031–1039.
- Jansen, E. J., Pieper, J., Gijbels, M. J., Guldmond, N. A., Riesle, J. et al. 2008. PEOT/PBT based scaffolds with low mechanical properties improve cartilage repair tissue formation in osteochondral defects. *Journal of Biomedical Materials Research Part A*. **89**(2), pp.444-52.
- Jay, G. D. and Cha, C. J. 1999. The effect of phospholipase digestion upon the boundary lubricating ability of synovial fluid. *J Rheumatol*. **26**(11), pp.2454-7.
- Jeong, C. G. and Hollister, S. J. 2010. A comparison of the influence of material on in vitro cartilage tissue engineering with PCL, PGS, and POC 3D scaffold architecture seeded with chondrocytes. *Biomaterials*. **31**(15), pp.4304-4312.
- Jin, R., Moreira Teixeira, L. S., Dijkstra, P. J., Karperien, M., van Blitterswijk, C. A., Zhong, Z. Y., and Feijen, J. 2009. Injectable chitosan-based hydrogels for cartilage tissue engineering. *Biomaterials*. **30**(13), pp.2544-2551.
- Jin, Z. M., Pickard, J. E., Forster, H., Ingham, E., and Fisher, J. 2000. Frictional behaviour of bovine articular cartilage. *Biorheology*. **37**(1-2), pp.57-63.
- Johnson, T. S., Xu, J. W., Zaporozhan, V. V., Mesa, J. M., Weinand, C. et al. 2004. Integrative repair of cartilage with articular and nonarticular chondrocytes. *Tissue Engineering*. **10**, pp.1308-1315.
- Johnstone, B., Alini, M., Cucchiari, M., Dodge, G. R., Eglin, D. et al. 2013. Tissue Engineering for Articular Cartilage Repair - The State of the Art. *Eur Cell Mater*. **25**, pp.248-267.
- Jordan, J. M., Luta, G., Stabler, T., B., Renner, J., Dragomir, A. D., and Vilim, V. 2003. Ethnic and sex differences in serum levels of cartilage oligomeric matrix protein: the Johnston County Osteoarthritis Project. *Arthritis & Rheumatism*. **48**, pp.675-81.
- Kang, Y., Yang, J., Khan, S., Anissian, L., and Ameer, G. A. 2006. A new biodegradable polyester elastomer for cartilage tissue engineering. *J Biomed Mater Res A*. **77**(2), pp.331-9.
- Kapoor, M., Martel-Pelletier, J., Lajeunesse, D., Pelletier, J. P., and Fahmi, H. 2011. The role of proinflammatory cytokines in the pathophysiology of osteoarthritis. *Nat Rev Rheumatol*. **7**(1), pp.33-42.
- Katta, J. 2007. *Self-assembling Peptide Networks for Treatment of Cartilage Degenerative Diseases*. Leeds: University of Leeds.
- Katta, J., Jin, Z., Ingham, E., and Fisher, J. 2008. Biotribology of articular cartilage — A review of the recent advances. *Medical Engineering and Physics*. **30**, pp.1349-1363.
- Katta, J., Jin, Z., Ingham, E., and Fisher, J. 2009. Effect of nominal stress on the long term friction, deformation and wear of native and glycosaminoglycan deficient articular cartilage. *Osteoarthritis and Cartilage*. **17**, pp.662-668.
- Katta, J., Pawaskar, S. S., Jin, Z. M., Ingham, E., and Fisher, J. 2007. Effect of load variation on the friction properties. *Proceedings of the Institution of Mechanical Engineers, Part J: Journal of Engineering Tribology*. **221**(3), pp.175–181.
- Katta, J., Stapleton, T., Ingham, E., Jin, Z. M., and Fisher, J. 2008. The effect of glycosaminoglycan depletion on the friction and deformation of articular cartilage. *Proc Inst Mech Eng H*. **222**(1), pp.1-11.
- Kellgren, J. H., Jeffrey, M. R., and Ball, J. 1963. *The epidemiology of chronic rheumatism. Atlas of standard radiographs of arthritis*. Oxford, UK: Blackwell Scientific Publications.

- Kellgren, J. H. and Lawrence, J. S. 1957. Radiological assessment of osteo-arthritis. *Annals of the Rheumatic Diseases*. **16**(4), pp.494-502.
- Kempson, G. E., Freeman, M. A., and Swanson, S. A. 1968. Tensile properties of articular cartilage. *Nature*. **220**(5172), pp.1127-8.
- Kempson, G. E., Freeman, M. A., and Swanson, S. A. 1971. The determination of a creep modulus for articular cartilage from indentation tests of the human femoral head. *J. Biomech.* **4**(4), pp.239-50.
- Kheir, E., Stapleton, T., Shaw, D., Jin, Z., Fisher, J., and Ingham, E. 2011. Development and characterization of an acellular porcine cartilage bone matrix for use in tissue engineering. *J Biomed Mater Res.* **99**, pp.283-94.
- Kim, J.E., Kim, S. H., and Jung, Y. 2015. In situ chondrogenic differentiation of bone marrow stromal cells in bioactive self-assembled peptide gels. *J Biosci Bioeng.* **120**(1), pp.91-8.
- Kim, S. E., Park, J. H., Cho, Y. W., Chung, H., Jeong, S. Y., Lee, E. B., and Kwon, I. C. 2003. Porous chitosan scaffold containing microspheres loaded with transforming growth factor-beta 1: implications for cartilage tissue engineering. *J Control Release.* **91**(3), pp.365-374.
- Kirkham, J., Firth, A., Vernals, D., Boden, N., Robinson, C. et al. 2007. Self-assembling Peptide Scaffolds Promote Enamel Remineralization. *J Dent Res.* **86**(5), pp.426-430.
- Kisiday, J., Jin, M., Kurz, B., Hung, H., Semino, C., Zhang, S., and Grodzinsky, A. J. 2002. Self-assembling peptide hydrogel fosters chondrocyte extracellular matrix production and cell division: Implications for cartilage tissue repair. *Proc Natl Acad Sci USA.* **99**(15), pp.9996-10001.
- Kleemann, R. U., Krockner, D., Cedraro, A., Tuischer, J., and Duda, G. N. 2005. Altered cartilage mechanics and histology in knee osteoarthritis: relation to clinical assessment (ICRS Grade). *Osteoarthritis Cartilage.* **13**(11), pp.958-63.
- Knutsen, G., Drogset, J. O., Engebretsen, L., Grøntvedt, T., Isaksen, V. et al. 2010. A randomized trial comparing autologous chondrocyte implantation with microfracture: findings at five years. *J Sports Med.* **38**(1), pp.68-77.
- Knutsen, G., Engebretsen, L., Ludvigsen, T.C., Drogset, J. O., Grøntvedt, T. et al. 2004. Autologous chondrocyte implantation compared with microfracture in the knee: A randomized trial. *J Bone Joint Surg Am.* **86**(3), pp.455-464.
- Kock, L. M., Schulz, R. M., van Donkelaar, C. C., Thummler, C. B., Bader, A., and Ito, K. 2009. RGD-dependent integrins are mechanotransducers in dynamically compressed tissue-engineered cartilage constructs. *J Biomech.* **42**(13), pp.2177-82.
- Kon, E., Delcogliano, A., Filardo, G., Montaperto, C., and Marcacci, M. 2008. Second generation issues in cartilage repair. *Sports Med Arthrosc Rev.* **16**(4), pp.221-9.
- Kon, E., Gobbi, A., Filardo, G., Delcogliano, M., Zaffagnini, S., and Marcacci, M. 2009. Arthroscopic second-generation autologous chondrocyte implantation compared with microfracture for chondral lesions of the knee: prospective nonrandomized study at 5 years. *Am J Sports Med.* **37**(1), pp.33-41.
- Kong, J. and Yu, S. 2007. Fourier Transform Infrared Spectroscopic Analysis of Protein Secondary Structures. *Acta Biochimica et Biophysica Sinica.* **39**(8), pp.549-59.
- Koppel, D.E., Axelrod, D., Schlessinger, J., Elson, E.L., and Webb, W.W. 1976. Dynamics of fluorescence marker concentration as a probe of mobility. *Biophys. J.* **16**, pp.1315-1329.

- Kramer, J., Hegert, C., Guan, K., Wobus, A. M., Müller, P. K., and Rohwedel, J. 2000. Embryonic stem cell-derived chondrogenic differentiation in vitro: activation by BMP-2 and BMP-4. *Mechanisms of Development*. **92**, pp.193-205.
- Krasnokutsky, S., Attur, M., Palmer, G., Samuels, J., and Abramson, S. B. 2008. Current concepts in the pathogenesis of osteoarthritis. *Osteoarthritis Cartilage*. **16**(Suppl. 3), pp.S1-3.
- Kreuz, P. C., Müller, S., Freymann, U., Erggelet, C., Niemeyer, P., Kaps, C., and Hirschmüller, A. 2011. Repair of Focal Cartilage Defects with Scaffold-Assisted Autologous Chondrocyte Grafts. *The American Journal of Sports Medicine*. **39**(8), pp. 1697-1706.
- Kreuz, P. C., Müller, S., Ossendorf, C., Kaps, C., and Erggelet, C. 2009. Treatment of focal degenerative cartilage defects with polymer-based autologous chondrocyte grafts: four-year clinical results. *Arthritis Research & Therapy*. **11**(2), p.R33.
- Kruger, T., Wohlrab, D., Reichel, H., and Hein, W. 2000. The effect of arthroscopic joint debridement in advanced arthrosis of the knee joint. *ZentralblChir*. **125**(6), pp.490-3.
- Kubelka, J. and Keiderling, T. A. 2001. Differentiation of β -Sheet-forming structures: An initio-based simulations of IR absorption and vibrational CD for model peptide and protein β -Sheets. *ournal of the American Chemical Society*. **123**(48), pp.12048-58.
- Kumagai, K., Suzuki, S., Kanri, Y., Matsubara, R., Fujii, K. et al. 2015. Spontaneously developed osteoarthritis in the temporomandibular joint in STR/ort mice. *Biomed Rep*. **3**(4), pp.453-6.
- Kunčická, L., Kocicha, R., and Lowe, T. C. 2017. Advances in metals and alloys for joint replacement. *Progress in Materials Science*. **88**, pp.232-280.
- Kuyinu, E. L., Narayanan, G., Nair, L. S., and Laurencin, C. T. 2016. Animal models of osteoarthritis: classification, update, and measurement of outcomes. *J Orthop Surg Res*. **11**(19), pp.1-27.
- Kyle, S., Aggeli, A., Ingham, E., and McPherson, M. J. 2009. Production of self-assembling biomaterials for tissue engineering. *Trends Biotechnol*. **27**(7), pp.423-33.
- Kyle, S., Aggeli, A., Ingham, E., and McPherson, M. J. 2010. Recombinant self-assembling peptides as biomaterials for tissue engineering. *Biomaterials*. **31**(36), pp.9395-9405.
- Kyle, S., Aggeli, A., Ingham, E., and McPherson, M. J. 2010. Recombinant self-assembling peptides as biomaterials for tissue engineering. *Biomaterials*. **31**(36), pp.9395-9405.
- Laffargue, P., Delalande, J. L., Maillet, M., Vanhecke, C., and Decoulx, J. 1999. Reconstruction of the anterior cruciate ligament: Arthrotomy versus arthroscopy. *Rev Chir Orthop Reparatrice Appar Mot*. **85**(4), pp.367-373.
- Lahiji, A., Sohrabi, A., Hungerford, D., and Frondoza, C. 2000. Chitosan supports the expression of extracellular matrix proteins in human osteoblasts and chondrocytes. *J Biomed Mater Res*. **51**, pp.586-95.
- Lai, W. M., Hou, J. S., and Mow, V. C. 1991. A triphasic theory for the swelling and deformation behaviors of articular cartilage. *J Biomech Eng*. **113**(3), pp.245-58.
- Lai, W. M., Mow, V. C., and Roth, V. 1981. Effects of nonlinear strain-dependent permeability and rate of compression on the stress behavior of articular cartilage. *J Biomech Eng*. **103**(2), pp.61-6.
- Lark, M. W., Bayne, E. K., J., Flanagan., Harper, C. F., Hoerrner, L. A., Hutchinson, N. I. et al. 1997. Aggrecan degradation in human cartilage. Evidence for both matrix metalloproteinase and aggrecanase activity in normal, osteoarthritic, and rheumatoid joints. *J Clin Invest*. **100**(1), pp.93 –106.

- Le Graverand, M. P., Eggerer, J., Vignon, E., Otterness, I. G., Barclay, L., and Hart, D. A. 2002. Assessment of specific mRNA levels in cartilage regions in a lapine model of osteoarthritis. *J Orthop Res.* **20**(3), pp.535-44.
- Leddy, H. and Guilak, F. 2003. Site-Specific Molecular Diffusion in Articular Cartilage Measured using Fluorescence Recovery after Photobleaching. *Annals of Biomedical Engineering.* **31**, pp.753-760.
- Lee, A. S., Ellman, M. B., Yan, D., Kroin, J. S., Cole, B. J., van Wijnen, A. J., and Im, H. J. 2013. A current review of molecular mechanisms regarding osteoarthritis and pain. *Gene.* **527**(2), pp.440-447.
- Lee, J. E., Kim, S. E., Kwon, I. C., Ahn, H. J., Cho, H. et al. 2004. Effects of a chitosan scaffold containing TGF-beta 1 encapsulated chitosan microspheres on in vitro chondrocyte culture. *Artif Organs.* **28**(9), pp.829-839.
- Lee, S. H. and Shin, H. 2007. Matrices and scaffolds for delivery of bioactive molecules in bone and cartilage tissue engineering. *Adv Drug Deliv Rev.* **59**(4-5), pp.339-359.
- Lee, K. H., Song, S. U., Hwang, T. S., Yi, Y., Oh, I. S. et al. 2001. Regeneration of hyaline cartilage by cell-mediated gene therapy using transforming growth factor beta 1-producing fibroblasts. *Human Gene Therapy.* **12**, pp.1805-1813.
- Leighton, R., Akermark, C., Therrien, R., Richardson, J. B, Andersson, M., Todman, M. G., and Arden, N. K. 2014. NASHA hyaluronic acid vs. methylprednisolone for knee osteoarthritis: a prospective, multi-centre, randomized, non-inferiority trial. *Osteoarthritis Cartilage.* **22**(1), pp.17-25.
- Li, W. J., Chiang, H., Kuo, Y. F., Lee, H. S., Jiang, C. C., and Tuan, R. S. 2009. Evaluation of articular cartilage repair using biodegradable nanofibrous scaffolds in a swine model: a pilot study. *J Tissue Eng Regen Med.* **3**(1), pp.1-10.
- Li, W. J., Danielson, K. G., Alexander, P. G., and Tuan, R. S. 2003. Biological response of chondrocytes cultured in three-dimensional nanofibrous poly(epsilon-caprolactone) scaffolds. *J Biomed Mater Res.* **67A**, pp.1105-1114.
- Li, Y., Tew, S. R., Russell, A. M., Gonzalez, K. R., Hardingham, T. E., and Hawkins, R. E. 2004. Transduction of passaged human articular chondrocytes with adenoviral, retroviral and lentiviral vectors and the effects of enhanced expression of SOX9. *Tissue Engineering.* **10**, pp.575-584.
- Little, C. B., Barai, A., Burkhardt, D., Smith, S. M., Fosang, A. J. et al. 2009. Matrix metalloproteinase 13-deficient mice are resistant to osteoarthritic cartilage erosion but not chondrocyte hypertrophy or osteophyte development. *Arthritis Rheum.* **60**(12), pp.3723-33.
- Li, W.J., Tuli, R., Okafor, C., Derfou, A., Daneilson, K. G., Hall, D. J., and Tuan, R. S. 2005. A three dimensional nanofibrous scaffold for cartilage tissue engineering using human mesenchymal stem cells. *Biomaterials.* **26**, pp.599-609.
- Liu, A., Jennings, L. M., Ingham, E., and Fisher, J. 2015. Tribology studies of the natural knee using an animal model in a new whole joint natural knee simulator. *Journal of Biomechanics.* **48**, pp.3004-3011.
- Liu, M., Zeng, X., Ma, C., Yi, H., Ali, Z. et al. 2017. Injectable hydrogels for cartilage and bone tissue engineering. *Bone Research.* **5**(17014).
- Livesley, P., Doherty, M., Needoff, M., and Moulton, A. 1991. Arthroscopic lavage of osteoarthritic knees. *J Bone Joint Surg Br.* **73**(6), pp.922-6.

- Lohan, A., Marzahan, U., Sayed, K. E., Haisch, A., Muller, R. D. et al. 2014. Osteochondral articular defect repair using auricle-derived autologous chondrocytes in a rabbit model. *Annals of Anatomy*. **196**(5), pp.317-326.
- Lohmander, L. S., Dahlberg, L., Ryd, L., and Heinegård, D. 1989. Increased levels of proteoglycan fragments in knee joint fluid after injury. *Arthritis Rheum*. **32**(11), pp.1434–1442.
- Longfield, M. D., Dowson, D., Walker, P. S., and Wright, V. 1969. Boosted lubrication of human joints by fluid enrichment and entrapment. *Biomed Eng*. **4**(11), pp.517-22.
- Loo, Y., Wong, Y. C., Cai, E. Z., Ang, C. H., Raju, A. et al. 2014. Ultrashort peptide nanofibrous hydrogels for the acceleration of healing of burn wounds. *Biomaterials*. **35**(17), pp.4805-14.
- Lorenz, H. and Richter, W. 2006. Osteoarthritis: Cellular and molecular changes in degenerating cartilage. *Prog Histochem Cytochem*. **40**(3), pp.135-163.
- Lorenz, H., Wenz, W., Ivancic, M., Steck, E., and Richter, W. 2005. Early and stable upregulation of collagen type II, collagen type I and YKL40 expression levels in cartilage during early experimental osteoarthritis occurs independent of joint location and histological grading. *Arthritis Res Ther*. **7**(1), pp.156-65.
- Lum, L. and Elisseeff, J. 2003. Injectable Hydrogels for Cartilage Tissue Engineering. *Topics in Tissue Engineering*. **30**, pp.1-25.
- Lu, J. X., Prudhommeaux, F., Meunier, A., Sedel, L., and Guillemin, G. 1999. Effects of Chitosan on rat knee cartilages. *Biomaterials*. **20**, pp.1937-1944.
- Lu, X. L., Sun, D. D., Guo, X. E., Chen, F. H., Lai, W. M., and Mow, V. C. 2004. Indentation determined mechano-electrochemical properties and fixed charge density of articular cartilage. *Ann Biomed Eng*. **32**(3), pp.370-9.
- Mak, A. F., Lai, W. M., and Mow, V. C. 1987. Biphasic indentation of articular cartilage – I. Theoretical analysis. *J. Biomechanics*. **20**(7), pp.703-714.
- Mankin, H. J. 1982. The response of articular cartilage to mechanical injury. *J Bone Joint Surg Am*. **64**(3), pp.460–466.
- Mankin, H. J. and Lippiell, L. 1971. The Glycosaminoglycans of Normal and Arthritic Cartilage. *J Clin Invest*. **50**(8), pp.1712–1719.
- Mankin, H. J., Mow, V. C., Buckwalter, J. A., Iannotti, J. P., and Ratcliffe, A. 1999. Articular cartilage structure, composition, and function (Chapter 17). *In: Orthopedic basic science: biology and biomechanics of the musculoskeletal system*, Rosemont : American Academy of Orthopaedic Surgeons, pp.444–70.
- Marcacci, M., Berruto, M., Brocchetta, D., Delcogliano, A., Ghinelli, D. et al. 2005. Articular cartilage engineering with Hyalograft C: 3-year clinical results. *Clin Orthop Relat Res*. **435**, pp.96-105.
- Marcacci, M., Zaffagnini, S., and Kon, E. 2002. Arthroscopic autologous chondrocyte transplantation: technical note. *Knee Surg Sports Traumatol Arthrosc*. **10**(3), pp.154-9.
- Marijnissen, A. C., van Roermund, P. M., TeKoppele, J. M., Bijlsma, J. W., and Lafeber, F. P. 2002. The canine ‘groove’ model, compared with the ACLT model of osteoarthritis. *Osteoarthritis Cartilage*. **10**(2), pp.145-55.
- Maroudas, A., Bullough, P., Swanson, S. A., and Freeman, M. A. 1968. The permeability of articular cartilage. *J Bone Joint Surg Br*. **50**(1), pp.166-177.

- Maroudas, A., Evans, H., and Almeida, L. 1973. Cartilage of the hip joint: Topographical variation of glycosaminoglycan content in normal and fibrillated tissue. *Ann Rheum Dis.* **32**(1), pp.1-9.
- Maroudas, A. and Venn, M. 1977. Chemical composition and swelling of normal and osteoarthrotic femoral head cartilage. *Ann Rheum Diss.* **36**, pp.399-406.
- Martel-Pelletier, J. 2004. Pathophysiology of osteoarthritis. *Osteoarthritis Cartilage.* **12**(Suppl A), pp.S31-3.
- Mason, S.J., Legge, G.E., and Kallie, C. S. 2005. Variability in the length and frequency of steps of sighted and visually impaired walkers. *Journal of Visual Impairment and Blindness.* **99**(12), pp.741-754.
- Matsiko, A., Levingstone, T, J., and O'Brien, F. J. 2013. Advanced Strategies for Articular Cartilage Defect Repair. *Materials.* **6**(2), pp.637-668.
- Maude, S., Ingham, E., and Aggeli, A. 2013. Biomimetic self-assembling peptides as scaffolds for soft tissue engineering. *Nanomedicine.* **8**(5), pp.823-847.
- Maude, S., Miles, D. E., Felton, S. H., Ingram, J., Carrick, L. M. et al. 2011. De novo designed positively charged tape-forming peptides: self-assembly and gelation in physiological solutions and their evaluation as 3D matrices for cell growth. *Soft Matter.* **7**(18), pp.8085-99.
- McCann, L., Ingham, E., Jin, Z., and Fisher, F. 2009. Influence of the meniscus on friction and degradation of cartilage in the natural knee joint. *Osteoarthritis Cartilage.* **17**(8), pp.995–1000.
- McCoy, A. M. 2015. Animal Models of Osteoarthritis: Comparisons and Key Considerations. *Vet Pathol.* **52**(5), pp.803-18.
- McCutchen, C. W. 1959. Sponge-hydrostatic and weeping bearings. *Nature.* **184**, pp.1284--1285.
- McDevitt, C., Gilbertson, E., and Muir, H. 1977. An experimental model of osteoarthritis; early morphological and biochemical changes. *J Bone Joint Surg Br.* **59**(1), pp.24-35.
- McGinley, B., Cushner, F., and Scott, W. 1999. Debridement arthroscopy. 10-year followup. *Clin Orthop Relat Res.* **367**, pp.667-72.
- McIlwraith, C. W., Frisbie, D. D., Kawcak, C. E., Fuller, C. J., Hurtig, M., and Cruz, A. 2010. The OARSI histopathology initiative recommendations for histological assessments of osteoarthritis in the horse. *Osteoarthr Cartil.* **18**(Supp 3), pp.S93-105.
- McNary, S. M., Athanasiou, K.A., and Reddi, A. H. 2012. Engineering Lubrication in Articular Cartilage. *Tissue Eng Part B.* **18**(2), pp.88-99.
- Mechanically Functional Scaffold Technology.* 2015. [online]. Available from World Wide Web: <<http://www.cellcotec.com/technology/mechanically-functional-scaffold/>>
- Meng, H., Chen, L., Ye, Z., Wang, S., and Zhao, X. 2009. The effect of a self-assembling peptide nanofiber scaffold (peptide) when used as a wound dressing for the treatment of deep second degree burns in rats. *Biomed Mater Res B Appl Biomater.* **89**(2), pp.379-91.
- Mesa, J. M., Zaporozjan, V., Weinand, C., Johnson, T. S., Bonassar, L. et al. 2006. Tissue engineering cartilage with aged articular chondrocytes in vivo. *Plastic and Reconstructive Surgery.* **118**, pp.41-49.
- Messier, S. P. 1994. Osteoarthritis of the knee and associated factors of age and obesity: effects on gait. *Med Sci Sports Exerc.* **26**(12), pp.1446-52.

- Messier, S., Loeser, R., Mitchell, M. N., Valle, G., Morgan, T. P., Rejeski, W. J., and Ettinger, W. H. 2000. Exercise and weight loss in obese older adults with knee osteoarthritis: a preliminary study. *J Am Geriatr Soc.* **48**(9).
- Messner, K., Fahlgren, A., Persliden, J., and Andersson, B. 2001. Radiographic joint space narrowing and histologic changes in a rabbit meniscectomy model of early knee osteoarthritis. *Am J Sports Med.* **29**(2), pp.151-60.
- Migliore, A. and Procopio, S. 2015. Effectiveness and utility of hyaluronic acid in osteoarthritis. *Clin Cases Miner Bone Metab.* **12**(1), pp.31-33.
- Milentijevic, D., Helfet, D. L., and Torzilli, P. A. 2003. Influence of stress magnitude on water loss and chondrocyte viability in impacted articular cartilage. *J Biomech Eng.* **125**(5), pp.594-601.
- Miles, D. E. 2012. *Self-assembling peptide/glycosaminoglycan hydrogels for spinal therapies*. Leeds: University of Leeds.
- Miles, D. E., Mitchell, E. A., Kapur, N., Beales, P. A., and Wilcox, R. K. 2016. Peptide:glycosaminoglycan hybrid hydrogels as an injectable intervention for spinal disc degeneration. *Journal of Materials Chemistry B.* **4**(19), pp.3225-31.
- Miller, K. L. and Clegg, D. O. 2011. Glucosamine and Chondroitin Sulfate. *Rheum Dis Clin North Am.* **37**(1), pp.103-118.
- Minas, T. 2001. Autologous chondrocyte implantation for focal chondral defects of the knee. *Clin Orthop Relat Res.* **391**(Suppl 1), pp.S349-61.
- Minas, T. and Bryant, T. 2005. The role of autologous chondrocyte implantation in the patellofemoral joint. *Clin Orthop Relat Res.* **436**, pp.30-9.
- Miosge, N., Hartmann, M., Maelicke, C., and Herken, R. 2004. Expression of collagen type I and type II in consecutive stages of human osteoarthritis. *Histochem Cell Biol.* **122**(3), pp.229-36.
- Mithoefer, K., Williams, R. J., Warren, R. F., Potter, H. G., Spock, C. R. et al. 2005. The microfracture technique for the treatment of articular cartilage lesions in the knee. A prospective cohort study. *J Bone Joint Surg Am.* **87**(9), pp.1911-20.
- Mobasher, A., Lewis, R., Maxwell, J. E., Hill, C., Womack, M., and Barrett-Jolley, R. 2010. Characterization of a stretch-activated potassium channel in chondrocytes. *J Cell Physiol.* **223**(2), pp.511-8.
- Morgan, C. E., Dombrowski, A. W., Rubert Pérez, C. M., Bahnson, E. S., Tsihli, N. D. et al. 2016. Tissue-Factor Targeted Peptide Amphiphile Nanofibers as an Injectable Therapy To Control Hemorrhage. *ACS Nano.* **10**(1), pp.899-909.
- Moroni, L., Hendriks, J. A., Schotel, R., Wijn, J. R., and Blitterswijk, C. A. 2007. Design of biphasic polymeric 3-dimensional fiber deposited scaffolds for cartilage tissue engineering applications. *Tissue Eng.* **13**(2), pp.361-371.
- Moskowitz, R. W., Altman, R. W., Hochberg, M. C., Buckwalter, J. A., and Goldberg, V. M. 2007. *Osteoarthritis: diagnosis and medical/surgical management*. Philadelphia: Lippincott Williams, and Wilkins.
- Mouw, J. K., Case, N. D., Gulberg, R. E., Plaas, A. H., and Levenston, M. E. 2005. Variations in matrix composition and GAG fine structure among scaffolds for cartilage tissue engineering. *Osteoarthritis Cartilage.* **13**(9), pp.828-836.
- Mow, V. C. and Ateshian, G. A. 1997. *Friction, lubrication and wear of diarthrodial joints*. New York: Raven Press.

- Mow, V. C., Flatow, E. L., and Ateshian, G. A. 2000. Biomechanics. *In: Orthopaedic basic science: Biology and biomechanics of the musculoskeletal system*, American Academy of Orthopaedic Surgeons, pp.140-42.
- Mow, V. C., Gibbs, M. C., Lai, W. M., Zhu, W. B., and Athanasiou, K. A. 1989. Biphasic indentation of articular cartilage – II. A numerical algorithm and an experimental study. *J Biomechanics*. **22**(8-9), pp.853-861.
- Mow, V. C. and Hayes, W. C. 1997. *Basic Orthopaedic Biomechanics*. Philadelphia: Lippincott-Raven Press.
- Mow, V. C., Holmes, M. H., and Lai, W. M. 1984. Fluid transport and mechanical properties of articular cartilage: a review. *J Biomech*. **17**(5), pp.377-94.
- Mow, V. C. and Hung, C. T. 1989. Biomechanics of articular cartilage. *In: Basic biomechanics of the musculoskeletal system*, Philadelphia: Lea & Febiger, pp.31-57.
- Mow, V. C., Kuei, S. C., Lai, W. M., and Armstrong, C. G. 1980. Biphasic creep and stress relaxation of articular cartilage in compression? Theory and experiments. *J Biomech Eng*. **102**(1), pp.73-84.
- Mow, V. C. and Lai, W. M. 1980. Recent developments in Synovial Joint Biomechanics. *SIAM Rev*. **22**(3), pp.275-317.
- Mow, V. C., Lai, W. M., and Hou, J. S. 1990. Triphasic theory for swelling properties of hydrated charged soft biological tissues. *Appl Mech Rev*. **43**(5), pp.S134 -S141.
- Mow, V. C., Wang, C. C., and Hung, C.T. 1999. The extracellular matrix, interstitial fluid and ions as a mechanical signal transducer in articular cartilage. *Osteoarthr Cartil*. **7**, pp.41-58.
- Muir, H. 1978. Proteoglycans of cartilage. *J Clin Pathol Suppl (R Coll Pathol)*. **12**, pp.67-81.
- Mwale, F., Wertheimer, M. R., and Antoniou, J. 2008. Novel nitrogen rich polymers and chitosan for tissue engineering of intervertebral discs. *Adv Sci Tech*. **57**, pp.117-124.
- Myers, S. L., Brandt, K. D., Ehlich, J. W., Braunstein, E. M., Shelbourne, K. D., Heck, D.A., and Kalasinski, L. A. 1990. Synovial inflammation in patients with early osteoarthritis of the knee. *J Rheumatol*. **17**(12), pp.1662-69.
- Nakamura, S., Ito, H., Nakamura, K., Kuriyama, S., Furu, M., and Matsuda, S. 2017. Long-Term Durability of Ceramic Tri-Condylar Knee Implants: A Minimum 15-Year Follow-Up. *The Journal of Arthroplasty*. **32**(6), pp.1874-1879.
- Nakamura, H., Yoshino, S., Kato, T., Tsuruha, J., and Nishioka, K. 1999. T-cell mediated inflammatory pathway in osteoarthritis. *Osteoarthritis Cartilage*. **7**(4), pp.401-2.
- Nakayama, Y., Narita, T., Mori, A., Uesaka, S., Miyazaki, K., and Ito, H. 2002. The Effects of Age and Sex on Chondroitin Sulfates in Normal Synovial Fluid. *Arthritis Rheum*. **46**(8), pp.2105-2108.
- Nakayama, Y., Shirai, Y., Yoshihara, K., and Uesaka, S. 2000. Evaluation of Glycosaminoglycans Levels in normal joint fluid of the knee. *J Nippon Med Sch*. **67**(2), pp.92-95.
- Nehrer, S1., Dorotka, R., Domayer, S., Stelzeneder, D., and Kotz, R. 2009. Treatment of Full-Thickness Chondral Defects With Hyalograft C in the Knee : A Prospective Clinical Case Series With 2 to 7 Years' Follow-up. *Am J Sports Med*. **37**(Suppl 1), pp.S81-7.
- Neu, C. P., Komvopoulos, K., and Reddi, A. H. 2008. The interface of functional biotribology and regenerative medicine in synovial joints. *Tissue Eng Part B Rev*. **14**(3), pp.235-47.
- Neyret, P., Donell, S., and Dejour, H. 1994. Osteoarthritis of the knee following meniscectomy. *Br J Rheumatol*. **33**(3), pp.267-8.

- Ng, L., Grodzinsky, A. J., Patwari, P., Sandy, J., Plaas, A., and Ortiz, C. 2003. Individual cartilage aggrecan macromolecules and their constituent glycosaminoglycans visualized via atomic force microscopy. *J Struct Biol.* **143**(3), pp.242-57.
- Niemeyer, P., Lenz, P., Kreuz, P. C., Salzmann, G. M., Südkamp, N. P., Schmal, H., and Steinwachs, M. 2010. Chondrocyte-Seeded Type I/III Collagen Membrane for Autologous Chondrocyte Transplantation: Prospective 2-Year Results in Patients With Cartilage Defects of the Knee Joint. *Arthroscopy.* **26**(8), pp.1074-1082.
- Nietfeld, J. J., Wilbrink, B., Den Otter, W., Huber, J., and Huber-Bruning, O. 1990. the effect of human interleukin 1 on proteoglycan metabolism in human and porcine cartilage explants. *J Rheumatol.* **17**(6), pp.818-26.
- Noel, D., Djouad, F., Bouffi, C., Mrugala, D., and Jorgensen, C. 2007. Multipotent mesenchymal stromal cells and immune tolerance. *Leukemia & Lymphoma.* **48**(7), pp.1283-1289.
- Nukavarapu, S. P.; Dorcenus, D. L. 2013. Osteochondral tissue engineering: Current strategies and challenges. *Biotechnol Adv.* **31**(5), pp.706-721.
- Ontario, H. Q. 2005. Arthroscopic lavage and debridement for osteoarthritis of the knee: an evidence-based analysis. *Ont Health Technol Assess Ser.* **5**(12), pp.1-37.
- Ossendorf, C., Kaps, C., Kreuz, P. C., Burmester, G. R., Sittinger, M., and Erggelet, C. 2007. Treatment of posttraumatic and focal osteoarthritic cartilage defects of the knee with autologous polymer-based three-dimensional chondrocyte grafts: 2-year clinical results. *Arthritis Research & Therapy.* **9**(R41), pp.1-11.
- Otsuki, S., Nakajima, M., Lotz, M., and Kinoshita, M. 2008. Hyaluronic acid and chondroitin sulfate content of osteoarthritic human knee cartilage: site-specific correlation with weight-bearing force based on femorotibial angle measurement. *J Orthop Res.* **26**(9), pp.1194-8.
- Ozeki, M., Kuroda, S., Kon, K., and Kasugai, S. 2011. Differentiation of bone marrow stromal cells into osteoblasts in a self-assembling peptide hydrogel: in vitro and in vivo studies. *J Biomater Appl.* **25**(7), pp.663-84.
- Panossian, A., Ashiku, S., Kirshhoff, C.H., Randolph, M. A., and Yaremchuk, M. J. 2001. Effects of cell concentration and growth period on articular and ear chondrocyte transplants for tissue engineering. *Plastic and Reconstructive Surgery.* **108**, pp.392-402.
- Park, S., Krishnan, R., Nicoll, S. B., and Ateshian, G. A. 2003. Cartilage interstitial fluid load support in unconfined compression. *J Biomech.* **36**(12), pp.1785-96.
- Pawaskar, S. S., Fisher, J., and Jin, Z. 2010. Robust and general method for determining surface fluid flow boundary conditions in articular cartilage contact mechanics modelling. *Journal of Biomechanical Engineering transactions of the American Society of Mechanical Engineers.* **132**, pp.1-8.
- Pawaskar, S. S., Grosland, N. M., Ingham, E., Fisher, J., and Jin, Z. 2011. Hemiarthroplasty of hip joint: An experimental validation using porcine acetabulum. *Journal of Biomechanics.* **44**, pp.1536-1542.
- Pelletier, J., Boileau, C., Altman, R. D., and Martel-Pelletier, J. 2010. Experimental models of osteoarthritis: usefulness in the development of disease-modifying osteoarthritis drugs/agents. *Therapy.* **7**(6), pp.621-34.
- Pelletier, J. P., Martel-Pelletier, J., Ghandur-Mnaymneh, L., Howell, D. S., and Woessner, Jr. J. F. 1985. Role of synovial membrane inflammation in cartilage matrix breakdown in the Pond-Nuki dog model of osteoarthritis. *Arthritis Rheum.* **33**(10), pp.554-61.

- Pelton, J. T. and McLean, L. R. 2000. Spectroscopic methods for analysis of protein secondary structure. *Analytical Biochemistry*. **277**, pp.167-176.
- Pfander, D., R., Rahmzadeh., and Scheller, E. E. 1999. Presence and distribution of collagen II, collagen I, fibronectin, and tenascin in rabbit normal and osteoarthritic cartilage. *J Rheumatol*. **26**(2), pp.386-94.
- Pickard, J., Ingham, E., Egan, J., and Fisher, J. 1998. Investigation into the effect of proteoglycan molecules on the tribological properties of cartilage joint tissues. *Proc. Instn Mech. Engrs, Part H: J. Engineering in Medicine*. **212**(H3), pp.177-182.
- Pitsillides, A. A. and Beier, F. 2011. Cartilage biology in osteoarthritis - lessons from developmental biology. *Nat Rev Rheumatol*. **7**(11), pp.654-663.
- Pond, M. J. and Nuki, G. 1973. Experimentally induced osteoarthritis in the dog. *Ann Rheum Dis*. **32**(4), pp.387-8.
- Poole, C. A. 1997. Articular cartilage chondrons: form, function and failure. *J Anat*. **191**(1), pp.1-13.
- Poole, A. R., Pidoux, I., Reiner, A., and Rosenberg, L. 1982. An immunoelectron microscope study of the organization of proteoglycan monomer, link protein, and collagen in the matrix of articular cartilage. *J Cell Biol*. **93**(3), pp.921-937.
- Proctor, C., Schmidt, M., Whipple, R., Kelly, M., and Mow, V. 1989. Material Properties of the Normal Medial Bovine Meniscus. *J. Orthop. Res*. **7**, pp.771-782.
- Radhakrishnan, J., Subramanian, A., Krishnan, U. M., and Sethuraman, S. 2017. Injectable and 3D Bioprinted Polysaccharide Hydrogels: From Cartilage to Osteochondral Tissue Engineering. *Biomacromolecules*. **18**(1), pp.1-26.
- Radin, E. L. and Rose, R. M. 1986. Role of subchondral bone in the initiation and progression of cartilage damage. *Clin Orthop Relat Res*. **213**, pp.34-40.
- Ramage, L., Nuki, G., and Salter, D. M. 2009. Signalling cascades in mechanotransduction: cell-matrix interactions and mechanical loading. *Scand J Med Sci Sports*. **19**(4), pp.457-69.
- Reboul, P., Pelletier, J. P., Tardif, G., Cloutier, J. M., and Martel-Pelletier, J. 1996. The new collagenase, collagenase-3, is expressed and synthesized by human chondrocytes but not by synoviocytes. A role in osteoarthritis. *J Clin Invest*. **97**(9), pp.2011-9.
- Ren, K., He, C., Li, G., and Chen, X. 2015. In-situ forming glycopolymer hydrogels as biomimetic scaffolds for cartilage tissue engineering. *J Control Release*. **213**, pp.e64-5.
- Rieppo, J., Toyras, J., Nieminen, M. T., Kovanen, V., Hyttinen, M. M. et al. 2003. Structure-function relationships in enzymatically modified articular cartilage. *Cells Tissues Organs*. **175**(3), pp.121-32.
- Rogers, B. A., David, L. A., and Briggs, T. W. 2010. Sequential outcome following autologous chondrocyte implantation of the knee: A six-year follow-up. *Int Orthop*. **34**(7), p.55.
- Rolfe, K. W., Martell, J. M., and Schmalzried, T. P. 2006. Joint reaction stress and osteoarthritis of the hip. In: *52nd Annual Meeting of the Orthopaedic Research Society*. Los Angeles: The University of Chicago Hospitals.
- Roth, S. H. and Fuller, P. 2011. Diclofenac sodium topical solution 1.5% w/w with dimethyl sulfoxide compared with placebo for the treatment of osteoarthritis: pooled safety results. *Postgraduate Med*. **123**(6), pp.180-8.
- Roth, V. and Mow, V. C. 1980. The intrinsic tensile behavior of the matrix of bovine articular cartilage and its variation with age. *J Bone Joint Surg Am*. **62**(7), pp.1102-17.

- Rozbruch, S., Wickiewicz, T., Di, C. E., and Potter, H. 1996. Osteonecrosis of the knee following arthroscopic laser meniscectomy. *Arthroscopy*. **12**(2), pp.245-50.
- Rusconi, F., Valton, E., Nguyen, R., and Dufourc, E. 2001. Quantification of sodium dodecyl sulfate in microliter-volume biochemical samples by visible light spectroscopy. *Analytical Biochemistry*. **295**(1), pp.31-7.
- Sakakibara, Y., Miura, T., Iwata, H., Kikuchi, T., Yamaguchi, T., Yoshimi, T., and Itoh, H. 1994. Effect of high-molecularweight sodium hyaluronate on immobilized rabbit knee. *Clin Orthop Relat Res*. **299**, pp.282-92.
- Saklatvala, J. 1986. Tumour necrosis factor alpha, stimulates resorption and inhibits synthesis of proteoglycan in cartilage. *Nature*. **322**, pp.547-549.
- Samouillan, V., Lamure, A., Maurel, E., Dandurand, J., Lacabanne, C., Ballarin, F., and Spina, M. 2000. Characterisation of elastin and collagen in aortic bioprostheses. *Med Biol Eng Comput*. **38**, pp.226-231.
- Sanchez, C., Pesesse, L., Gabay, O., Delcour, J. P., Msika, P., Baudouin, C., and Henrotin, Y. E. 2012. Regulation of subchondral bone osteoblast metabolism by cyclic compression. *Arthritis Rheum*. **64**(4), pp.1193-203.
- Sandell, L. J. and Aigner, T. 2001. Articular cartilage and changes in arthritis. An introduction: cell biology of osteoarthritis. *Arthritis Res*. **3**(2), pp.107-13.
- Sandy, J. D., Barrach, H. J., Flanner, C. R., and Plaas, A. H. 1987. The biosynthetic response of the mature chondrocyte in early osteoarthritis. *J Rheumatol*. **14**, pp.16-19.
- Sasada, T., Abe, T., Morita, M., and Mabuchi, K. 2005. Role of chondroitin sulfate in the low friction property of articular cartilages. In *Proceedings of the Fifth Kobe International Forum on Biotribology, Kobe, Japan.*, pp.64-67.
- Scanzello, C. R., Umoh, E., Pessler, F., Diaz-Torne, C., Miles, T. et al. 2009. Local cytokine profiles in knee osteoarthritis: elevated synovial fluid interleukin-15 differentiates early from endstage disease. *Osteoarthritis Cartilage*. **17**(8), pp.1040-48.
- Schinagl, R. M., Gurskis, D., Chen, A. C., and Sah, R. L. 1997. Depth-dependent confined compression modulus of full-thickness bovine articular cartilage. *J Orthop Res*. **15**(4), pp.499-506.
- Schiphof, D., Boers, M., and Bierma-Zeinstra, S. M. 2008. Differences in descriptions of Kellgren and Lawrence grades of knee osteoarthritis. *Ann Rheum Dis*. **67**, pp.1034-36.
- Schmidt, M. B., Mow, V. C., Chun, L. E., and Eyre, D. R. 1990. Effects of proteoglycan extraction on the tensile behavior of articular cartilage. *J Orthop Res*. **8**(3), pp.353-63.
- Schneider, A., Garlick, J. A., and Egles, C. 2008. Self-assembling peptide nanofiber scaffolds accelerate wound healing. *PLoS One*. **3**(1), p.e1410.
- Scott, W. W. Jr., Lethbridge-Cejku, M., Reichle, R., Wigley, F. M., and Tobin, J. D., Hochberg, M.C. 1993. Reliability of grading scales for individual radiographic features of osteoarthritis of the knee. The Baltimore longitudinal study of aging atlas of knee osteoarthritis. *Investigate Radiology*. **28**, pp.497-501.
- Séguin, C. A. and Bernier, S. M. 2003. TNF- α suppresses link protein and type II collagen expression in chondrocytes: Role of MEK1/2 and NF- κ B signaling pathways. *J Cell Physiol*. **197**(3), pp.356-69.
- Sellam, J. and Berenbaum, F. 2010. The role of synovitis in pathophysiology and clinical symptoms of osteoarthritis. *Nat Rev Rheumatol*. **6**(11), pp.625-35.

- Semino, C. E. 2008. Self-assembling Peptides: From Bio-inspired Materials to Bone Regeneration. *J Dent Res.* **87**(7), pp.606-616.
- Seshadri, S., Khurana, R., and Fink, A. L. 1999. Fourier transform infrared spectroscopy in analysis of protein deposits. *Methods in Enzymology.* **309**, pp.559-576.
- Shaha, R. N., Shah, N. A, Lim, M. M. R., Hsieh, C., Nuber, G., and Stupp, S. I. 2010. Supramolecular design of self-assembling nanofibers for cartilage regeneration. *PNAS.* **107**(8), pp.3293–3298.
- Sharif, M., Osborne, D. J., Meadows, K., Woodhouse, S. M., Colvin, E. M., Shepstone, L., and Dieppe, P. A. 1996. The relevance of chondroitin and keratan sulphate markers in normal and arthritic synovial fluid. *Br J Rheumatol.* **35**, pp.951-957.
- Shen, G. 2005. The role of type X collagen in facilitating and regulating endochondral ossification of articular cartilage. *J Orthod Craniofac Res.* **8**(1), pp.11-17.
- Sherman, A. L., Ojeda-Correal, G., and Mena, J. 2012. Use of Glucosamine and Chondroitin in Persons With Osteoarthritis. *PM R.* **4**(5), pp.S110-S116.
- Short, A. R., Koralla, D., Deshmukh, A., Wissel, B., Stocker, B. et al. 2015. Hydrogels That Allow and Facilitate Bone Repair, Remodeling, and Regeneration. *J Mater Chem B Mater Biol Med.* **3**(40), pp.7818-7830.
- Siebert, F. and Hildebrandt, P. 2007. *Vibrational Spectroscopy in Life Science.* Wiley-VCH.
- Silver, F. H., Bradica, G., and Tria, A. J. 2001a. Viscoelastic behavior of osteoarthritic cartilage. *Connect Tissue Res.* **42**(3), pp.223-233.
- Silver, F. H., Bradica, G., and Tria, A. 2004. Do changes in the mechanical properties of articular cartilage promote catabolic destruction of cartilage and osteoarthritis? *Matrix Biol.* **23**(7), pp.467-476.
- Slynarski, K., Widuchowski, W., Snow, M., and Verdonk, P. 2015. Primary chondrocytes and bone marrow cells on a 3D co-polymer scaffold: 2-year results of a prospective, multicenter, single-arm clinical trial in patients with cartilage defects of the knee. *Revue de Chirurgie Orthopédique et Traumatologique.* **101**(8), pp.e17-e18.
- Smith, H. 2005. *Autologous Chondrocyte Transplantation / Implantation Versus Existing treatments.* [online]. Available from World Wide Web: <<http://www.active-trial.org.uk/ChondralDefects.htm>>
- Smith, M. D., Triantafillou, S., Parker, A., Youssef, P. P., and Coleman, M. 1997. Synovial membrane inflammation and cytokine production in patients with early osteoarthritis. *J Rheumatol.* **24**(2), pp.365-371.
- Solheim, E., Hegna, J., Oyen, J., Austgulen, O. K., Harlem, T., and Strand, T. 2010. Osteochondral autografting (mosaicplasty) in articular cartilage defects in the knee: results at 5 to 9 years. *Knee.* **17**(1), pp.84-87.
- Soppimath, K. S., Aminabhavi, T. M., Dave, A. M., Kumbar, S. G., and Rudzinski, W. E. 2002. Stimulus-responsive smart hydrogels as novel drug delivery systems. *Drug Dev Ind Pharm.* **28**(8), pp.957-974.
- Sprague, N. F. 1981. Arthroscopic debridement for degenerative knee joint disease. *Clin Orthop.* **160**, pp.118-23.
- Squires, G. R., Okouneff, S., Ionescu, M., and Poole, A. R. 2003. The pathobiology of focal lesion development in aging human articular cartilage and molecular matrix changes characteristic of osteoarthritis. *Arthritis Rheum.* **48**(5), pp.1261-70.

- Stapleton, T, Ingram, J, Katta, J, Knight, R, Korossis, S, Fisher, J, and Ingham, E. 2008. Development and characterisation of an acellular porcine medial meniscus for use in tissue engineering. *Tissue Eng Part A*. **14**(4), pp.505-18.
- Stephanopoulos, N., Ortony, J. H., and Stupp, S. I. 2013. Self-assembly for the synthesis of functional biomaterials. *Acta Materialia*. **61**(3), pp.912-930.
- Stemplewski, A., Hintze, V., and Fertala, A. 2007. Molecular basis of organization of collagen fibrils. *J Struct Biol*. **157**(2), pp.297-307.
- Stolz, M., Raiteri, R., Daniels, A.U., VanLandingham, M.R., Baschong, W., and Aebi, U. 2004. Dynamic Elastic Modulus of Porcine Articular Cartilage Determined at Two Different Levels of Tissue Organization by Indentation-Type Atomic Force Microscopy. *Biophysical Journal*. **86**(5), pp.3269-3283.
- Strand, V., Simon, L. S., Dougados, M., Sands, G. H., Bhadra, P., Breazna, A., and Immitt, J. 2011. Treatment of osteoarthritis with continuous versus intermittent celecoxib. *J Rheumatol*. **38**(12), pp.2625-34.
- Stuart, B. H. 2004. *Infrared Spectroscopy: Fundamentals and Applications*. Wiley.
- Stuart, B. H. and George, B. McIntyre, P. 1996. *Modern Infrared Spectroscopy, Volume 40 of Analytical Chemistry by Open Learning*. John Wiley & Sons.
- Suh, J. and Matthew, H. 2001. Application of chitosan-based polysaccharide biomaterials in cartilage tissue engineering: a review. *Biomaterials*. **21**, pp.2589-98.
- Susi, H. 1972. Infrared spectroscopy - Conformation. *Methods in Enzymology*. **26**, pp.455-472.
- Susi, H. and Byler, D. M. 1986. Resolution-enhanced Fourier transform infrared spectroscopy of enzymes. *Methods in Enzymology*. **130**, pp.290-311.
- Sutton, S., Clutterbuck, A., Harris, P., Gent, T., Freeman, S. et al. 2009. The contribution of the synovium, synovial derived inflammatory cytokines and neuropeptides to the pathogenesis of osteoarthritis. *Vet J*. **179**(1), pp.10-24.
- Swann, A. C. and Seedhom, B. B. 1989. Improved techniques for measuring the indentation and thickness of articular cartilage. *Proc Inst Mech Eng H*. **203**(3), pp.143-50.
- Swift, S. R and Trinkle-Mulcahy, L. 2004. Basic principles of FRAP, FLIM and FRET. *Proc. Royal Mic. Soc*. **39**, pp.3-10.
- Swoboda, B. 2001. Epidemiological arthrosis research. *Orthopade*. **30**(11), pp.834-40.
- Tabib, W., Beaufils, P., Blin, J., Tremoulet, J., and Hardy, P. 1999. Arthroscopic meniscectomy with Ho-Yag laser versus mechanical meniscectomy. Mid-term results of a randomized prospective study of 80 meniscectomies. *Rev Chir Orthop Reparatrice Appar Mot*. **85**(7), pp.713-21.
- Tao, H., Wu, Y., Li, H., Wang, C., Zhang, Y. et al. 2015. BMP7-Based Functionalized Self-Assembling Peptides for Nucleus Pulposus Tissue Engineering. *ACS Appl. Mater. Interfaces*. **7**(31), pp.17076-17087.
- Tatman, P. D., Gerull, W., Sweeney-Easter, S., Davis, J. I., Gee, A. O., and Kim, D. H. 2015. Multiscale Biofabrication of Articular Cartilage: Bioinspired and Biomimetic Approaches. *Tissue Eng Part B Rev*. **21**(6), pp.543-59.
- Tay, A. G., Farhadi, J., Suetterlin, R., Pierer, G., Heberer, M., and Martin, I. 2004. Cell yield, proliferation, and postexpansion differentiation capacity of human ear, nasal, and rib chondrocytes. *Tissue Engineering*. **10**, pp.762-770.

- Teepie, E., Jay, G. D., Elsaid, K. A., and Fleming, B. C. 2013. Animal Models of Osteoarthritis: Challenges of Model Selection and Analysis. *AAPS J.* **15**(2), pp. 438–446.
- Teixeira, L. S. M., Patterson, J., and Luyte, F. P. 2014. Skeletal tissue regeneration: where can hydrogels play a role? *International Orthopaedics.* **38**(9), pp.1861-1876.
- Temple-Wong, M. M., Bae, W. C., Chen, M. Q., Bugbee, W. D., Amiel, D. et al. 2009. Biomechanical, structural, and biochemical indices of degenerative and osteoarthritic deterioration of adult human articular cartilage of the femoral condyle. *Osteoarthritis Cartilage.* **17**(11), pp.1469-1476.
- The Center for Orthopaedics & Sports Medicine. 2003. *ACI: General Information*. [online]. Available from World Wide Web: <<http://www.arthroscopy.com/sp08024.htm>>
- The collagen molecule: Collagen structure*. 2014. [online]. Available from World Wide Web: <<https://www.proto-col.com/blog/2014/07/collagen/>>
- The INSTRUCT Products*. 2015. [online]. Available from World Wide Web: <<http://www.cellcotec.com/technology/instruct-products/>>
- Therapeutic trajectory following intra-articular hyaluronic acid injection in knee osteoarthritis - meta-analysis. 2011. R.R. Bannuru, N.S. Natov, U.R. Dasi, C.H. Schmid, T.E. McAlindon. **19**, pp.611-619.
- Thorpe, A. A., Boyes, V. L., Sammon, C., and Le Maitre, C. L. 2016. Thermally triggered injectable hydrogel, which induces mesenchymal stem cell differentiation to nucleus pulposus cells: Potential for regeneration of the intervertebral disc. *Acta Biomater.* **36**, pp.99-111.
- Tortorella, M. D., Malfait, A. M., Deccico, C., and Arner, E. 2001. The role of ADAM-TS4 (aggrecanase-1) and ADAM-TS5 (aggrecanase-2) in a model of cartilage degradation. *Osteoarthritis Cartilage.* **9**(6), pp.539-552.
- Tortorella, M. D., Pratta, M., Liu, R. Q., Austin, J., Ross, O. H. et al. 2000. Sites of aggrecan cleavage by recombinant human aggrecanase-1 (ADAMTS-4). *J Biol Chem.* **275**(24), pp.18566– 73.
- Torzilli, P. A. and Grigiene, R. 1998. Continuous cyclic load reduces proteoglycan release from articular cartilage. *Osteoarthritis Cartilage.* **6**(4), pp.260-8.
- Torzilli, P. A., Grigiene, R., Borrelli, Jr. J., and Helfet, D. L. 1999. Effect of impact load on articular cartilage: cell metabolism and viability, and matrix water content. *J Biomech Eng.* **121**(5), pp.433-41.
- Trattnig, S., Ba-Ssalamah, A., Pinker, K., Plank, C., Vecsei, V., and Marlovits, S. 2005. Matrix-based autologous chondrocyte implantation for cartilage repair: noninvasive monitoring by high-resolution magnetic resonance imaging. *Magn Reson Imaging.* **23**, pp.779-787.
- Tu, R. S. and Tirrell, M. 2004. Bottom-up design of biomimetic assemblies. *Adv Drug Deliv Rev.* **56**(11), pp.1537-1563.
- Ulijn, R. V. and Smith, A. M. 2008. Designing peptide based nanomaterials. *Chem Soc Rev.* **37**(4), pp.664-675.
- University of Arizona. 2001. *Peptide Bond Formation*. [online]. Available from World Wide Web: <<http://www.blc.arizona.edu/courses/schaffer/182/peptidebond.HTM>>
- Urban, J. P. 1994. The Chondrocyte: a cell under pressure. *British Journal of Rheumatology.* **33**, pp.901-908.

- Vacanti, C. A., Langer, R., Schloo, B., and Vacanti, J. P. 1991. Synthetic Polymers seeded with chondrocytes provides a template for new cartilage formation. *Plast Reconstr Surg.* **88**, pp.753-759.
- Van den Berg, W. B. 1997. Lessons for joint destruction from animal models. *Curr Opin Rheumatol.* **9**(3), pp.221-8.
- Van Lent, P. L., Blom, A. B., van der Kraan, P., Holthuisen, A. E., Vitters, E. et al. 2004. Crucial role of synovial lining macrophages in the promotion of transforming growth factor beta-mediated osteophyte formation. *Arthritis Rheum.* **50**(1), pp.103-11.
- Van Osch, G. J., Mandi, E.W., Jahr, H., Koevoet, W., Nolst-Trenite, G., and Verhaar, J. A. 2004. Considerations on the use of ear chondrocytes as donor chondrocytes for cartilage tissue engineering. *Biorheology.* **41**, pp.411-421.
- Vangsness, C. T. Jr., Spiker, W., and Erickson, J. 2009. A Review of Evidence-Based Medicine for Glucosamine and Chondroitin Sulfate Use in Knee Osteoarthritis. *Arthroscopy.* **25**(1), pp.86-94.
- Varaprasad, K., Raghavendra, G. M., Jayaramudu, T., Yallapu, M. M., and Sadiku, R. 2017. A mini review on hydrogels classification and recent developments in miscellaneous applications. *Materials Science and Engineering: C.* **79**, pp.958-971.
- Vasiliadis, H. S. and Tsikopoulos, K. 2017. Glucosamine and chondroitin for the treatment of osteoarthritis. *World J Orthop.* **18**(8), pp.1-11.
- Veje, K., Hyllested-Winge, J. L., and Ostergaard, K. 2003. Topographic and zonal distribution of tenascin in human articular cartilage from femoral heads: normal versus mild and severe osteoarthritis. *Osteoarthritis Cartilage.* **11**(3), pp.217-27.
- Versier, G. and Dubrana, F. 2011. Treatment of knee cartilage defect in 2010. *Orthop Traumatol Surg Res.* **97**(8), pp.S140-S153.
- Vinatier, C. and Guicheux, J. 2016. Cartilage tissue engineering: From biomaterials and stem cells to osteoarthritis treatments. *Annals of Physical and Rehabilitation Medicine.* **59**, pp.139-144.
- Vincent, K. R., Conrad, B. P., Fregly, B. J., and Vincent, H. K. 2012. The Pathophysiology of Osteoarthritis: A Mechanical Perspective on the Knee Joint. *PM R.* **4**(5 Supp), pp.S3-9.
- Visser, M., Bouter, L. M., McQuillan, G. M., Wener, M. H., and Harris, T. B. 1999. Elevated C-reactive protein levels in overweight and obese adults. *JAMA.* **282**(22), pp.2131-5.
- Voet, D. and Voet, J. G. 1995. *Biochemistry.* New York: John Wiley and Sons.
- Voss, B., El-Othmani, M. M, Schnur, A. K., Botchway, A., Mihalko, W. M., and Saleh, K. J. 2016. A Meta-Analysis Comparing All-Polyethylene Tibial Component to Metal-Backed Tibial Component in Total Knee Arthroplasty: Assessing Survivorship and Functional Outcomes. *The Journal of Arthroplasty.* **31**(11), pp.2628-2636.
- Wachs, R. A., Hoogenboezem, E. N., Huda, H. I., Xin, S., Porvasnik, S. L., and Schmidt, C. E. 2017. Creation of an injectable in situ gelling native extracellular matrix for nucleus pulposus tissue engineering. *The Spine Journal.* **17**(3), pp.435-444.
- Walker, P. S., Dowson, D., Longfield, M. D., and Wright, V. 1968. Boosted lubrication in synovial joints by fluid entrapment and enrichment. *Ann Rheum Dis.* **27**(6), pp.512-20.
- Walsh, D. A., Bonnet, C.S., Turner, E.L., Wilson, D., Situ, M., and McWilliams, D. F. 2007. Angiogenesis in the synovium and at the osteochondral junction in osteoarthritis. *Osteoarthritis Cartilage.* **15**, pp.743-51.

- Wan, S., Borland, S., Richardson, S. M., Merry, C. L. R., Saiani, A., and Gough, J. E. 2016. Self-assembling peptide hydrogel for intervertebral disc tissue engineering. *Acta Biomaterialia*. **46**, pp.29-40.
- Wang, J. H., Jia, F., Gilbert, T. W., and Woo, S. L. 2003. Cell orientation determines the alignment of cell-produced collagenous matrix. *J Biomech*. **36**(1), pp.97–102.
- Wilder, F. V., Hall, B. J., Barrett, J. P. Jr., and Lemrow, N. B. 2002. History of acute knee injury and osteoarthritis of the knee: a prospective epidemiological assessment. The Clearwater Osteoarthritis Study. *Osteoarthritis & Cartilage*. **10**, pp.911-6.
- Williams, D. A., Farrell, M. J., Cunningham, J., Gracely, R. H., Ambrose, K., and Cupps, T. 2004. Knee pain and radiographic osteoarthritis interact in the prediction of levels of self-reported disability. *Arthritis & Rheumatism*. **51**, pp.558-61.
- Williams, D. H. and Fleming, I. 1995. *Spectroscopic methods in organic chemistry*. Maidenhead: McGraw-Hill Book Company.
- Williams, A., Sharma, L., McKenzie, C. A., Prasad, P. V., and Burstein, D. 2005. Delayed gadolinium-enhanced magnetic resonance imaging of cartilage in knee osteoarthritis: Findings at different radiographic stages of disease and relationship to malalignment. *Arthritis & Rheumatism*. **52**, pp.3528-35.
- Wilshaw, S. P., Aggeli, A., Fisher, J., and Ingham, E. 2008. The biocompatibility and immunogenicity of self-assembling peptides for use in tissue engineering and regenerative applications. *Tissue Eng Part A*. **14**, pp.785-785.
- Wilson, W., Huyghe, J. M., and Donkelaar, C. C. v. 2007. Depth-dependent compressive equilibrium properties of articular cartilage explained by its composition. *Biomechan Model Mechanobiol*. **6**, pp.43-53.
- Wise, B. L., Niu, J., Yang, M., Lane, N. E., Harvey, W. et al. 2012. Patterns of compartment involvement in tibiofemoral osteoarthritis in men and women and in Caucasians and African Americans. *Arthritis Care Res*. **64**(4), pp.847-52.
- Withdrawal Assessment Report: Hyalograft C Autograft*. 2013. London.
- Wu, J. L., Liao, C. Y. Zhang, J., Cheng, W. Z., Zhou, N., Wang, S., and Wan, S. 2011. Incorporation of protein-loaded microspheres into chitosan–polycaprolactone scaffolds for controlled release. *Carbohydr Polym*. **86**(2), pp.1048-1054.
- Xavier, J. R., Thakur, T., Desai, P., Jaiswal, M. K., Sears, N. et al. 2015. Bioactive nanoengineered hydrogels for bone tissue engineering: a growth-factor-free approach. *ACS Nano*. **9**(3), pp.109-18.
- Xie, Z., Aphale, N. V., Kadapure, T. D., Wadajkar, A. S., Orr, S. et al. 2015. Design of antimicrobial peptides conjugated biodegradable citric acid derived hydrogels for wound healing. *J Biomed Mater Res A*. **103**(12), pp.3907-18.
- Xu, F. F., Wang, Y. C., Sun, S., Ho, A. S., Lee, D. et al. 2015. Comparison between self-assembling peptide nanofiber scaffold (SAPNS) and fibrin sealant in neurosurgical hemostasis. *Clin Transl Sci*. **8**(5), pp.490-4.
- Yamagata, T., Saito, H., Habuchi, O., and Suski, S. 1968. Purification and Properties of Bacterial Chondroitinases and Chondrosulfatases. *The Journal of Biological Chemistry*. **243**(7), pp.1523-1535.
- Yan, L. P., Wang, Y. J., Ren, L., Wu, G., Caridade, S. G. et al. 2010. Genipin-cross-linked collagen/chitosan biomimetic scaffolds for articular cartilage tissue engineering applications. *J Biomed Mater Res A*. **95**(2), pp.465-475.

- Young, A. A., Smith, M. M., Smith, S. M., Cake, M. A., Ghosh, P. et al. 2005. Regional assessment of articular cartilage gene expression and small proteoglycan metabolism in an animal model of osteoarthritis. *Arthritis Res Ther.* **7**(4), pp.852-61.
- Zanetti, M., Ratcliffe, A., and Watt, F. M. 1985. Two subpopulations of differentiated chondrocytes identified with a monoclonal antibody to keratan sulfate. *J Cell Biol.* **101**(1), pp.53-59.
- Zaslav, K., Cole, B., Brewster, R., DeBerardino, T., Farr, J., Fowler, P., and Nissen, C. 2009. A prospective study of autologous chondrocyte implantation in patients with failed prior treatment for articular cartilage defect of the knee e results of the Study of the Treatment of Articular Repair (STAR) Clinical Trial. *Am J Sports Med.* **37**(1), pp.42-55.
- Zhang, S., Gelain, F., and Zhao, X. 2005. Designer self-assembling peptide nanofiber scaffolds for 3D tissue cell cultures. *Semin Cancer Biol.* **15**(5), pp.413-420.
- Zhang, Y. and Jordan, J. M. 2010. Epidemiology of Osteoarthritis. *Clin Geriatr Med.* **26**(3), pp.355–369.
- Zhang, Y., Xu, L., Nevitt, M.C., Aliabadi, P., Yu, W., and Qin, M. 2001. Comparison of the prevalence of knee osteoarthritis between the elderly Chinese population in Beijing and whites in the United States: The Beijing Osteoarthritis Study. *Arthritis & Rheumatism.* **44**, pp.2065-71.
- Zhao, G., Yin, S., Liu, G., Cen, L., Sun, J. et al. 2009. In vitro engineering of fibrocartilage using CDMP1 induced dermal fibroblasts and polyglycolide. *Biomaterials.* **30**(19), pp.3241-50.